An integrated solution for school renovation: Double-skin facade with diffuse ceiling ventilation

Master's Thesis

Aalborg University
BUILD

BUILD
Aalborg University
http://www.aau.dk

AALBORG UNIVERSITY
STUDENT REPORT

Title:
An integrated solution for school renovation: Double-skin facade with diffuse ceiling ventilation

Project Period:
Autumn Semester 2023

Participant(s):
Eimante Kazukalovaite
Sarolta Kereszturi

Supervisor(s):
Chen Zhang
Olena Kalyanova Larsen

Page Numbers: 124

Date of Completion:
11.01.2024

Abstract:

The I-DIFFER renovation solution, implementing a double-skin facade with diffuse ceiling ventilation, is investigated in this report via experimental methods. The experiments were conducted in the FACADE laboratory of AAU, within a scaled-down classroom (Test room). The aim of the research is to evaluate the performance of the currently applied control strategy of the cooling and heating modes, and its influence on the temperature distribution within the DSF and DCV cavities, and on the global and local thermal comfort of the Test room. The measurements occurred across diverse seasons, including a summer, an intermediate, and a winter week. The results displayed that the control strategy is able to perform according to its purpose under favourable conditions, however, it requires optimization. The global thermal comfort analysis revealed overheating during the summer and winter periods, while dominantly low operative temperature defined the intermediate period. The local comfort analysis only posed a risk of discomfort due to radiant temperature asymmetry for a sitting position in the middle of the room during the intermediate and winter periods.

Abbreviations

AAU	Aalborg University
BR	Building regulations
BR18	Building regulations 2018
CO_2	Carbon dioxide
DCV	Diffuse Ceiling Ventilation
DR	Draught Rate
DS	Danish Standard
DSF	Double Skin Facade
I-DIFFER	Double Skin Facade and Diffuse Ceiling Ventilation for School Renovation
IEQ	Indoor Environmental Quality
MRT	Mean Radiant Temperature
PD	Predicted percent Dissatisfied due to draft
PMV	Predicted Mean Vote
PPD	Predicted Percentage of Dissatisfied
RTA	Radiant Temperature Asymmetry
WM	WindowMaster

Contents

Chapter 1

Introduction

The prevailing majority of the building stock within the European Union reveals a lack of energy efficiency, as 85% of it was constructed before 2001. Given their anticipated continued utilization through 2050, the necessity for comprehensive renovation efforts emerges. In alignment with this, the European Commission has introduced the Climate Target Plan 2030, proposing a substantial reduction (55%) in greenhouse gas emissions by 2030, relative to 1990. Considering that the existing buildings account for 40% of the EU's total energy consumption and contribute 36% of its GHG emissions, a need for improvement within the building sector in the form of refurbishment is evident. In order to meet the established objectives, a reduction of 60% in GHG emissions, an 18% decrease in heating and cooling energy demand, and a 14% reduction in final energy consumption are essential [3].

Considering the Danish building stock, it is essential to address the need for refurbishment of schools, as approximately 90% of schools predate 1995, and were predominantly constructed between the years 1960 and 1980. Consequently, the criteria outlined in BR95, including specifications regarding ventilation requirements and indoor temperature, apply to only about 10% of the existing school buildings. Additionally, the implementation of energy framework guidelines commenced in 2006, with less than 5% of school constructions occurring thereafter, leading to the prevalent energy rating of D in this building typology [6] [12].

The currently applied Building Regulations (BR18) incorporate requirements concerning the indoor climate of schools, addressing the thermal, atmospheric, acoustic, and visual parameters due to their profound impact on students' performance [22] [12]. Discomfort arising from inadequate indoor environments can cause challenges in sustaining focus, irritability, heightened stress, and drowsiness. Insufficient ventilation, in particular, significantly impairs concentration, comprehension, memory retention, and reading and mathematical abilities. Furthermore, inadequate study environments can manifest in the absence of students, contributing to a decline in academic performance[10].

As the BR18 also defines guidelines regarding energy frameworks, the potential renovation solutions for establishing an optimal indoor climate are limited [22] [12]. An influential initiative addressing these challenges was the "School of the Future" project, funded by the European Union, which incorporated a Danish school. This project aimed to illustrate holistic renovations focusing on enhancing indoor environmental quality and energy con-

servation, resulting in superior building performance [8].

However, the traditional construction process can negatively impact school life by causing disturbance in various ways due to factors such as noise, vibrations, emissions, etc [1]. These disruptions not only interrupt the educational program but also compromise the learning environment for students. While conducting renovations during holidays and school breaks can mitigate disturbances to students, this approach limits the available time frame and affects the workflow for the renovation process [7]. Furthermore, an emerging challenge of improving atmospheric comfort through retrofitting involves the integration of a balanced mechanical ventilation system, as it is expensive, and the majority of buildings lack adequate space for installing the ducts and air handling units. Consequently, this obstacle has led to the exploration and application of simplified ventilation systems [13].

To avoid the difficulties associated with traditional renovations, the concept of the I-DIFFER (Integrated Solution – Double Skin Facade and Diffuse Ceiling Ventilation for School Renovation) renovation solution is introduced, which implements the combination of a double skin facade (DSF) and diffuse ceiling ventilation (DCV). The DSF structure comprises of an external and an internal facade surrounding an air cavity between them. In the I-DIFFER approach, the original construction of the facade (which becomes the internal facade) remains intact while adding an external glazed facade. Moreover, the strategically positioned openings on the external glazing are equipped with integrated control mechanisms. The DCV structure within this renovation solution incorporates an air cavity (plenum box) situated above the room, bounded by diffuse ceiling panels. This design facilitates air distribution across the entire ceiling surface area via thermal buoyancy enhanced by mechanical extraction. Moreover, there is a partition between the DSF and DCV cavities, providing the flexibility to open or close according to the functional requirements. Consequently, the operation of the system can adapt to the specific heating or cooling needs of the occupied space [11] [14] [2].

Additionally, the incorporation of efficient building control systems during renovation can result in establishing an indoor environment that prioritizes the comfort of the occupants while optimizing energy utilization. In order to obtain a satisfactory operation of these advanced building controls, the ability to adapt to dynamic environmental factors and the occupants, while integrating occupant feedback into control logic and fulfilling the set objectives is required. The energy efficiency of the I-DIFFER solution, which is designed for advanced control system integration, is therefore dependent on the adequate commissioning and performance monitoring of the control strategies. Conversely, challenges associated with the implementation of control systems are significant to consider, e.g. standardization, system complexity, and compatibility. Furthermore, inadequate control performance presents a risk, as it could inadvertently increase energy consumption. This emphasizes the necessity for system testing, and continual monitoring to ensure that these advanced control systems deliver the anticipated benefits [24] [15] [4].

1.1 State-of-the-Art

Previous research has been conducted on the performance of the I-DIFFER renovation solution in comparison to a traditional renovation solution that includes the replacement of windows and additional insulation of the building envelope. The main focus was on evaluating which solution is more energy efficient while providing satisfactory thermal and atmospheric IEQ. Intending to define the most adequate I-DIFFER solution that can adapt to seasonal weather changes, different variations of the parameters of computational models using IDA-ICE were investigated, regarding the DSF glazing properties, cavity thicknesses, orientation, facade material and its thermal mass, occupant density, and future and extreme weather [11] [14].

From the results of *"A novel solution for school renovations: Combining diffuse ceiling ventilation with double skin facade"* it was concluded that considering the simulation with the lowest total primary energy consumption of both the traditional and I-DIFFER solutions, the latter performed better by 11%. However, it was also determined that for the traditional renovation, the main energy-consuming system was the ventilation, while for the I-DIFFER solution, it was the heating system. Regarding the IEQ, when double-glazing was implemented into the simulation, the I-DIFFER solution fulfilled the criteria and was more energy-efficient than the traditional renovation solution which also satisfied the criteria. Furthermore, the glazing properties have a more significant influence than altering the DSF cavity thickness, as single-glazing for the DSF leads to larger energy consumption in comparison to the traditional renovation. However, the performance of the I-DIFFER solution is heavily influenced by the ambient temperature and solar radiation[11].

Further simulations were inspected and analyzed in the article *"Exploring the potential of combining diffuse ceiling and double-skin facade for school renovations"*, where the results discovered that the I-DIFFER solution performs better or similarly to the traditional renovation solution with an orientation toward E, SE, S, SW, and W. However, with a northern orientation, the traditional renovation appears to be more favourable, considering the total primary energy consumption and the thermal comfort of the occupants. The results regarding the facade material (thermal mass and reflectivity) displayed that the highest thermal comfort and lowest energy consumption are achieved with a facade construction of high thermal mass and low reflectance. However, the influence of the facade material is minimal on the energy demand and IEQ. When simulating extreme climate conditions, the traditional renovation solution performs better during extremely cold weather; while the I-DIFFER solution is more favourable under hot and sunny conditions, and mild winters. Considering the future climates of 2050 and 2090 with the increasing global warming, the I-DIFFER solution displays the trend of decreasing energy consumption and increasing thermal comfort, in contrast to the traditional renovation. The results are similar for both renovation solutions in terms of altering the number of occupants in the classrooms[14].

Consequently, a different method was introduced in the research study of *"Experimental investigation of an integrated renovation solution combining diffuse ceiling ventilation and double skin facade"* in the form of an experimental research, which inspected the performance of the I-DIFFER renovation solution in the FACADE laboratory of AAU that functions as a scaled-down classroom. From the experiment, it was concluded that the I-DIFFER solu-

tion appeared to be a competitive solution to a traditional renovation, as under favourable circumstances it is able to provide better thermal comfort with a lower energy demand. During winter, the thermal mass of the ceiling was activated leading to a reduction and shift of the peak temperatures into later hours of the investigated days. Similarly, in summer, the peak temperatures were reduced as the DSF cavity was ventilated and the heat gain by solar radiation was removed from the cavity. However, the system is more easily affected by outdoor and indoor conditions, and the performance is more sensitive to the design parameters. Furthermore, the implemented simple control was not sufficient [2].

To sum up, from the currently existing research on the topic, the most adequate structural parameters have been investigated and defined via building performance simulations, which led to the conclusion that the I-DIFFER solution can compete with a traditional renovation, concerning IEQ and energy efficiency. However, adequate implementation is important in order to avoid the risks of unsatisfactory potential. Additionally, the need for further investigations regarding the optimization of control strategies, to achieve a system that can perform sufficiently regardless of the altering outdoor and indoor conditions, was revealed through experimental methods [2] [11] [14].

1.2 Problem formulation

The objective of the report is to conduct further experimental research on the topic of the I-DIFFER renovation solution, implementing a double-skin facade with diffuse ceiling ventilation. A Test room built in the FACADE laboratory of Aalborg University functions as a scaled-down classroom with the purpose of investigating the control strategies of the system and the indoor environmental quality in the room. As the activation of the distinct control modes is dependent on the outdoor conditions, multiple sets of experiments are performed to establish the operation of the system during a summer week, a transient week, and a winter week. Consequently, the report aims to investigate and answer the following questions:

- *How do the efficacy and performance of existing control strategies differ across the summer, intermediate, and winter seasons?*
- *How do the cooling and heating modes impact the temperature distribution in the DSF and DCV cavities across distinct seasons?*
- *What is the influence of implementing the I-DIFFER renovation solution on the expression of global and local thermal comfort within the Test room across distinct seasons?*

Chapter 2

Methodology

The methodology chapter outlines the research process to address the questions raised in the subsection *1.2. Problem formulation.* Focusing on the project outline and approach of performing the thermal comfort analysis.

General research outline
An experimental investigation is conducted in a scaled-down classroom to explore the performance of a double skin facade combined with diffuse ceiling ventilation system heating and cooling control modes and its impact on occupant thermal comfort.

The initial phase of the general project outline includes three steps:

1. Preparation for conducting the measurements. It involves defining the preliminary problem and the measurement campaign, coupled with a literature review to assimilate existing research findings. This phase further incorporates thermocouple calibration procedures and examination of equipment. Entailing validating WindowMaster monitor thermal sensors against K-type thermocouples and IC-meters, evaluating thermocouple protection methods such as a silver tube, silver foil and no protections against solar radiation and determining the efficacy of polished versus unpolished silver tubes in the DSF cavity. Which are described in appendix *9.3 Validation of equipment*. Concurrently, test measurements are conducted throughout the preparation phase to address and resolve any issues, laying a robust foundation for the rest of the research stages.

2. After the preparation, the actual measurements for the analysis are conducted. The analysis contains two measurements for the heating season: intermediate measurements are taken from 23-26.10.2023 (4 full days of data) and winter measurements from 30-11-2023 to 02-12-2023 (3 full days). Due to time constraints, acquiring data for the system operating in cooling mode during summer conditions was not feasible. However, data was obtained from previously conducted research for 24-30.07.2023, providing seven full days of data. The experimental room is described in *3.1 The Test room*, and control modes in *3.2 Control strategy*.

DATA RECEIVED		DATA COLLECTED
COOLING SEASON	HEATING SEASON	
Summer	Intermediate	Winter
(24-30).07.2023	(23-26).10.2023	(30.10-06.11).2023

Figure 2.1: Experimental investigation cases with durations.

Figure 2.2 shows which thermal comfort areas are investigated and what is measured, as well as supplementary measures to get an overview of how the system reacts in the changing outdoor conditions. A more detailed description of the sensors and equipment can be found in chapter *3.1 Setup of the Test room*.

THERMAL COMFORT		SUPPLEMENTARY
GLOBAL	LOCAL	Weather conditions
Operative temperature	Draught Rate	t_o (°C), I_{sol} (W/m²), w_s(m/s)
t_{op} (°C)	$t_{a,l}$ (°C), $v_{a,l}$ (m/s), Tu (%)	DSF & DCV cavities
PMV and PPD	Vertical Air Temperature Difference	$t_{a,l}$ (°C)
$t_{a,l}$ (°C), RH (%), $v_{a,l}$ (m/s)	$t_{a,l}$ (°C)	Ventilation
	Radiant Temperature Asymetry	$t_{a,l}$ (°C), V_{air} (l/s), CO_2 (ppm)
	t_s (°C)	Other:
	Floor temperature	Window openings (%)
	t_s (°C)	
Mean Radiant Temperature		
t_s (°C)		

CO_2	carbon dioxide from humans
I_{sol}	solar irradiance
$t_{a,l}$	temperature at the specific location
t_{air}	air temperature
t_o	outdoor air temperature
t_{op}	operative temperature
t_s	surface temperature
Tu	turbulence intensity
V_{air}	air volume flow
$v_{a,l}$	air velocity at the specific location

Figure 2.2: The investigated fields and measures performed during the measurement campaign.

3. After collecting the measurements, the logs are extracted, treated, analysed and visualised. Data is gathered from various apparatuses for analysis, with calculations for thermal comfort being guided by the Danish standard (DS), with detailed explanations and methodologies, including the data treatment and actions regarding missing data to follow in the subsequent subchapter.

To define which control is active at given time the window opening are investigated. If the bottom and middle row windows are opened, it indicates that the system is running in cooling mode. This mode cools the DSF cavity by drawing fresh air in through the bottom row windows and releasing it through the middle row windows. Furthermore, during the cooling mode, the top window is also open as cold air is directly admitted into the DCV cavity. Conversely, when only the bottom row windows are open, it suggests the system is in heating mode, as cold air is directly admitted into the DSF cavity, where it is preheated and supplied further into the DCV cavity and Test room.

2.1 Thermal comfort

People can experience thermal comfort/discomfort globally or locally. When considering global comfort, the thermal condition of the overall body is assessed by the operative temperature in the room and indices such as Predicted Mean Vote (PMV) and Predicted Percentage Dissatisfied (PPD). However, local discomfort occurs when undesired heating or cooling targets part of the body, which can be caused by draught, vertical air temperature difference, warm/cold surfaces, and radiant asymmetry. People with sedentary activity mostly experience the perception of local discomfort, as they are more thermally sensitive than people with higher activity levels [20].

Meanwhile, IEQ categories guide the design of climate-controlled buildings, setting expected comfort levels. Application of these categories is voluntary and used as guidelines to ensure safety and quality if the national building regulations (BR) do not say otherwise. According to the Danish standards (DS), high expectations (Category I) may be selected for occupants with special consideration, such as children, elderly and disabled. The lower categories are not associated with health risks but may reduce comfort levels. [18] For more detailed explanation of the IEQ categories see Appendix 9.1.

IEQ Category	Level of expectation
I	High
II	Medium
III	Moderate
IV	Low

Figure 2.3: Categories of indoor environmental quality. [18]

2.1.1 Global thermal comfort

The parameters investigated in the report concerning global thermal comfort and the recommended values according to DS 17772 can be viewed in Figure 2.4.

Type of space	Activity, W/m²	IEQ categories		Operative temperature,°C		Thermal state of the body as a whole	
		Category	Level of expectation	Summer, cooling season (0.5 clo)	Winter, heating season (1.0 clo)	PPD, %	PMV
Classroom	70 (1.2 met)	I	High	23.5 - 25.5	21 - 23	< 6	-0.2 < PMV < 0.2
		II	Medium	23 - 26	20 - 24	< 10	-0.5 < PMV < 0.5
		III	Moderate	22 - 27	19 - 25	< 15	-0.7 < PMV < 0.7
		IV	Low	21 - 28	17 - 26	< 25	-1.0 < PMV < 1.0

Figure 2.4: Global thermal environment parameter ranges for classrooms according to the categories of indoor environmental quality. [18]

Operative temperature

Operative temperature is a uniform temperature within an enclosure, where an occupant would exchange the same amount of heat by radiation and convection as in the actual non-uniform environment. [20] The optimal operative temperature range satisfies the greater percentage of occupants at a given clothing and activity level in the current thermal environment. In a classroom with typical sedentary activity (70W/m² at 1.2 met) and clothing levels of 1.0 clo (heating season) and 0.5 clo (cooling season), the recommended operative temperatures are shown in Figure 2.4.

Operative temperature estimation in the Test Room:

The operative temperature for the test room is obtained from a thermocouple placed in a grey table tennis ball located on the Middle pole at 1.1 height from the floor. For the analysis, the running five-minute averages are used.

However, an alternative calculation is adopted when this method becomes unreliable due to data errors, notably during summer and winter measurements. Which involves averaging the readings from thermocouples measuring air temperature at the North, Middle, and South poles, ranging in height from 0.1 meters to 1.7 meters above the floor.

Alongside operative temperature analysis, Fanger's comfort model estimates the PMV and PPD, with the specific calculation methods detailed in DS 7730.

PMV

The PMV is estimating a group's average comfort in a space based on seven factors: occupants' activity level, clothing insulation, air temperature, radiant temperature, air velocity, and water vapour pressure. It yields a value on a 7-point scale, where +3 signifies hot, -3 signifies cold, and 0 represents a neutral, balanced thermal state where the body's heat production equals heat loss. [20]

PPD

When the PMV has been determined, it allows for calculating the PPD. The PPD is an index that quantifies the proportion of people likely to feel thermally uncomfortable in a

given environment, representing all votes besides 0. The PPD can be a value between 5-100%, acknowledging that someone will always be dissatisfied with indoor environmental conditions due to the subjective nature of thermal comfort. [20]

$$PPD = 100 - 95 \cdot e^{-0.3353 \cdot PMV^4 - 0.2179 \cdot PMV^2} \quad (2.1)$$

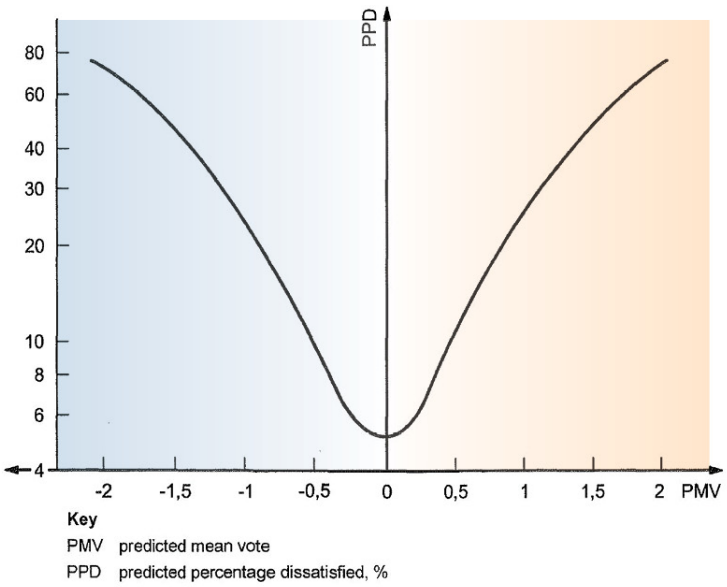

3	Hot
2	Warm
1	Slightly warm
0	Neutral
-1	Slightly cool
-2	Cool
-3	Cold

Figure 2.5: PPD as a function of PMV (right) and the seven-point thermal sensation scale (left).[20]

Mean radiant temperature

According to DS 7726, the mean radiant temperature can be defined as *"the uniform temperature of an imaginary enclosure in which radiant heat transfer from the human body is equal to the radiant heat transfer in the actual non-uniform enclosure"*. When calculating the mean radiant temperature, the surface temperatures of the surrounding surfaces, and the angle factors in relation to the subject's position in the enclosure and the surrounding surfaces have to be considered. Furthermore, the reflectivity of the building materials can be disregarded due to their high emissivity. The mean radiant temperature can be calculated with the following equation:

$$\overline{T}_r{}^4 = T_1{}^4 \cdot F_{p\text{-}1} + T_2{}^4 \cdot F_{p\text{-}2} + ...T_N{}^4 \cdot F_{p\text{-}N} \quad (2.2)$$

Where
$\overline{T}_r$ is the mean radiant temperature [K]
T_N is the surface temperature of surface N [K]
$F_{p\text{-}N}$ is the angle factor between a person and surface N [-]
[19]

When determining the angle factors, the position of the occupant (standing or sitting) is considered, along with the assessment of the positions of relevant surfaces being horizontal or vertical.

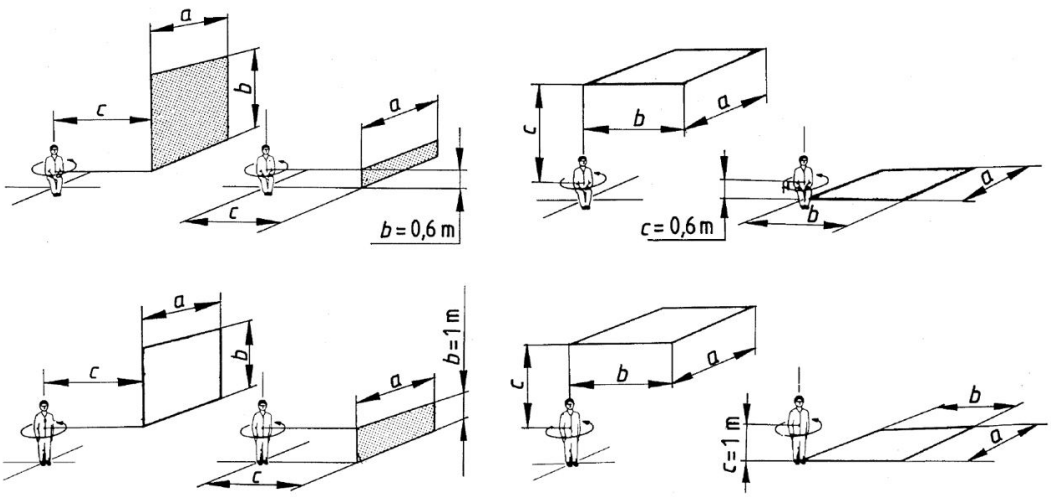

Figure 2.6: Illustration for determining the angle factors considering the position of the occupant in relation to the surrounding surfaces.[19]

The determination of angle factors can be calculated with the following equation:

$$Anglefactor = F_{\max} \cdot (1 - e^{-(a/c)/\tau}) \cdot (1 - e^{-(b/c)/\gamma}) \tag{2.3}$$

Where

$$\tau = A + B \cdot (a/c) \tag{2.4}$$

$$\gamma = C + D \cdot (b/c) + E \cdot (a/c) \tag{2.5}$$

[19]

For solving the equation, the dimensions of the relevant surfaces of the enclosure are indicated by the lowercase letters (a, b, c); and the capital letters (A-F) demonstrate standard values (see Figure 2.7) regarding the occupant's position.

	$F_{\max}$	A	B	C	D	E
SEATED PERSON, figure B.2 Vertical surfaces: Wall, Window	0,118	1,216	0,169	0,717	0,087	0,052
SEATED PERSON, figure B.3 Horizontal surfaces: Floor, Ceiling	0,116	1,396	0,130	0,951	0,080	0,055
STANDING PERSON, figure B.4 Vertical surfaces: Wall, Window	0,120	1,242	0,167	0,616	0,082	0,051
STANDING PERSON, figure B.5 Horizontal surfaces: Floor, Ceiling	0,116	1,595	0,128	1,226	0,046	0,044

Figure 2.7: Standard values for calculating the angle factors.[19]

PMV and PPD calculation inputs:

The calculations PMV and PPD are conducted for individuals who are either sitting or standing in three specific locations within a room: the North pole, Middle pole, and South pole. These calculations are performed for the occupancy hours spanning from 8:00 to 15:00 over the measurement time: summer 6 days, intermediate 4 days, and winter 3 days.

For PMV calculations, standard DS values are used for classroom analysis: 1.2 met for activity level, 0.5 clo for summer clothing insulation, and 1 clo for intermediate and winter.

K-type thermocouples are utilised to determine the air temperature. Air velocities are measured using an anemometer, with both instruments providing running five-minute average data. For a person sitting, the readings from the first three thermocouples and anemometers at ground level (0.1m, 0.6m, 1.1m) are used to calculate an average. In the case of a standing person, the readings include an additional measurement taken at 1.7m above ground level to account for their height.

The MRT is calculated for all six positions (North pole: Sitting and Standing, Middle pole: Sitting and Standing, South pole: Sitting and Standing.) according to the five minute running averages of the measured surface temperatures in the Test room and the angle factor calculation displayed in Appendix 9.6.

The partial water vapour pressure (P) is derived from the IC-meter's RH readings in the Test room every five minutes. The gaps are filled using the last known value to ensure minute-by-minute data. The P is calculated from measured air temperature (t_{air}) and RH of the room with the equation:

$$P = RH \times 10 \times \exp\left(16.6536 - \frac{4030.183}{t_{\text{air}} + 235)}\right) \tag{2.6}$$

[19]

2.1.2 Local thermal comfort

The parameter values for assessing thermal local discomfort, as shown in DS 17772 and DS 7730, which are utilized for the analysis in both cooling and heating seasons, are presented in Figure 2.8.

IEQ	Draught	Vertical air temperture difference (heand-ankle)		Range of floor temperature		Radiant temperature asymmetry				
Category	DR, %	PD, %	Temp. Diference, °C	PD, %	Floor surface tempertaure range, °C	PD, %	Warm ceiling, °C	Cool wall, °C	Cool ceiling, °C	Warm wall, °C
I / A	10	3	2	10	19 - 29	5	< 5	< 10	< 14	< 23
II / B	20	5	3	10	19 - 29	5	< 5	< 10	< 14	< 23
III / C	30	10	4	15	17 - 31	10	< 7	< 13	< 18	< 35

Figure 2.8: Local discomfort design parameters according to the categories of indoor environmental quality. [18]

Radiant temperature asymmetry
The temperature of other surfaces, including walls and the ceiling of an enclosure can influence the thermal comfort of the occupant due to the radiant temperature asymmetry between the opposite surfaces. The most dominant factors are the warm ceiling and cold walls/windows as humans tend to be more sensitive to the temperatures of these surfaces. The equations for determining the PD due to the temperature of the different surfaces are the following:

- Warm ceiling, when the Δt_{pr} is less than 23°C:

$$PD = \frac{100}{1 + exp \cdot (2.84 - 0.174 \cdot \Delta t_{pr})} - 5.5 \tag{2.7}$$

- Cool wall, when the Δt_{pr} is less than 15°C:

$$PD = \frac{100}{1 + exp \cdot (6.61 - 0.345 \cdot \Delta t_{pr})} \tag{2.8}$$

- Cool ceiling, when the Δt_{pr} is less than 15°C:

$$PD = \frac{100}{1 + exp \cdot (9.93 - 0.50 \cdot \Delta t_{pr})} \tag{2.9}$$

- Warm wall, when the Δt_{pr} is less than 35°C:

$$PD = \frac{100}{1 + exp \cdot (3.72 - 0.052 \cdot \Delta t_{pr})} - 3.5 \tag{2.10}$$

[20]

The categorization of thermal comfort regarding the horizontal temperature gradient created by the surface temperatures of different surfaces is displayed in Figure 2.8.

Radiant temperature asymmetry estimation in the Test Room:

The radiant temperature asymmetry (RTA) is determined for both sitting and standing positions for a central, Northern, and Southern location in the Test Room within the occupied hours.

The surface temperatures are obtained via centrally placed K-type thermocouples glued with thermopaste to the following surfaces: floor, ceiling, walls (East, West, North, South), and windows (East, West). For the South facade, the weighted average of the South wall, East window and West window is implemented in the calculations. The recorded data is converted into five-minute running averages.

The plane radiant temperature for each surface is calculated by the multiplication of the surface temperatures with the relevant angle factors. The calculation of angle factors are displayed in Appendix 9.6. Lastly, the RTA is determined by calculating the difference in plane radiant temperatures of the opposing surfaces: North-South, West-East, and floor-ceiling.

Warm and cool floors
Local discomfort of the feet due to the surface temperature of the floor can be expressed as the function of the PD. To calculate the PD, the following equation is used:

$$PD = 100 - 94 \cdot exp \cdot (-1.387 + 0.118 \cdot t_f - 0.0025 \cdot {t_f}^2) \tag{2.11}$$

Where
t_f is the floor temperature [°C] [20]

The thermal comfort categories defined by DS 7730, regarding the surface temperature of the floors are displayed in Figure 2.8.

Floor surface temperature estimation in the Test Room:

The floor surface temperature is measured in the Test Room by a centrally placed K-type thermocouple glued to the floor surface by thermopaste, and secured with tape and silver foil. The recorded data is treated for analysis as five-minute running averages, and only considering the occupied period for the categorization according to DS 7730.

Vertical air temperature difference
Discomfort occurs when a vertical air temperature gradient can be detected between the head and ankles. The PD as the function of vertical air temperature difference is calculated according to the following equation:

$$PD = \frac{100}{1 + exp \cdot (5.76 - 0.856 \cdot \Delta t_{a,v})} \tag{2.12}$$

Where
$\Delta t_{a,v}$ is the vertical air temperature difference [°C][20]

The equation applies when the vertical air temperature difference is less than 8°C.

To categorize the thermal comfort regarding the local discomfort due to vertical air temperature gradient, Figure 2.8 displays the temperature differences measured at ankle level (0.1m) and at head level of a sitting person (1.1m).

Vertical air temperature difference estimation in the Test Room:

The vertical air temperature difference between a sitting person's head (1.1m) and ankle (0.1m) is evaluated within the occupied period for three positions in the room: North, Middle, and South poles. For each position, the data is obtained from the measurement campaigns conducted in a summer week, an intermediate week and a winter week via K-type thermocouples located at the relevant heights. For the analysis, the data is treated as five-minute running averages. The results are acquired by calculating the differences between the temperatures recorded at 0.1m and 1.1m heights, and categorized according to DS 7730.

Draught rate
Draught is one of the most common thermal local discomfort factors, which occurs when unwanted cooling or heating of a body part is caused by air movement in the room. From draught, most affected are occupants in light sedentary activity (> 1.2 met). The Draught Rate (DR) can be estimated by the number of People Dissatisfied (PD) due to the drought in %. [20]

$$DR = (34 - t_{a,l}) \cdot (\overline{v}_{a,l} - 0.05)^{0.62} \cdot (0.37 \cdot \overline{v}_{a,l} \cdot Tu + 3.14) \tag{2.13}$$

Where
$t_{a,l}$ is the local air temperature in °C
$\overline{v}_{a,l}$ is the local mean air velocity in m/s
Tu is the local turbulence intensity in %
[20]

The local turbulence intensity varies from 10-60% (if unknown, 40% must be used) and can be found in Danish standard graphs, or if more accurate values are needed, the matter can be calculated.

$$Tu = 100 \cdot \frac{SD}{v_a} \tag{2.14}$$

Where
SD is the standard deviation of air velocity in the m/s measurement period by three minutes

There are no requirements for minimum local air velocities. However, the maximum is recommended not to exceed 0.15m/s in sedentary activity. To be within the three thermal comfort environment categories, the draught rate must be lower than 30% see Figure 2.8. [20]

Draught rate estimation in the Test Room:

The Draught Rate (DR) in the Test room is calculated according to the DS 7730 standard using local air temperature, velocity, and turbulence intensity data at the North, Middle, and South pole positions at 0.1m, 0.6m, 1.1m, and 1.7m height from the ground for every minute. The temperature data is sourced from the thermocouples, while velocity and turbulence intensity are measured using anemometers. Both sensors are placed at the exact locations, and the data is treated to show running five-minute averages.

2.2 Limitations

Experimental measurement duration
Due to time constraints, the summer data for the Test room was obtained from earlier research. However, it is essential to note that the duration of data collection varied across different cases. While the initial goal was to gather at least 7 full days of data, this was not achievable in both the intermediate and winter heating season measurements. This limitation was due to the computers running the measurements shutting off unexpectedly because of software updates that could not be disabled. Additionally, the WindowMaster was deactivated during the rest of the winter measurement period. These unexpected issues impacted the consistency and continuity of data collection.

Indoor environmental analysis
An analysis such as thermal comfort must be carefully considered as the DS guided recommendations are designed for adults rather than children. The IEQ analysis reveals critical data, highlighting that the settings in the Test room do not account for breaks between classes, lunch breaks, students opening the doors, or occasional exits. Regarding PMV and PPD of the global comfort, it is important to note that based on the activity level's standard input, this general classification provides a rough estimation and carries a significant risk of error in the resulting calculations [21].

Analysing aspects such as the floor surface temperature may be less critical if the occupants wear shoes. Furthermore, it is important to note that the experimental room is situated on the 5th floor, directly beneath a heated room. This setup may not accurately represent the more common layout of typical classrooms in Denmark, usually located on the ground floor.

The standard DS 15251:2007, utilised in this research, has been withdrawn and updated to DS 16798-01:2019. However, this update has not changed the ranges and design parameters. Four heat emitters representing occupants in the Test Room necessitate a modification in the positioning of the south pole. To minimise interference from the thermal plume, the south pole is relocated closer to the wall, positioned at an offset of 0.2m from the wall instead of the 0.6m recommended in DS 7730. Additionally, it is essential to highlight that the heat emitters, simulating occupants, can only produce sensible heat, which restricts the scope of air quality analysis in the Test Room.

Data treatment

The heating and cooling modes are defined according to the window opening. The system is not set to log the bypass opening, which must bring the preheated air to the DCV plenum bow. The report assumes that the bypass opens at the same time the heating mode starts when only the bottom row windows are open. The missing data is treated differently, which is explained more in the *9.1 Thermal comfort*.

Chapter 3

Experimental setup

The experimental setup chapter includes a description of the Test room, its systems, and the instruments set up within the room. Subsequent subchapters explain the control of the WindowMaster, detailing how the system operates in both cooling and heating modes. Lastly, the validation of the equipment can be seen in Appendix 9.3, an essential factor to evaluate before beginning the data collection process.

3.1 The Test room

The measurements are set to be conducted in a room designed to mimic a small classroom located within the Indoor Environment and Energy Universal Facade laboratory on the 5th floor at AAU Build. The Test Room has dimensions of 2750mm (width) x 2905mm (length) x 2715mm (height), with a floor area of 8m^2 and a volume of 22m^3. The room has a floor, a roof/ceiling, three interior walls and a south-oriented double-skin facade.

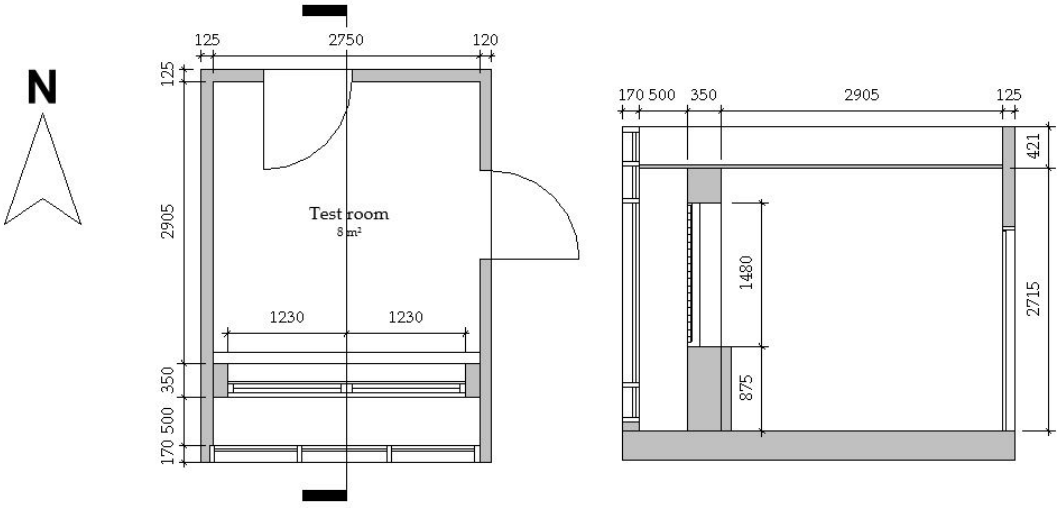

Figure 3.1: Floor plan (right) and a section (left) view of the Test Room.

People do not use all floor area and volume in the room. Therefore, when analysing IEQ, the room space is limited to the occupied zone. Which indicates the volume of air in the room used by the occupants determined by the distance from the inner surfaces of the room. The height from the floor of the occupied zone can vary depending on the seated or standing occupant position being analysed. Distances, according to DS 447 requirements,

are illustrated in Figure 3.2.

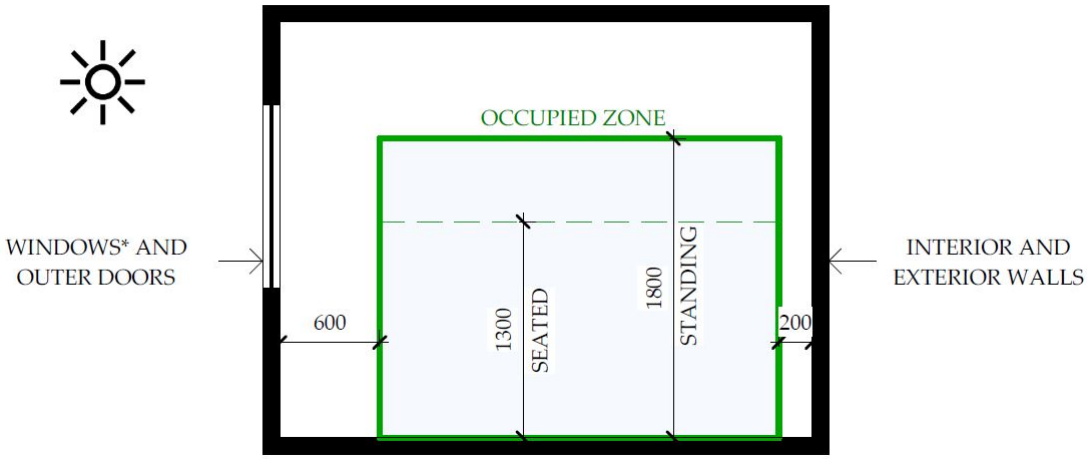

Figure 3.2: Definition of the occupied zone according to DS 447.
*Windows of 1500x800mm or larger size.

The interior facade is a heavy structure consisting of brick insulation and brick with a total U-value of 0.30W/m^{2}K. The wall has two fixed double-glazed windows of 1480x1230mm each, with a U-value of 1.6W/m^{2}K, a frame fraction of 0.88, a solar heat gain coefficient (g-value) of 0.63 and a light transmittance (LT value) of 0.80. [2]

The exterior facade has 12 double-glazed windows, of which 9 can be opened. The small window 380x930mm U-value is 1.53W/m^{2}K, and the frame faction is 0.63, while the big one, 1900x930mm, is 1.33W/m^{2}K and 0.83. Both windows have a g-value of 0.73 and an LT value of 0.84. [2]

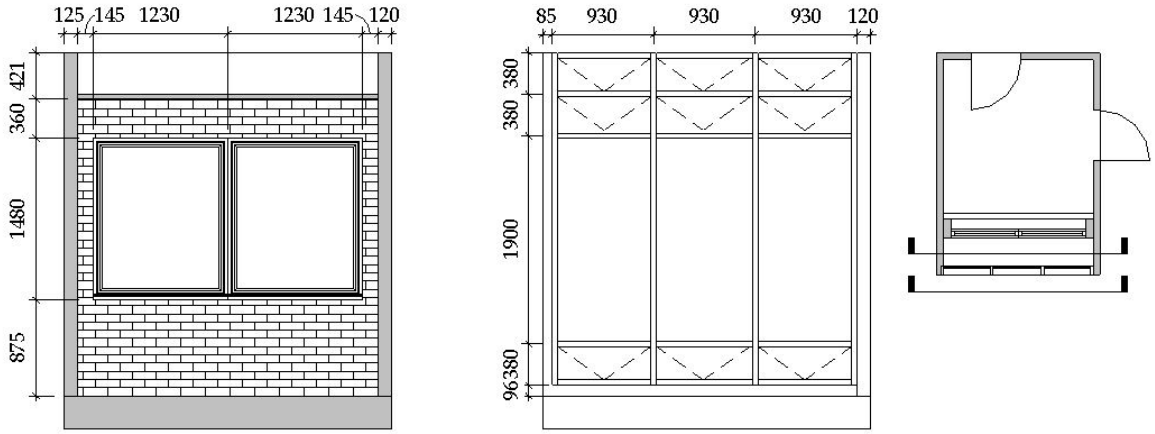

Figure 3.3: Interior (left) and exterior (middle) facades.

3.1.1 Systems in the Test room

Space heating
An electrical space heater, model EWT E2TS, is placed as a freestanding unit on feet in the Test Room beneath the east window (refer to Figure 3.4 and 3.6). This heater has a maximum power capacity of 2000W and features two operational settings: setting I, where the heater operates at half its heat output, and setting II, where it operates at full heat output. The thermostat comes with seven settings, including frost damage protection marked as *, I, II, III, IIII, IIIII, IIIIII. During the heating season measurements, the space heater is utilized—operating at full output with setting I for the intermediate case and setting II for the winter case.

Figure 3.4: Electric space heater location in the Test room .

Ventilation
The experimental room is equipped with a DCV system, which includes a plenum box. This box is a cavity within the ceiling, measuring 421mm thick. It is completely lined with cement-bonded wood wool panels, each measuring 600mm in width, 1200mm in length, and 35mm in height. Air is mechanically extracted from the room through an opening at the floor level on the interior north wall.

Occupancy and internal heat load
In the Test room, four heat-emitting sources are installed to simulate the presence of four children and their equipment, operational from Monday to Friday between 8:00-16:00, mirroring a standard school day. Each "student" contributes an internal heat load of 100W, representing a sedentary activity level with a metabolic rate of 1.2 met and a clothing insulation of 1 clo. As per the guidelines from "Branchevejlednings for indeklima på skoler," it is assumed that a laptop accompanies each student, and the room includes a smartboard and a projector. The internal heat load assumptions for the Test room are detailed in Figure 3.5.

Heat source	Heat load
4 occupants	400W
4 laptops	40W
1 smartboard with projector	175W
Total	**615W**

Figure 3.5: Internal heat load in the Test room.

However, prior research [2] suggests this internal heat load may be overly optimistic, particularly when considering the ratio of the glazed area to the floor area and the designated space per student. As a result, the total internal heat load has been revised downward to 377W, as calculated and shown in 3.5.

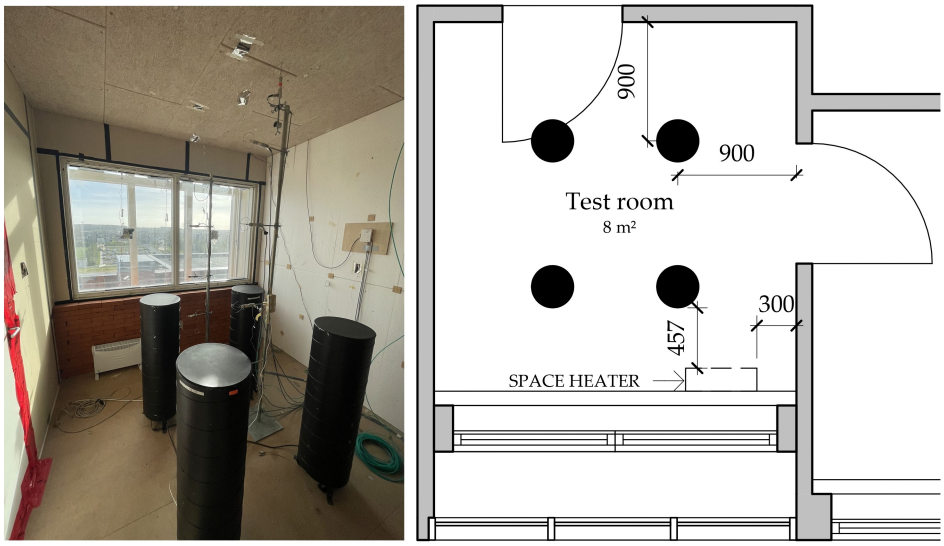

Figure 3.6: Placement of four heat emitters (occupants + equipment) and electric space heater in the Test room.

3.1.2 Set up of the instruments

Test room

Figure 3.7 presents a sectional view of the Test Room, highlighting three vertical steel structures termed the South, Middle, and North poles. These poles are equipped with sensors: thermocouples (K-type), coloured orange, and anemometers (Dantec), coloured blue, strategically placed at four heights significant for thermal comfort assessment for the occupants. At 0.1m, sensors capture conditions at ankle level; at 0.6m, they measure the centre of gravity of a seated person; at 1.1m, the head level of a seated person; and at 1.7m, the head level of a standing person. The South and North poles are positioned 200mm from the walls. The Middle pole is centrally located, placing it marginally closer to the southern heat sources. Additionally, on the Middle pole at a height of 1.1m, there is a (grey-coloured) thermocouple housed inside a grey table tennis ball, which is utilized to measure the operative temperature of the room.

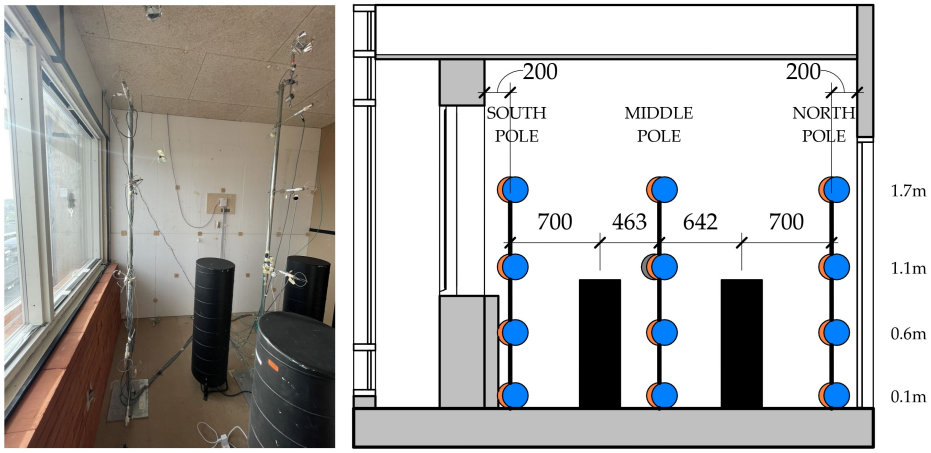

Figure 3.7: Air temeprture and velocity sensor locations in the Test room.

At the same spot where the thermocouple measures the room's operative temperature, an IC-meter device is positioned to record relative humidity data every 5 minutes, which is used for calculating the PMV.

Figure 3.8: In the Test Room, an IC-meter device is used to measure the relative humidity.

Surface temperatures of the walls, floor, and diffuse ceiling are measured to assess the potential for discomfort from radiant temperature asymmetry and floor temperature. These measurements also allow for calculating the room's mean radiant temperature. Thermocouples are attached to these surfaces using a thermally conductive paste and shielded with silver foil to guard against direct solar radiation.

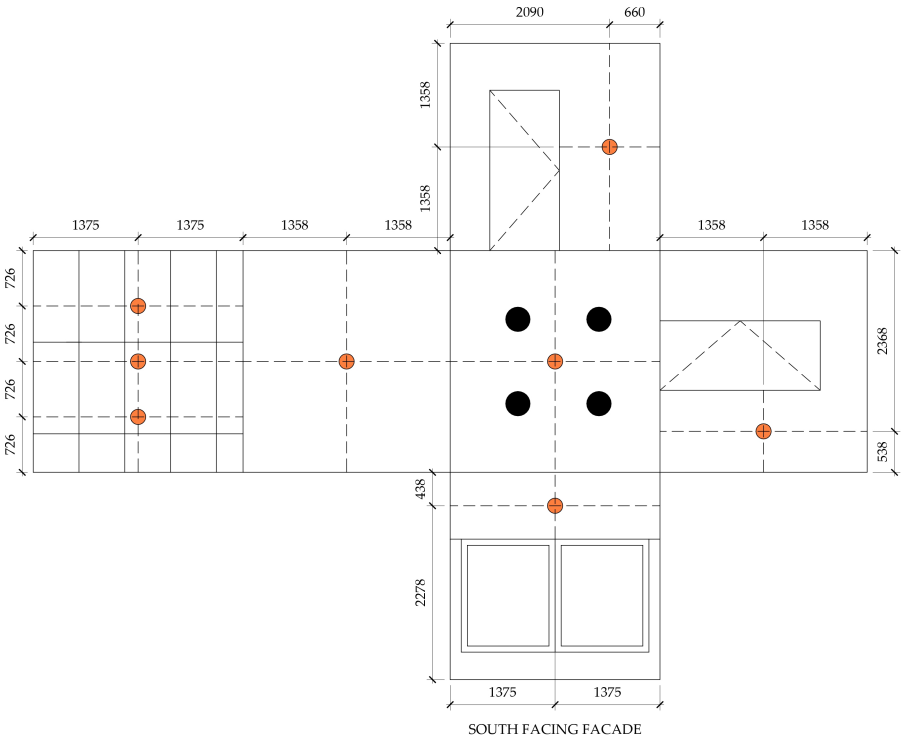

Figure 3.9: Test room surface temperature sensor locations.

Additionally, two thermocouples (to ensure accuracy in case of errors) are installed inside the exhaust diffuser to monitor the temperature of the air removed from the room.
The heater's energy use is tracked via a Power Detective device to quantify the energy needed to maintain set thermal comfort. This device, connected to the heater and power source, records consumption data in its 'energy consumption' mode during measurement periods.

DSF

Air temperature in the DSF cavity is monitored to determine the temperature gradient in heating and cooling modes using Type K thermocouples within ventilated silver tubes. These thermocouples are positioned within silver tubes that receive airflow from an electric mini fan, directing air downwards to avoid heat from the fan affecting the readings. The thermocouples are positioned to avoid contact with the tubes, ensuring accurate measurements. Installed along three vertical axes (West, Middle, and East lines), the tubes are set at heights from 0.265m to 2.410m. Figure 3.10 visualizes the arrangement of these air temperature thermocouples.

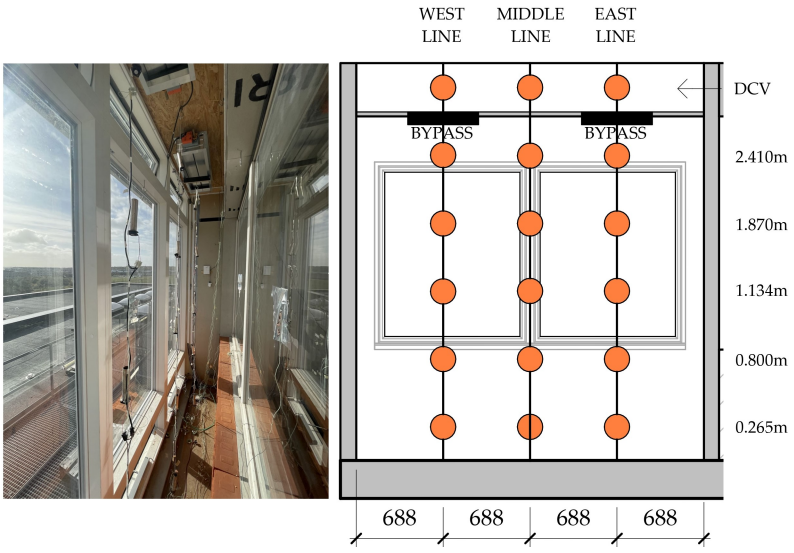

Figure 3.10: Air temperature sensor placement in the DSF cavity.

DCV

To analyse the supply air temperature and the air distribution within the DCV cavity, air temperatures are measured along two vertical lines—West and East—in the plenum box at distances of 1m, 2m, and 2.75m from the bypass opening. Thermocouples are suspended on fishing lines and shielded with silver foil on the South side to protect them from direct solar radiation.

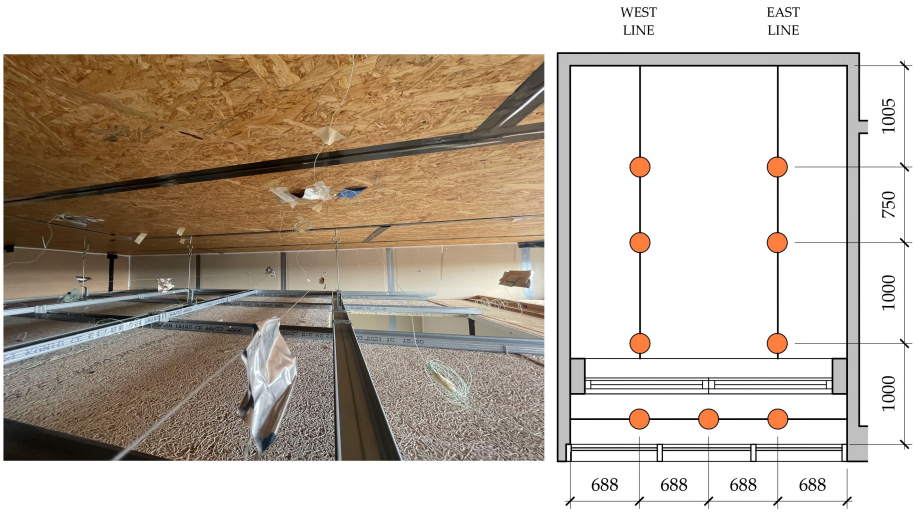

Figure 3.11: Placement of thermocouples within the DCV cavity.

Alongside the specified sensors, outdoor conditions are tracked by Aalborg University's weather station at Thomas Manns Vej 23, which is available for research at *www.vejrradar.dk/weatherstation/TMV23/*. This station provides minute-by-minute data, such as solar radiation and outdoor temperature, which is crucial for analysing the test room's control system performance.

3.2 Control strategy

The built I-DIFFER system in the Test room is equipped with demand-controlled ventilation, and the current control strategy is operating according to the measured data by the sensors (room temperature, CO_2 concentration) located in the room, and sensors measuring the outdoor conditions (outdoor temperature, precipitation, wind speed). There is a possibility for operating with diverse ventilation modes corresponding to the priorities concerning the indoor environmental qualities in the Test room, and the maximum window opening percentages can be defined accordingly. Moreover, due to extreme weather conditions, the closure of the windows is ensured; and a value for maximum temperature drop in the room can also be defined to achieve the closed position in case of low temperatures.

The following ventilation modes are possible with the currently applied control strategy:

- **Fresh air (morning ventilation):** Utilized before occupancy begins to ensure fresh air.
- **Night cooling:** Implemented outside of occupancy (during nights) to cool the room down in order to avoid overheating the following day.
- **Pulse ventilation:** Short period of the window opening, followed by immediate closing to provide the minimum air exchange rate.
- **Temperature-controlled natural ventilation:** The window openings are regulated according to the outdoor temperature, and CO_2 concentration and temperature in the room.
- **Gap ventilation:** The windows are opened for a longer interval due to the outdoor conditions, and CO_2 concentration and temperature in the room, while a continuous air exchange rate is ensured.
- **Manual operation:** The manual override of the window openings by the occupants, after 30 minutes the automatic control resets.

Two control modes are differentiated in the strategy, corresponding to the cooling or heating requirements in the room. The operation of both control strategies is described in the following sections.

3.2.1 Cooling mode

When the cooling mode is activated, all the facade openings are fully opened. The DSF cavity is ventilated as the outside air enters the cavity from the bottom row openings, and due to thermal buoyancy, the warm air leaves the cavity through the middle row openings. Therefore, the excess heat is removed from the DSF cavity, which provides a cooling effect for the test room.

The partition between the DSF and DCV cavities is closed off during the cooling mode. The top row openings of the facade are open, therefore, the outside air directly enters the plenum box, and the fresh cool air is supplied to the test room through the diffuse ceiling. The flow of air is enhanced by mechanical extraction from the Test room, through a diffuser

placed at floor level.

The following ventilation modes are possible during the cooling mode: fresh air (morning ventilation), night cooling, pulse ventilation, temperature-controlled natural ventilation, gap ventilation, and manual operation.

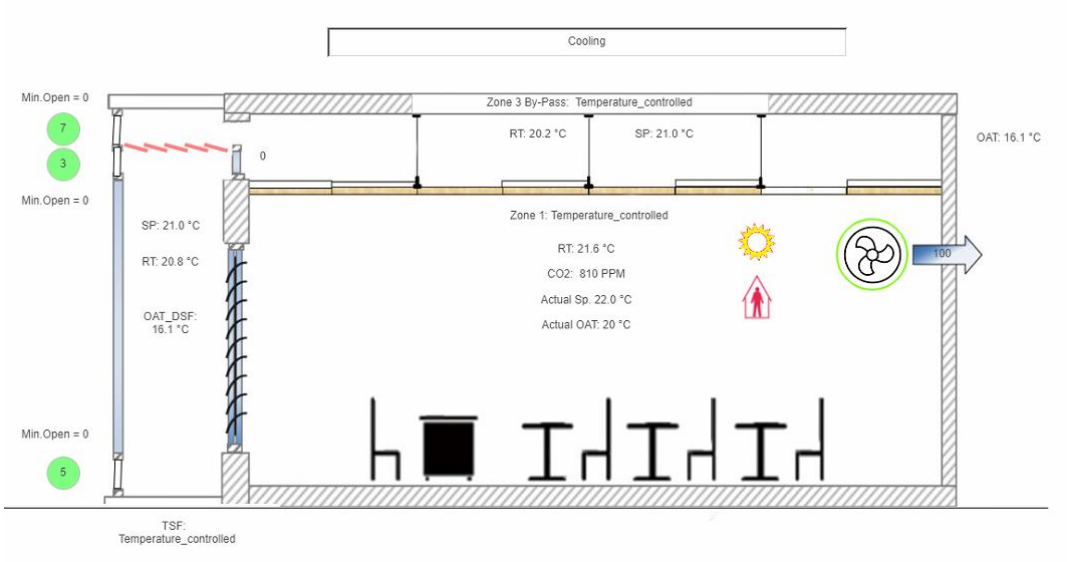

Figure 3.12: Example of cooling mode on 10.10.2023 - WindowMaster.

Figure 3.13: The separation between the DSF cavity and plenum box is closed during the cooling mode.

3.2.2 Heating mode

The principle of the heating mode is to ensure that the supply air is heated up in the DSF cavity before entering the plenum box and the test room. During this mode, the bottom row openings of the DSF cavity are open, while the middle and top row openings are closed. The separation between the DSF cavity and the plenum box is opened. Therefore, the supply air enters the DSF cavity from the bottom, flows upwards in the DSF cavity, enters the plenum box, and flows through the diffuse ceiling toward the Test room. The airflow is ensured by thermal buoyancy in the DSF cavity, and mechanical ventilation in the form of extraction through a diffuser at floor level in the Test room.

The following ventilation modes are possible during the heating mode: fresh air (morning ventilation), pulse ventilation, gap ventilation, and manual operation.

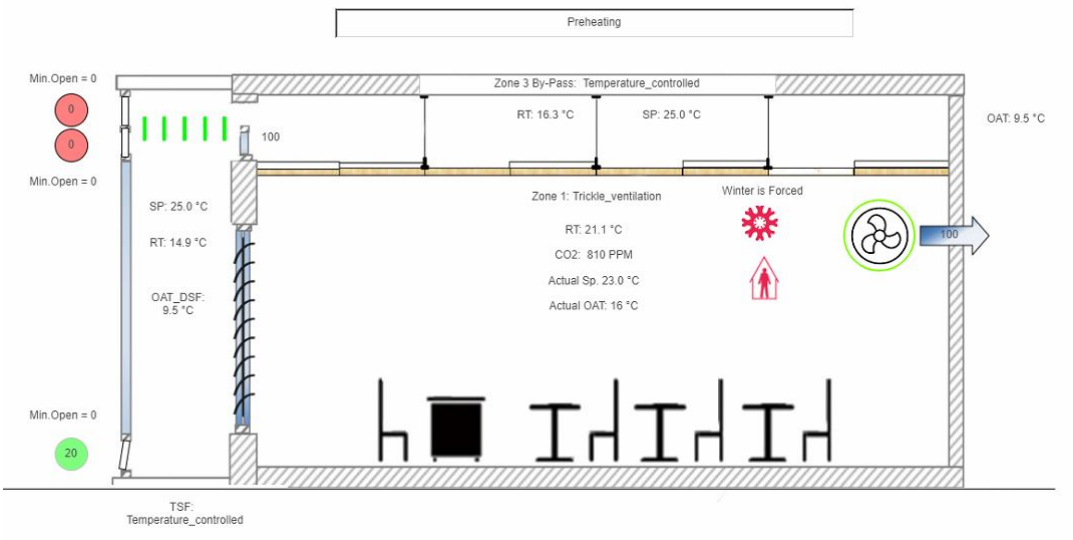

Figure 3.14: Example of heating mode on 19.10.2023 - WindowMaster.

Figure 3.15: The separation between the DSF cavity and plenum box is open during the heating mode.

Chapter 4

Control strategy - Cooling mode

In this chapter, the cooling mode of the control strategy is investigated during the summer measurement period, concerning its efficiency, its influence on the temperature distribution in the DSF and DCV cavities, and its relation with the operation of the building systems.

4.1 Summer case

The cooling control was prevailing during the measurement period, however, the heating mode activated on the second, third, and fourth days. The temperature-controlled natural ventilation mode and the night cooling ventilation mode defined the cooling mode. The heating mode operated with the gap and pulse ventilation modes.

4.1.1 Overview

Window openings
During the observation period, the behaviour of the bottom, middle, and top row windows is analysed see Figure 4.2. Window 1, among the bottom set, was open 98.6% of the time, up to 50% more frequently than Windows 2 and 3. However, there were occasions, accounting for 1.4% of the time, when Windows 2 and 3 opened more frequently, surpassing Window 1 by up to 7%.

Similarly, for the middle windows, Window 4 was open 97.8% of the time, outperforming Windows 5 and 6 by up to 8%. However, in 2.2% of instances, Windows 5 and 6 opened more than Window 4, by as much as 6%.

The data reveals a consistent pattern of individual windows in each row (Window 1 in the bottom and Window 4 in the middle) registering a higher percentage of window opening than those under shared control. Additionally, the logs indicate that Windows 1 and 4 typically respond about one minute faster response than the other windows.

Windows 1-6 generally opened first and closed earlier than the top windows (7-9). The top windows (7-9) tended to stay open for extended periods, often overnight, indicating their role in continuous ventilation or cooling.

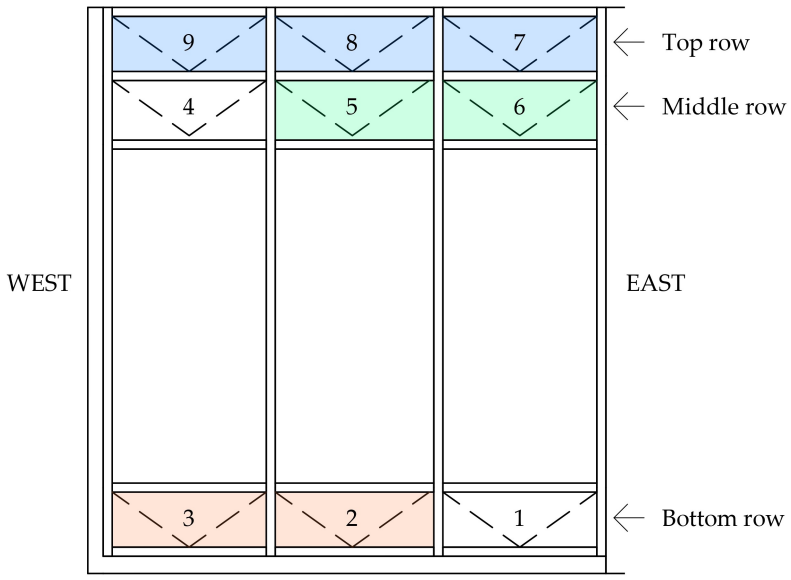

Figure 4.1: Windows 2-3, 5-6, and 7-9 are automatically controlled together through the WindowMaster system on the exterior DSF.

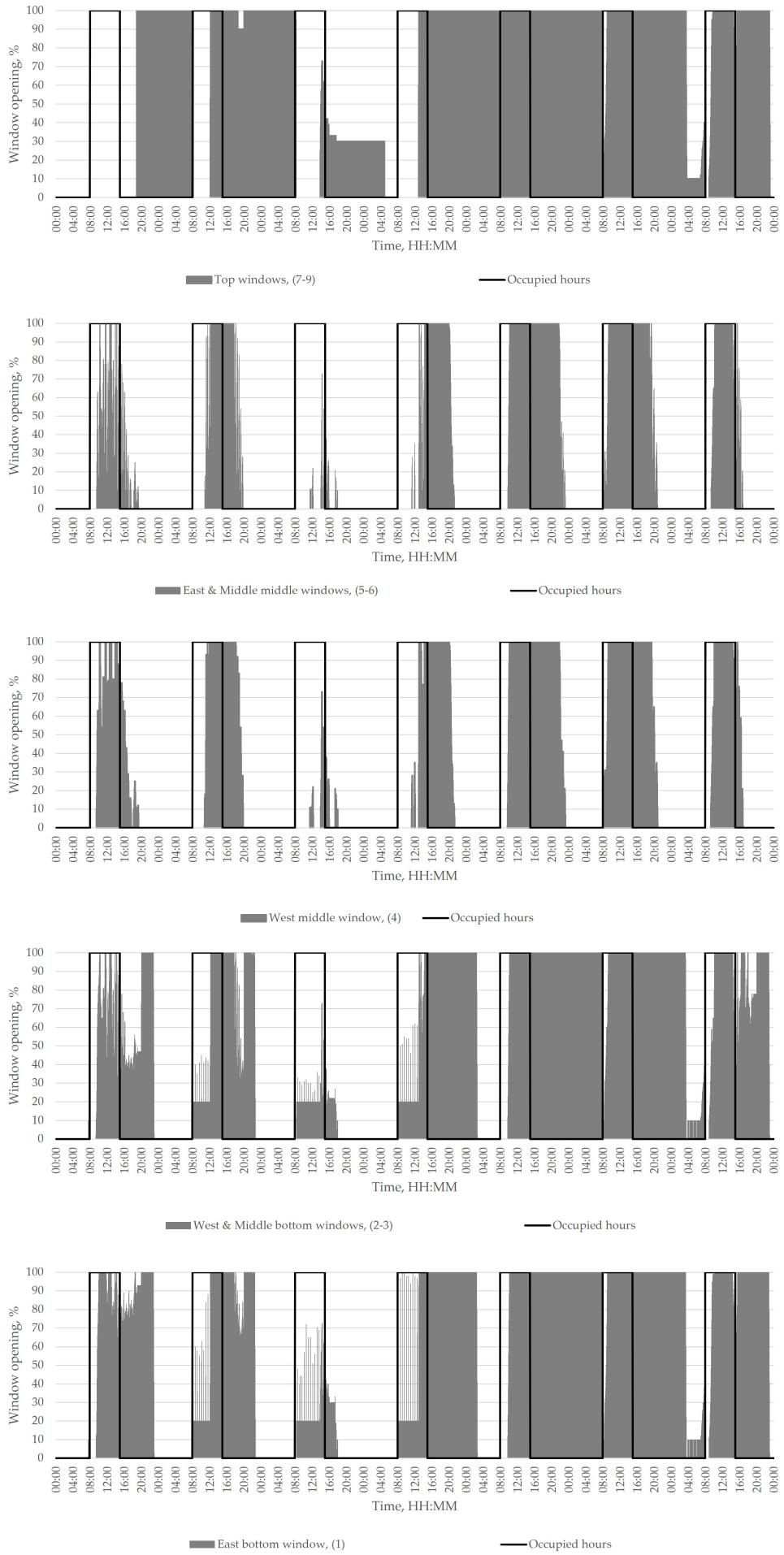

Figure 4.2: Window openings during the summer measurements in the Test room. (24-30.07.2023)

Outdoor weather conditions

The outdoor air temperature fluctuates from night to early morning, dropping to 9.6°C and then increasing during the day to as high as 23.4°C. The coldest day during the occupied hours was the 3rd measurement day, with an average temperature of 15.4°C, while the warmest was the 6th day, with an average air temperature of 20.0°C.

The solar radiation data points are most densely distributed around midday when the sun's intensity is at its peak, and become sparse during the early and late hours of the day. However, throughout all measured summer days, solar radiation is consistently present, ranging from a minimum of 931 minutes to a maximum of 993 minutes of sunlight. The outdoor temperatures and solar radiation is presented in figure below.

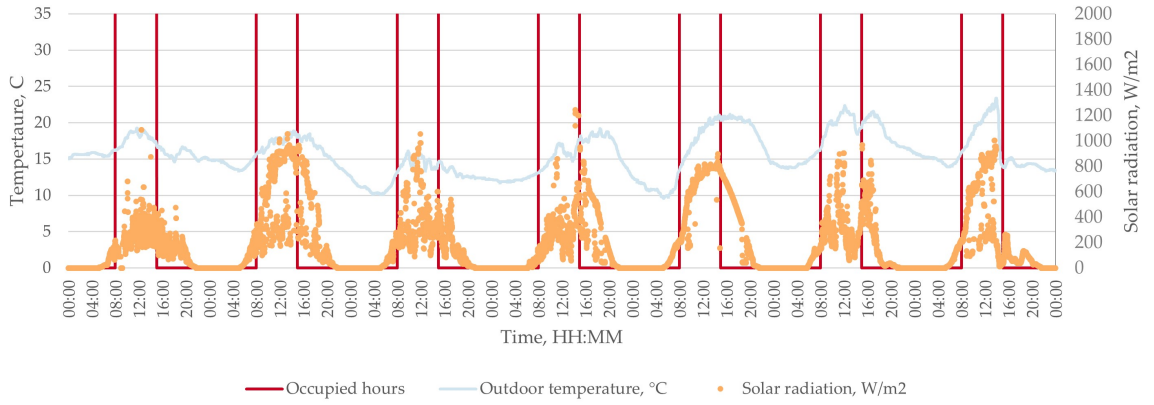

DAY	Outdoor air temperature, °C 24h				Solar radiadio, W/m² 24h		
	MIN	AVE	MAX	Std	AVE	MAX	SUNLIGHT, Minutes
1	14.6	16.3	19.3	1.2	126	1088	973
2	12.7	15.8	18.9	1.7	250	1088	993
3	10.1	12.8	16.1	1.5	163	1055	962
4	11.8	14.9	19.2	2.4	176	1245	934
5	9.6	16.1	21.2	4.1	291	898	980
6	13.7	17.6	22.4	2.7	161	969	931
7	13.4	15.9	23.4	2.7	166	1002	977

Figure 4.3: The outdoor air temperature and solar radiation during the summer measurements. (24-30.07.2023)

The overall control of the WindowMaster system is significantly influenced by wind speed due to its limitations in adverse weather conditions, which pose a risk of damage to the windows. However, the WindowMaster did not log the collected wind speed data from the Wind/Rain sensor (WLA 330) during the summer measurement period. Consequently, Figure 4.4 displays data from the AAU Built weather stations. From the heating mode measurement, it was observed that the weather station logs higher wind speeds than the WindowMaster, which is expected due to the sensor's different location/environment. Therefore, the figure is referenced to understand the outdoor conditions, considering that the actual wind speed for the DSF windows is somewhat lower.

Window opening patterns are notably more dynamic during the first three days, coinciding with higher wind speeds. The most significant speed was recorded on the third day,

surpassing 10m/s (classified as a fresh breeze, see Appendix 9.21). On this particular day, the top windows (7-9) closed early in the occupied hours (8:05) and reopened later at 13:54. Their subsequent openings were variable but consistently below 70%, which is less than the usual 100% seen on other days. The middle and bottom rows of windows were the least open on the third day, indicating that window control is likely influenced by wind speed constraints.

On the second day of measurements, the wind speed approached 7m/s. Despite this, the windows did not begin to close, suggesting that the WindowMaster system responds to wind speeds higher than 7m/s, as recorded by the university weather station.

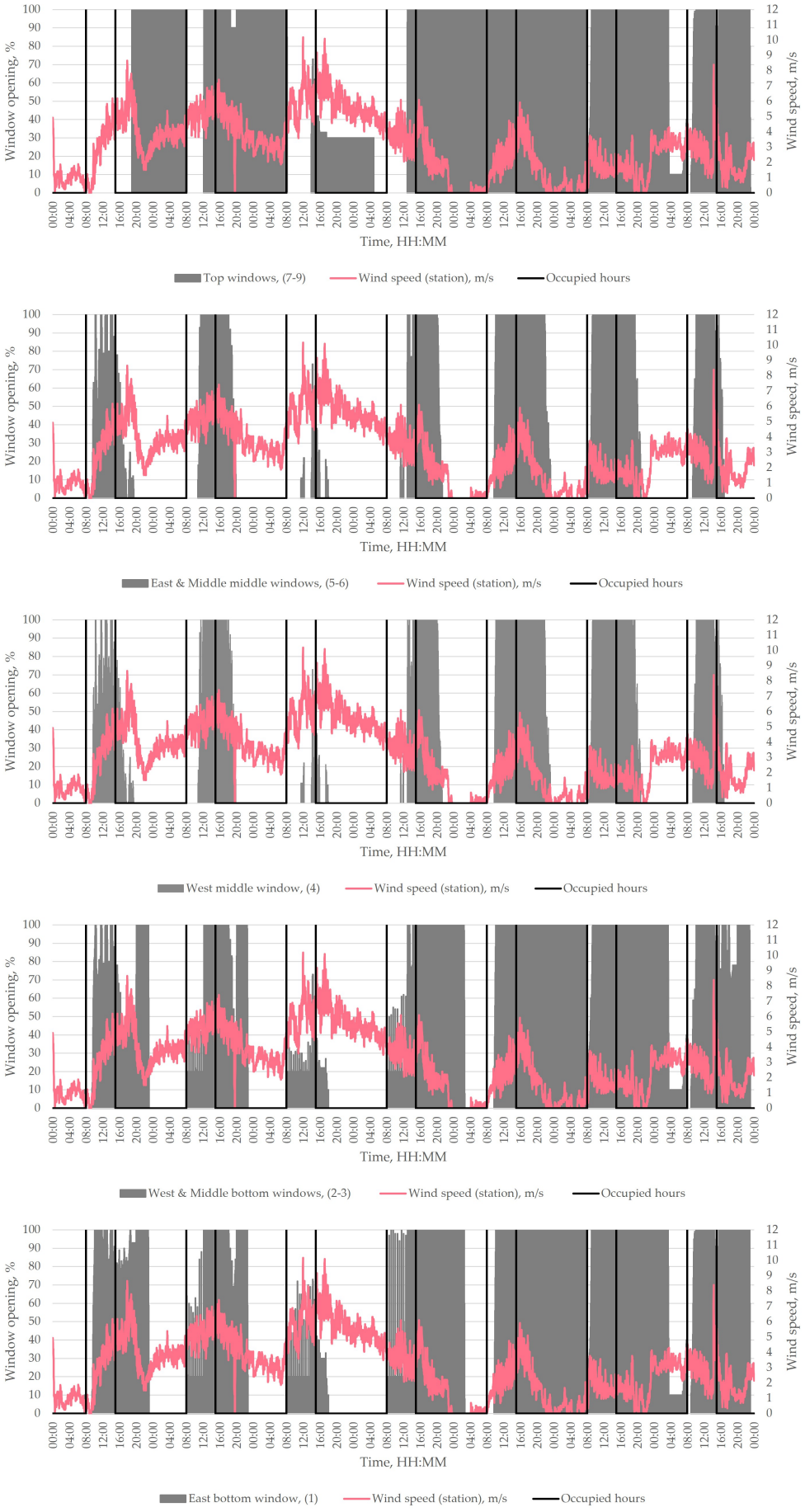

Figure 4.4: Window openings during the summer measurement week with regards to windspeed data from Weather station (AAU Built). (24-30.07.2023)

WindowMaster setpoints
The WindowMaster setpoints for the DSF, DCV cavities, and the Test Room are set according to the cooling mode control, as seen in Figure 4.5.

Figure 4.5 also indicates on the x-axis the operational mode of the system at any given time through colour coding: non-active (no mode) is grey, the heating mode is red, and the cooling mode is blue. The mode of operation is further apparent from the positions of the window openings. In cooling mode, the system focuses on the interaction between the bottom windows (1-3) and the middle top windows (4-6). This arrangement is designed to cool the DSF cavity, consequently lowering the indoor temperature of the Test Room. Simultaneously, the top windows (7-9) introduce outdoor air directly into the DCV cavity. Closed bypass openings are strategically utilized throughout the cooling process for two main purposes: directly supplying air to the DCV and assisting in cooling both the DSF cavity and the Test Room. When no mode is selected and all operable windows are closed, the room remains neutral - neither cooled nor heated. During the heating mode, fresh air enters through the bottom row of windows (1-3, the only ones open) and ascends through the DSF cavity. This air is then preheated and circulated to the room via the DCV cavity and the ceiling. The colour code reflects the variation in control mode throughout the day.

On the first day, the system activated cooling mode at 9:23 as the Test Room's air temperature surpassed the setpoint established in WindowMaster (23°C). After the day's peak, the DSF cavity's cooling windows closed once the temperature fell below the setpoint (21°C). Meanwhile, the top row windows (7-9) remained fully open at 100%, indicating night cooling was maintained until the next day's occupancy hours.

On the second day, the system switched from cooling to heating mode just a minute before the top windows closed (8:05 – 10:47), then reverting to cooling mode for the remainder of the time. The shift to heating mode was triggered by the Test Room's temperature falling below the set point (23°C) and continued until the DSF cavity temperature, as detected by WindowMaster, exceeded the setpoint (25°C).

Days 3 and 4 have similar system performance. On Day 3 of the measurement, the system began with night cooling, which lasted until 8:06. At 8:07, the bottom row windows opened for two minutes, indicating a switch to heating mode. This was followed by a twelve-minute period where the system was in no mode, with all windows closed. At 8:20, the bottom windows opened again, resuming heating mode, which continued until 11:26. Then, the middle row windows opened to cool the temperature in the DSF cavity. This cycle of heating and cooling occurred several times over a short duration.

At the beginning of the 4 day, the system was in cooling mode until 4:52. After that, it switched to no mode, with all windows closed. At exactly 8:00, the bottom row windows opened, signalling the start of heating mode. At this point, none of the setpoints in the system were being reached. The DSF cavity (25°C) at 11:12 was the first space to reach its setpoint. Two minutes later, the middle row windows opened to cool the DSF cavity. This phenomenon, where the DSF temperature fluctuated and exceeded the setpoint, occurred four more times in a short period, indicating that the system struggled to maintain the DSF setpoint. At 12:55, all windows were opened as all setpoints were exceeded. The first

middle row window closed at 23:48 when the DSF cavity air temperature dropped below the setpoint (21°C). These rapid transitions between heating and cooling modes were due to the DSF cavity temperatures briefly exceeding and falling below the set point. This indicates that the system is highly sensitive and capable of reacting within 1 minute to temperature changes. The rest of the time, the open top and middle row windows indicate continued cooling mode.

In the Test room, air temperatures at night are typically the highest, followed by those in the DSF and DCV cavities. Interestingly, the DCV cavity's temperature is consistently lower than the Test room's. Nevertheless, there are times when these temperatures intersect. For example, during occupancy hours, the DSF cavity's temperature often surpasses that of the Test room. This trend can extend beyond occupancy hours as well. The most notable instance was on the fifth measurement day when the DSF cavity's temperature soared to 34°C. This pattern further demonstrates that under certain conditions, the current control strategy faces challenges in effectively cooling and maintaining the air temperature within the DSF cavity.

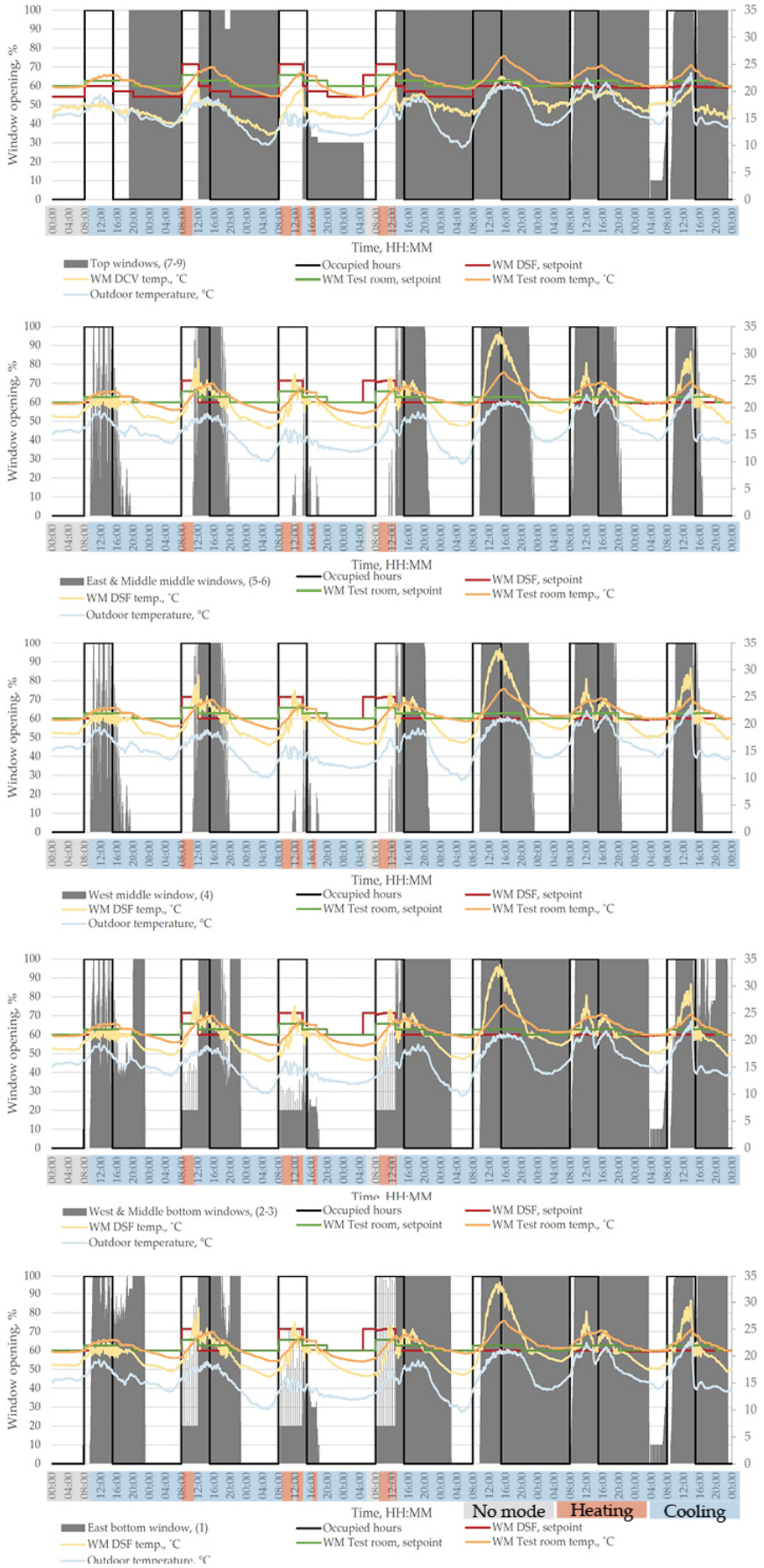

Figure 4.5: Window openings during the summer measurements in the Test room with indications of active control mode, WindowMaster setpoints, and different air temperatures. (24-30.07.2023)

4.1.2 DSF cavity

The temperature distribution in the DSF cavity is illustrated as a box-and-whiskers plot in Figure 4.6, where the boxes represent the lower and upper quartiles including 50% of the data, and the whiskers indicate the deviation outside of these quartiles. The outlier temperatures below and above the quartiles are indicated with dots. The measured air temperatures by each thermocouple include data for all hours between 24-30.07.2023.

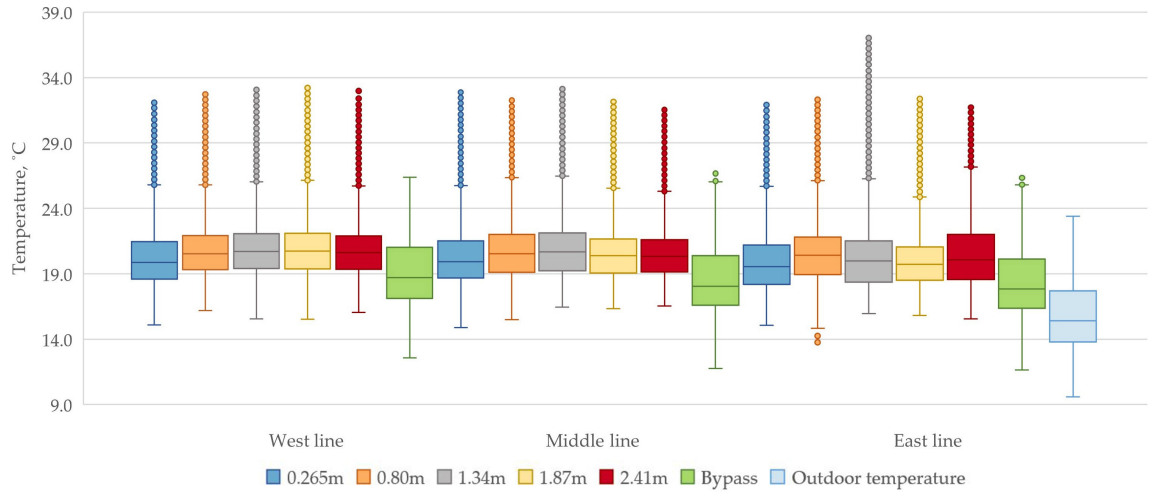

Figure 4.6: Whiskers-and-box plots of the measured temperatures in the DSF cavity for all hours. (24-30.07.2023)

The temperature distribution for the West and Middle lines followed the same tendency, as the lowest temperatures occurred near the bottom opening (0.265m) and at the middle opening (2.41m) of the cavity, while the centrally placed thermocouples (0.80m, 1.34m, 1.87m) showed higher temperatures. Therefore, the data represents the function of the prevailing cooling control mode as the outdoor air enters the cavity at the bottom and the heated-up air leaves the cavity at the top opening; however, the opened windows at the top influenced the temperatures measured by the thermocouples near it (2.41m).

For the East line, the temperature distribution was slightly different for the 3 upper thermocouples, as generally lower temperatures were present for the one located at 1.34m, while the thermocouple at 2.41m height showed the highest temperatures. Figure 4.7 illustrates this matter with regard to the relevant window openings, from which it can be obtained that the higher temperatures for the East line thermocouple at 2.41m occurred due to the small opening percentage of the middle windows (first day 10:30-16:00) and the closed state of the middle windows (from 20:00 on the sixth day until 4:00 on the seventh day). For the thermocouple located at 1.34m, the lower temperatures occurred during the closed state of the middle windows. However, when the middle windows opened, the measured temperatures of this thermocouple exceeded the temperatures of the other thermocouples in the DSF cavity, reaching the highest peak with a maximum of 37.2°C on the fifth day at 13:52.

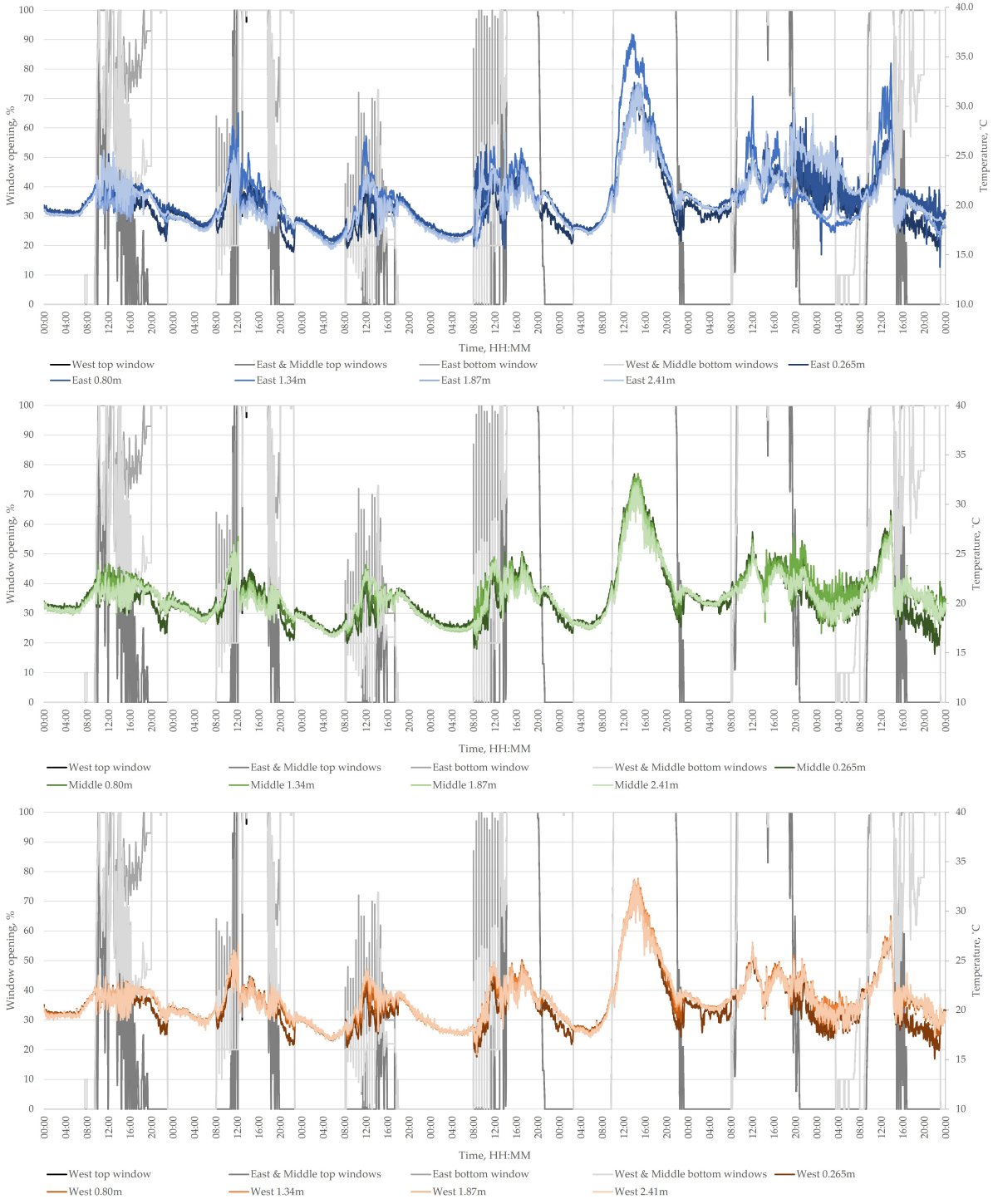

Figure 4.7: Window openings and temperature distribution in the DSF cavity for all hours. (24-30.07.2023)

Furthermore, critically high temperatures (above 30°C) had been occurring in the entire DSF cavity on the fifth day, while the opened state of all the windows was at 100%, indicating the limitations of the system and the need for improvement of the cooling strategy.

Since the separation between the DSF and DCV cavity was mainly closed, the top row windows were open, providing fresh air which was further distributed into the DCV cavity and Test room. Therefore, the lowest temperatures were measured by the thermocouples at the bypass, located right next to the opened windows (see Figure 4.8).

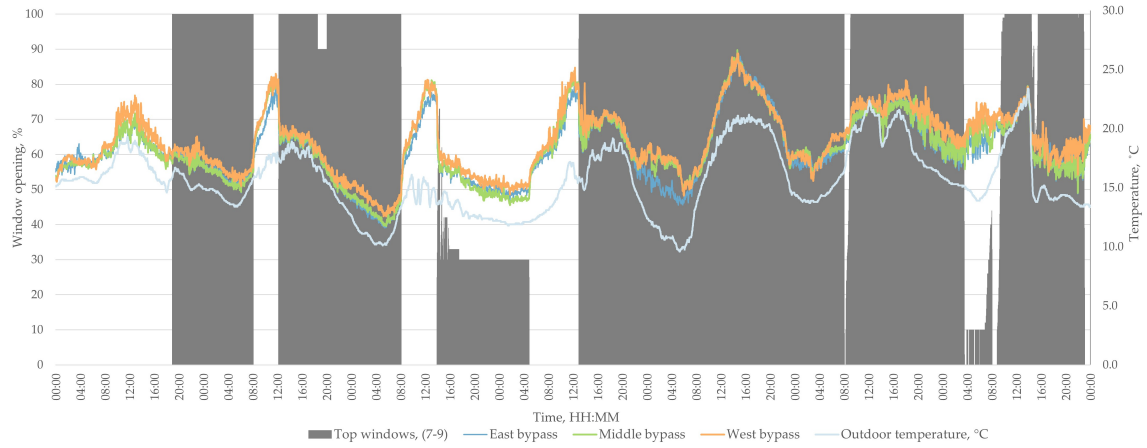

Figure 4.8: Window openings and temperature distribution in the bypass area for all hours. (24-30.07.2023)

Evidently, all three thermocouples displayed similar temperatures, that were highly dependent on the outdoor temperature when the windows were open. Moreover, during the opened window state, the thermocouples measured slightly higher temperatures than the outdoor temperature measured by the weather station, which indicates the preheating of the air when it enters the cavity. Most of the measurement days indicated effective cooling, although an exception of this is visible on the fifth day, as the temperature difference between the cavity and the outdoor temperature increased during the occupancy, while a reduction began only when the occupancy period ended and the solar radiation started to decrease. In addition, it is significant to note that during the summer measurement week, the three thermocouples located at the bypass inside the silver tubes were not equipped with minifans. Therefore, the lack of airflow (same amount as for the ones in the DSF cavity at 0.265-2.41m) through the silver tubes might have influenced the measured data, resulting in higher temperatures.

When the temperature distribution is analysed in relation to the outdoor temperature, the thermocouples at the bottom and middle opening of the DSF cavity are included, as well as the thermocouple located next to the top opening. Generally, the measured air temperatures in the cavity were always higher than the outdoor temperature. The lowest temperatures occurred at the top opening during the unoccupied hours, where a linear increase in the cavity temperature can be observed as the outdoor temperature increased. This indicates the cooling effectiveness of the system, as it has more potential during lower outdoor temperatures. Within the occupied hours the temperatures at the bypass were higher than outside of the occupancy, considering the same outdoor temperature. A similar tendency can be noted for the measured air temperatures at 0.265m and 2.41m, as the temperatures

were lower within the unoccupied hours.

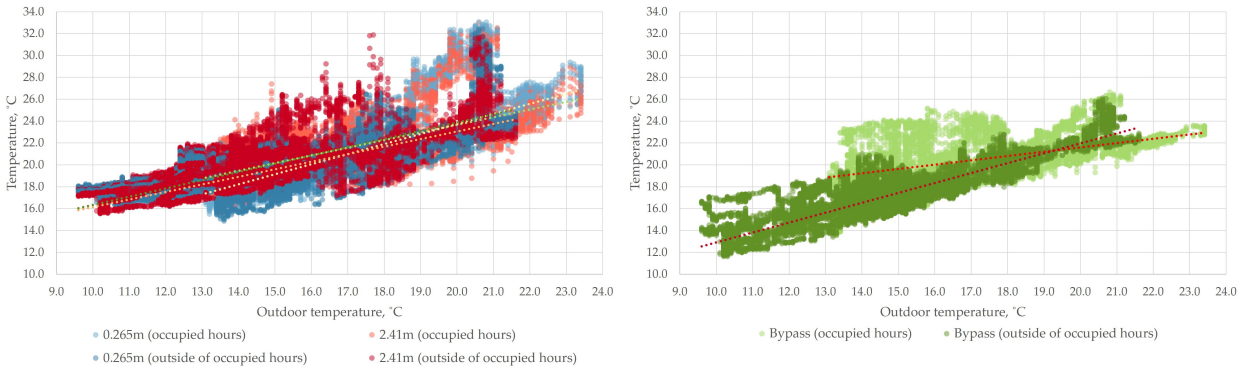

Figure 4.9: Dot plot of the measured temperatures at 0.265m, 2.41m, and at the bypass in the DSF cavity as a function of outdoor temperature for all hours. (24-30.07.2023)

The same air temperatures are plotted in Figure 4.10 (at the height of 0.265m, 2.41m, and at the bypass) as a function of solar radiation with the differentiation of occupied and unoccupied hours. In general, the lowest temperatures were measured when the solar radiation was also low, and a tendency of increasing temperature with increasing solar radiation can be noted. However, the highest temperatures occurred when the solar radiation was around 800W/m^2, while not as high temperatures were experienced above 1000W/m^2. This phenomenon can be explained by thermal energy release from the building mass, and additionally due to the connection between the window control and the outdoor temperature: lower outdoor temperatures were recorded above 1000W/m^2 while the windows were 100% open for an extended period. For example, on 27.07.2023 at 14:16-14:22 the solar incidence was between 1121-1245W/m^2 when the outdoor temperature was 15.7-16.4°C (all windows are 100% open); while outdoor temperatures above 20°C regularly occurred below 1000W/m^2, occasionally with a lower percentage of window openings. Moreover, as the daylight hours are longer in summer, the occurrence of high solar radiation outside of occupied hours was common until 18-19h in the evenings; although the control system was also active during these hours to avoid heat accumulation. Furthermore, the air temperatures in the bypass area appeared to be less sensitive towards the solar radiation.

This leads to the conclusion that the highest temperatures in the cavity arose as the combination of the high outdoor temperature and solar radiation. The ability of the control strategy is evidently limited when these outdoor conditions occur for a longer interval. However, with lower outdoor temperatures, the effect of high solar radiation can be reduced, and therefore the cooling mode is more effective with lower outdoor temperatures.

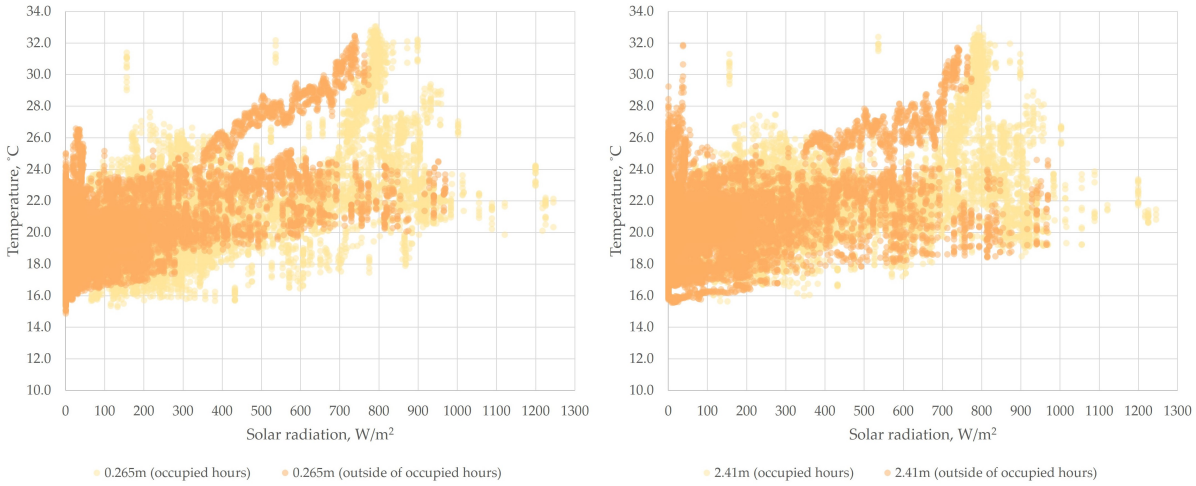

Figure 4.10: Dot plot of the measured temperatures at 0.265m and 2.41m in the DSF cavity as a function of solar radiation for all hours. (24-30.07.2023)

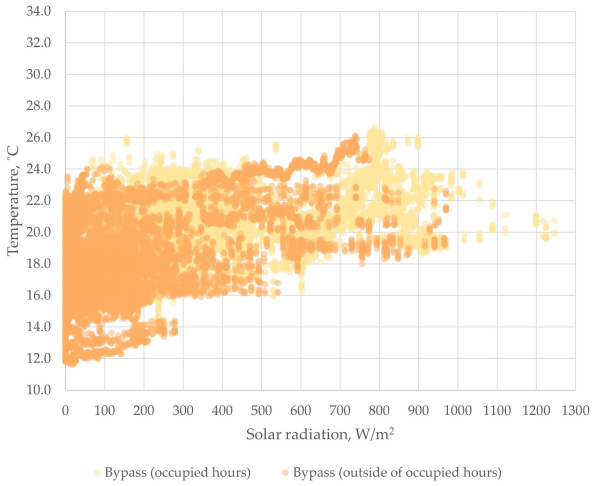

Figure 4.11: Dot plot of the measured temperatures at the bypass in the DSF cavity as a function of solar radiation for all hours. (24-30.07.2023)

To inspect the hourly averages of the air temperature distribution for three occupied hours during a day, Figure 4.12 displays an example of the data from 28.07.2023 as the highest air temperatures in the cavity occurred that day with the combination of the high outdoor temperature and solar radiation. From the tables, it can be concluded that the temperatures in the cavity increased parallelly to the increasing outdoor temperature and solar radiation, while the lowest temperatures were experienced at the bypass. In addition, the release of the accumulated heat from the building structures is notable towards the later hours of the occupied period. Generally, the highest temperatures were measured by the thermocouples located at the height of 1.34m and 1.87m in all the lines. Furthermore, when the solar radiation was high, the thermocouple at 1.34m in the East line experienced the highest temperatures, which indicates the possibility of incorrect installation of the thermocouple: the sensor was in contact with the wall of the silver tube.

Day 5				28/07/2023
	Averages - 8:00-9:00			Average outdoor temperature: 14.43
	West line	Middle line	East line	Average solar radiation: 273
Bypass	16.62	16.25	16.26	
2.41m	19.15	19.04	18.88	
1.87m	19.25	19.01	18.82	
1.34m	19.28	19.10	19.11	
0.80m	19.37	19.04	18.99	
0.265m	19.43	19.40	19.03	
	Averages - 11:00-12:00			Average outdoor temperature: 18.63
	West line	Middle line	East line	Average solar radiation: 733
Bypass	21.89	21.95	21.58	
2.41m	26.31	25.57	24.97	
1.87m	26.70	26.04	25.69	
1.34m	26.57	26.51	30.72	
0.80m	26.49	26.10	25.68	
0.265m	26.52	26.93	25.67	
	Averages - 14:00-15:00			Average outdoor temperature: 20.73
	West line	Middle line	East line	Average solar radiation: 749
Bypass	25.60	25.69	25.51	
2.41m	31.20	30.49	30.42	
1.87m	31.85	31.21	31.20	
1.34m	32.01	31.91	34.26	
0.80m	31.70	31.18	31.08	
0.265m	31.16	31.71	30.34	

Figure 4.12: Hourly averages of the measured temperatures in the DSF cavity. (28.07.2023)

4.1.3 DCV cavity

When inspecting the temperature distribution in the plenum box, only 3 thermocouples are included in the data analysis, as the other three (located in the East line at 1 meter and 2 meters, and in the West line at 2 meters away from the South facade) appeared to have been performing defectively by providing unreliable data. The box-and-whiskers plot in Figure 4.13 includes measurements during all hours in the period of 24-30.07.2023. From the figure, it can be concluded that all the adequately functioning thermocouples displayed a uniform temperature distribution throughout the plenum box. During the summer measurements, the temperatures were between 16.6-19.5°C for 50% of the time, while the lowest occurring temperature was 12.6°C and the highest was 23.2°C.

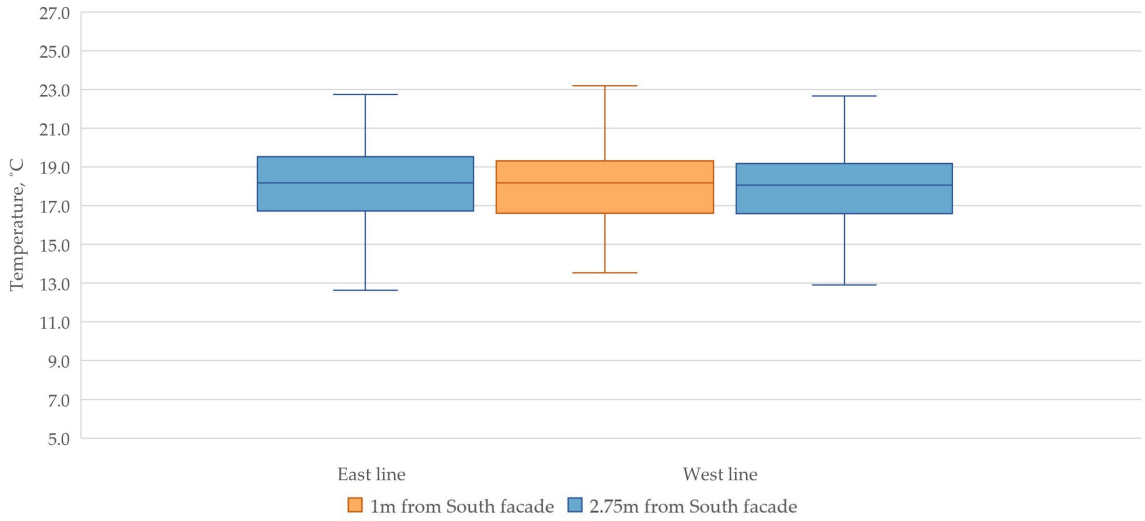

Figure 4.13: Whiskers-and-box plots of the measured temperatures in the plenum box for all hours. (24-30.07.2023)

As the cooling mode was prevailing during the summer measurements, the top windows were often open, and the temperature distribution in the plenum box was significantly dominated by the outdoor temperatures. Therefore, to analyse the temperature of the plenum box as the function of outdoor temperature, Figure4.14 visualises the results, including the differentiation between the occupied and unoccupied hours. Visibly, the air temperature in the DCV cavity was always higher than the outdoor temperature, and the highest temperatures were measured during the occupied period. This is due to the control strategy, as within the occupied hours the heating and cooling modes activated according to the thermal requirements in the Test room, resulting in generally higher temperatures during occupancy, while night cooling was implemented during the evenings. Furthermore, the tendency of increasing temperatures within the cavity can be observed along with the increasing outdoor temperature.

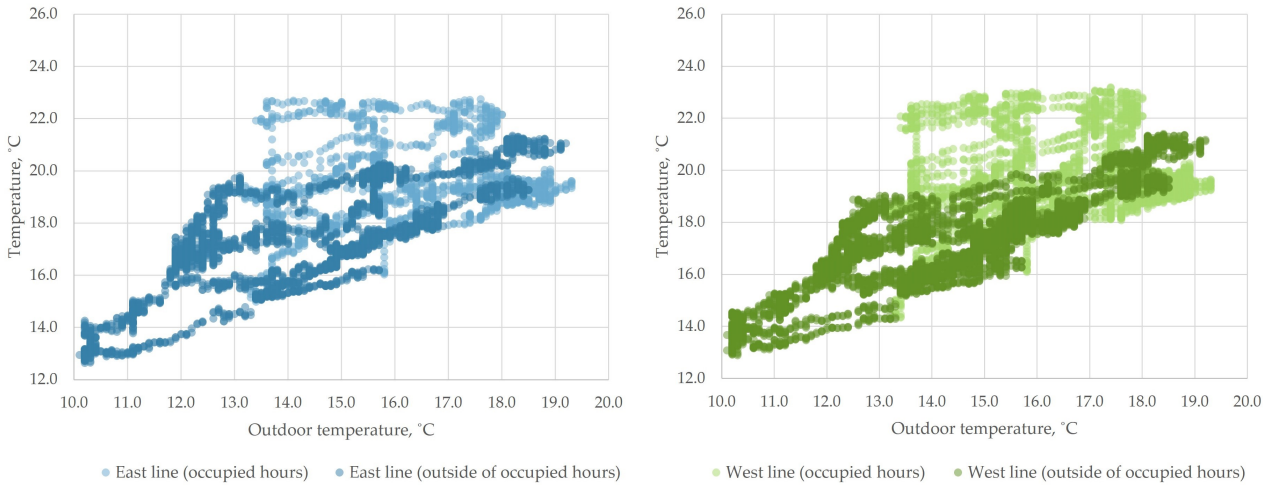

Figure 4.14: Dot plot of the measured temperatures in the plenum box as a function of outdoor temperature for all hours. (23-26.10.2023)

All three thermocouples displayed similar tendencies to the thermocouples located at the bypass during the measurement period (4.8 and 4.15), although with slightly less fluctuation as they are located further away from the windows. The control strategy appears to have operated efficiently for the vast majority of the week, as the opening percentage of the windows influenced the temperatures in the cavity accordingly: a larger difference between the outdoor and indoor temperatures occurred with a lower opening percentage. However, issues with the capacity of cooling during the fifth day can also be noticed here, as the night cooling (started on the fourth day) did not achieve similar temperatures to the outdoor temperature, resulting in overheating during the occupied period. This issue is assumed to be linked to the low thermal mass of the construction.

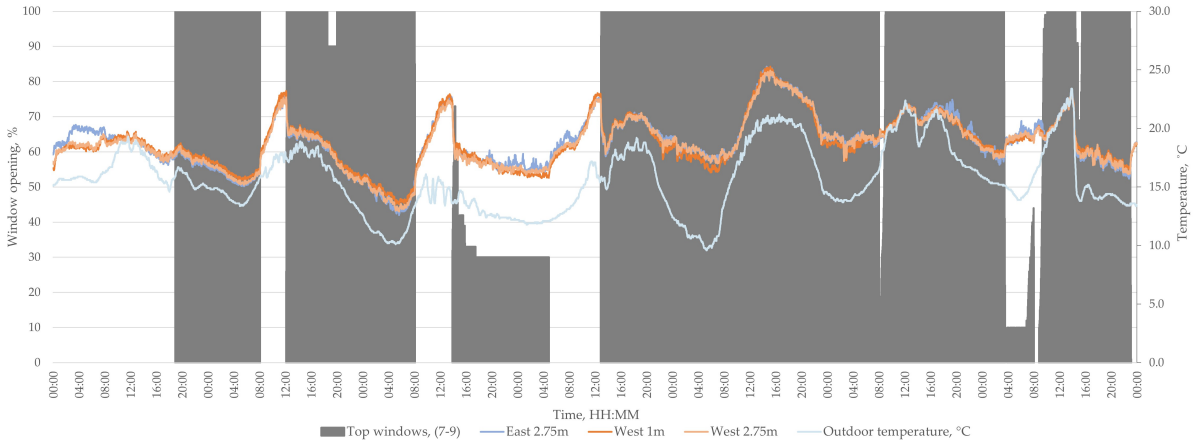

Figure 4.15: Window openings and temperature distribution in the DCV cavity for all hours. (24-30.07.2023)

In Figure 4.16, hourly air temperature averages for three occupied hours on 28.07.2023 are displayed. The influence of the combination of increasing outdoor temperature and solar radiation can be noted as the temperatures in the cavity were rising accordingly. Additionally, the temperature difference between the thermocouple measurements was insignificant and indicated uniform temperature distribution throughout the entire plenum box. This even temperature distribution can be attributed to the directly supplied air into the DCV cavity from outdoors, including the control of synchronized openings for the three windows, and to the low influence of the heat source located in the Test room.

Day 5			28/07/2023
Averages - 8:00-9:00		Average outdoor temperature:	14.43
	East line	West line	Average solar radiation:	273
1m	N/A	17.42		
2m	N/A	N/A		
2.75m	17.58	17.69		
Averages - 11:00-12:00		Average outdoor temperature:	18.63
	East line	West line	Average solar radiation:	733
1m	N/A	21.32		
2m	N/A	N/A		
2.75m	21.27	21.07		
Averages - 14:00-15:00		Average outdoor temperature:	20.73
	East line	West line	Average solar radiation:	749
1m	N/A	24.82		
2m	N/A	N/A		
2.75m	24.69	24.50		

Figure 4.16: Hourly averages of the measured temperatures in the DCV cavity. (28.07.2023)

4.1.4 Systems

Ventilation

The graphs present data on window opening percentages and carbon dioxide (CO_2) levels in parts per million (ppm) over time, displayed in hours and minutes (HH:MM) as referenced in Figure 4.17. During occupied hours, from 8:00 to 15:00, the CO_2 concentration is 810 ppm, while during non-occupied hours, it drops to 500 ppm. These figures show that the WindowMaster system is configured to simulate the presence of occupants in the Test room, as actual CO_2 levels would typically fluctuate more in real-life conditions.

As the bypass is closed during cooling, the air is indirectly supplied from the top windows (7-9) to the Test Room through the diffuse ceiling panels. However, the window opening schedules indicate that these windows are mostly closed during occupied times. A notable correlation between window openings and indoor CO_2 concentration in the Test Room is observed, particularly with the middle and especially bottom row windows. These windows begin to operate during occupancy hours and remain active for some time, even after these hours have ended. Although the middle and bottom row windows are intended primarily to cool the DSF cavity, they are expected to somewhat lower indoor CO_2 concentration as well, although not as their primary function. Therefore, it is highly unlikely that the control strategy demonstrates the potential to maintain air quality by managing bottom and middle row widows alone.

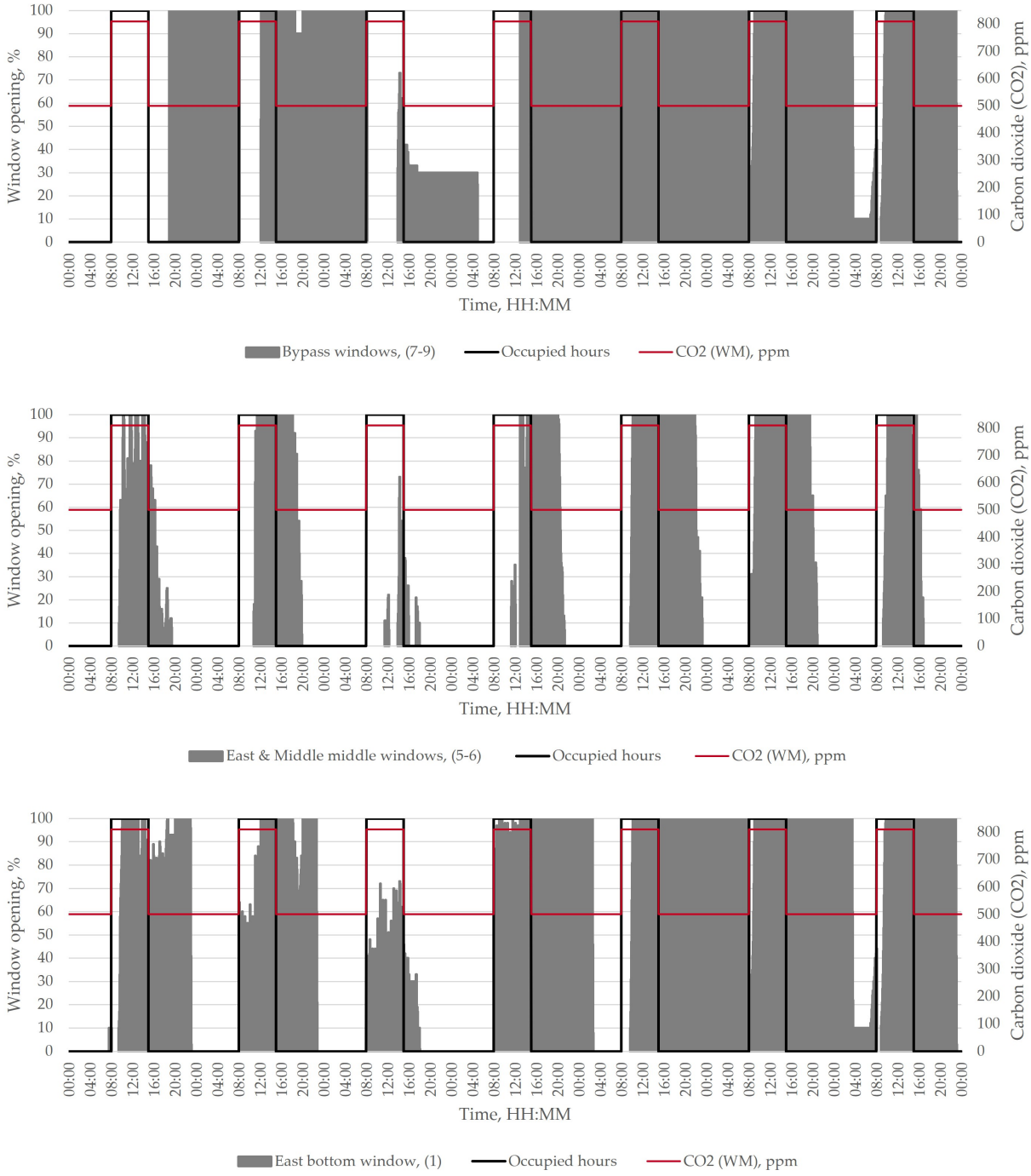

Figure 4.17: Window openings with regards to CO2 concentration in the Test room. (23-26.10.2023)

The supply air temperature, indicated by the orange line in Figure 4.18, shows a fluctuation throughout the day that generally follows the outdoor temperature trend but remains consistently higher than the outdoor air temperature.

The red line indicates that the exhaust air temperature in the Test room, measured near the exhaust outlet is consistently higher than the supply air and outdoor temperatures. There is a visible correlation between the occupancy hours and the increase in exhaust air temperature, suggesting that the building's usage directly impacts the temperature of the air being exhausted.

The opening of top row windows appears to lower the air temperatures in the Test room. The effect is evidenced by a subsequent decrease in exhaust air temperature, indicating that the cooler outside air replaces the warmer indoor air. For example, this effect is noticeable on measurement day 2 at noon. Conversely, at around 8:00 on day 3, there is an immediate increase in the temperature within the room and the DCV cavity when the top row windows close, highlighting the impact of window operations on indoor temperature control.

On the first measurement day, the top row windows remained inactive within the occupancy hours. In contrast, the middle and bottom rows opened at 9:24 to cool the air in the DSF cavity and the Test room. Despite this, the exhaust air temperature maintains a relatively stable profile, with minor variations reflecting outdoor air temperature changes. However, the cooling impact from opening the middle and bottom rows is less marked than that observed when the top row windows are opened.

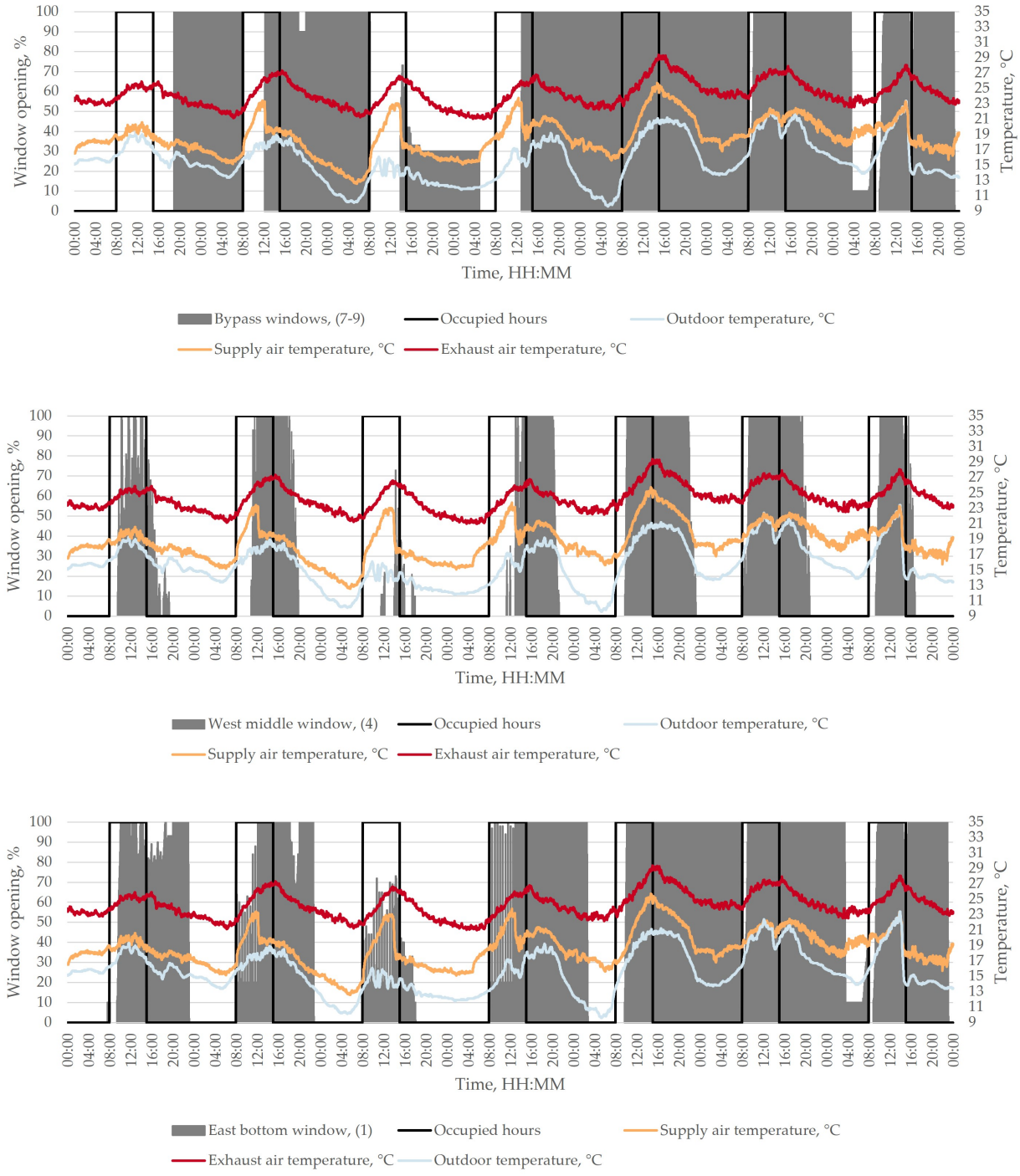

Figure 4.18: Window openings with regards to supply and exhaust air temperature in the Test room. (23-26.10.2023)

Space heating
During the cooling season, the electric space heater remains inactive because the main objective is to cool the space in response to the already warm or hot ambient conditions rather than to heat it.

4.2 Summary

The study found that the individually controlled windows (Window 1 and Window 4) were quicker to respond to changes by approximately one minute and generally had a higher opening percentage than the rest of the openable windows. However, there were moments when other windows surpassed these usual leaders in usage. Top windows operated independently from the bottom and middle rows, often remaining open for extended periods, including overnight, highlighting their role in providing continuous ventilation – night cooling.

Wind speed, as measured by AAU Built weather stations, significantly impacts window behavior, particularly on days with speeds exceeding 7m/s, affecting both the frequency and timing of window openings.

The system displayed rapid responsiveness to temperature variations, reacting within minutes. However, it struggled to maintain the DSF cavity air temperature, frequently exceeding and falling below the setpoint, which led to rapid transitions between modes. This agility is beneficial for promptly responding to indoor temperature fluctuations and sustaining thermal comfort. However, the continual mode shifting has its downsides. While it ensures the system's reactivity to environmental shifts, the noise from frequent window operations may disturb occupants. Moreover, this constant switching may decrease energy efficiency and hasten the system's wear and tear, potentially affecting its longevity.

DSF cavity

The DSF cavity's temperature distribution in summer measurement indicated the temperature variations, with the West and Middle lines showing the lowest temperatures near the cavity's bottom and top, while centrally placed thermocouples recorded higher temperatures. This distribution aligns with the cooling strategy, where cooler outdoor air enters from the bottom and heated air exits from the top.

For the East line, the temperature distribution was slightly different, particularly at the upper thermocouples. The highest temperatures were generally at the top, influenced by the smaller opening percentage and the closed state of the top windows. The temperatures at the bypass, where fresh air enters, were typically the lowest, and the lack of mini fans at the thermocouples might have affected the measurements.

Analysis against outdoor temperature revealed that the cavity's air temperatures were consistently higher. Lower temperatures were noted at the bypass during unoccupied hours, with a linear temperature rise as outdoor temperatures increased. During occupied hours, temperatures at the bypass were higher than outside the same period for a given outdoor temperature. The study concluded that the combination of high outdoor temperatures and

solar radiation had a significant impact on the DSF cavity's air temperature distribution. The highest temperatures were usually at 1.34m and 1.87m, and high solar radiation led to exceptionally high temperatures at 1.34m in the East line, suggesting a potential issue with thermocouple installation.

DCV cavity

In the summer analysis of the plenum box, only three thermocouples provided reliable data, revealing a uniform temperature distribution. During the week, temperatures mostly ranged between 16.6-19.5°C, with extremes at 12.6°C and 23.2°C. The temperature in the plenum box was influenced by the outdoor temperatures, especially during the cooling mode when the windows near the bypass were open. Analysis showed that the air temperature in the DCV cavity was consistently higher than outdoors, with the highest readings during occupied hours. Furthermore, as the outdoor temperature increased, so did the cavity's temperature. The three thermocouples showed similar temperature trends to those at the bypass, with slight fluctuations due to their distance from the windows. A day's analysis indicated that the temperature in the cavity rose with increasing outdoor temperature and solar radiation, maintaining a uniform distribution due to the direct outdoor air supply and window opening control.

Systems

The window opening data indicates that the top-row windows, which are meant to supply fresh air directly during the cooling mode, were barely open during the occupied hour the first four days, despite the system mainly being in cooling mode. During this period, the bottom and middle row windows were open. However, the effectiveness of this window operation strategy in maintaining optimal air quality remains uncertain, as its primary function is to cool the DSF cavity/Test room rather than regulate CO_2 levels.

On the first measurement day, only the middle and bottom row windows were active, leading to a relatively stable exhaust air temperature profile, although the cooling effect was less pronounced than when the top row windows were opened. The electric space heater remains inactive during the cooling season, emphasising the system's focus on cooling rather than heating due to the warm ambient conditions.

Chapter 5

Control strategy - Heating mode

The chapter discusses the effectiveness of the currently incorporated heating mode of the control strategy within two measurement periods: intermediate and winter. Both cases include the analysis of the control's effect on the temperature distribution in the DSF and DCV cavities, and its relation with the operation of the building systems.

5.1 Intermediate case

The heating control operated during the entire measurement period with the implementation of the gap and pulse ventilation modes.

5.1.1 Overview

Window openings
The window opening tendencies differ from day to day during the measurement week and are illustrated in Figure 5.1. The system was operating during the occupied period, therefore, the windows were opening and closing between the hours of 8:00-15:00. As the heating mode was active, only the bottom windows were opening. A slight difference within the opening percentages was experienced, reaching up to 59%, as Window 1 and Windows 2-3 are controlled separately. On the first and third days all three windows opened to a similar percentage, while on the second and fourth days the Window 1 had a larger opening than the other two. Additionally, it is visible that the highest opening percentage occurs on the fourth, while the lowest is on the third day.

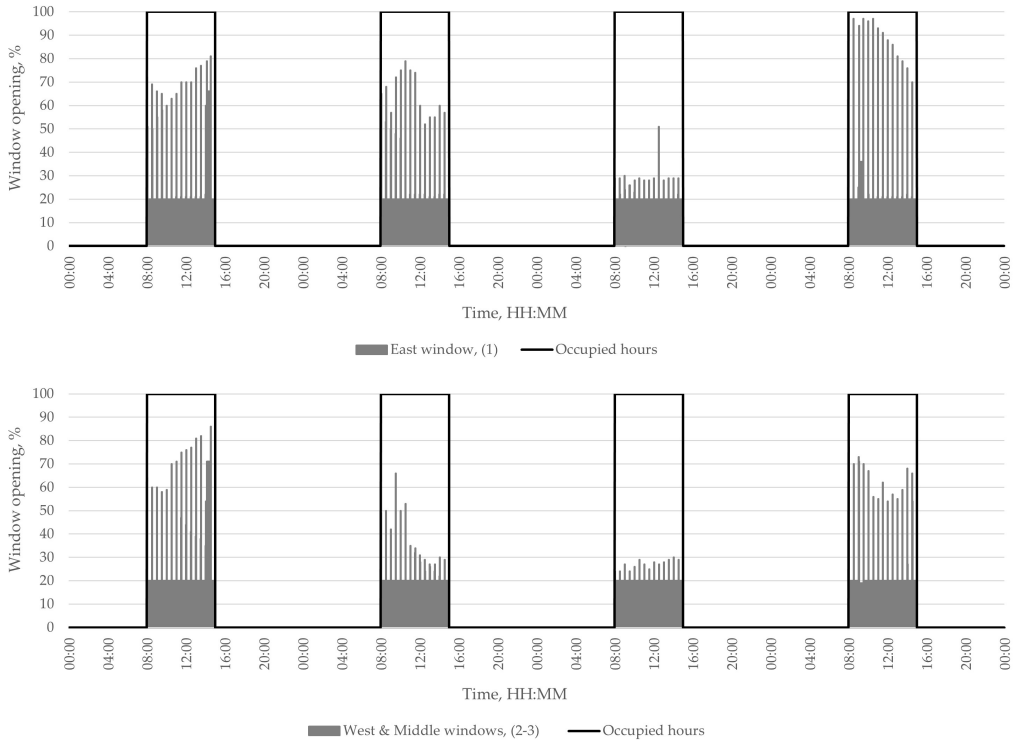

Figure 5.1: Window openings during the intermediate measurement week. (23-26.10.2023)

Outdoor weather conditions

The outdoor temperature varied between 5.5°C and 10.8°C with higher temperatures on the first two days, and lower temperatures on the last two days. Furthermore, the displayed relation between the outdoor temperature and the window opening demonstrates the tendency of a higher opening percentage along with a higher outdoor temperature (5.4). The highest solar radiation occurred on the second day, with 266W/m^2.

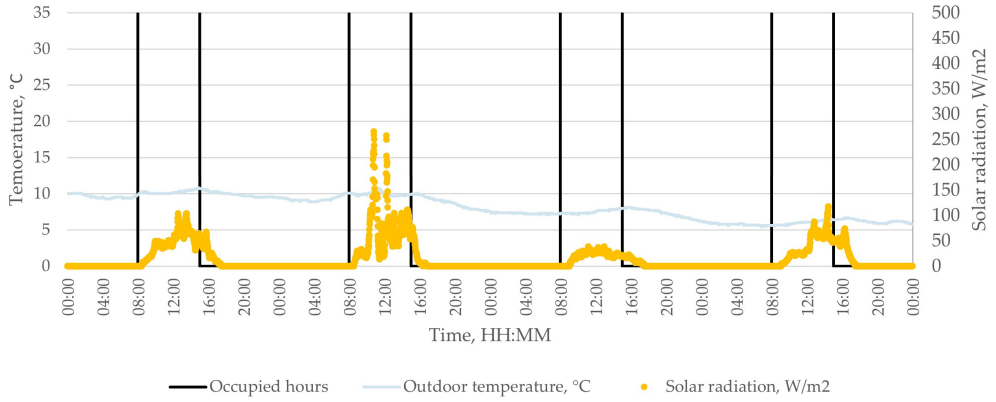

DAY	Outdoor air temperature, °C 24h				Solar radiadio, W/m^2 24h		
	MIN	AVE	MAX	Std	AVE	MAX	SUNLIGHT, Minutes
1	9.3	9.9	10.8	0.4	16	104	540
2	7.6	9.3	10.8	0.7	21	266	493
3	6.2	7.4	8.1	0.4	7	39	506
4	5.5	6.0	6.7	0.3	14	118	505

Figure 5.2: The outdoor air temperature and solar radiation during the intermediate measurements. (23-26.10.2023)

Concerning the wind conditions, a correlation can be obtained from Figure 5.3, in which the opening percentage of the windows decreases as the wind speed increases. As an example, on the first day, the wind speed peaks around 9:30 with 2.3m/s (measured by WindowMaster), thus a drop within the opening percentages can be observed. Additionally, as the wind speed was the highest on the third day (7.0m/s), it explains why the windows were only opened to a small percentage, with a maximum of 51% for Window 1, and 30% for Window 2-3. Furthermore, it is important to note that the WindowMaster records lower wind speed than the weather station, with an average difference of 1.4m/s during the intermediate measurement period.

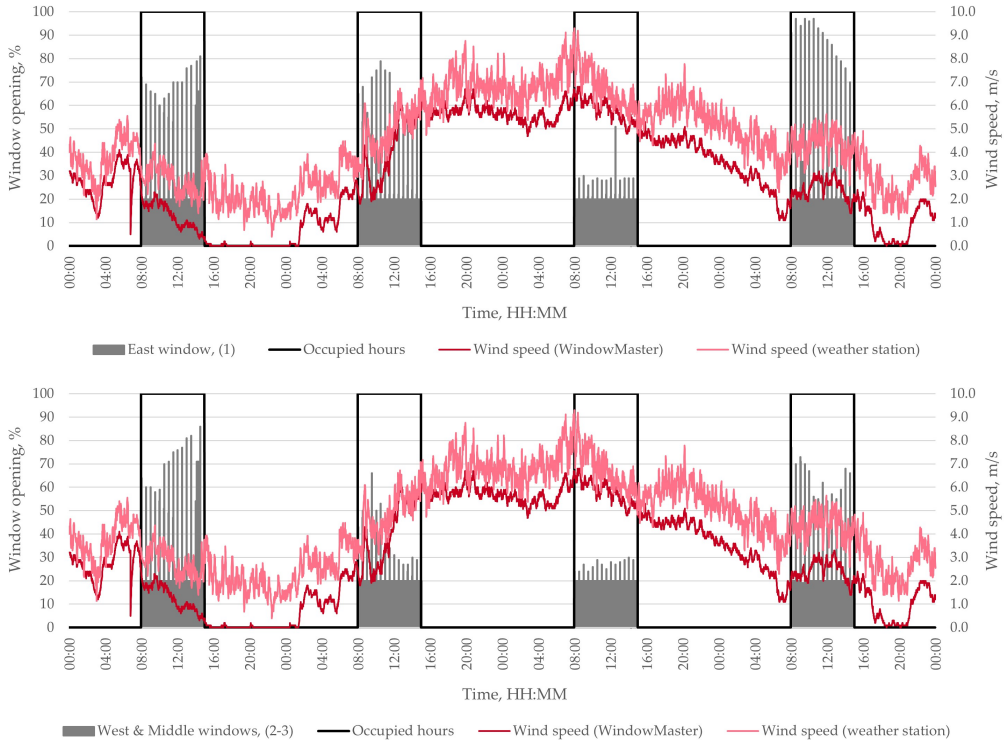

Figure 5.3: Window openings during the intermediate measurement week with regards to wind speed. (23-26.10.2023)

WindowMaster setpoints

The WindowMaster setpoints for the DSF, DCV cavities, and the Test Room are set according to the heating mode control, as seen in Figure 5.4. However, the temperature setpoints were not reached during the four days.

When analysing the response of the DSF and DCV cavities to the operation of the system, it can be asserted that when the windows open in the morning at 8:00, the temperature in both cavities starts to decrease. The temperature change recorded by the WindowMaster sensor in the DSF cavity occurred 2-4 minutes after the windows first opened in the morning, with the slowest response time on the third day when the opening percentage of the windows was the lowest. For the DCV, this reaction time was between 1-3 minutes, where the fastest reaction occurred on the last day with the largest window opening in the morning. Moreover, the temperature in the DSF cavity appears to be more sensitive to changes in outdoor temperatures than the air temperatures in the plenum box, which can be seen in Figure 5.4 as the peaks in outdoor temperature are followed by similar peaks in the DSF cavity temperatures, and with reduced peaks in the DCV cavity temperatures. For instance, on the second day, the outdoor temperature increased from 9.9°C to 10.8°C (ΔT = 0.9°C) in the timespan from 10.01 to 11.04, and with a delay of 6 minutes the temperatures in the DFS (measured by the WindowMaster sensor) increased from 14.7°C up to 16.9°C (ΔT = 2.2°C). This temperature increase in the DSF cavity is assumed to be affected by not only the outdoor temperature but also by the heat transfer occurring between the cavity and the Test room. On the other hand, the air temperatures in the DCV cavity started to increase with a 30-minute delay from 16.6°C to 16.9°C (ΔT = 0.3°C). Furthermore, the temperature setpoint of 25°C for the DSF and DCV cavities was never reached during the

intermediate measurements.

With regards to the operative temperature in the room, it drops approximately in the first 30 minutes, as the windows open at 8:00 and the mechanical extraction in the room starts. However, after 8:30, the operative temperature starts to increase due to the internal heat load. Although an increase in operative temperature within the occupied hours can be observed during the measurement week, the setpoint of 23°C for the heating mode was never reached.

An increase in operative temperature can be observed every day between 15:00-16:00, as the system is set to operate until 15:00, however, the simulated occupants are scheduled to operate until 16:00. Therefore, additional heat is delivered to the room. After 16:00, the operative temperatures start to decrease as the artificial occupants are turned off.

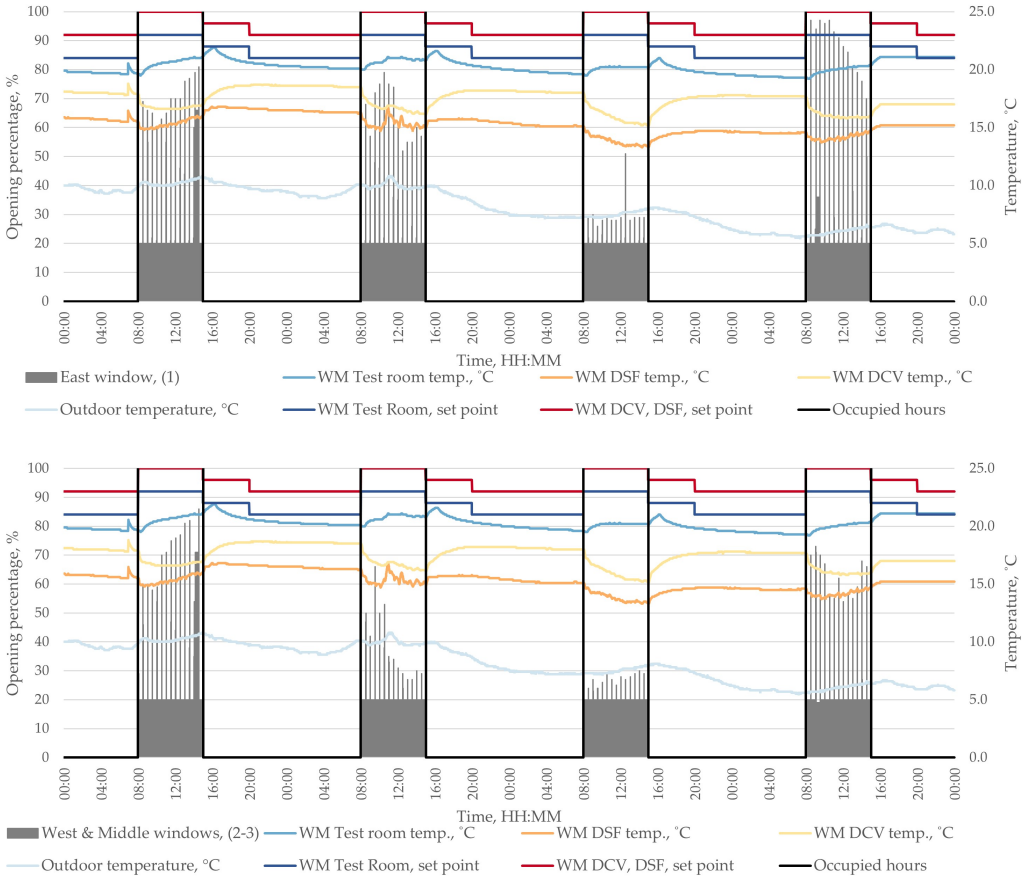

Figure 5.4: Window openings with regards to control setpoints, outdoor temperature, and temperatures in the Test room and cavities. (23-26.10.2023)

5.1.2 DSF cavity

When inspecting the temperature distribution in the DSF cavity during the heating mode, all hours are taken into consideration. The box-and-whiskers plots in Figure 5.5 represent the data collected from each thermocouple. It can be observed that the lowest temperatures occurred at the height of 0.265m in the West and Middle lines, closest to the opening bottom windows. Furthermore, the measured air temperatures were increasing with the increasing height of sensor placements. For all three lines (East, Middle, and West), the highest temperatures were measured by the thermocouples at the bypass area, which confirms that the airflow was preheated in the DSF cavity before it was transferred into the plenum box, correspondingly to the purpose of the control mode. Furthermore, by plotting the outdoor temperature data, it is visible that the temperatures in the DSF cavity are always higher than the temperature outside.

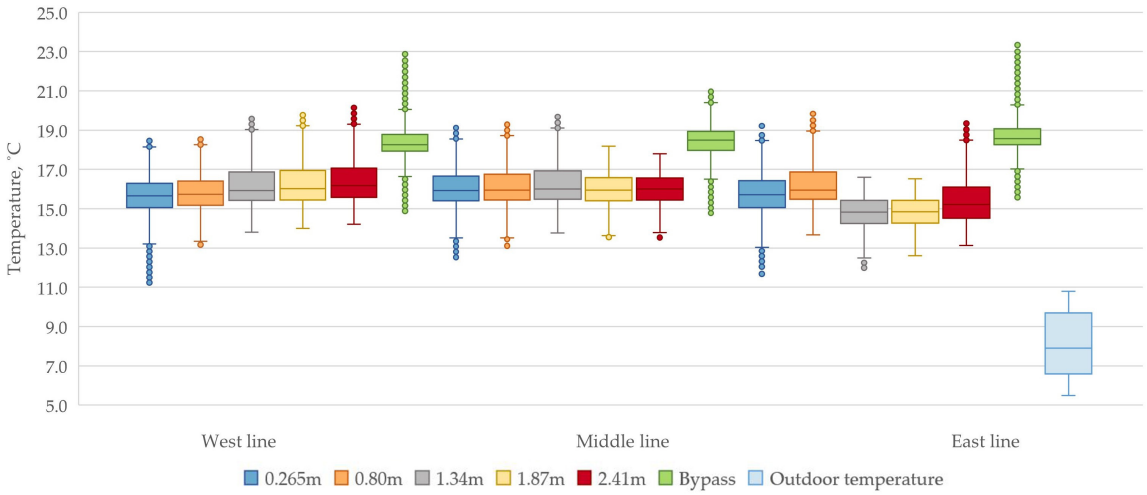

Figure 5.5: Whiskers-and-box plots of the measured temperatures in the DSF cavity for all hours. (23-26.10.2023)

Interestingly, in the East line, generally lower temperatures were measured at the height of 1.34m, 1.87m, and 2.41m. In Figure 5.6, this issue is further investigated with regards to the control system; however, as the measured temperatures by these 3 thermocouples were lower with an average range of 0.9-2.0°C during the unoccupied hours when the windows were closed, it poses the risk of incorrectly calibrated thermocouples.

Additionally, the influence of opened windows was most dominant at the lower part of the cavity near the operating bottom windows, and the effect decreased with height, meaning that the bypass was the least sensitive to the opening percentage of windows.

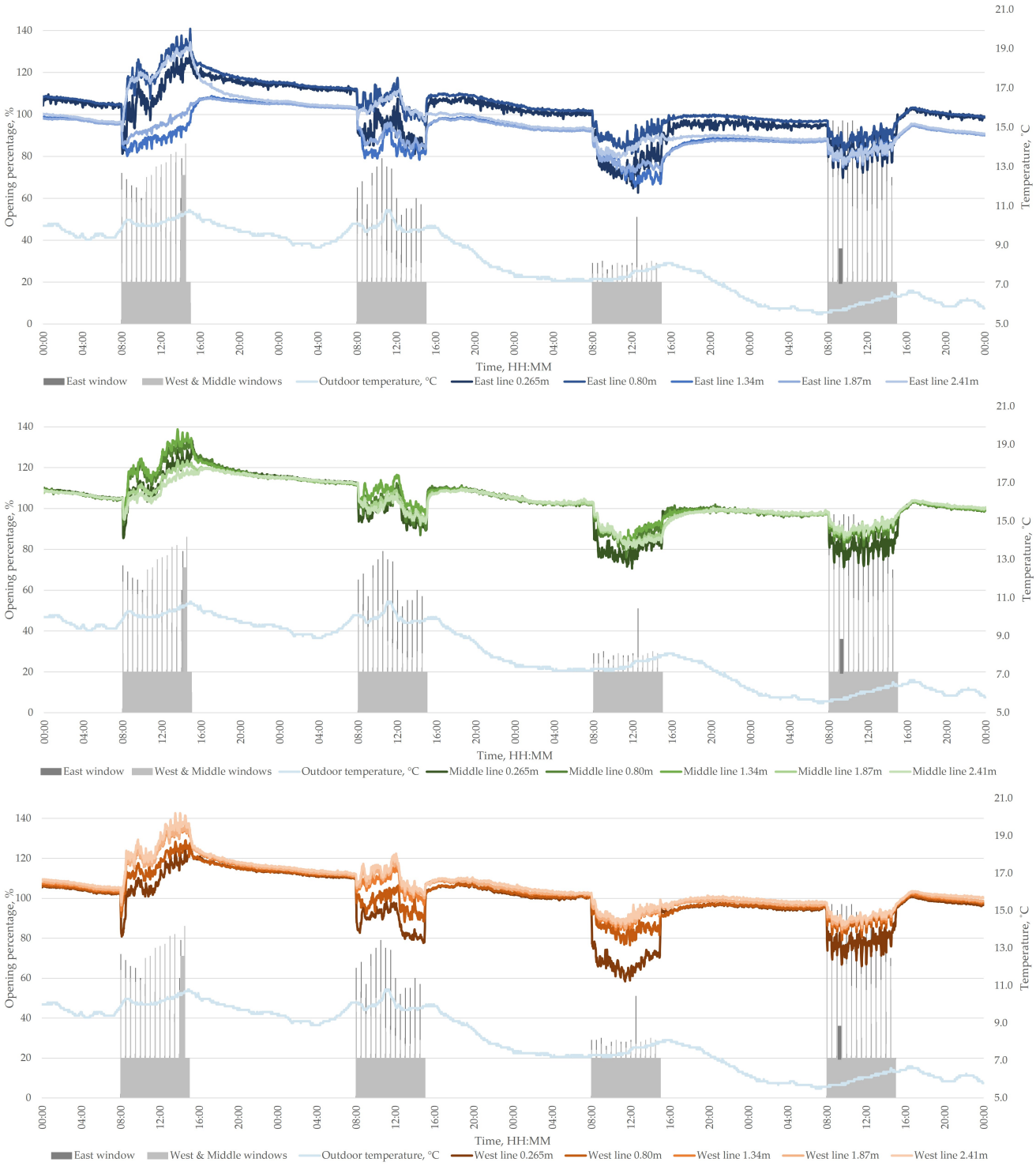

Figure 5.6: Window openings and temperature distribution in the DSF cavity for all hours. (23-26.10.2023)

In Figure 5.7, the measured air temperatures from the thermocouples located at 0.265m and at the bypass area are displayed as a function of outdoor temperature. The data is distinguished as temperatures in the occupied hours and outside the occupancy. It can be concluded, that the measured temperatures were more stable outside of the occupied hours (as the windows were closed), and slightly rose along with the rising outdoor temperatures.

However, within the occupied period, the measured temperatures varied and appeared to be more sensitive to changes in the outdoor temperature. When the outdoor temperature was below 8°C, all the thermocouples measured lower temperatures within the occupied hours. Though with higher outdoor temperatures than 9.5°C, the sensors at 0.265m showed lower values, and the sensors at the bypass showed both higher and lower temperatures than in the period outside of the occupancy. This phenomenon was due to the increasing temperatures along with the increasing height in the cavity, and the slightly different window openings during the four days at the same temperatures (although under different wind conditions).

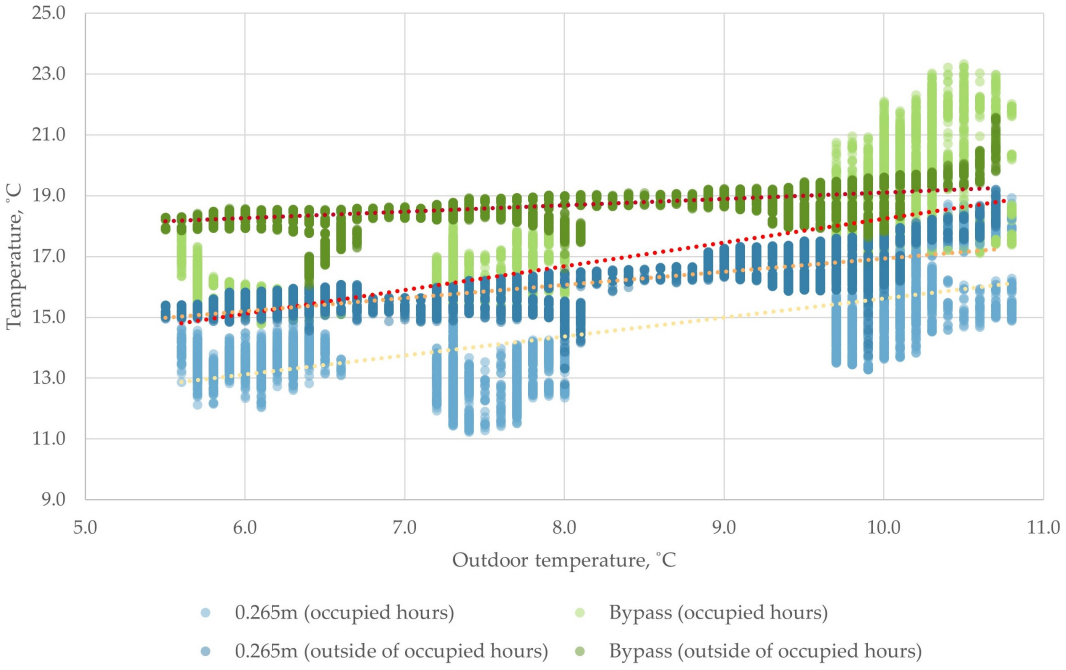

Figure 5.7: Dot plot of the measured temperatures at 0.5m and at the bypass in the DSF cavity as a function of outdoor temperature for all hours. (23-26.10.2023)

The measured temperatures in the DSF cavity at the height of 0.265m and at the bypass are illustrated in Figure 5.8, as the function of solar radiation. During the intermediate measurement week, the solar radiation occurred between 8:30-17:30; however, its incidence was low, mainly between 0-120W/m^2. Generally, the tendency of increasing temperatures in the cavity along with the increasing solar radiation can be noted, although the slightly different tendencies between the thermocouples at 0.265m and at the bypass indicate that the bypass was less sensitive to the changes in solar intensity. In addition, the presence of solar radiation positively affected the control, as it marginally (due to the low intensity) helped with preheating the supply air.

The highest solar radiation occurred on the second day with a maximum value of 266W/m^2 (at 10:47), while the highest temperatures in the cavity were measured on the first day with the solar radiation between 65-100W/m^2. As during these first two days, the window-opening tendencies and the outdoor temperatures were similar, the higher temperature on the first day could have possibly occurred due to the thermal mass of the room, with more heat released from the construction compared to the second day. Furthermore, the high temperature at 0.265m during lower solar radiation outside of the occupancy can be explained by the closed state of the windows.

Figure 5.8: Dot plot of the measured temperatures at 0.5m and at the bypass in the DSF cavity as a function of solar radiation for all hours. (23-26.10.2023)

To inspect the temperature distribution within the cavity in detail, the averages for 3 hours each day during the occupied period are inspected for each thermocouple (see Figure 5.9 and Appendix 9.30 - 9.32). As an example, the results from 23.10.2023 are displayed in Figure 5.9. It can be determined that the highest temperatures appeared in the bypass at the East line; while the lowest temperatures were around the height of 1.34-1.87m in the East line and at 0.265m in the West line. Furthermore, in the bypass area, the air temperature appeared to be non-uniform as lower values occurred in the middle of the cavity than in the West and East corners. This could have occurred due to the realise of the accumulated heat from the building structures, and the thermocouples placed at the corners are more affected as the middle thermocouple is located further away from the surrounding walls.

Day 1				23/10/2023
Averages - 8:00-9:00			Average outdoor temperature:	10.20
	West line	Middle line	East line	Average solar radiation:	5
Bypass	19.22	17.58	19.91	
2.41m	17.11	15.77	16.48	
1.87m	16.87	15.99	14.34	
1.34m	16.76	16.68	13.93	
0.80m	16.16	16.53	16.49	
0.265m	14.98	15.63	15.06	
Averages - 11:00-12:00			Average outdoor temperature:	10.04
	West line	Middle line	East line	Average solar radiation:	43
Bypass	20.19	18.86	20.54	
2.41m	18.17	16.32	17.69	
1.87m	17.89	16.70	15.03	
1.34m	17.89	17.71	14.41	
0.80m	17.16	17.45	17.68	
0.265m	16.27	16.69	16.47	
Averages - 14:00-15:00			Average outdoor temperature:	10.65
	West line	Middle line	East line	Average solar radiation:	55
Bypass	22.05	20.49	22.25	
2.41m	19.70	17.51	18.95	
1.87m	19.37	17.97	15.79	
1.34m	19.31	19.29	15.01	
0.80m	18.38	18.97	19.22	
0.265m	17.80	18.29	18.27	

Figure 5.9: Hourly averages of the measured temperatures in the DSF cavity. (23.10.2023)

5.1.3 DCV cavity

The air temperature distribution in the plenum box is illustrated in Figure 5.10, including the measurements from 6 thermocouples for all hours during the measurement period. It can be obtained that in the West line, the thermocouple closest to the bypass area had the lowest temperatures, and the mean temperatures rose towards the northern wall of the plenum box. However, in the East line, the lowest temperatures occurred in the middle, and the mean temperature was highest closest to the bypass.

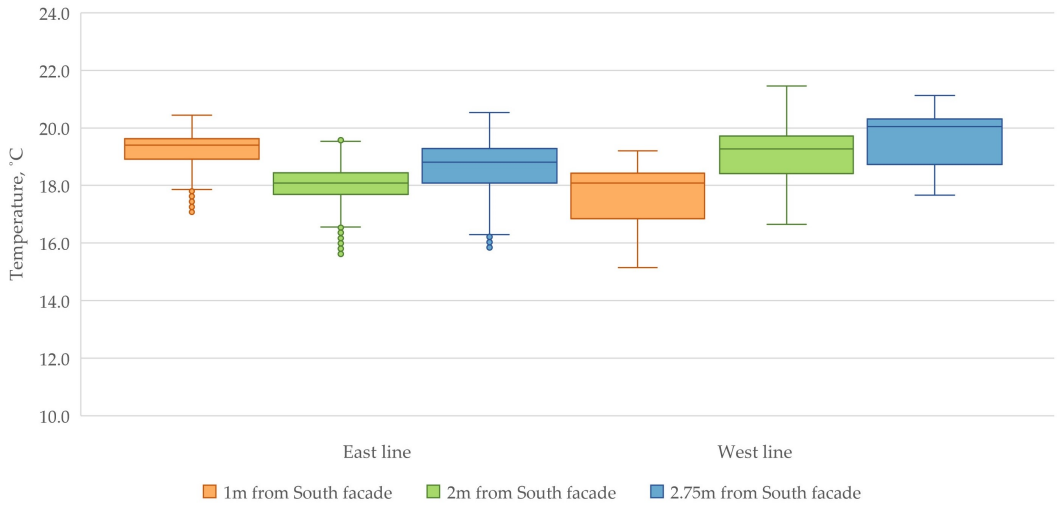

Figure 5.10: Whiskers-and-box plots of the measured temperatures in the plenum box for all hours. (23-26.10.2023)

When analysing the air temperatures with regards to the outdoor temperature in the plenum box, the temperatures ranged from 15-21.5°C. Generally, higher temperatures occurred in the West line, and mostly outside of the occupied hours, as the tendency of dropping temperatures can be observed when the windows opened at 8:00 every day. With such low temperatures of airflow occurring in the plenum box, which was further supplied into the Test room, the risk of local thermal discomfort due to draught within the occupied hours is investigated in section 7.2 Draught rate.

Furthermore, the air temperature in the plenum was dependent on the air temperature of the DSF cavity, therefore, it was also influenced by the outdoor temperature. However, the temperatures in the plenum box were less sensitive to the changes in outdoor conditions, and the opening percentage of the windows influenced the reaction time.

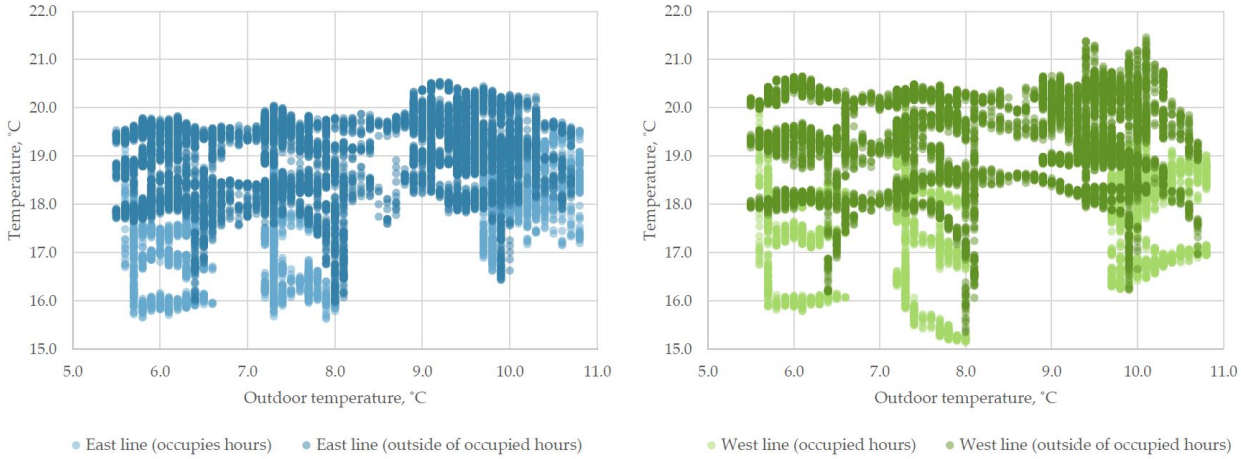

Figure 5.11: Dot plot of the measured temperatures in the plenum box as a function of outdoor temperature for all hours. (23-26.10.2023)

With the aim of inspecting how hourly averages altered during the days (see Appendix 9.43 - 9.46), Figure 5.12 functions as an example for 23.10.2023. Similarly to Figure 5.10, it can be observed that the air temperature in the East line decreased from the South towards the North, and the opposite tendency is true for the West line. However, the mixing of air in the plenum box caused uniform temperatures towards the North wall (at the distance of 2.75m from the South facade).

The non-uniform temperatures measured by the thermocouples close to the South facade are assumed to have occurred due to the uneven installation of the diffuse ceiling panels. Figures 5.13 and 5.14 display the pictures taken with a FLIR thermal camera of the ceiling, where the difference in gaps between the installed ceiling panels is visible. Due to the larger gaps, the local air temperatures measured in the DCV were influenced by the Test room air temperatures.

Overall, the purpose of the heating mode was achieved as the air was preheated before it reached the Test room. However, the need for improvement in the control strategy is implied, with the aim of attaining uniform temperatures of the supply air throughout the entire occupied zone.

Day 1			23/10/2023
Averages - 8:00-9:00		Average outdoor temperature:	10.20
	East line	West line	Average solar radiation:	5
1m	19.19	17.02	
2m	18.19	18.53	
2.75m	18.18	18.56	
Averages - 11:00-12:00		Average outdoor temperature:	10.04
	East line	West line	Average solar radiation:	43
1m	18.79	16.72	
2m	18.13	18.27	
2.75m	17.90	17.92	
Averages - 14:00-15:00		Average outdoor temperature:	10.65
	East line	West line	Average solar radiation:	55
1m	19.41	17.04	
2m	18.61	18.83	
2.75m	18.27	18.76	

Figure 5.12: Hourly averages of the measured temperatures in the plenum box. (23.10.2023)

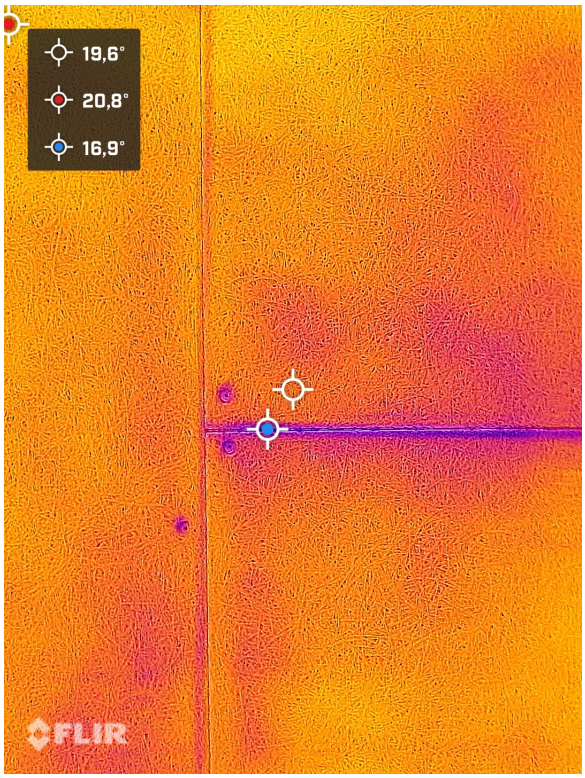

Figure 5.13: Connection of diffuse ceiling panels.

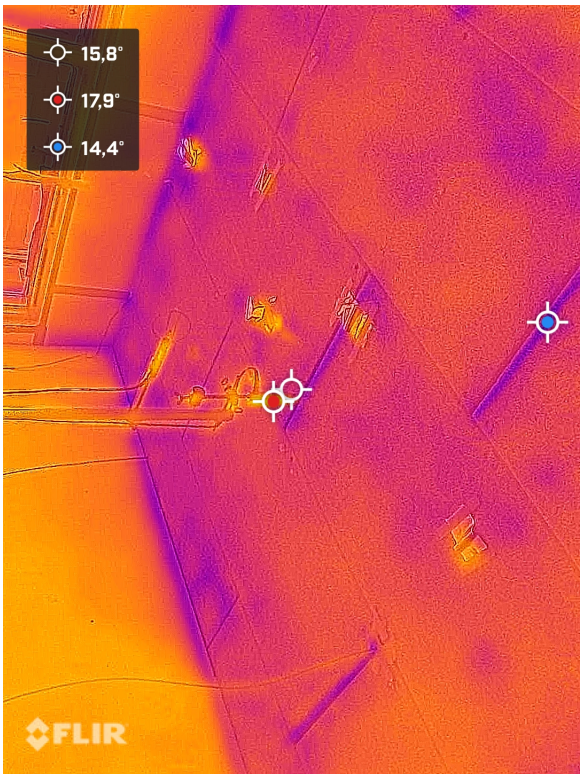

Figure 5.14: Connection of diffuse ceiling panels.

5.1.4 Systems

Ventilation

In the Test room, four occupants are simulated by a heat source that does not emit CO_2. The WindowMaster system is configured to automatically register a CO_2 level of 810 ppm during the occupancy hours, from 8:00 to 15:00. See Figure 5.15.

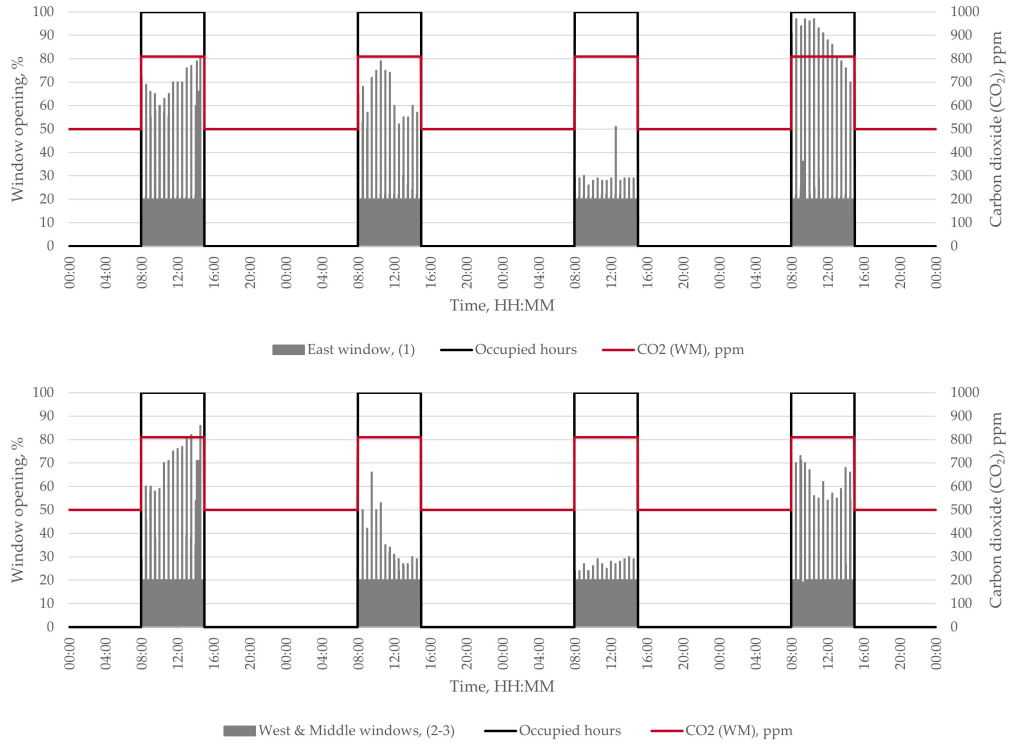

Figure 5.15: Window openings with regards to CO_2 concentration in the Test room. (23-26.10.2023)

The increased CO_2 concentration in the Test room triggers the activation of the exhaust ventilation system to maintain the amount of pollutants from the occupants in the classroom. Figure 5.16 shows that the Test room has an airflow of 34.5l/s (8.6l/s per person), representing an 8.9 times per hour air change rate in the room.

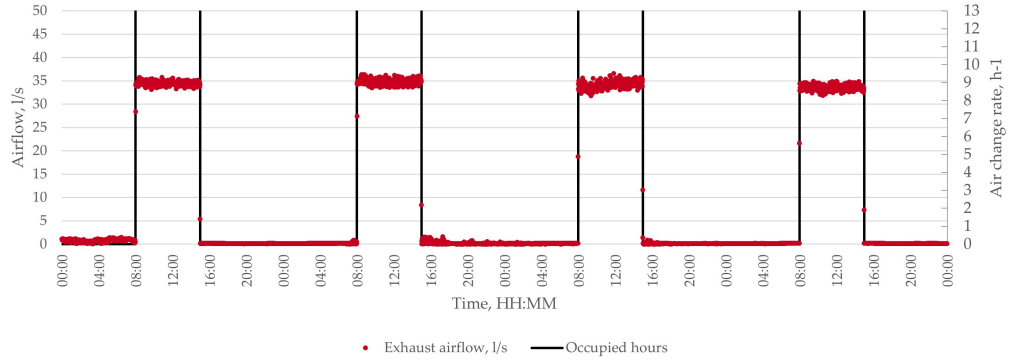

Figure 5.16: Exhaust airflow and air change rate in the Test room. (23-26.10.2023)

The supply air, exhaust air, and room operative temperatures come closer when the windows are closed and the ventilation system is inactive – unoccupied hours. See Figure 5.17

During occupied hours, when the windows are open, the supply temperature (average air temperature from thermocouples placed in the DCV cavity) experiences a decrease, influenced by the lower outdoor temperature as the WindowMaster windows in DSF open.

The operative temperature shows slight fluctuations but rises gradually throughout the occupied period due to heat gains — notably, the exhaust temperature registers as the highest among the monitored temperatures during these hours.

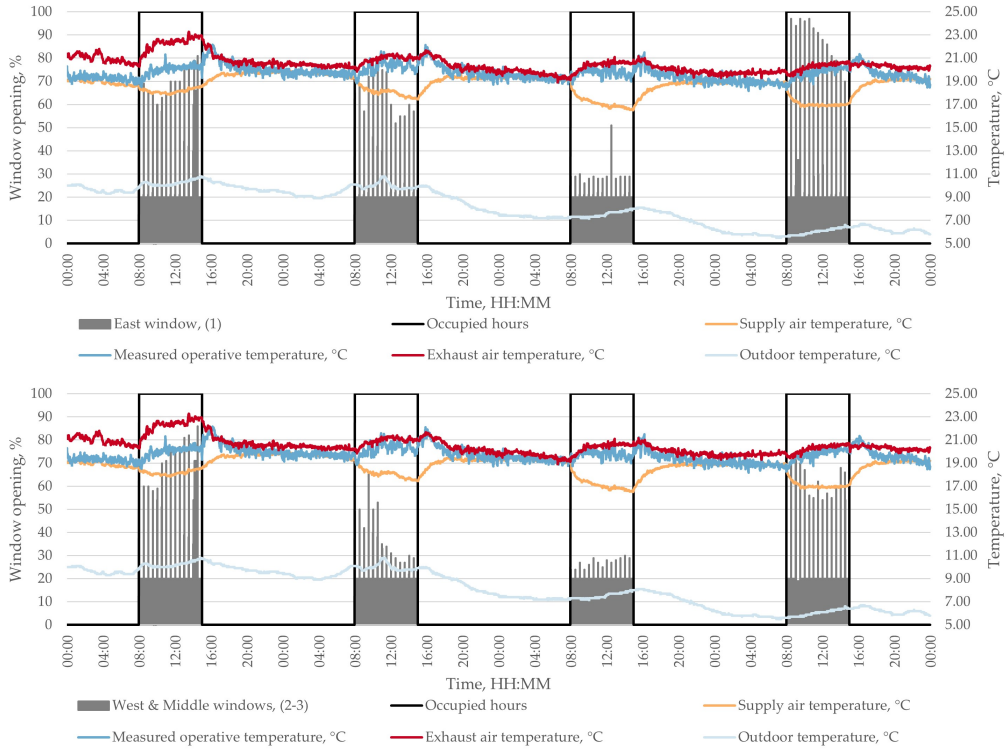

Figure 5.17: Window openings with regards to supply and exhaust air temperature in the Test room. (23-26.10.2023)

Space heating

During the intermediate measurement phase, the electric space heater, which was set to position (I), did not activate. This suggests that the set temperature was maintained consistently throughout the period, indicating no need for additional heating.

5.2 Winter case

The heating control operated during the entire measurement period with the implementation of the gap and pulse ventilation modes.

5.2.1 Overview

Window openings
Figure 5.18 illustrates window opening percentages during a three-day winter measurement period in which the system runs in heating mode. After analysing the data, Window 1 is shown to be opened more than Windows 2-3 99.5% of the time, occasionally by as much as 28%. Conversely, for 0.5% of the time, Windows 2-3 opens up to 11% more than Window 1. Despite the predominant trend of Window 1 being opened more frequently, the instances where Windows 2-3 are opened more highlight an inconsistency in window opening behaviour.

The black vertical lines indicate the hours of occupancy. It is observable that the windows were first opened each day after the start of occupancy and remained open for a duration beyond the end of occupancy.

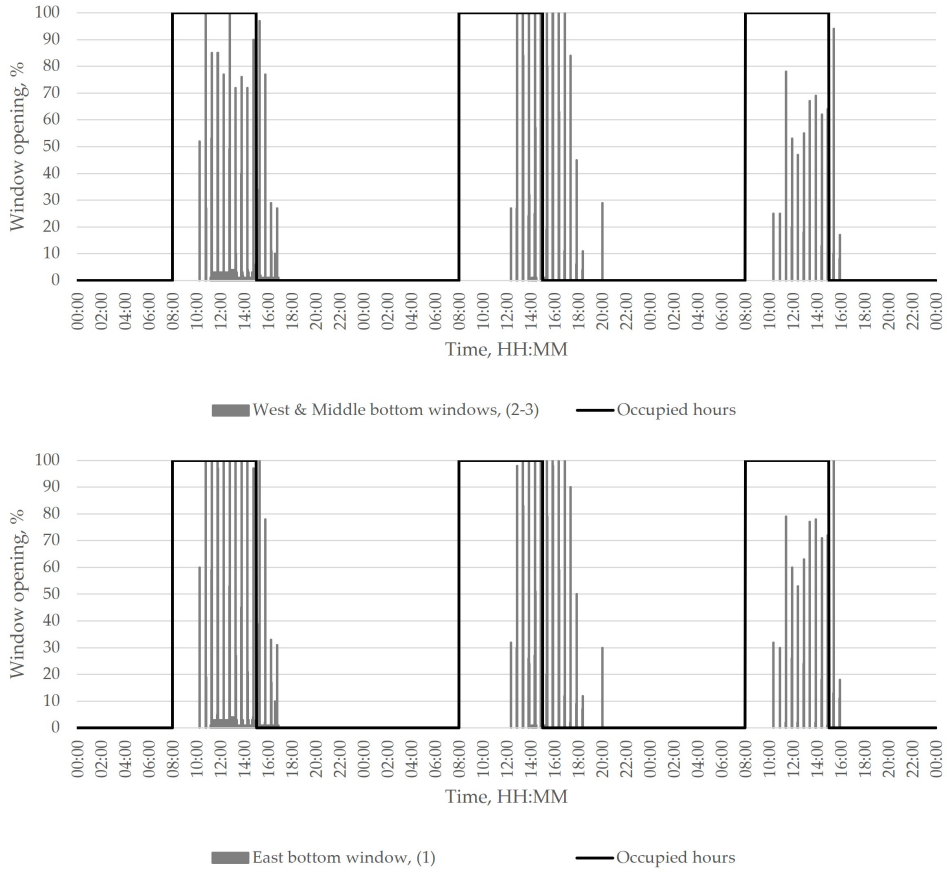

Figure 5.18: Window openings during the winter measurements in the Test room. (30-11.2023 - 02.12.2023)

Outdoor weather conditions

The outdoor air temperature experienced a notable drop from -0.8 to -6.2°C between 15:00 on the second day and 02:00 the following day. Other than these specific hour dips over three days, the temperature remained relatively stable, just below 0°C. The highest solar irradiance was recorded on the first measurement day, reaching 255W/m². It was slightly lower on subsequent days, as shown in the figure below.

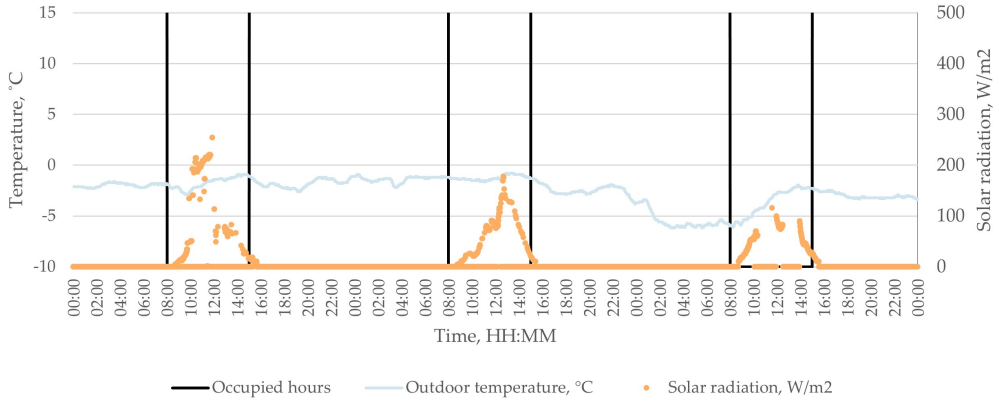

DAY	Outdoor air temperature, °C 24h				Solar radiadio, W/m² 24h		
	MIN	AVE	MAX	Std	AVE	MAX	SUNLIGHT, Minutes
1	-2.9	-1.8	-0.9	0.4	13	255	357
2	-3.8	-1.7	-0.8	0.7	6	178	115
3	-6.2	-4.0	-1.9	1.4	7	116	228

Figure 5.19: The outdoor air temperature and solar radiation during the winter measurements. (30-11.2023 - 02.12.2023)

Regarding wind speed, data from the WindowMaster sensor indicated a light breeze, peaking at 2.4m/s, on the first day of measurement. During the occupied hours in the remaining days, wind speeds were generally calm, falling below 1m/s. See Figure 5.20. The wind speed data logged by the WindowMaster is up to 3.8m/s lower than the weather station data. The observed difference can arise from various factors, including environmental conditions, technical aspects, and the geographical positioning of the weather stations. The light wind speed does not seem to influence the window openings during the three measurement days.

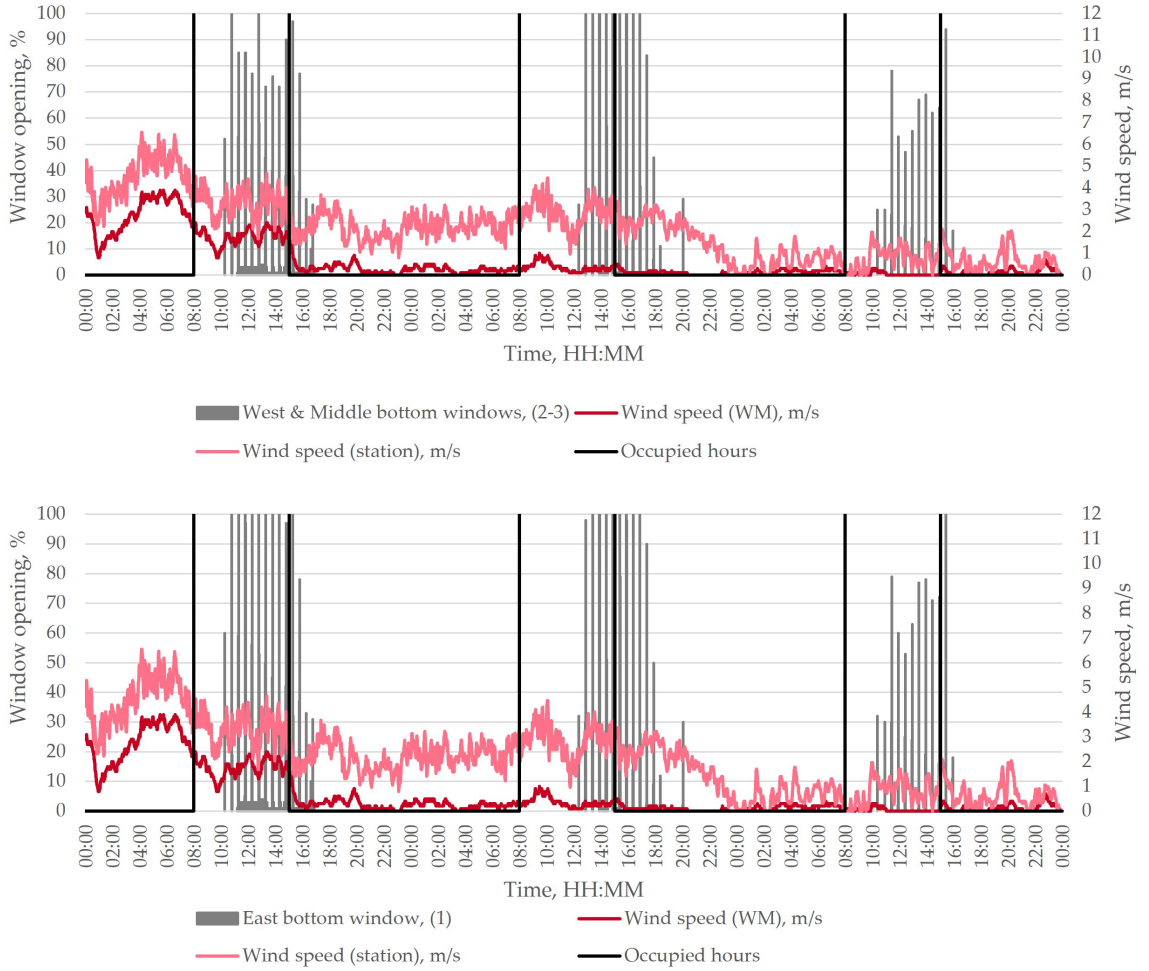

Figure 5.20: Window openings during the winter measurement case with regards to wind speed. (30-11.2023 - 02.12.2023)

WindowMaster setpoints

The WindowMaster setpoints for the DSF, DCV cavities, and the Test Room are set according to the heating mode control, as seen in Figure 5.21.

WindowMaster opening opened for the first time during the occupancy hour on the first day at 10:16 (4 minutes after the Test Room set point is reached (10:12; 23°C), second day 12:21 (28 minutes after the Test Room set point is reached (11:52; 23°C) and third day 10:22 (11 minutes after the Test Room set point is reached (10:11; 23°C). Which shows that the system is controlled according to the set temperature setpoints.

During the intermediate measurement case, the air temperatures maintained distinct levels without intersecting. The highest temperatures were recorded in the Test Room, with slightly cooler readings in the DCV cavity, and the lowest temperatures were observed in the DSF cavity (Figure 5.4). In the winter measurement case, the air temperature within the DSF cavity exceeded the temperatures in both the Test Room and the DCV cavity during occupied hours. Notably, on the first day, the air temperature in the DCV cavity surpasses the Test Room's temperature from 10:55 to 12:05 by up to 2.2°C. See Figure 5.21.

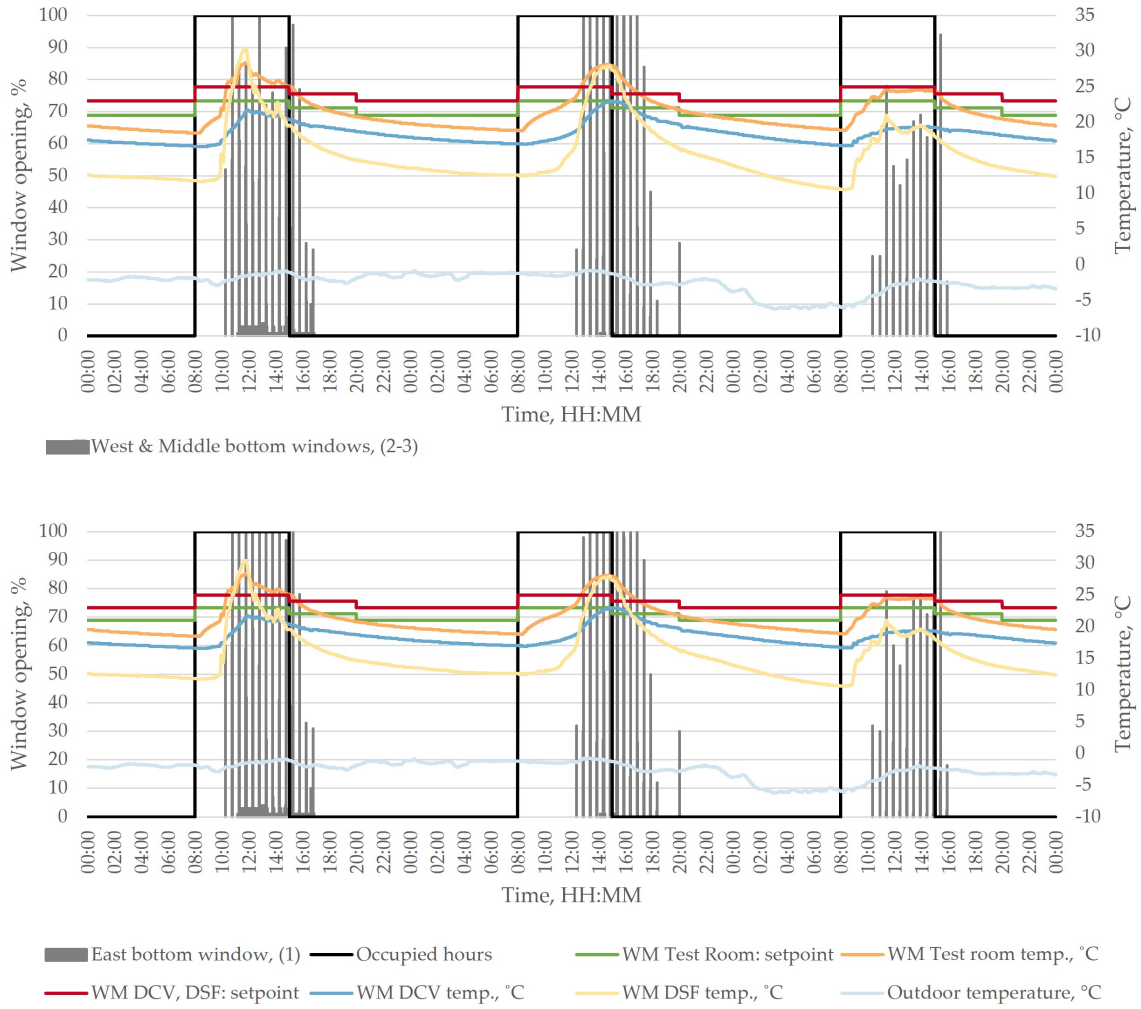

Figure 5.21: Window openings with regards to control set points, outdoor and air temperatures in the Test room and cavities. (30-11.2023 - 02.12.2023)

5.2.2 DSF cavity

For the three measurement days during winter, the air temperatures measured by the thermocouples located in the DSF cavity are illustrated as box-and-whiskers plots in Figure 5.22. Nonetheless the cold temperatures outdoors (between -6.2°C and 2.3°C), the air temperature in the cavity stayed above 9.8°C, implying an effective heating function of the control.

Generally, the temperatures up until the height of 2.41m mainly ranged between 9.8-23.5°C, although the maximum temperature of 29.1°C was reached. For all three lines, the highest average temperatures occurred in the bypass, as the temperatures ranged between 15.6-22.9°C, with a maximum temperature increasing up to 28.4°C. The occurrence of the minimum temperatures being significantly higher in the bypass than in the lower parts of the DSF cavity can be explained by the control strategy of the system, as the separation between the DSF and DCV cavity was closed off as long as the windows were closed. Therefore, during the closed state of the windows, the thermocouples in the bypass measured similar

temperatures to the DCV cavity air temperatures, and as visualised in Figure 5.22, there were mostly higher temperatures in the plenum box.

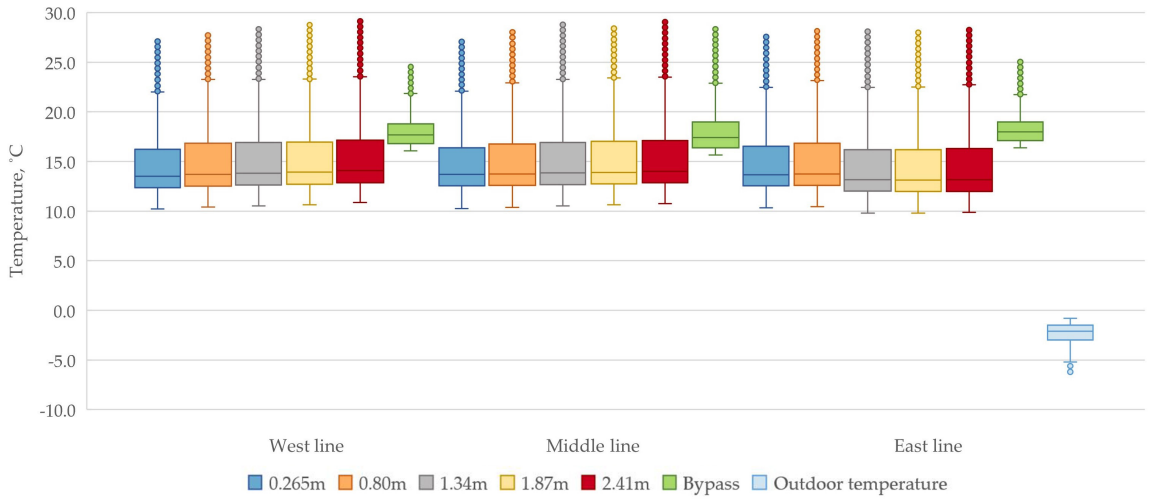

Figure 5.22: Whiskers-and-box plots of the measured temperatures in the DSF cavity for all hours. (30.11.2023-02.12.2023)

In the West and Middle lines, the air temperatures for the thermocouples located at the heights between 0.265m and 2.41m appeared to be nearly uniform, however, a slight increase in temperatures along with the increase in height was evident. On the other hand, for the East line, similarly to the intermediate case, the tendency of lower temperatures is notable in the case of the thermocouples at the height of 1.34m, 1.87m, and 2.41m. During the intermediate case, the issue of incorrect calibration of those 3 thermocouples was raised, and in Figure 5.23, the same matter can be observed. However, the difference between the thermocouple measurements outside of the occupied hours in the winter case was minor as it ranged between an average of 0.5-0.7°C.

Additionally, with regards to the window opening tendencies of the pulse ventilation mode, the sensitivity of the lower thermocouples was obvious, in contrast to the higher-placed ones. In Figure 5.23, the sudden drops in air temperatures were evident (dominantly for the thermocouples at the heights of 0.265m and 0.80m) after the windows opened, followed by increasing temperatures when the windows were closed again.

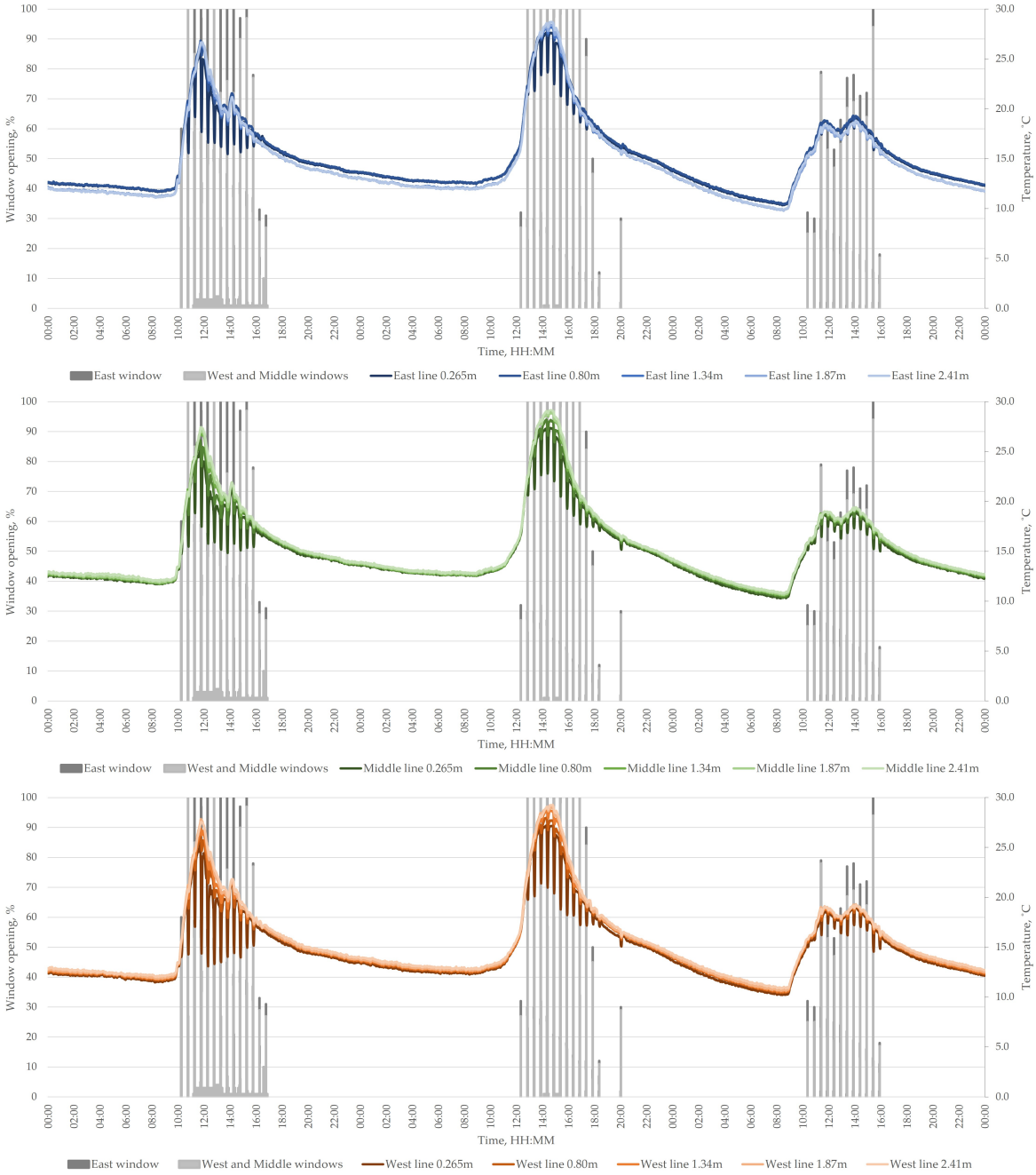

Figure 5.23: Window openings and temperature distribution in the DSF cavity for all hours. (30.11.2023-02.12.2023)

When analysing the temperature distribution within the cavity as a function of outdoor temperature, the measurements of the thermocouples at the height of 0.265m and at the bypass are included for all hours, although with the differentiation in occupied and unoccupied hours. Within the unoccupied periods, the temperatures appeared to be steady, with a slight increase as the outdoor temperature rose, due to the mainly closed state of the windows. However, during the occupied hours, both lower and higher temperatures occurred than outside of occupancy, indicating a higher sensitivity towards outdoor temperature, due to the operating windows.

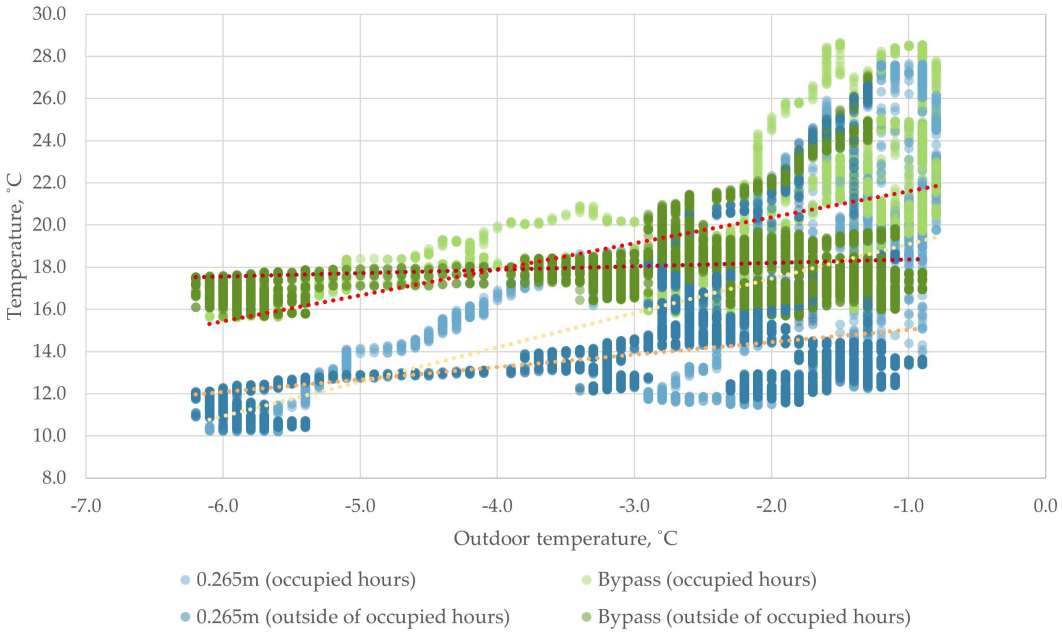

Figure 5.24: Dot plot of the measured temperatures at 0.5m and at the bypass in the DSF cavity as a function of outdoor temperature for all hours. (30.11.2023-02.12.2023)

With the aim of assessing the influence of solar radiation on the temperature distribution in the DSF cavity, the dot plot in Figure 5.25 displays the measurements. It appears that the highest solar radiation recorded by the pyranometer was 255W/m^2 on the first day (at 11:52), when also the highest temperature measurement occurred in the bypass area. The lower air temperatures at the height of 0.265m can be explained by the constant state of the opened windows up to 4%, during this period of high solar intensity. On the other hand, high temperatures (above 26°C) occurred during lower solar incidence (40-110W/m^2), due to the fluctuation in the solar radiation while the air temperature in the cavity was stable with a slower reaction time to the changing outdoor conditions. Overall, the influence of solar radiation can be obtained due to the increasing temperature in the cavity with the increasing solar radiation.

Furthermore, during the whole measurement week, there was snow outside, which is an essential factor to consider, especially in its potential impact on the weather station's solar radiation readings. The snow may have caused the recorded solar radiation levels to be lower than they were. Furthermore, snow introduces a significant variable on sunny days due to its high albedo effect, which involves the snow's ability to reflect incoming sunlight. It could have notably increased the light intensity in the Test Room and in the cavities. As

this amplified light was absorbed by the materials in the room, it likely led to an increase in indoor air temperatures, as the absorbed light converted to heat. However, this fact cannot be concluded as no light measures in the room were performed.

The above-mentioned findings concerning the high air temperatures in the DSF cavity in contrast to the combination of low outdoor temperatures and the influence of solar radiation, lead to the conclusion that there is a demand for optimization of the control, as the currently incorporated strategy did not manage to remove the excessive heat accumulation in the cavity.

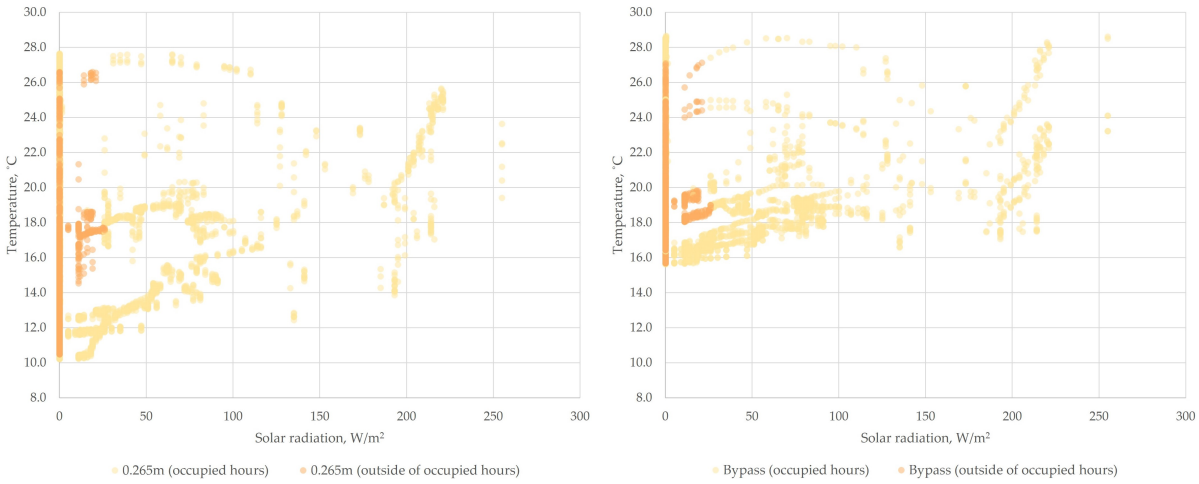

Figure 5.25: Dot plot of the measured temperatures at 0.265m and at the bypass in the DSF cavity as a function of solar radiation for all hours. (30.11.2023-02.12.2023)

The temperature distribution is further analysed in Figure 5.26 for three occupied hours on 02.12.2023, as the coldest outdoor temperatures occurred on that measurement day (see Appendix 9.33-9.35 for all the measurement days). The coldest temperatures in the cavity occurred in the first occupied hour, and the outdoor temperature and solar radiation were also the lowest at that time. However, the thermocouples in the bypass showed higher temperatures, with up to 6°C. This significant difference between the thermocouples at the height of 2.41m and the bypass was due to the closed state of the separation between the DSF and DCV cavities, as the first time the windows opened that day was at 10:46. Therefore, between the hours of 11:00-12:00 when the separation was open, the West and East corners of the bypass displayed uniform temperatures with the thermocouples located at 2.41m. On the other hand, the centrally placed thermocouple still showed slightly higher temperatures as it is not located right above the openable part of the separation, while the other two thermocouples are (see Figure 5.27). Towards the end of the occupied period, the temperatures equalized in the bypass area.

Day 3				02/12/2023
	Averages - 8:00-9:00			Average outdoor temperature: -5.80
	West line	Middle line	East line	Average solar radiation: 4
Bypass	16.21	15.73	16.50	
2.41m	10.97	10.92	10.03	
1.87m	10.75	10.79	9.99	
1.34m	10.64	10.70	10.00	
0.80m	10.54	10.55	10.59	
0.265m	10.33	10.43	10.49	
	Averages - 11:00-12:00			Average outdoor temperature: -3.29
	West line	Middle line	East line	Average solar radiation: 8
Bypass	18.50	20.17	18.45	
2.41m	18.50	18.52	17.87	
1.87m	18.60	18.48	17.70	
1.34m	18.39	18.50	17.77	
0.80m	18.26	18.26	18.32	
0.265m	17.81	18.01	18.20	
	Averages - 14:00-15:00			Average outdoor temperature: -2.26
	West line	Middle line	East line	Average solar radiation: 41
Bypass	18.86	19.34	18.85	
2.41m	18.76	18.85	18.12	
1.87m	18.65	18.75	18.00	
1.34m	18.59	18.69	18.00	
0.80m	18.51	18.50	18.60	
0.265m	18.17	18.15	18.35	

Figure 5.26: Hourly averages of the measured temperatures in the DSF cavity. (02.12.2023)

Figure 5.27: Thermocouples located at the bypass area. (The picture serves as a reference for the thermocouple location, and the open state of the windows should be ignored as it was taken within the cooling mode.)

Additionally, a general increase in the air temperatures in the DSF cavity can be noted, from the morning hours until the afternoon hours, which can be explained by the increasing outdoor temperature, solar radiation, and heat exchange between the cavity and the Test room. Due to the occupancy in the room, the internal heat load was increased, as well as the presence of an electrical heater further increased the temperatures in the room. Therefore, the heat exchange through the internal South facade influenced the DSF cavity air temperatures. In Figure 5.28, on the picture taken with a FLIR thermocamera, the critical points in the construction are indicated with blue colour, where heat transfer occurs at a higher level due to the lack of adequate insulation.

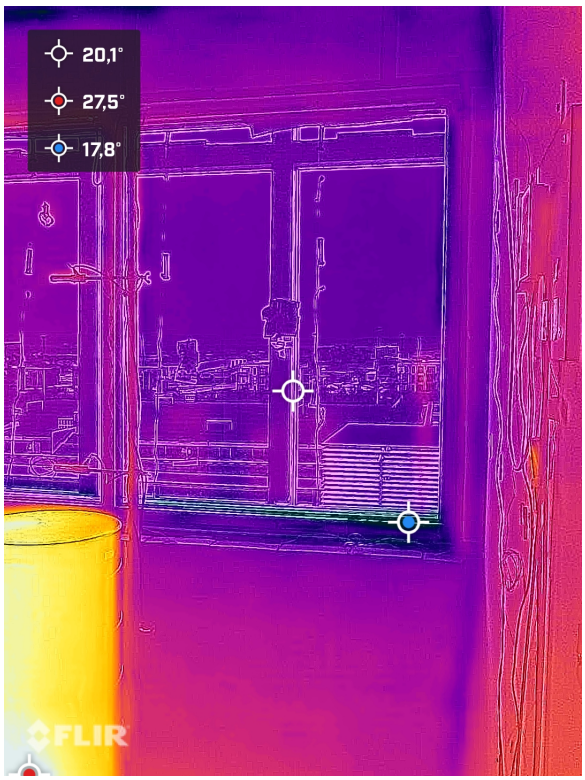

Figure 5.28: Thermal picture of South facade, taken with FLIR thermocamera.

5.2.3 DCV cavity

During the winter measurements, only 3 out of 6 thermocouples showed reliable data, therefore, Figure 5.29 only includes the measured temperatures from the thermocouples located at 2.75m from the South facade on the East line, and at 1m and 2.75m on the West line. The lowest temperature (16.6°C) occurred closest to the South facade, while the highest temperature (31.3°C) occurred in the West line near the northern part of the cavity.

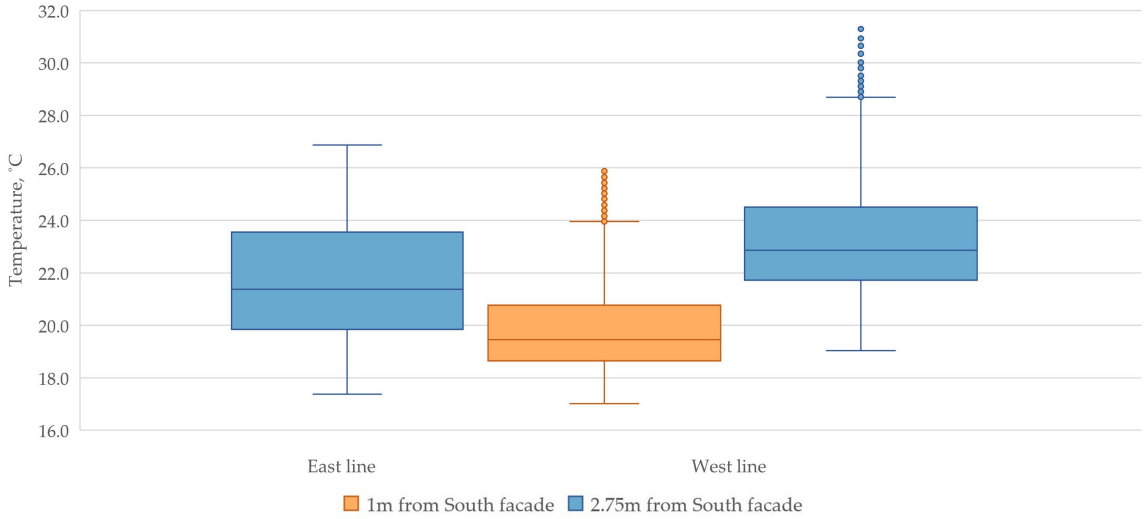

Figure 5.29: Whiskers-and-box plots of the measured temperatures in the plenum box for all hours. (30.11.2023-06.12.2023)

With regards to the outdoor conditions, Figure 5.30 visualises the air temperature distribution in the plenum box as a function of outdoor temperature. As during the winter measurement week the heating mode was operating, the temperature distribution in the DCV cavity was influenced by the air temperatures in the DSF cavity, therefore it was also dependent on the outdoor conditions. In both the East and West lines, generally lower temperatures occurred when the outdoor temperature was also low, while the highest temperatures can be observed when the outdoor temperature was the highest. In the East line, the temperature distribution was similar within and outside of the occupied period. Although, in the West line slightly higher temperatures are present between 8:00-15:00.

The need for optimization of the system is obvious in the DCV cavity analysis as well, considering that temperatures exceeded 30°C while the outdoor temperature was below 0°C. Consequently, the control strategy did not perform the required actions to optimize the temperature of the supply air to the Test room, resulting in the increased air temperature in the cavity affected by the internal load of the Test room.

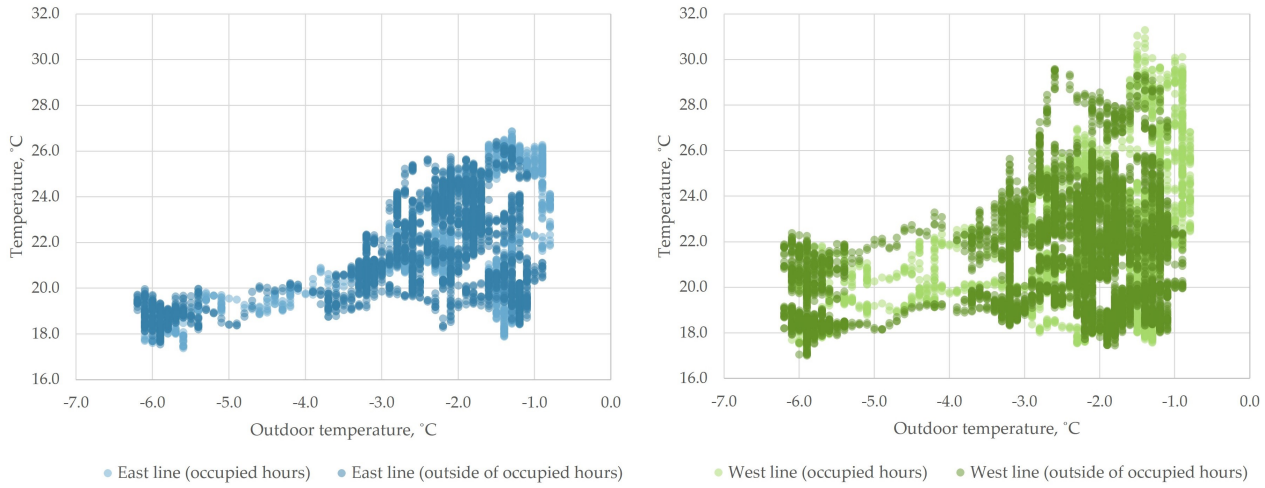

Figure 5.30: Dot plot of the measured temperatures in the plenum box as a function of outdoor temperature for all hours. (30.11.2023-06.12.2023)

When inspecting the hourly temperature distribution within the occupied period, 02.12.2023 (see Figure 5.31) serves as an example due to its coldest temperatures, however, the measurements for the first two days can be seen in Appendix 9.47-9.49. Noticeably, a non-uniform temperature distribution defines the DCV cavity, in which the temperatures increased during the day with the increasing outdoor temperatures and Test room temperatures. As described previously in section 5.1.3, the results of non-uniform temperatures in the plenum box are assumed to have occurred due to the uneven installation of the diffuse ceiling panels, causing irregular gaps.

Day 3			02/12/2023
Averages - 8:00-9:00			Average outdoor temperature: -5.80
	East line	West line	Average solar radiation: 4
1m	N/A	18.11	
2m	N/A	N/A	
2.75m	17.94	20.57	
Averages - 11:00-12:00			Average outdoor temperature: -3.29
	East line	West line	Average solar radiation: 8
1m	N/A	20.14	
2m	N/A	N/A	
2.75m	20.70	22.81	
Averages - 14:00-15:00			Average outdoor temperature: -2.26
	East line	West line	Average solar radiation: 41
1m	N/A	19.02	
2m	N/A	N/A	
2.75m	21.47	25.68	

Figure 5.31: Hourly averages of the measured temperatures in the DCV cavity. (02.12.2023)

5.2.4 Systems

Ventilation

The CO_2 concentration within the test room remained relatively stable at approximately 500 ppm, with minor fluctuations of ±60 ppm observed during the first and second days. This stability is to be expected, given the absence of human occupancy during these periods (see Figure 5.32). However, it is unknown why WindowMaster did not keep the artificially set 810ppm in the test room during the occupied hours as it did before in the intermediate case. This has changed since the November 20th.

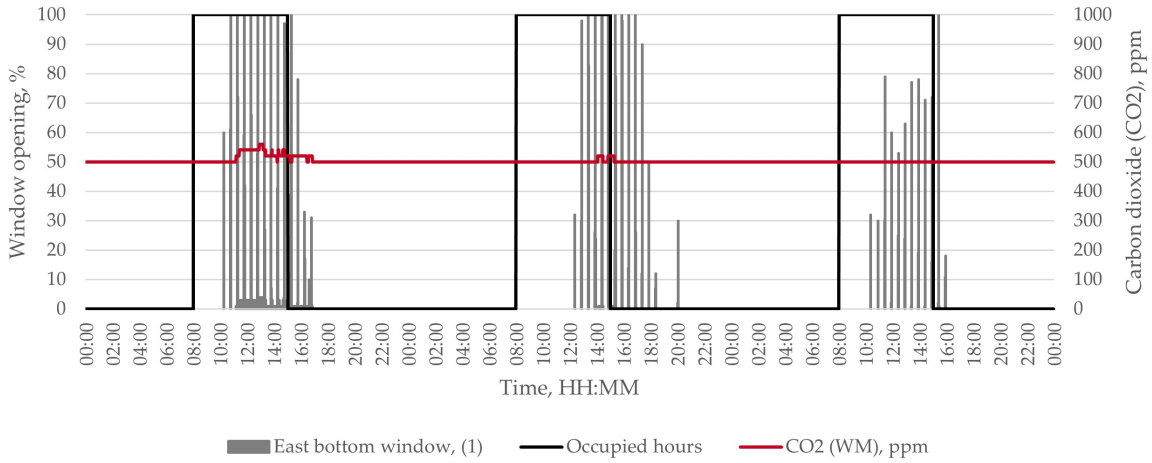

Figure 5.32: Window openings with regards to CO_2 concentration in the Test room. (30-11.2023 - 02.12.2023)

The exhaust ventilation from the collected data from Ultralink is seen on the first day to activate at 10:14, the second day at 12:19 and the third day at 10:21. See Figure 5.33. Compared to the first time the window opened during the occupancy, the exhaust ventilation was activated 2 minutes later the first two days and 1 minute later the last day.

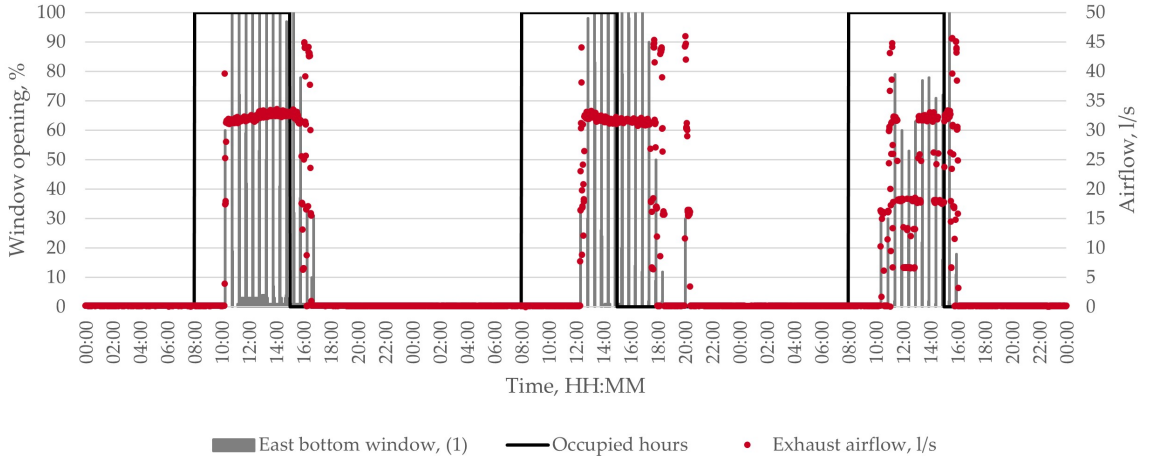

Figure 5.33: Window openings with regards to exhaust airflow in the Test room. (30-11.2023 - 02.12.2023)

In the exhaust ventilation, when not activated, the airflow sensor constantly logs around -0.18-0.19l/s, indicating some air movement between the spaces (The test room and the corridor where the air is discharged). During the occupied hours, the airflow at more lin-

ear times of the day is 32l/s, representing an air change rate of slightly above $8h^{-1}$, which suggests that the air in the space is changed more than eight times per hour. See Figure 5.34.

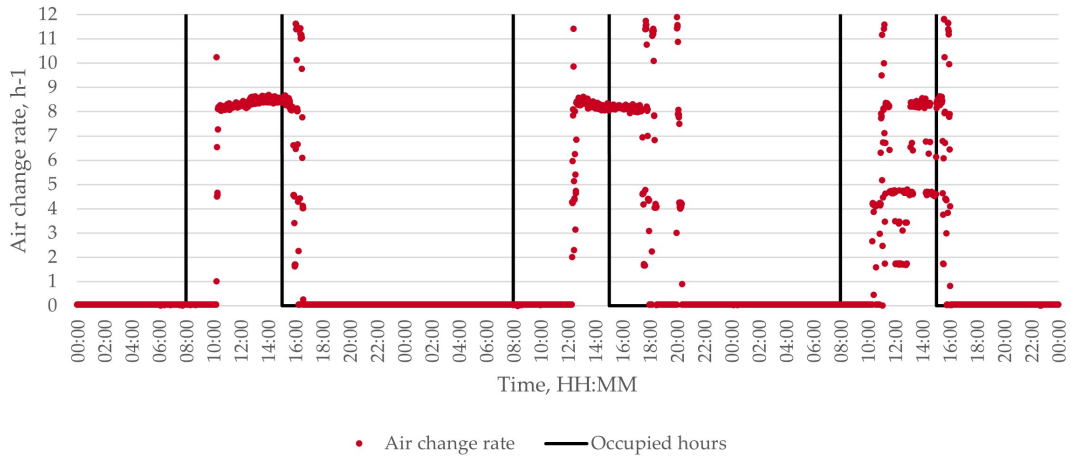

Figure 5.34: Window openings with regards to air change rate in the Test room. (30-11.2023 - 02.12.2023)

On the second day, the WindowMaster system initiated the opening of all bottom windows (1, 2, and 3) for a two-minute interval at 20:01-20:02, which may suggest a one-minute delay. Concurrently, the exhaust ventilation operated for 6 minutes starting at 20:00 with an airflow of approximately 44.3 l/s. Eighteen minutes into the cycle, the system reached a steady-state value. This change coincided with the WindowMaster setpoint transitioning to a lower value. The reason for fluctuating airflow during specific hours on the first two days and throughout the third day is due to the pulse ventilation, aiming to keep the minimum air change rate as the outdoor temperature is low.

The temperature data obtained from the thermocouples in the exhaust ventilation was deemed invalid due to errors. Consequently, the exhaust air temperature data presented in Figure 5.35 is a 5-minute running average calculated from all thermocouples on the north, middle, and south poles, ranging from 0.1 to 1.7m above the ground.

During the initial day and the next day until 8:00, during non-occupied hours, the temperature within the DCV cavity was higher than in the Test room. This phenomenon is likely due to heat generated during the day, rising towards the ceiling and accumulating in the cavity, particularly when the space is not ventilated. On the second day, a contrasting pattern emerged, with the DCV cavity temperature remaining lower throughout the occupancy hours. The reason for this inversion is not immediately apparent. Notably, a drop in the DCV temperature was recorded when the window was opened. On the third day, the most significant temperature disparity was experienced, coinciding with the lowest recorded outdoor air temperatures.

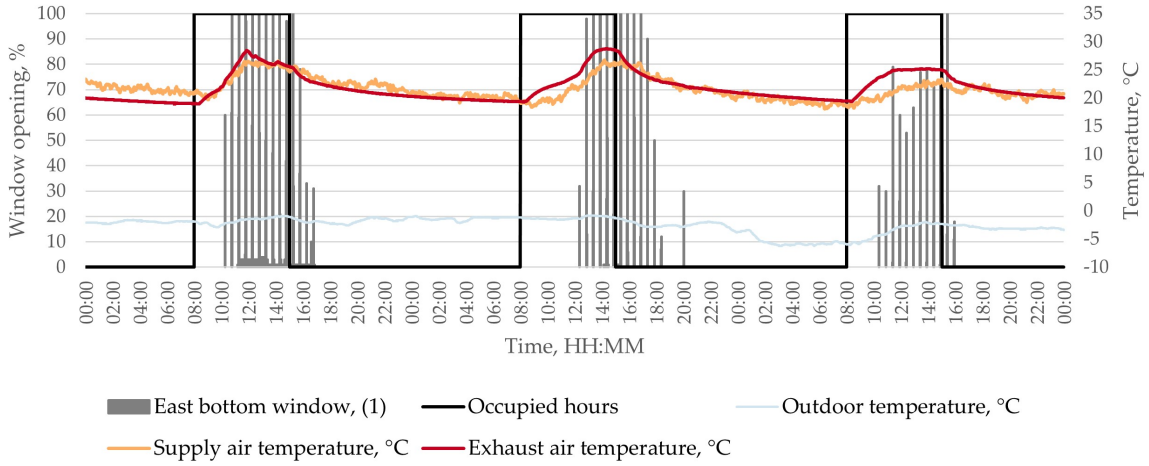

Figure 5.35: Window openings with regards to supply and exhaust air temperature in the Test room. (30-11.2023 - 02.12.2023)

Space heating

During the winter case measurement, the electric space heater operated from 8:22 to 15:16 on the first two days and from 8:22 to 15:14 on the third day. According to data collected from the Power Detective device, the daily energy consumption was 790W on the first day, 767W on the second, and 774W on the third.

In Figure 5.36, the graph illustrates the variance in the frequency of the heater's operation over three days. On the first day, the heater cycled down to 1Wh 40 times, increased to 63 times on the second day, and then decreased to 52 times on the third day. More frequent cycling is expected to occur on days when internal and external conditions lead to greater heat loss or when the heater responds to more significant temperature fluctuations.

Examining the outdoor air temperature raises the question of why the space heater did not consume the most energy to maintain the indoor temperature at the "II" setting predominantly on the third day, especially since it was the coldest. This inconsistency suggests that factors other than the outdoor temperature influenced the heater's energy usage and operational frequency.

The window opening analysis observed that the window was opened less frequently on the third day due to the DCV and DSF cavity temperatures being below the setpoint, as depicted in Figure 5.21. The reduced window opening would lead to less room cooling, resulting in a lower air change rate. Additionally, it was noted that the wind speed, according to WindowMaster, was below 1m/s on that day (5.20), which could indicate a lower infiltration rate. These factors combined might explain why the space heater did not need to use as much energy to maintain the indoor temperature on the coldest day, as both reduced window openings and lower wind speeds would contribute to retaining more heat inside the room. Furthermore, the retained heat from heat emitters (such as occupants, equipment, and space heating) and solar radiation, though it was the lowest that day, could have played a role. Additionally, the building materials in the room could have stored heat energy from the previous day and slowly released it, further contributing to a warmer indoor environment.

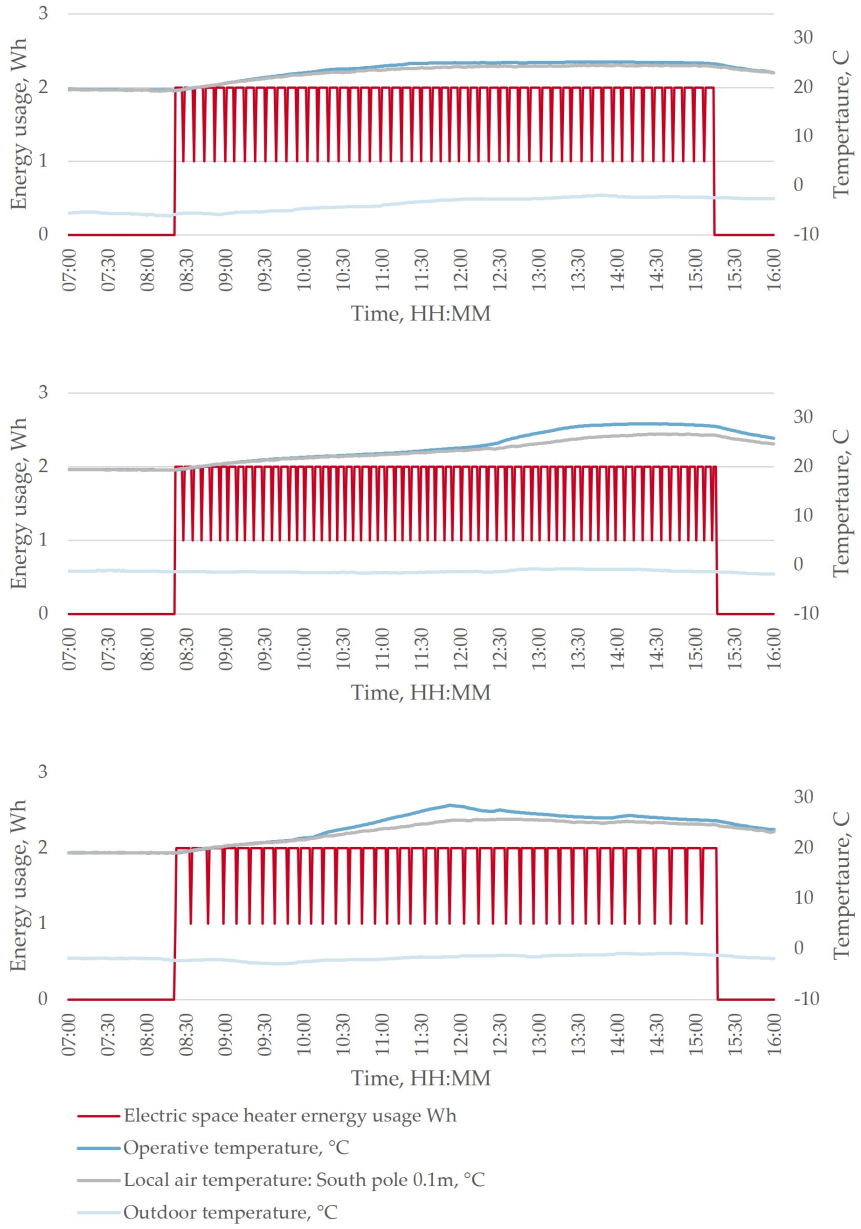

Figure 5.36: Data of electric space heater energy usage in the Test Room during winter measurements, with Day 1 at the bottom, ascending to Day 3 at the top.(30-11.2023 - 02.12.2023)

5.3 Summary

The heating control mode is investigated in two measurement periods: for an intermediate week between 23-26.10.2023, and for a winter week between 30.11.2023-02.12.2023.

During the intermediate week, the control mode activated the bottom row windows to open in the occupied period, every day from 8:00-15:00. The outdoor conditions affected the opening percentage of the windows, as with a higher windspeed the windows opened to a smaller degree, while with a higher outdoor temperature, the windows opened to a

larger degree. Within approximately half an hour after the first window opening in the mornings, the operative temperature in the Test room decreased, however, after that the operative temperature increased. This implies the need to optimize the control focusing on preheating in the mornings, to provide a comfortable environment by the occupants arrive. However, sufficient preheating of the air was confirmed during the occupancy, as the highest temperatures were recorded in the Test room, while the temperatures in the DCV cavity were lower, and the lowest temperatures occurred in the DSF cavity. Additionally, neither the setpoint for the Test room nor the setpoints for the cavities were ever reached during the intermediate measurement week.

On the contrary, during the winter measurement week, the windows first opened when the setpoint in the Test room was reached and kept operating until the setpoint was no longer exceeded. Therefore, an inconsistent window opening trend was present during all three days. Concerning the outdoor conditions, primarily the outdoor temperature defined the opening percentages of the windows as it was snowing and the temperature was mainly below zero, while the windspeed was insignificantly low during the three measurement days. The presence of snow during the measurement period is an essential factor to consider, especially in its potential impact on the weather station's solar radiation readings, and its high albedo effect. Accordingly, a constant increase in operative temperature in the room can be observed from 8:00 due to the internal loads, as the WindowMaster only started operating after the setpoint was reached, a minimum of 2 hours after the occupied period began. Remarkably, the air temperatures in the DSF cavity even exceeded (first day) or were equal (second day) to the Test room's operative temperature. However, the air temperatures in the DCV cavity were mostly lower than in the DSF cavity during the occupied hours, while the opposite was true outside of the occupancy. This phenomenon highlights the requirement of the control system to improve the control strategy in order to avoid overheating even during cold outdoor temperatures.

DSF cavity

The preheating of air during the intermediate week is notable within the temperature distribution in the West and middle lines, as the tendencies of increasing temperature with the increasing height of the thermocouples were demonstrated, with the highest temperatures occurring at the bypass area. However, for the East line the thermocouples located at 1.34m, 1.87m, and 2.41m, the temperatures were lower than the temperatures recorded by the ones placed at 0.265m and 0.80m, and the doubt of adequate calibration is posed. Furthermore, the influence of the operating WindowMaster was evident in the bottom thermocouples that are located close to the windows, as the opening/closing of the windows was followed by temperature decrease/increase, indicating the system's sensitivity towards the outdoor conditions. This effect was reduced for the higher-located thermocouples. The setpoint was not reached during the intermediate week, identifying that the heating mode could be optimized to aim for higher preheating performance.

Comparably to the intermediate case, during winter, the temperature distribution displayed similar tendencies, with the same issue occurring in the East line at the heights of 1.34m, 1.87m, and 2.41m. As the separation between the cavities was closed during the occupied hours until the WindowMaster first opened the windows, the bypass thermo-

couples measured significantly higher temperatures during this period, which equalized during the day with the opened state of the separation. Furthermore, temperatures appeared to be more uniform and generally higher in the cavity (0.265m-2.41m), despite the lower outdoor temperatures. However, the sensitivity towards the opening windows of the thermocouples located close to them was more obvious. While the high temperatures measured in the cavity displayed great potential for the heating mode during winter, the risk of overheating should be addressed.

DCV cavity

The measurements from the intermediate week indicated a generally non-uniform temperature distribution within the DCV cavity, due to the internal heat load in the Test room. Moreover, the opened state of the separation between cavities during the heating mode caused the dependency of the air temperatures in the DCV cavity on the temperatures in the DSF cavity. Therefore, indicating a sensitivity towards the altering outdoor conditions as well. As the lowest temperature measured in the cavity was 15°C, the risk of local discomfort due to draught emerges. Consequently, the optimization of control is recommended to ensure a uniform and possibly higher supply air temperature within the occupied zone.

The winter measurements displayed a similar tendency to the intermediate case, regarding the non-uniform temperature distribution. However, higher temperatures occurred in the cavity, proving the possibility of a more efficient preheating result. Additionally, the risk of overheating should be considered by improving the control hence optimal air temperatures can be supplied into the Test room. The dependency of DCV cavity temperatures on the DSF cavity temperatures is similarly significant when the separation is open between the cavities.

Systems

The mechanical extraction within the intermediate measurement week was activated between 8:00-15:00, as the CO_2 level was automatically set to exceed the allowed limit and to be constantly at 810ppm during occupancy, and as the windows were correspondingly opening/closing within the same time interval. Therefore, a continual airflow extraction of 34.5l/s was established during the occupied hours, while during the unoccupied hours, the mechanical ventilation was not operating. This confirms the appropriate operation of control concerning providing fresh air continuously to the Test room. Additionally, during the occupancy, the highest temperature was measured by the thermocouples placed inside the exhaust diffuser, while the operative temperature was slightly lower, and the supply temperature displayed the lowest temperatures. However, outside of the occupancy when the system was not operating, all three locations showed similar values with insignificant temperature differences. Lastly, the electrical space heater did not activate with the set position of (I).

Opposingly to the intermediate week, during winter the scheduled presence of occupants was not detectable by the automatically set CO_2 concentration as it stagnated around

500ppm during the three days. Likewise, the operation of mechanical ventilation showed inconsistency, especially on the third day. The extraction started with a 1-2 minute delay after the first window openings in the mornings; however, the airflow in the first two days did not reach the steady value of 32l/s until approximately 10-20 minutes had passed, while fluctuations defined the third day. Consequently, this finding poses the risk of unsatisfactory air quality, as fresh air was not provided in the Test in the first couple hours of the occupancy period. Therefore, the control system needs to be adjusted to consider this issue, despite severe outdoor conditions. In addition, for the supply and exhaust temperatures, the same tendency was valid as for the intermediate case, as the average temperatures measured in the DCV cavity were lower than the operative and exhaust temperatures. Additionally, the electrical space heater setting was increased to position (II), resulting in operating during the three days, with the energy consumption between 767-790W.

Chapter 6

Global thermal comfort in the Test room

The analysis begins with examining the operative temperature at a given clothing and activity level in the Test room. Following this, a standardised global thermal comfort analysis method is applied, which involves calculating the PMV and determining if the given environment meets the required comfort category. In addition, the PPD is calculated to quantify the proportion of individuals likely to be thermally dissatisfied. Finally, the findings from these assessments are used to determine the IEQ categories into which the analysed environment falls. These analyses are performed for different year periods: summer, intermediate, and winter.

This section presents only the results from analysed data regarding global thermal comfort. For details on the calculation method, refer to Chapter 2.1.

6.1 Summer case

Operative temperature

In the summer analysis of the Test room, from July 24th to 30th, 2023, data show operative temperatures varying in sync with the patterns of solar radiation and outside air temperatures—increasing during the day and decreasing at night. See Figure 6.1.

These variations sometimes lead to indoor temperatures falling below the IEQ Category III comfort standard for summer classrooms, ideally between 22-27°C for an assumed clothing insulation of 0.5 and a metabolic rate of 1.2 met.

The WindowMaster system consistently recorded temperatures about 2.5°C higher than the estimated room operative temperatures, indicating a possible discrepancy due to calibration issues, environmental influences, or inaccurate temperature estimations.

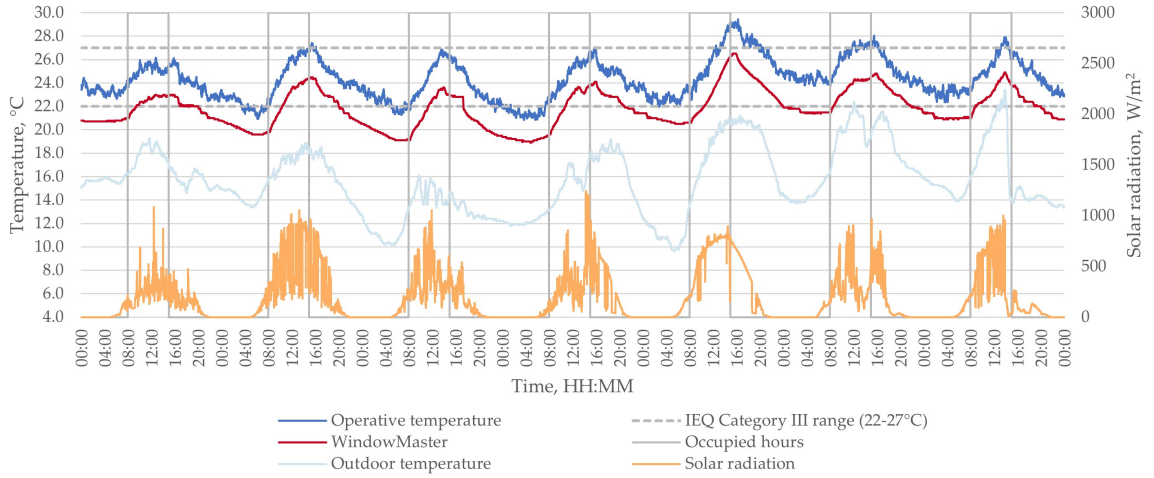

Figure 6.1: Operative temperature in the Test room and outdoor conditions (24-30.07.2023; All hours).

During the occupancy hours of 8:00 to 15:00 in the Test room, the operative temperature was within the optimal IEQ range for 41% of the time in Category I, 59% in Category II, 87% in Category III, and 98% in Category IV. See Figure 6.2. These statistics indicate a risk for overheating, as the percentages for temperatures are too high, particularly in Categories I and II. Conversely, too-low temperatures affect less than 12% of the occupied time across the first three categories.

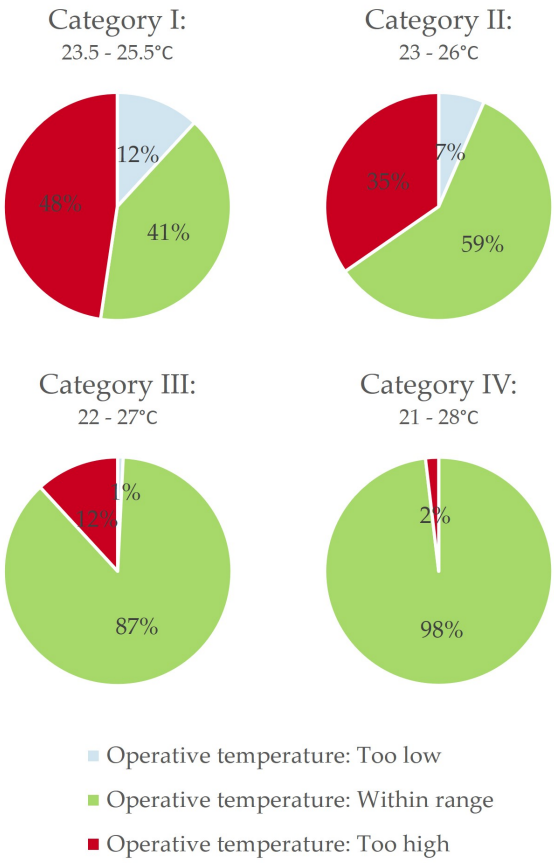

Figure 6.2: Percentage occupied time, the operative temperature in the Test room is within the indoor environmental quality categories.
(24-30.07.2023; 8:00-15:00)

Predicted mean vote (PMV) and predicted percentage of dissatisfied (PPD)

The MRT data, pivotal for assessing the PMV and PPD during occupancy hours, indicates warmer conditions at the South pole, likely influenced by more intense direct sunlight or warmer surroundings. The North pole's average MRT is notably cooler, registering 4°C less than the South pole. The MRT at the Middle pole is marginally lower than that at the North pole. See Figure 6.3.

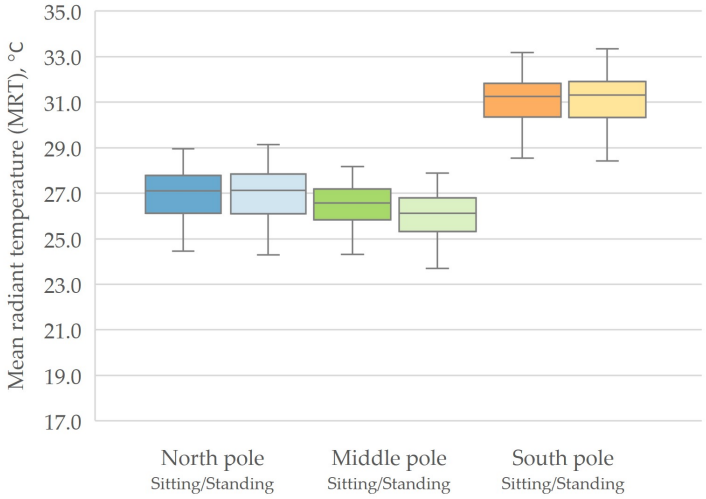

Figure 6.3: Mean radiant temperatures (MRT) for a sitting and standing person in three positions (North, Middle, South) in the Test room during the occupied hours. (24-30.07.2023; 8:00-15:00)

The thermal comfort analysis is restricted to sitting positions at the Middle and South poles due to the absence of data for other conditions. At the Middle pole, occupants experience cooler thermal comfort, with the PMV falling below zero most of the time, indicating a cooler bias in thermal sensation. Correspondingly, the predicted dissatisfaction is low, with less than 17% of occupants likely to be uncomfortable. See Figure 6.5.

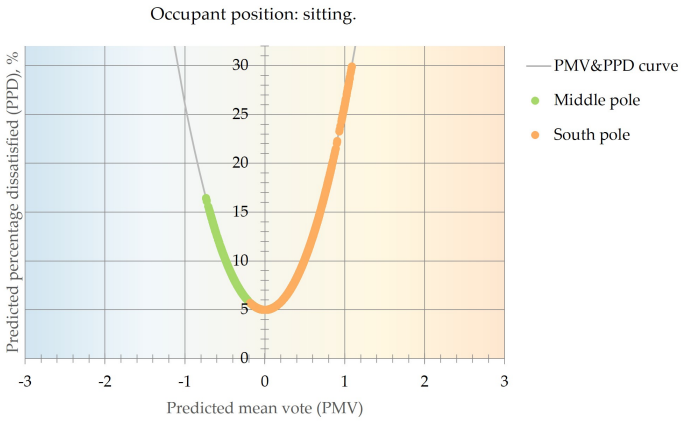

Figure 6.4: Predicted mean vote (PMV) and Predicted percentage dissatisfied (PPD) for a sitting and standing person in three positions (North, Middle, South) in the Test room during the occupied hours. (24-30.07.2023; 8:00-15:00)

In contrast, while not extreme, the South pole leans towards a warmer thermal sensation as indicated by the positive PMV values. Up to 30% of occupants are predicted to be dissatisfied here, suggesting a less comfortable environment compared to the Middle pole.

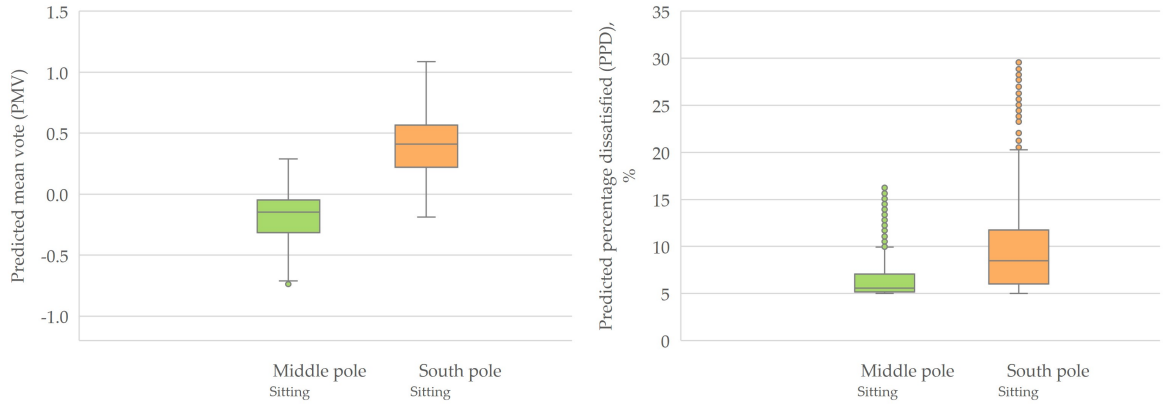

Figure 6.5: Predicted mean vote (PMV) and Predicted percentage dissatisfied (PPD) for a sitting and standing person in three positions (North, Middle, South) in the Test room during the occupied hours. (24-30.07.2023; 8:00-15:00)

When evaluating the IEQ Categories for the PMV, data for sitting positions at both the Middle and South poles span all four IEQ categories. At the South Pole, there is a deviation where 2% of the occupied time records a PMV exceeding the value of 1, placing it outside the standard categories. This detail is illustrated in Figure 6.6. The Middle pole demonstrates a more thermally comfortable position within the room, with higher percentages of time falling within the more desirable first categories for both PMV and PPD, compared to the sitting position at the South pole. Data for standing positions and the sitting position at the North pole are not available due to errors in the datalogs.

PMV		Category I (-0.2<PMV<0.2)	Category II (-0.5<PMV<0.5)	Category III (-0.7<PMV<0.7)	Category IV (-1.0<PMV<1.0)	Out of categories
Sitting	North pole	N/A	N/A	N/A	N/A	N/A
	Middle pole	58%	92%	100%	100%	0%
	South pole	22%	65%	89%	99%	1%
Standing	North pole	N/A	N/A	N/A	N/A	N/A
	Middle pole	N/A	N/A	N/A	N/A	N/A
	South pole	N/A	N/A	N/A	N/A	N/A

PPD		Category I (PPD<6%)	Category II (PPD<10%)	Category III (PPD<15%)	Category IV (PPD<25%)	Out of categories
Sitting	North pole	N/A	N/A	N/A	N/A	N/A
	Middle pole	62%	91%	100%	100%	0%
	South pole	25%	64%	88%	98%	2%
Standing	North pole	N/A	N/A	N/A	N/A	N/A
	Middle pole	N/A	N/A	N/A	N/A	N/A
	South pole	N/A	N/A	N/A	N/A	N/A

Figure 6.6: As a percentage of occupied time, the PMV and PPD was within the Indoor Environmental Quality (IEQ) category ranges for a sitting and standing person in three positions (North, Middle, South) in the Test room. (24-30.07.2023; 8:00-15:00)

6.2 Intermediate case

Operative temperature

The room's operative temperature was comparatively stable for the intermediate season, spanning November 23rd to 26th, 2023, with modest fluctuations during daylight hours. The indoor temperature reflected the solar radiation patterns, while outdoor temperatures remained relatively steady. See Figure 6.7.

During non-occupied and early occupied hours (first day for 01:11h, second day for 00:56h, third day for 00:58h, fourth day for 2:23h), the indoor temperatures fell below the IEQ Category III standard for winter classrooms, where the ideal temperature range is 20-24°C, accounting for clothing insulation of 1.0 and metabolic rate of 1.2 met.

In contrast to the summer observations, the WindowMaster measurements closely matched the operative temperatures recorded by the K-type thermocouple in the Test room during this intermediate season.

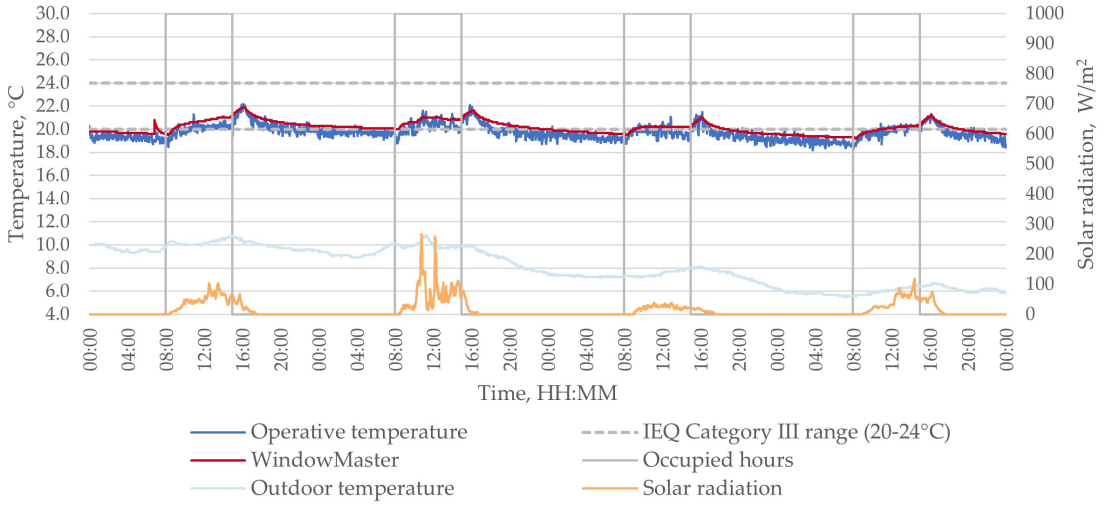

Figure 6.7: Operative temperature in the Test room and outdoor conditions (23-26.10.2023; All hours).

In the intermediate measurement period, the occupied time percentages within the IEQ range are 2% for Category I, 49% for Category II, 96% for Category III, and 100% for Category IV. The pie charts in Figure 6.4 suggest a prevalent issue of temperatures falling below the recommended range, particularly in Categories I and II, where there is a significant risk of the operative temperature being too low for a big part of the occupied time.

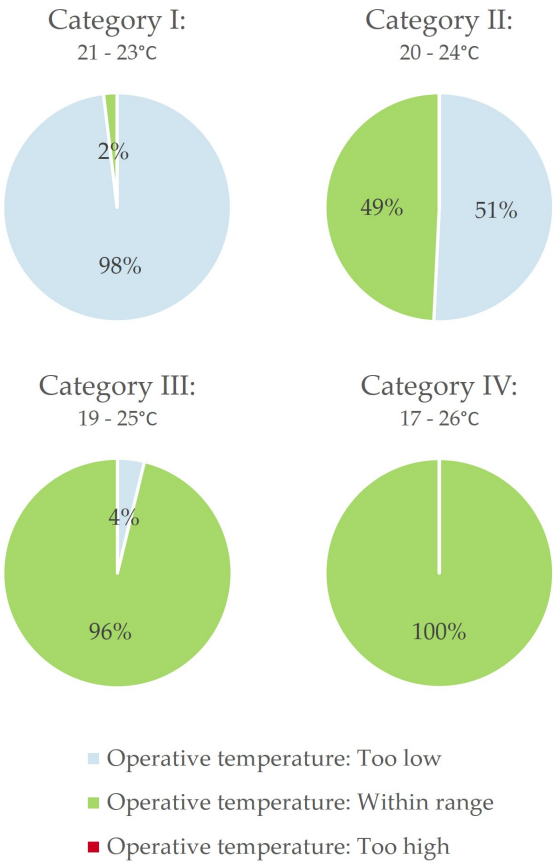

Figure 6.8: Percentage occupied time, the operative temperature in the Test room is within the indoor environmental quality categories.
(23-26.10.2023; 8:00-15:00)

Predicted mean vote (PMV) and predicted percentage of dissatisfied (PPD)

The South pole consistently records the highest MRT in line with the summer conditions. The North pole follows with an MRT average that is 4°C cooler, while the Middle pole's MRT values are just slightly below those of the North pole. See Figure 6.9.

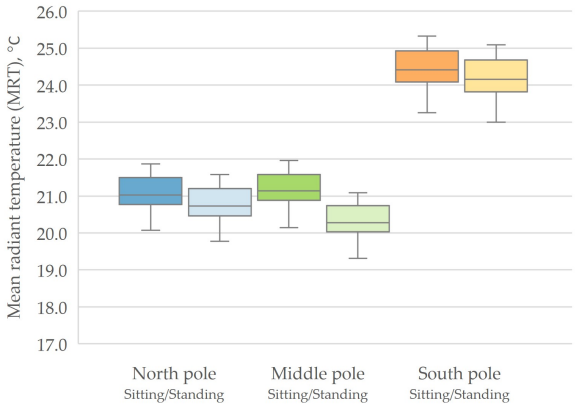

Figure 6.9: Mean radiant temperatures (MRT) for a sitting and standing person in three positions (North, Middle, South) in the Test room during the occupied hours. (23-26.10.2023; 8:00-15:00)

The box plot, in Figure 6.10, offers insight into the thermal experiences at various room locations during occupancy. The PMV index points to a generally cool environment, with most values falling between -0.2 and -1.0. It is observed that individuals in sitting positions report better thermal comfort than those standing, based on their respective PMV scores. The North and Middle poles show similar PMV patterns, ranging from -0.6 to -1.0, associated with a PPD of 14-27%. Conversely, the South pole presents a tighter PMV span of -0.2 to -0.6, corresponding to a notably lower PPD of 6-13%, suggesting a slight deviation from the cooler comfort conditions at the other poles.

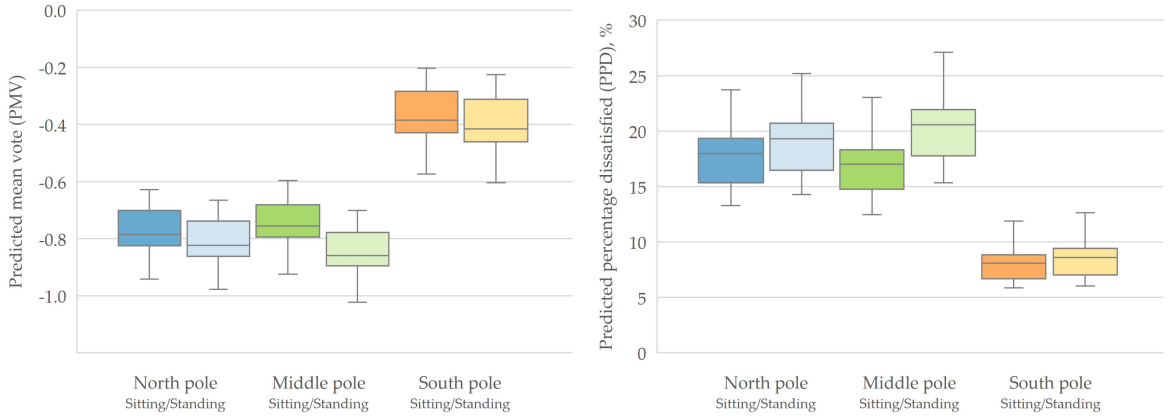

Figure 6.10: Predicted mean vote (PMV) and Predicted percentage dissatisfied (PPD) for a sitting and standing person in three positions (North, Middle, South) in the Test room during the occupied hours. (23-26.10.2023; 8:00-15:00)

The data on IEQ categories for sitting and standing persons in three distinct room positions (North, Middle, South) during occupancy hours present a clear differentiation in comfort levels. See Figure 6.12. A significant portion of the time, specifically over 83%, occupants in the South pole, whether sitting or standing, have their PMV and PPD within Category II. This suggests a thermal comfort where the PMV is between -0.5 and 0.5, and the PPD is below 10%, indicating minimal thermal dissatisfaction among the occupants.

In other positions—North and Middle poles—primarily fall within Category IV for both sitting and standing postures during the occupied times. Category IV represents a less

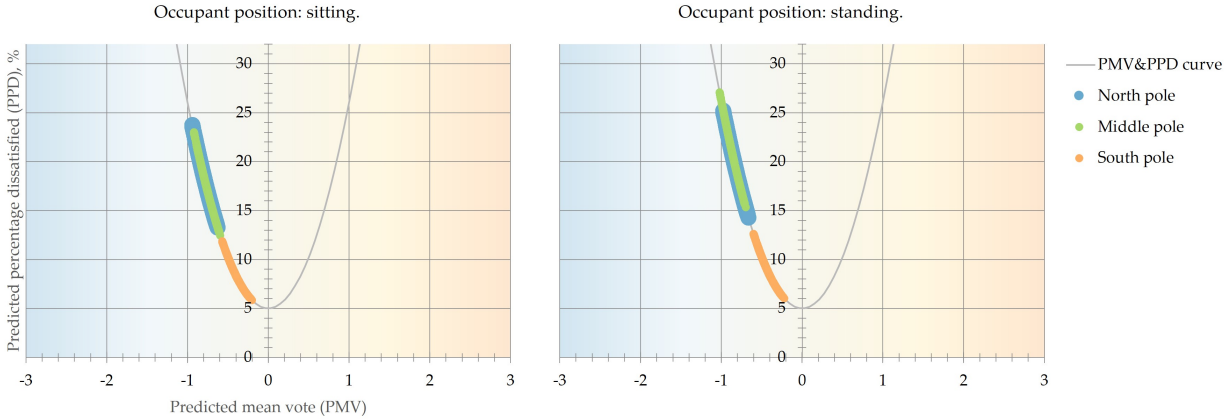

Figure 6.11: Predicted mean vote (PMV) and Predicted percentage dissatisfied (PPD) for a sitting and standing person in three positions (North, Middle, South) in the Test room during the occupied hours. (23-26.10.2023; 8:00-15:00)

desirable thermal environment where the PMV deviates further from the neutral range and the PPD reaches up to 25%.

PMV		Category I (-0.2<PMV<0.2)	Category II (-0.5<PMV<0.5)	Category III (-0.7<PMV<0.7)	Category IV (-1.0<PMV<1.0)	Out of categories
Sitting	North pole	0%	0%	25%	100%	0%
	Middle pole	0%	0%	33%	100%	0%
	South pole	0%	92%	100%	100%	0%
Standing	North pole	0%	0%	10%	100%	0%
	Middle pole	0%	0%	0%	98%	2%
	South pole	0%	86%	100%	100%	0%

PPD		Category I (PPD<6%)	Category II (PPD<10%)	Category III (PPD<15%)	Category IV (PPD<25%)	Out of categories
Sitting	North pole	0%	0%	23%	100%	0%
	Middle pole	0%	0%	28%	100%	0%
	South pole	1%	88%	100%	100%	0%
Standing	North pole	0%	0%	5%	99%	1%
	Middle pole	0%	0%	0%	94%	6%
	South pole	0%	83%	100%	100%	0%

Figure 6.12: As a percentage of occupied time, the PMV and PPD was within the Indoor Environmental Quality (IEQ) category ranges for a sitting and standing person in three positions (North, Middle, South) in the Test room. (23-26.10.2023; 8:00-15:00)

Operative temperature validation

Figure 6.13 shows the operative temperature data obtained via different methods and instruments in the Test room during the intermediate case measurement time 23-26.10.2023:

- **K-type thermocouple:** Inside a tennis ball, this sensor is designed to mimic the thermal absorption characteristics of the human body. It is mounted on the middle pole at a height of 0.6 meters above the floor, aligning with the average centre of mass for a person seated to yield a measure of temperature that is representative of the conditions experienced by occupants.
- **IC-meter:** Positioned near the K-type thermocouple.
- **WindowMaster:** This sensor is placed on the interior east wall of the Test room.
- **Summer method:** This approach determines operative temperature by averaging air temperature data collected at various heights on three poles – North, Middle, and South – within the room.
- **DS 7726 standard:** According to this standard, the operative temperature is computed by the equation $t_o = A \cdot t_a + (1 - A) \cdot t_r$, where t_a is the air temperature, t_r is the mean radiant temperature, and A is a coefficient adjusted for air velocity. [19]

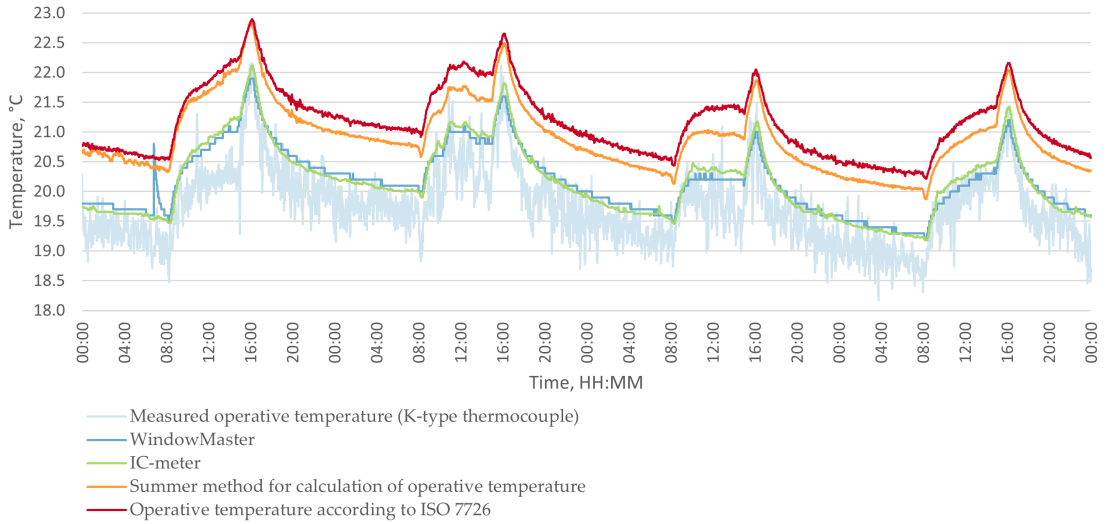

Figure 6.13: Operative temperature? analysis in the Test room. (23-26.10.2023; All hours)

The operative temperatures recorded using these methods generally range between 18.5°C and 22.5°C. The trends, including the peaks and downturns in temperature, are observed consistently across all methods. The K-type thermocouple, IC-meter, and WindowMaster sensor display closely matching temperature readings. In contrast, the summer method and the DS 7726 standard, while mirroring the same trends, report temperatures that are consistently about 0.5°C higher than those measured by the K-type thermocouple, IC-meter, and WindowMaster sensor.

6.3 Winter case

Operative temperature

During the three measurement days, the operative temperature—an average derived from thermocouples at the North, Middle, and South poles at heights from the ground of 0.1, 0.6, 1.1, and 1.7m—varied between 19.0°C and 28.8°C. See Figure 6.14 Compared with the room's air temperature measured by WindowMaster, the estimated operative temperature shows nearly identical readings, with an average discrepancy of just 0.5°C.

The trend observed in the graph indicates that the operative temperature consistently falls below the optimal IEQ Category III range (20-24°C) during the night and early morning each day. Conversely, the temperature exceeds this range during midday, likely due to internal loads and solar radiation. This pattern suggests a risk of temperatures being uncomfortably cold in the morning and too warm around midday within the same day, highlighting potential challenges in maintaining thermal comfort throughout the day.

Although the coldest outdoor air temperatures are recorded during the early morning hours of the last days, the operative temperature within the room does not correspondingly reach its lowest at those times. This indicates that the indoor environment may have some thermal inertia or other moderating factors that prevent the operative temperature from dropping as quickly as the outdoor temperature, resulting in a more stable indoor climate in the morning.

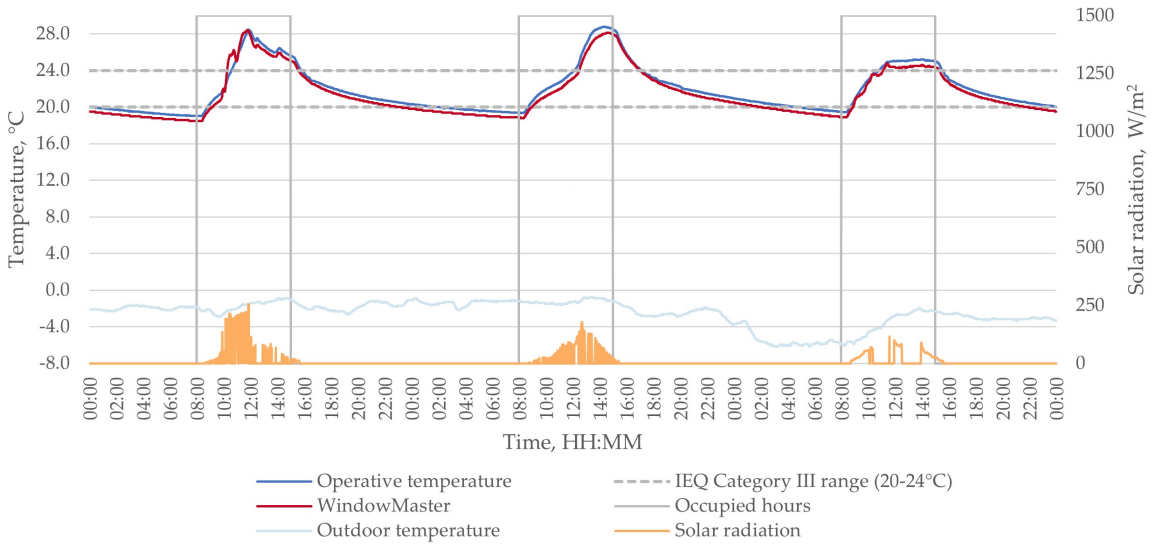

Figure 6.14: Operative temperature in the Test room and outdoor conditions (30-11.2023 - 02.12.2023; All hours).

Data in Figure 6.15 indicates that during the total occupied time, the operative temperature was within the optimal range for IEQ Category I only 19% of the time, Category II 35% of the time, Category III 53% of the time, and Category IV 74% of the time, which highlights the difficulty in maintaining ideal temperature conditions within all categories. While only the first two categories experienced too low operative temperatures, all categories

experienced too high temperatures.

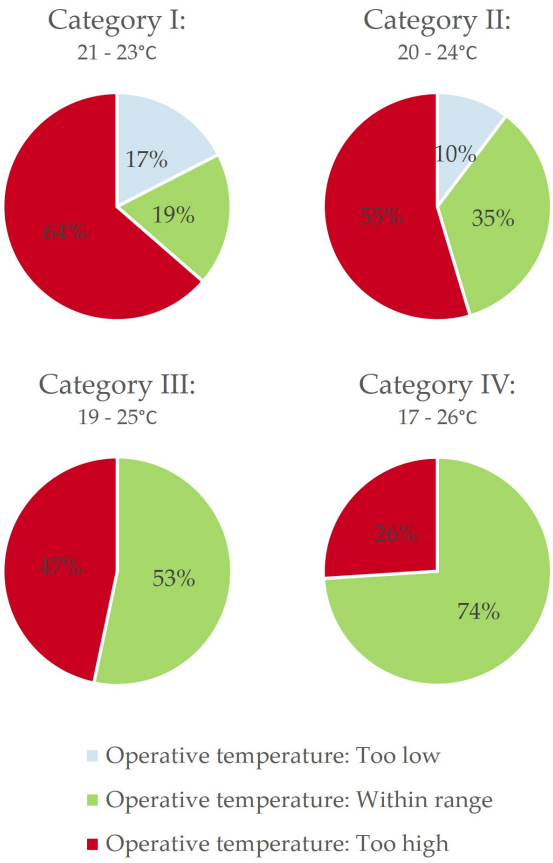

Figure 6.15: Percentage occupied time, the operative temperature in the Test room is within the indoor environmental quality categories.
(30-11.2023 - 02.12.2023; 8:00-15:00)

Predicted mean vote (PMV) and predicted percentage of dissatisfied (PPD)

The box plot in Figure 6.16 illustrates MRT measured at three different positions within a room: North pole, Middle pole, and South pole, considering both sitting and standing positions.

The South pole's sitting and standing positions display mean radiant temperatures that are approximately 5°C higher on average compared to the North and Middle pole positions. Additionally, the overlap of interquartile ranges for sitting and standing at each pole indicates that posture minimally impacts the mean radiant temperature experienced at these locations.

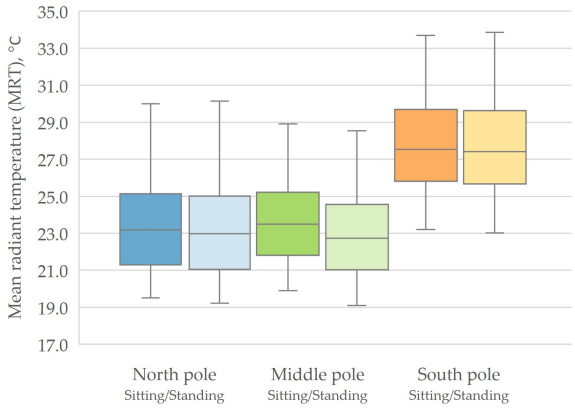

Figure 6.16: Mean radiant temperatures (MRT) for a sitting and standing person in three positions (North, Middle, South) in the Test room during the occupied hours. (30-11.2023 - 02.12.2023; 8:00-15:00)

The boxplots in Figure 6.17 illustrate the PMV and PPD at the North and South poles, encompassing both sitting and standing positions. The analysis excludes data from the Middle pole due to errors at the ankle level, 0.1m off the ground.

PMV values for the North pole are predominantly negative, suggesting a cooler sensation for occupants in both sitting and standing positions. Correspondingly, the PPD values average around 9.6%, with an interquartile range from about 5.8% to 17.6%.

Conversely, at the South pole, PMV values are primarily positive, indicating a warmer sensation. The PPD values here are slightly lower, averaging 8.1%, with a narrower IQR extending from 5.9% to 11.9%, reflecting a lower average dissatisfaction among occupants. However, there is a cluster of extreme outliers, with PPD values as high as approximately 38.4%, suggesting an increased discomfort.

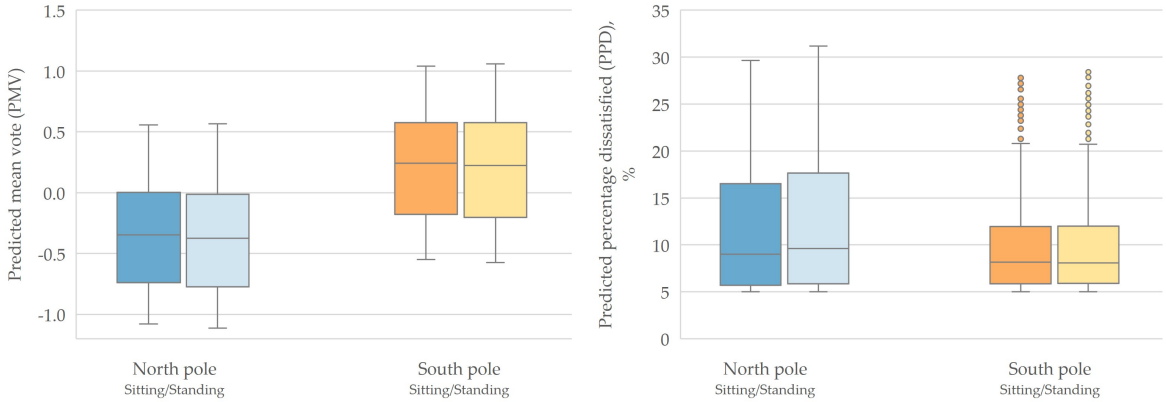

Figure 6.17: Predicted mean vote (PMV) and Predicted percentage dissatisfied (PPD) for a sitting and standing person in three positions (North, Middle, South) in the Test room during the occupied hours. (30-11.2023 - 02.12.2023; 8:00-15:00)

The PMV and PPD values for the winter measurement days during occupied hours, according to the IEQ Categories, show a distribution of comfort across all categories, including instances that fall outside these categories. See Figure 6.19.The data indicates that the sitting and standing positions at the South pole are more thermally acceptable than those at

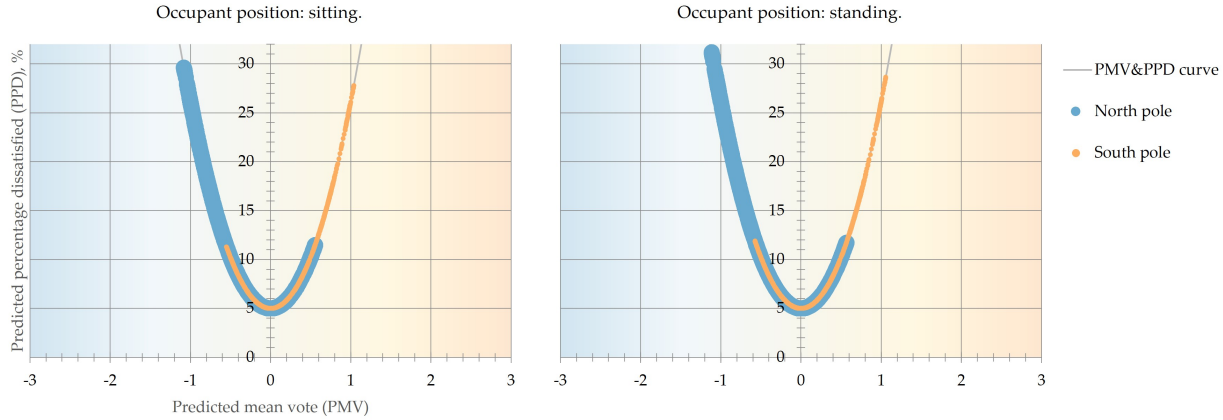

Figure 6.18: Predicted mean vote (PMV) and Predicted percentage dissatisfied (PPD) for a sitting and standing person in three positions (North, Middle, South) in the Test room during the occupied hours. (30-11.2023 - 02.12.2023; 8:00-15:00)

the North pole. Data for sitting and standing positions at the Middle pole are unavailable due to errors in the datalogs.

PMV		Category I (-0.2<PMV<0.2)	Category II (-0.5<PMV<0.5)	Category III (-0.7<PMV<0.7)	Category IV (-1.0<PMV<1.0)	Out of categories
Sitting	North pole	29%	57%	72%	94%	6%
	Middle pole	N/A	N/A	N/A	N/A	N/A
	South pole	25%	70%	86%	99%	1%
Standing	North pole	25%	53%	70%	90%	10%
	Middle pole	N/A	N/A	N/A	N/A	N/A
	South pole	23%	67%	86%	98%	2%

PPD		Category I (PPD<6%)	Category II (PPD<10%)	Category III (PPD<15%)	Category IV (PPD<25%)	Out of categories
Sitting	North pole	33%	55%	71%	90%	10%
	Middle pole	N/A	N/A	N/A	N/A	N/A
	South pole	27%	69%	85%	97%	3%
Standing	North pole	29%	52%	69%	88%	12%
	Middle pole	N/A	N/A	N/A	N/A	N/A
	South pole	26%	65%	85%	96%	4%

Figure 6.19: As a percentage of occupied time, the PMV and PPD was within the Indoor Environmental Quality (IEQ) category ranges for a sitting and standing person in three positions (North, Middle, South) in the Test room. (30-11.2023 - 02.12.2023; 8:00-15:00)

6.4 Comparing thermal comfort in the Test room: Classrooms vs. Kindergarten

The primary global comfort analysis for the PMV and PPD for classroom occupants, both seated and standing, the DS 17772 recommended values were adopted. However, in reality, the metabolic rate is more complex and dynamic. As indicated by DS 8996, the metabolic rate varies based on several factors: the intensity of the body segment involved, age - with younger people generally exhibiting higher rates than adults, and gender - where women typically have a slightly lower metabolic rate than men. Generally, a standing person has a higher metabolic rate, approximately 20W more, than a sitting person.

Clothing insulation can also vary according to occupants' adjustment: occupants might wear a sweater when they feel cold or remove it if the indoor environment becomes excessively warm. Nonetheless, research indicates that younger occupants are less likely to modify their clothing insulation in response to minor deviations in temperature [5]. Furthermore, it has been noted that the recommended clothing insulation values in the DS designed for adults align with the younger humans during the winter season [9].

In other standards, such as DS 15251, for kindergarten spaces, the metabolic rate increases to 1.4. At the same time, the clothing insulation remains the same at 0.5 for the summer season and 1.0 for winter. This standard also provides a table with slightly lower recommended temperature ranges for indoor environments across three categories than those in DS 17772. See Figure 6.20.

Type of space	Activity, W/m²	IEQ	Operative temperature,°C	
		Category	Summer, cooling season (0.5 clo)	Winter, heating season (1.0 clo)
Kindergarten	81 (1.4 met)	I	22.5 - 24.5	19 - 21
		II	21.5 - 25.5	17.5 - 22.5
		III	21 - 26	16.5 - 23.5

Figure 6.20: Recommended temperature ranges for kindergartens with an activity level of 1.4 were met. [**DS 15251**]

In the next part, the analysis investigates the Test room as both a classroom and a kindergarten, examining the operative temperature ranges for overall thermal comfort according to DS 17772. To understand the suitability of the Test room.

In the same Test room environment, the operative temperatures measured in summer (see Figure 6.21) and winter (see Figure 6.22) are compared against the recommended temperature ranges for both classroom and kindergarten settings. These settings consider a metabolic rate of 1.2 met and clothing insulation levels of 0.5 clo in summer and 1.0 clo in winter, in line with the four (IEQ) categories outlined in DS 17772 for classrooms. Conversely, the kindergarten room scenario, characterized by a metabolic rate of 1.4 met and identical clothing insulation values, is examined under the three IEQ categories specified by DS 15251.

The Figures illustrate the percentage of time the temperature remains within the optimal range (green), falls too low (blue), or rises too high (red) for each category in both settings.

The classroom environment, with a metabolic rate of 1.2 met, exhibits a higher percentage of operative temperature within the ideal range across all categories compared to the kindergarten, which has a metabolic rate of 1.4 met. The kindergarten, on the other hand, shows a higher percentage where the temperature exceeds the maximum recommended range for all three categories in summer and winter conditions. While the classroom experiences slightly cooler than ideal temperatures for Category I, II and III, the kindergarten predominantly maintains temperatures above the ideal range, with only Category I experiencing instances of being too cool in summer data.

To ensure the classroom remains within the appropriate temperature ranges for a higher percentage of the time, it is necessary to maintain the temperature at the start of occupancy at no less than 23°C to meet Category II's minimum during the cooling season, and at least 20°C during the heating season. Additionally, it is crucial to cool the room effectively during midday peaks to prevent exceeding the recommended temperature range, which varies depending on the targeted IEQ category.

The analysis also considered the PMV and the North, Middle, and South Pole locations for both space scenarios. (See Appendix 9.8). However, the results showed a deviation from the optimal operative temperature ranges. Suggesting that with a metabolic rate of 1.4 met—a rate representative of activity levels in a kindergarten—fewer individuals are likely to be dissatisfied with the thermal comfort. This discrepancy can likely be attributed to the need to adjust the body surface area in the PMV calculation to represent better pupils, as well as modify the PMV ranges themselves.

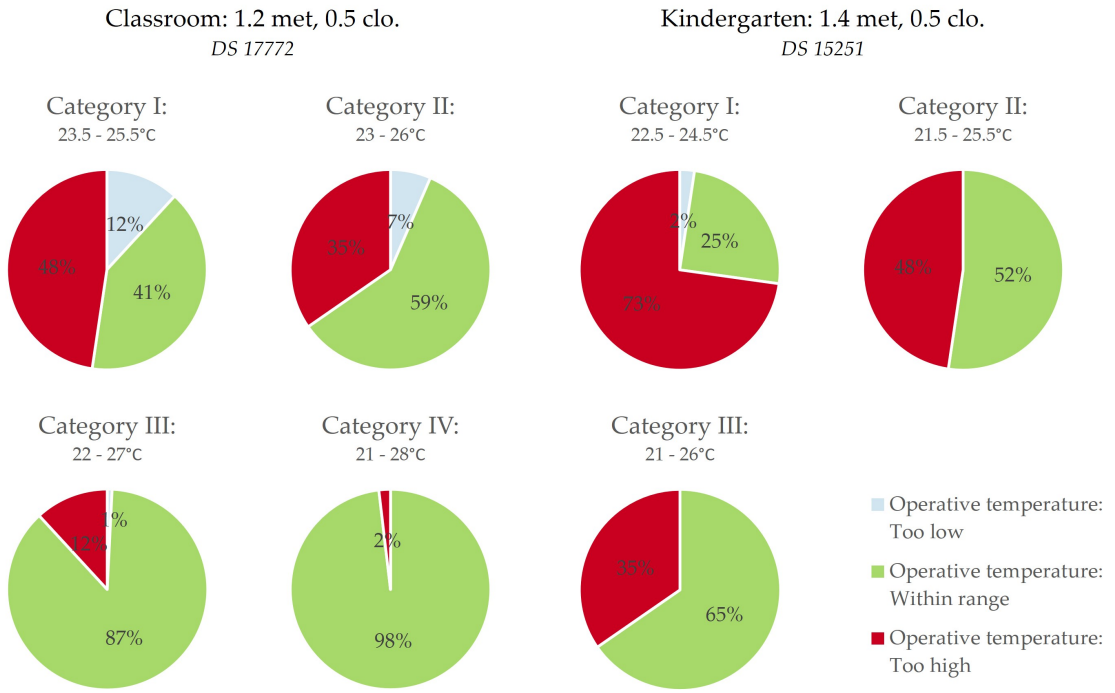

Figure 6.21: Percentage occupied time, the operative temperature in the Test room is within the indoor environmental quality categories for classroom and kindergarten cases. (24-30.07.2023 SUMMER; 8:00-15:00)

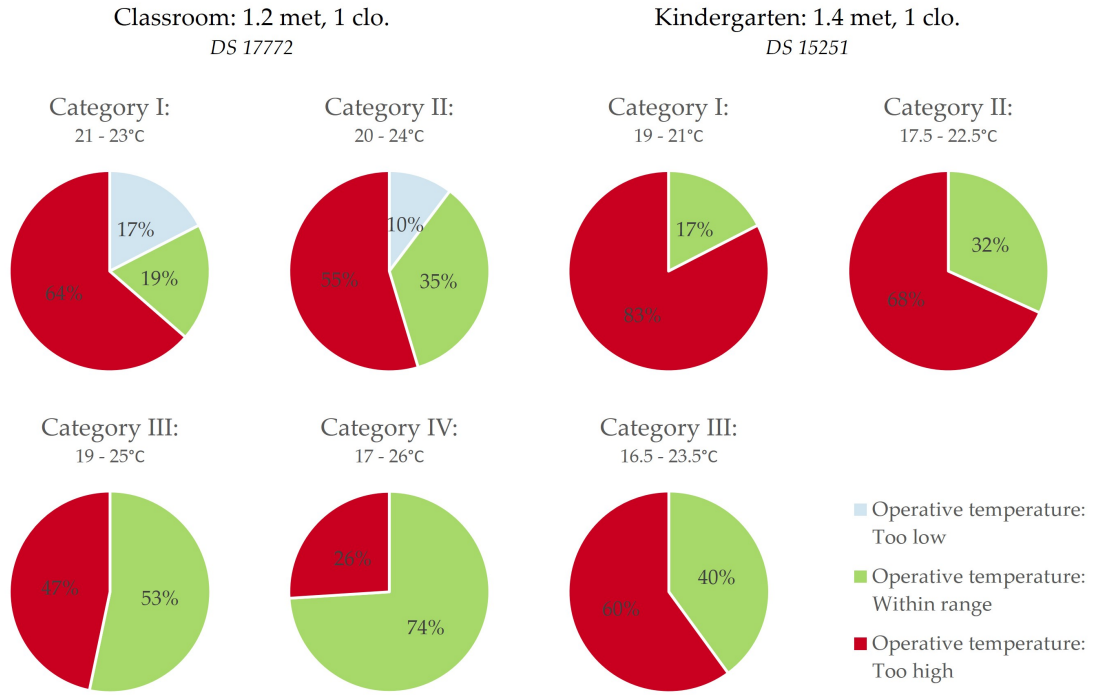

Figure 6.22: Percentage occupied time, the operative temperature in the Test room is within the indoor environmental quality categories for classroom and kindergarten cases. (30.11.2023-06.12.2023 WINTER; 8:00-15:00)

6.5 Summary

With the aim of summarising the assessment of global comfort in the Test room, Figure 6.23 displays the findings concerning the categorisation of the operative temperature, predicted mean vote and predicted percentage of dissatisfied across the three investigated seasons.

The operative temperature during the summer measurement period predominantly satisfied category I (with 40.5%) according to DS 17772, although the temperatures generally appear to be too high, and 1.9% does not fulfil any categories due to overtemperatures. Moreover, large daily fluctuations occur within the operative temperature measurements that align with the change in outdoor conditions. In contrast, during the intermediate measurement period, the temperatures within the Test room remained stable with minor fluctuations within the occupancy. The categorisation of operative temperature mainly falls into categories II (47.3%) and III (47.0%) due to the too low temperatures occurring in the mornings. To avoid these low temperatures, an electric space heater was incorporated into the measurement campaign during winter, which resulted in overheating in the Test room. Therefore, for 26.0% of the occupancy, none of the DS 17772 categories were achieved, while category I was fulfilled for 19.0%. Furthermore, low temperatures (minimum of 19.0°C) defined the beginning of the occupied hours, followed by a significant increase (up to 28.8°C) during the day.

With regards to PPD and PMV, for the summer case, only the Middle and South locations are evaluated with a sitting position due to data availability. The assessment revealed that the Middle position is more favourable, as the thermal sensation is “slightly cool”, mainly achieving category I. However, the thermal sensation at the South position falls on the “warm” side of the scale, primarily fulfilling category II.

For the intermediate scenario, both the sitting and standing positions for all locations display a “slightly cool” sensation, although the sitting position generally indicates better thermal satisfaction. The North and Middle positions display similar values, as the highest category achieved both for PMV and PPD during the measurements was category III. Furthermore, the least favourable position is a standing position at the Middle pole, as the PPD resulted in 94.4%, in category IV while 5.6% did not achieve any categories. On the contrary, the South location results in higher values on the scale, for which the majority of results regarding PMV and PPD belong to category II, both for the sitting and standing positions.

During the winter measurement period, the calculation of PMV and PPD values for the Middle location are excluded due to data availability. The PMV calculation indicates a prevailing "cool" environment for the North location, while opposingly a "slightly warm" environment is dominant at the South location. Consequently, the South location provides a smaller dissatisfaction rate than the North location amongst the occupants. However, in all cases, it occurred that the PPD calculation did not reach any categories defined by DS 7730.

The comparison of optimal operative temperature ranges between classrooms and kindergartens indicates that younger pupils, with their smaller body surface area and higher

metabolic rate, would require even stricter temperature control in the Test room, as they tend to prefer lower indoor temperatures. However, these results are not included in the summary tables.

			SUMMER					INTERMEDIATE					WINTER				
			Category I	Category II	Category III	Category IV	No category	Category I	Category II	Category III	Category IV	No category	Category I	Category II	Category III	Category IV	No category
Operative temperature			40.5%	18.3%	28.6%	10.7%	1.9%	1.9%	47.3%	47.0%	3.8%	0.0%	19.0%	16.1%	18.2%	20.7%	26.0%
PMV	Sitting position	North			N/A			0.0%	0.0%	24.9%	75.1%	0.0%	28.7%	27.9%	15.4%	22.2%	5.8%
		Middle	58.0%	34.0%	7.7%	0.3%	0.0%	0.0%	0.0%	33.0%	67.0%	0.0%			N/A		
		South	22.4%	43.0%	23.4%	9.9%	1.3%	0.0%	91.7%	8.3%	0.0%	0.0%	24.8%	45.4%	15.8%	13.1%	0.9%
	Standing position	North			N/A			0.0%	0.0%	9.5%	90.5%	0.0%	24.8%	28.1%	16.7%	19.9%	10.5%
		Middle			N/A			0.0%	0.0%	0.0%	97.5%	2.5%			N/A		
		South			N/A			0.0%	85.5%	14.5%	0.0%	0.0%	23.3%	43.4%	19.1%	12.5%	1.7%
PPD	Sitting position	North			N/A			0.0%	0.0%	23.2%	76.8%	0.0%	33.2%	21.7%	15.7%	19.6%	9.8%
		Middle	62.1%	29.2%	8.3%	0.4%	0.0%	0.0%	0.0%	28.4%	71.6%	0.0%			N/A		
		South	25.0%	38.9%	24.6%	9.6%	1.9%	1.0%	87.2%	12.8%	0.0%	0.0%	26.9%	41.9%	16.0%	11.9%	3.3%
	Standing position	North			N/A			0.0%	0.0%	4.9%	94.1%	1.0%	29.4%	22.4%	16.9%	19.3%	12.0%
		Middle			N/A			0.0%	0.0%	0.0%	94.4%	5.6%			N/A		
		South			N/A			0.0%	83.0%	17.0%	0.0%	0.0%	25.9%	39.6%	19.4%	11.0%	4.1%

Figure 6.23: Summary of the evaluation of the global thermal comfort in the Test room.

Chapter 7

Local thermal comfort in the Test room

This chapter presents the assessment of local thermal comfort in the Test room, including the determination of the draught rate, vertical air temperature difference, discomfort due to the floor surface temperature, and radiant temperature asymmetry. Moreover, the percentage of dissatisfied is calculated for each factor, and the evaluation of results is categorized according to DS 7730. The analysis is concluded for the following seasonal periods: summer, intermediate, and winter.

As only the results regarding local thermal comfort from the analysed data are displayed in this section, see Chapter 2.1 for details on the calculation method.

7.1 Summer case

Draught rate

During the summer measurement period, the draught rate analysis faced limitations due to incomplete velocity and air temperature data. Nevertheless, the evaluation proceeded for the Middle and South poles at heights of 0.1m, 0.6m, and 1.1m from the floor, with the North pole included at 0.1m and 0.6m.

Figure 7.1 illustrates that the majority of DR values stayed below the 10% threshold. During occupancy hours, the DR remained within Category I for 98.5% of the time, signifying comfortable airflow conditions for occupants. Only 1.5% of the time did the DR touch upon Category II, indicating a negligible increase in perceived draught. See Figure 7.2.

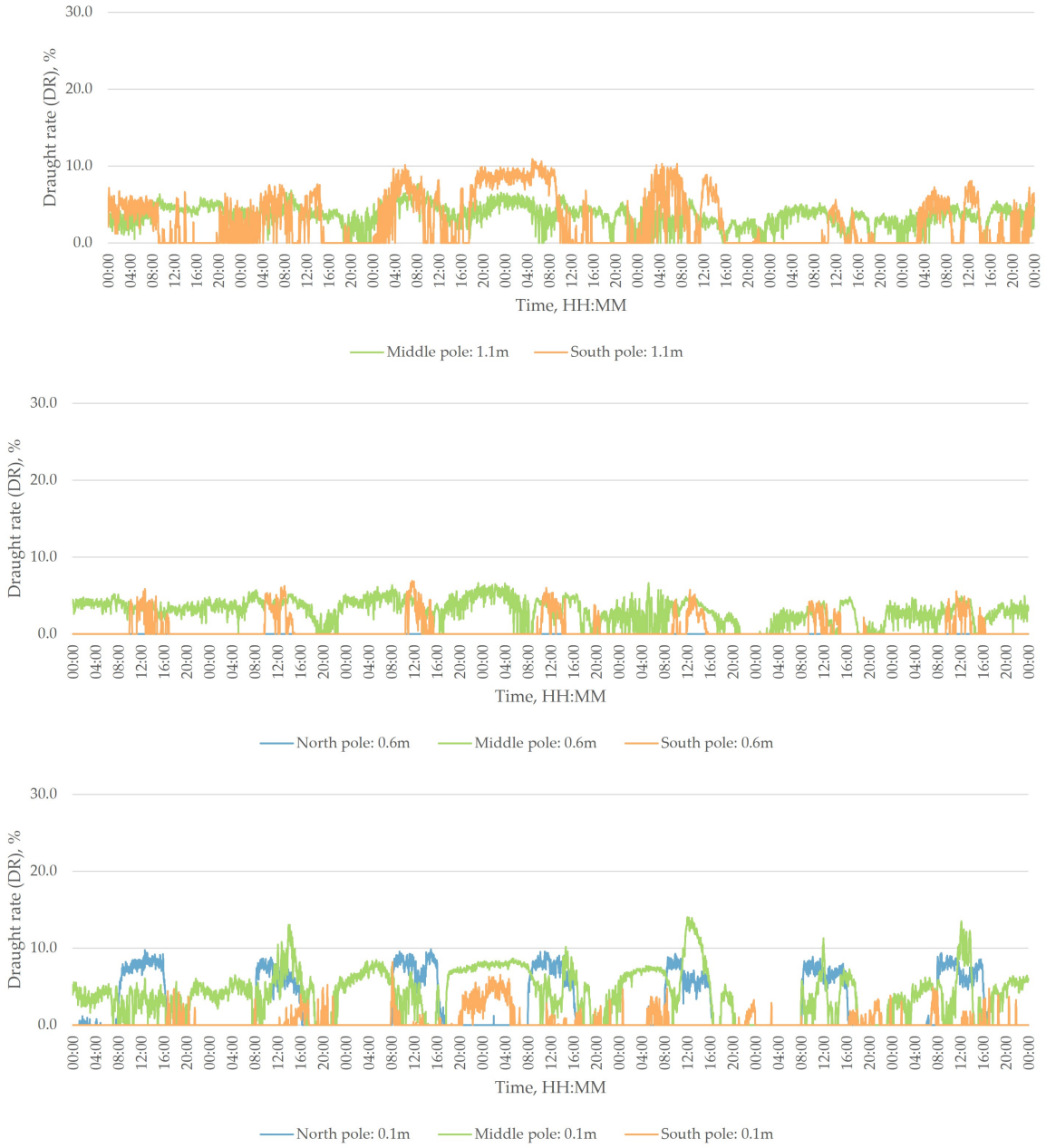

Figure 7.1: North, Middle and South pole draught rates at at differetn height from the ground (Occupied zone) in the Test room. (24-30.07.2023; All hours)

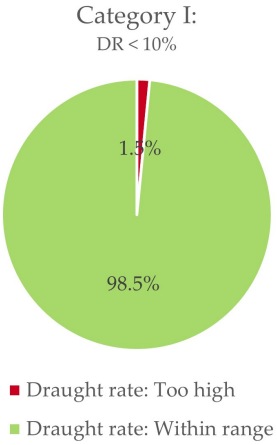

Figure 7.2: Percentage of total occupied time, the draught rate in the Test room is within the IEQ Category I range (23-26.10.2023; 08:00-15:00)

Vertical air temperature difference

The vertical air temperature difference between the ankle and head of a sitting person is analysed during the occupied hours for three positions in the Test room: North pole, Middle pole, and South pole. From Figures 7.3 and 7.4, it can be concluded that for the vast majority of the measurement period, the vertical air temperature difference falls into category A according to DS 7730 (see Figure 2.8). However, the results for the North and South positions exceed 2°C for 11.0% and 7.4% respectively of the total measurement time. Therefore, 8.3% of the North pole results fall into category B and 2.6% to category C, whereas for the South pole 7.3% belong to category B and 0.1% to category C. Furthermore, 0.1% of the results for the North position did not satisfy any categories, as on 28.07.2023 the temperature difference reached a maximum of 4.02°C.

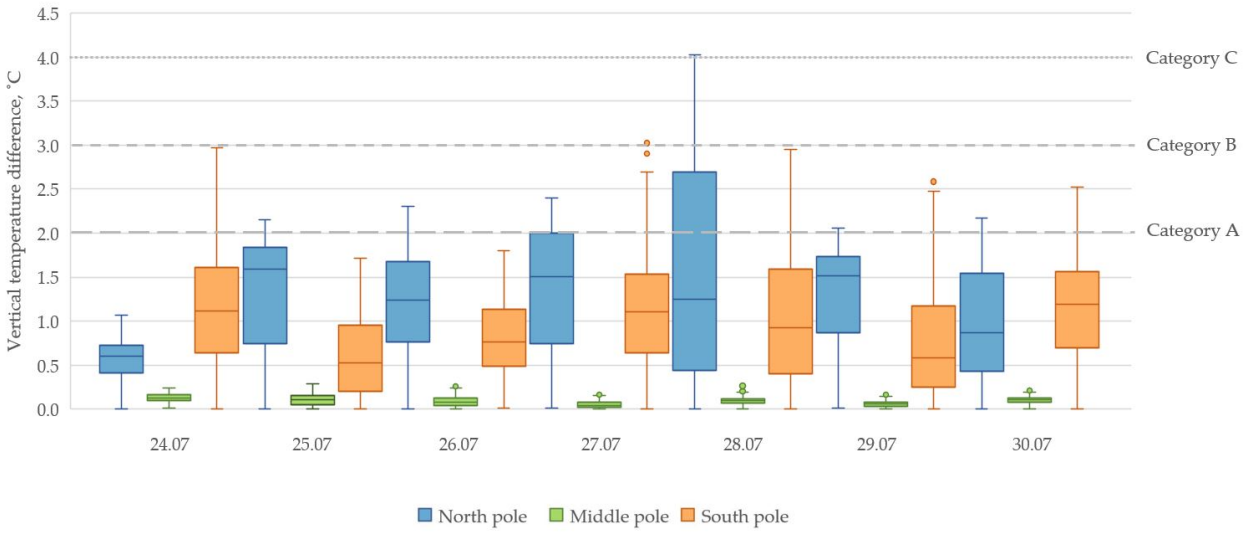

Figure 7.3: Vertical air temperature difference between ankle (0.1m) and head of a sitting person (1.1m) during occupied hours. (24-30.07.2023; 8:00-15:00)

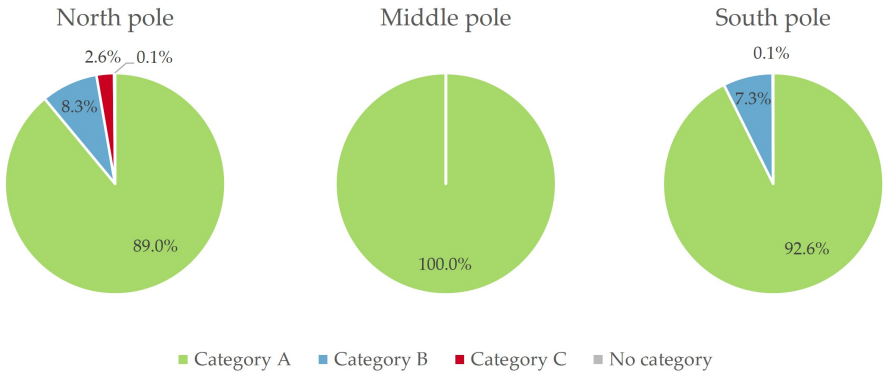

Figure 7.4: Vertical air temperature difference between ankle (0.1m) and head of a sitting person (1.1m) during occupied hours. (24-30.07.2023; 8:00-15:00)

Considering the percentage of dissatisfied, Figure 7.5 demonstrates that 0.3-0.4% of the occupants located in the middle of the room are dissatisfied, while up to 4.0% at the South position, and up to 8.9% at the North position are dissatisfied. Therefore, the Northern part of the room is the most critical regarding the vertical air temperature difference.

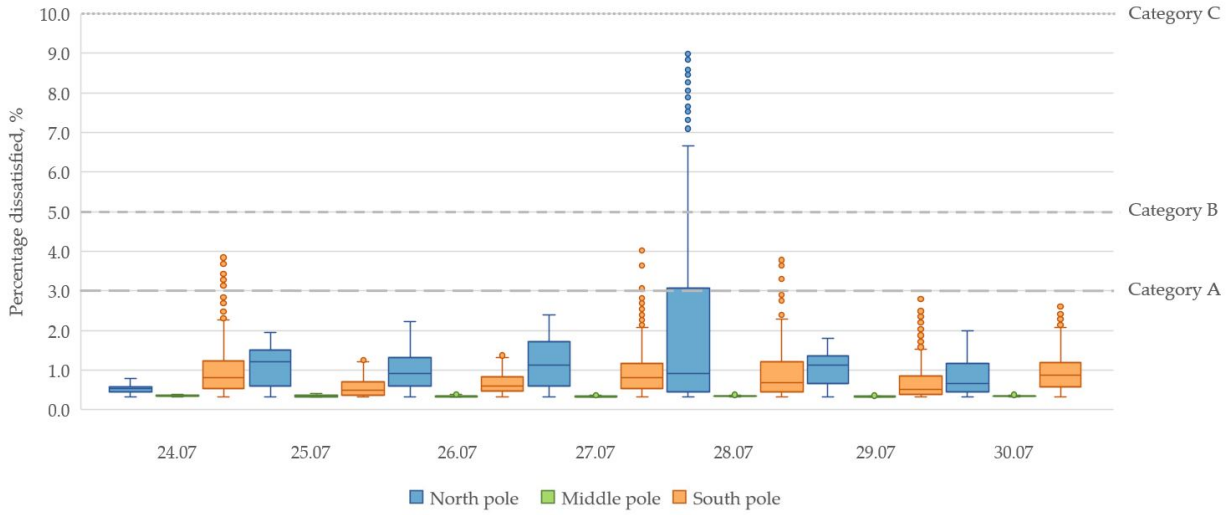

Figure 7.5: Percentage dissatisfied due to vertical air temperature difference between ankle (0.1m) and head of a sitting person (1.1m). (24-30.07.2023; 8:00-15:00)

Floor surface temperature

As the recorded data displays unrealistic temperatures during the summer measurement period, the discomfort due to the surface temperature of the floor is not evaluated.

Radiant temperature asymmetry

To assess the risk of thermal discomfort due to radiant asymmetry, the calculations are carried out for the cases of a sitting and a standing person placed in the middle of the room, 0.2m away from the North wall, and 0.2m away from the South wall during the occupied hours. However, the lack of data concerning the floor surface temperature resulted in including only the RTA due to the walls. Furthermore, as 100% of the values for each

position fall into the highest comfort category, the findings are displayed for the case of a sitting person located in the middle of the room as an example, while the results for the remaining positions can be obtained in Appendix 9.9. The relevant angle factors are calculated according to DS 7726, and can be seen in 9.6 Appendix D.

Sitting person in the middle of the room

In the case of a centrally placed subject in a sitting position, the plane radiant temperature difference between the opposite walls is displayed in Figure 7.6. For the North-South asymmetry the results vary between 0.7°C and 2.0°C, while for the West-East asymmetry, it is between 0.3°C and 1.9°C. As the values are below 23°C, category A/B is fulfilled according to DS 7730. Furthermore, the calculation the percentage of dissatisfied occupants revealed that there is no risk of discomfort due to the radiant temperature asymmetry from the walls.

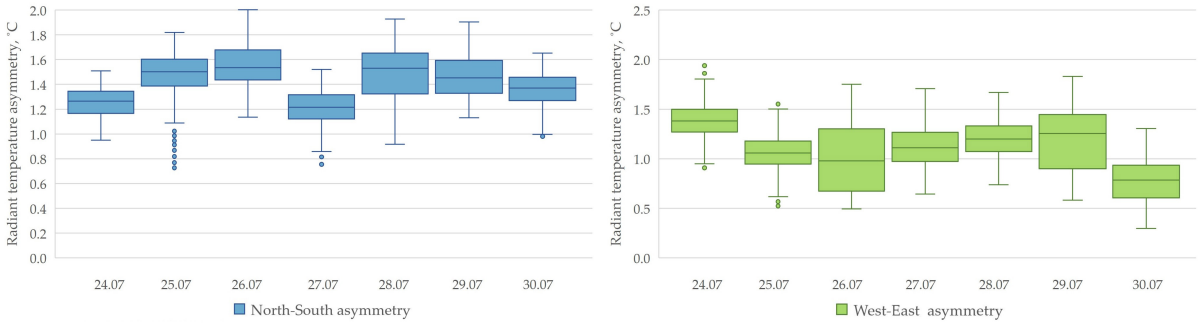

Figure 7.6: Radiant temperature asymmetry due to walls in the case of a sitting person located in the middle of the room during occupied hours. (24-30.07.2023; 8:00-15:00)

7.2 Intermediate case

Draught rate

Figure 7.7 shows the DR values at north, middle, and south pole locations at 0.1m, 0.6m, 1.1m and 1.7m from the ground level during the measurement period 23-26.10.2023.

The DR fluctuates throughout the day, with peaks corresponding to changes in the Test room during the occupancy hours (8:00-16:00), which might be the influence of the electric space heater, the presence of people (heat emitters), as well as the actions of the Window-Master and exhaust ventilation systems. Despite these variations, the DR remains below the 10% threshold for IEQ Category I most of the time, indicating that the environmental conditions are within a comfortable or acceptable range according to the set standards for draught comfort.

Figure 7.7: North, Middle and South pole draught rates at 0.1m, 0.6m, 1.1m and 1.7m from the ground (Occupied zone) in the Test room. (23-26.10.2023; All hours)

Figure 7.8 also displays that the DR stayed within Category I for 96.6% of the occupied time over four full days. The remaining 3.4% of the time, when the DR exceeded the 10% mark, corresponds to instances at the middle pole at all measured heights and the 0.6m height at the south pole, suggesting localized areas where drought conditions were less than ideal.

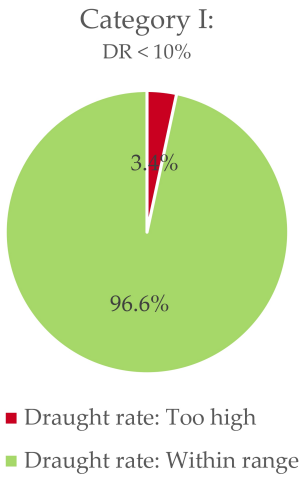

Figure 7.8: North, Middle and South pole draught rates at 0.1m, 0.6m, 1.1m and 1.7m from the ground (Occupied zone) in the Test room. (23-26.10.2023; All hours)

Vertical air temperature difference

When analysing whether there is thermal discomfort due to the vertical air temperature difference between the ankle and the head of a sitting person, the results show that during the measurement period, all the values are in category A, according to DS 7730 (see Figure 2.8). Figure 7.9 displays that for 3 days out of 4, the temperature difference is highest in the northern part of the room, with a maximum of 1.1°C, occurring on 26.10.2023 at 8:00. As all the values during the occupied hours are below 2°C, it can be concluded that the vertical air temperature difference does not pose a risk for the thermal comfort of the occupants.

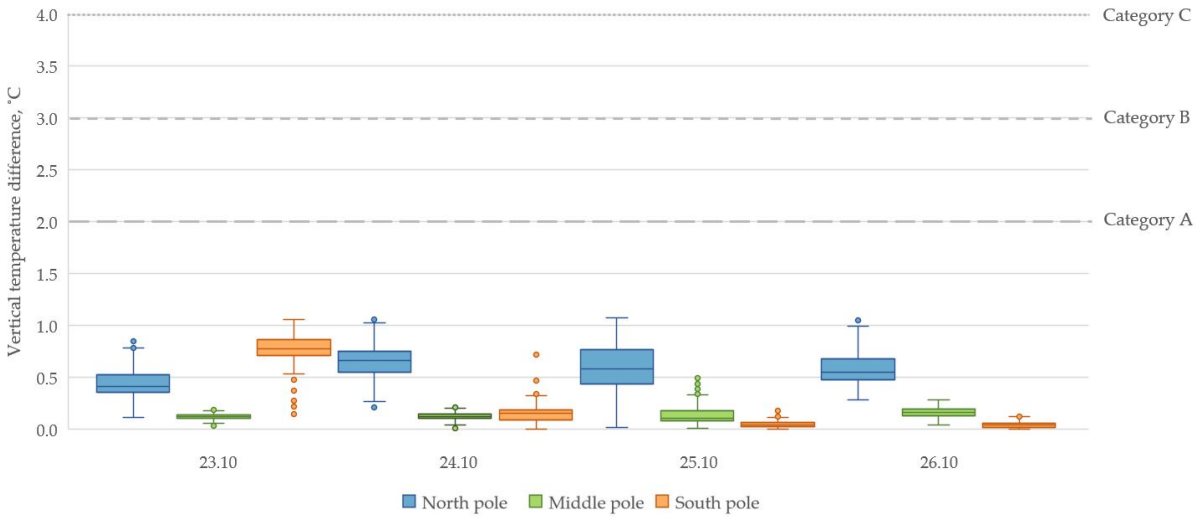

Figure 7.9: Vertical air temperature difference between ankle (0.1m) and head of a sitting person (1.1m) during occupied hours. (23-26.10.2023; 8:00-15:00)

Consequently, when calculating the percentage dissatisfied according to Equation 2.12, the values are between 0.1-0.7%. As less than 1% of the occupants are dissatisfied with the vertical temperature difference during the measurement period, category A is achieved (see Figure 2.8).

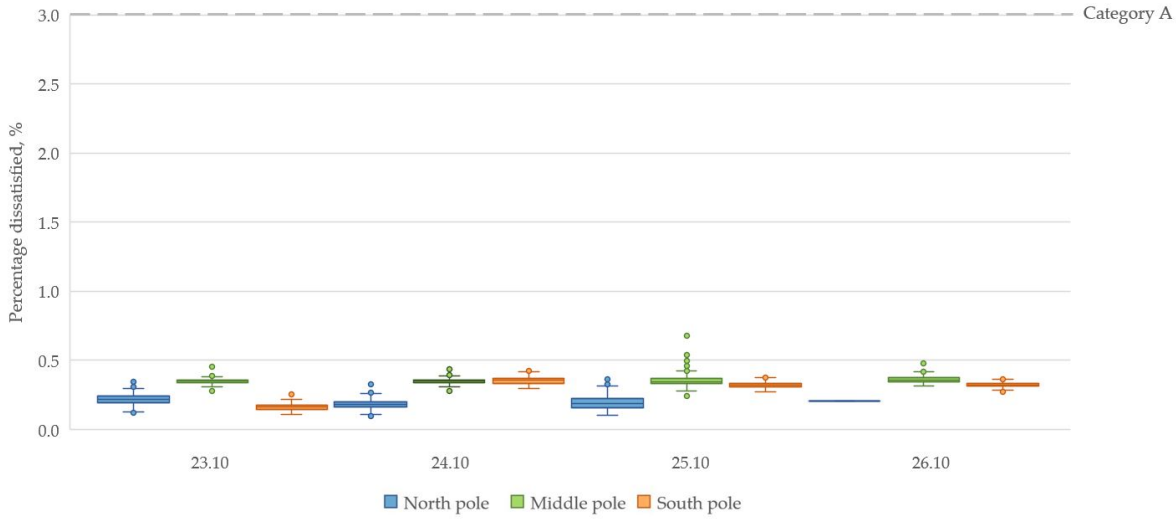

Figure 7.10: Percentage dissatisfied due to vertical air temperature difference between ankle (0.1m) and head of a sitting person (1.1m). (23-26.10.2023; 8:00-15:00)

Floor surface temperature

In Figure 7.11, the results of measuring the floor surface temperature during all hours are displayed. The tendency of rising surface temperature during the day can be noted, as well as the temperature drop outside of the occupied hours.

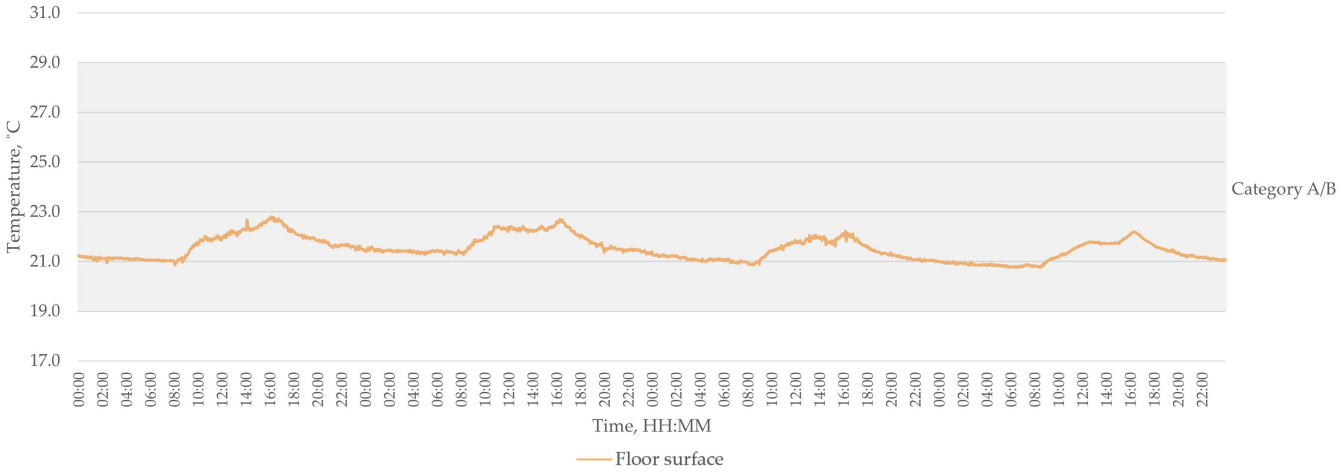

Figure 7.11: Floor surface temperature during all hours. (23-26.10.2023; 00:00-23:59)

To further inspect the temperatures during the occupied hours, figure 7.12 illustrates the results in the form of box-and-whiskers plots for each day. It can be observed that the surface temperature varies between 20.7-22.9°C, therefore, it falls into the best category, according to DS 7730 (see Figure 2.8).

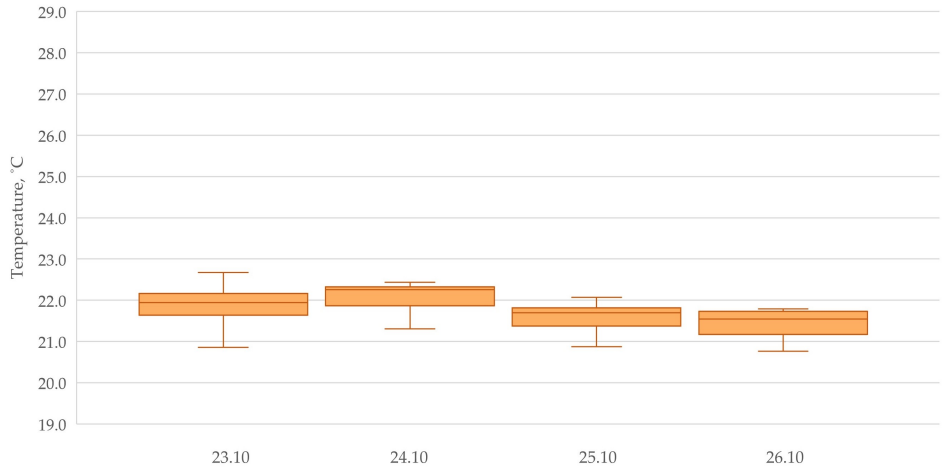

Figure 7.12: Floor surface temperature during occupied hours. (23-26.10.2023; 8:00-15:00)

As the percentage of dissatisfied occupants decreases with the rising floor temperatures, figure 7.13 illustrates the calculated PD results. Category A/B is achieved during the occupied hours in the measurement period with regards to PD, as the maximum value is 7.4%, occurring on 26.10.2023 at 8:31.

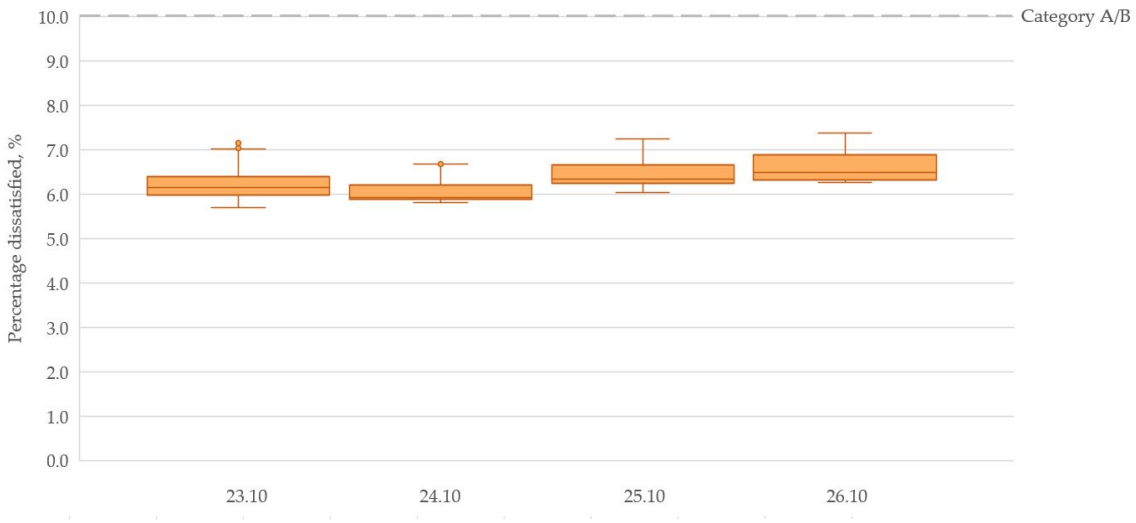

Figure 7.13: Percentage dissatisfied due to floor surface temperature during occupied hours. (23-26.10.2023; 8:00-15:00)

Radiant temperature asymmetry

To assess the risk of thermal discomfort due to radiant asymmetry, the calculations are carried out for the cases of a sitting and a standing person placed in the middle of the room, 0.2m away from the North wall, and 0.2m away from the South wall during the occupied hours. The relevant angle factors are calculated according to DS7726, and can be seen in 9.6 Appendix D. Furthermore, in this section only the case of a sitting person located in the middle of the room is displayed, as it appeared to be the only critical placement, while the remaining positions fulfill category A/B for 100% during the measurement period. Therefore, the cases of the sitting position at the North and the South of the room, and the standing positions in the middle, North and South of the room can be viewed in Appendix 9.9.

Sitting person in the middle of the room

The results show that the radiation from the walls does not cause any thermal discomfort, as the plane radiant temperature difference between the North and South walls varies between 0.9-1.0°C, and for the West and East walls it varies between 0.0-0.3°C. Therefore, the values for the walls are in category A/B in the occupied hours during the measurement period, according to DS 7730.

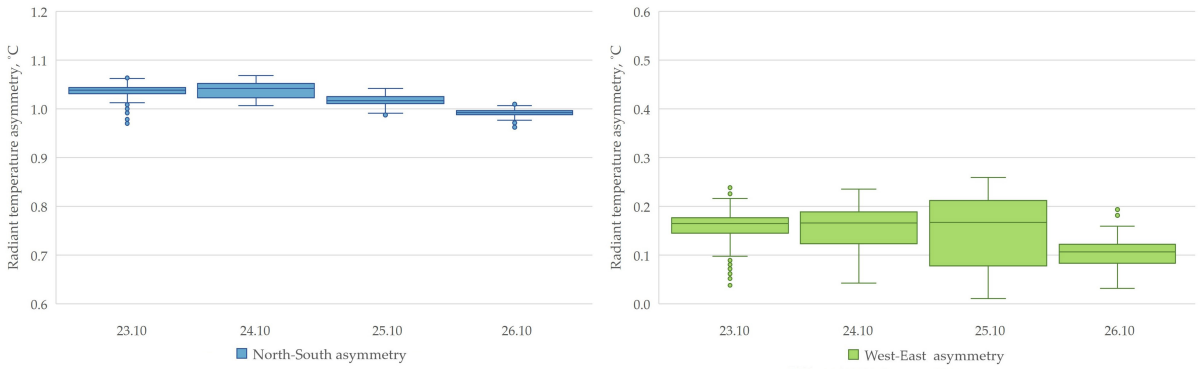

Figure 7.14: Radiant temperature asymmetry due to walls in the case of a sitting person located in the middle of the room during occupied hours. (23-26.10.2023; 8:00-15:00)

When analysing the plane radiant temperature differences between the ceiling and the floor, the result varies between 4.6-5.2°C (see figure 7.15). As the category A/B for radiant temperature asymmetry ranges from 0°C up to 5°C, only 65.6% of the occupied time falls into category A/B, and 34.4% falls into category C.

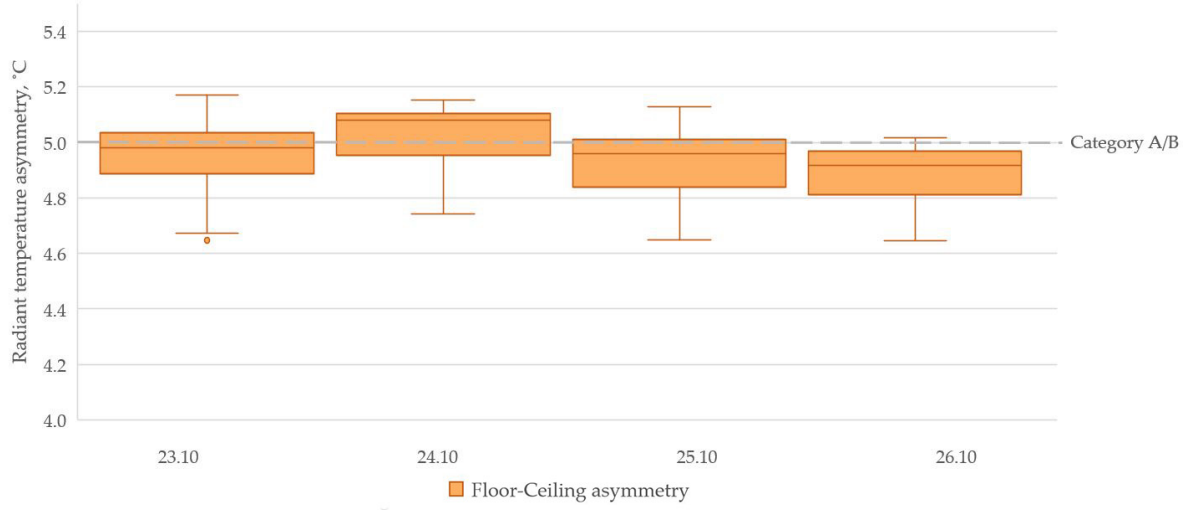

Figure 7.15: Radiant temperature asymmetry due to ceiling and floor in the case of a sitting person located in the middle of the room during occupied hours. (23-26.10.2023; 8:00-15:00)

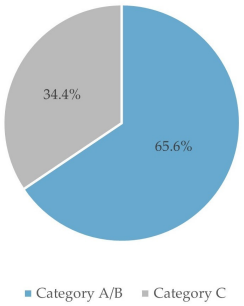

Figure 7.16: Comfort categories for radiant temperature asymmetry due to ceiling and floor in the case of a sitting person located in the middle of the room during occupied hours. (23-26.10.2023; 8:00-15:00)

The percentage of dissatisfied occupants is displayed in Figure 7.17, which is calculated according to Equation 2.10 for the walls and Equation 2.7 for the ceiling. It can be concluded that there is no dissatisfaction due to the radiant asymmetry of the walls. However, as the ceiling causes 6-7% to be dissatisfied, only category C is achieved.

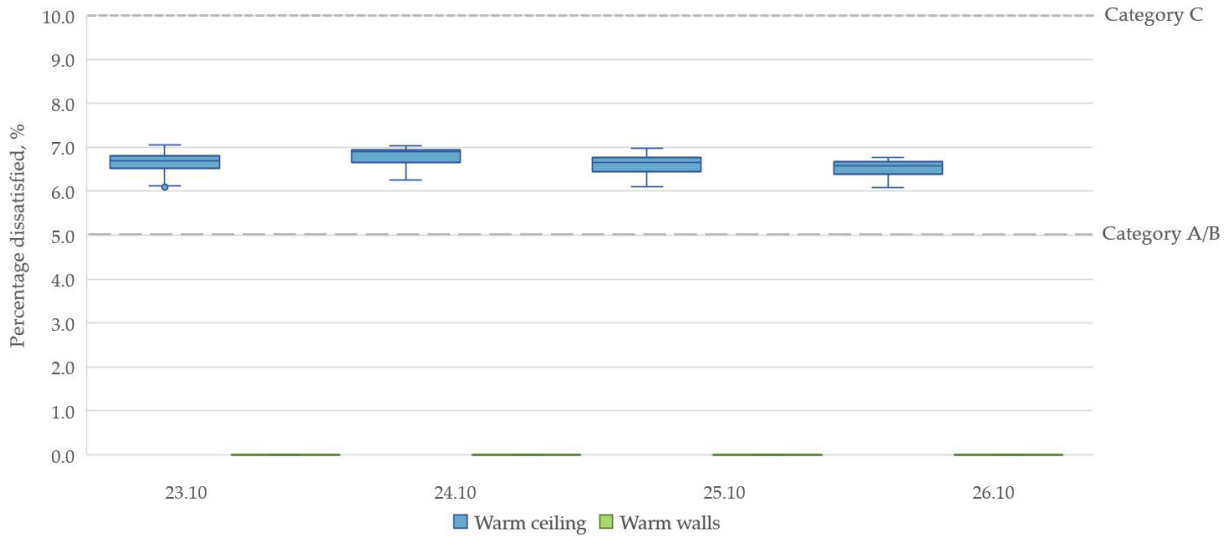

Figure 7.17: Percentage dissatisfied due to radiant temperature asymmetry in the case of a sitting person located in the middle of the room during occupied hours. (23-26.10.2023; 8:00-15:00)

7.3 Winter case

Draught rate

During the three-day winter measurement period, Figure 7.18 shows that DR are influenced by the measurement height, aligning with the known fact that environmental conditions can differ with elevation, even within a single room. At 0.1m and 0.6m from the floor, DR are present throughout the day. In contrast, at heights of 1.1m and 1.7m, significant DR are primarily observed during occupied hours. It is notable that only at ankle level do the DR occasionally surpass 10%, yet they remain below 20% at all times. This data highlights a stratified pattern of air movement, with the lowest levels experiencing more consistent draught conditions across both occupied and unoccupied periods.

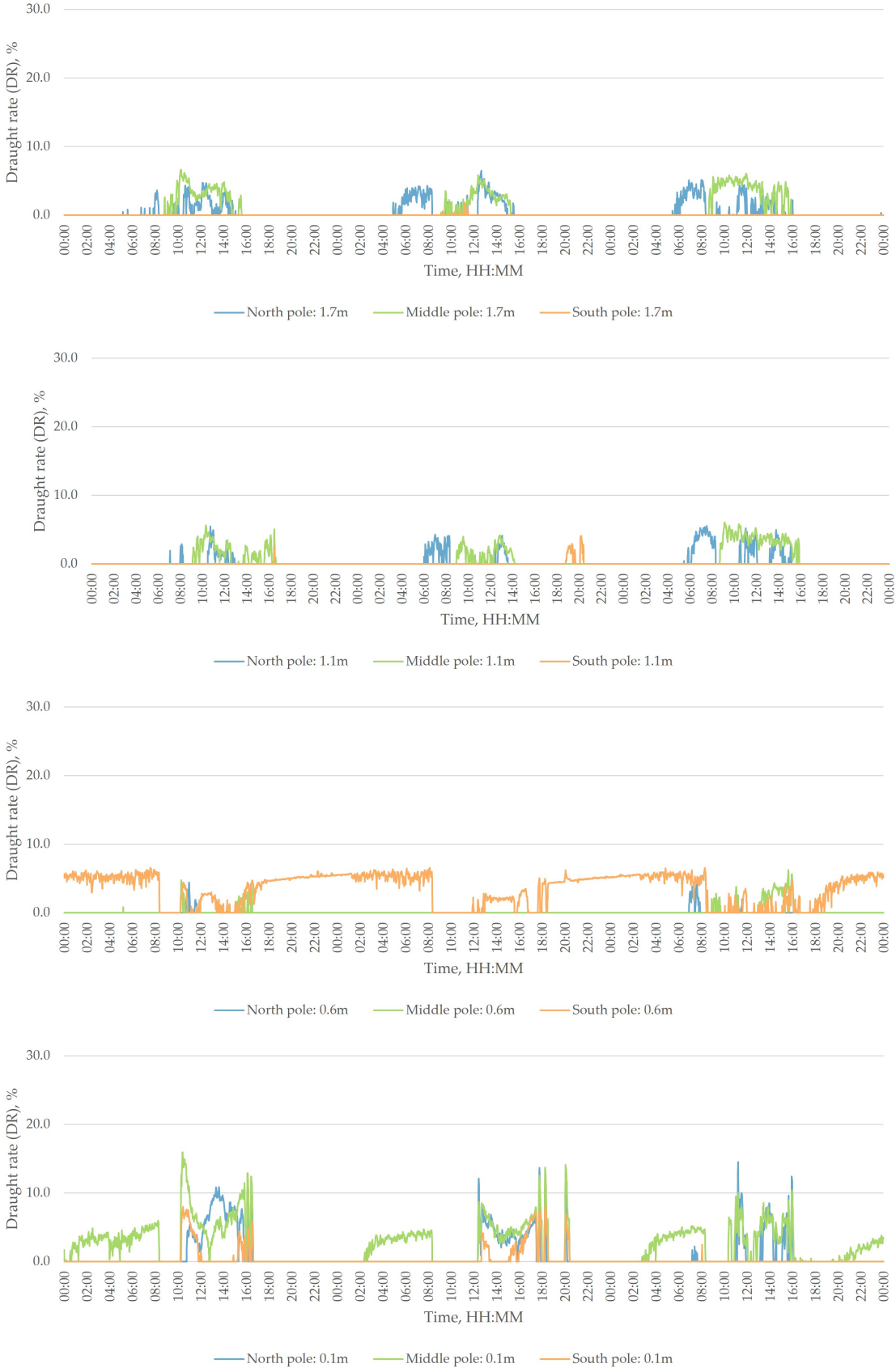

Figure 7.18: North, Middle and South pole draught rates at at differetn height from the ground (Occupied zone) in the Test room. (30.11.2023-02.12.2023; All hours)

Over the three-day period during occupied hours, the draught rate is within the optimal IEQ Category I (DR<10%) for 97.6% of the time, exceeding this level only 2.4% of the time. See the pie diagram in Figure 7.19.

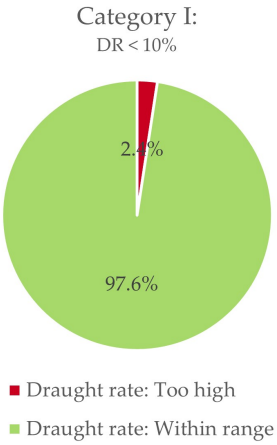

Figure 7.19: Percentage of total occupied time, the draught rate in the Test room is within the IEQ Category I range (30.11.2023-02.12.2023; 08:00-15:00)

Vertical air temperature difference

During the winter measurement period, the local discomfort caused by the temperature difference between the head and the ankle of a sitting person was determined for the North and South locations, as the thermocouple placed at ankle level (0.1m) on the middle pole displayed unreasonable temperatures, and therefore it was excluded from the evaluation. For the other two positions, category A was fulfilled for 79% of the occupied hours during the three days. However, the first two measurement days appeared to be more critical, as the difference at the North pole reached its maximum of 5.3°C on the first day at 11:40, and the South pole reached its maximum on the second day at 14:13 with 3.7°C. Consequently, the temperature difference at the North location did not reach any category defined by DS 7730 for 4.5% of the time, while the difference at the South location fell into the lowest category for 14.6%.

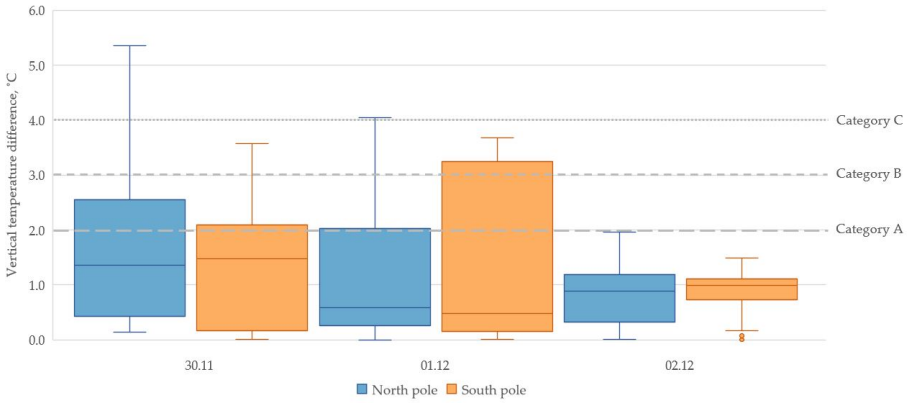

Figure 7.20: Vertical air temperature difference between ankle (0.1m) and head of a sitting person (1.1m) during occupied hours. (30.11.2023-02.12.2023; 8:00-15:00)

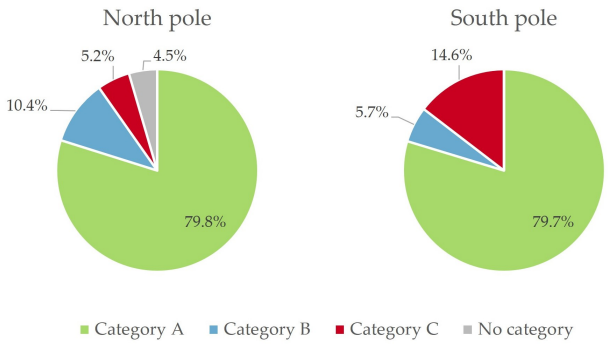

Figure 7.21: Vertical air temperature difference between ankle (0.1m) and head of a sitting person (1.1m) during occupied hours. (30.11.2023-02.12.2023; 8:00-15:00)

The high temperature difference is apparent during the PD analysis, as on the first day the maximum value (23.4%) for the North pole is significantly higher than the rest of the values during the measurement period, resulting in 4.0% outside of the comfort categories. Furthermore, both positions reached category C on the first two days, while on the third day category A was achieved during the entire occupied period.

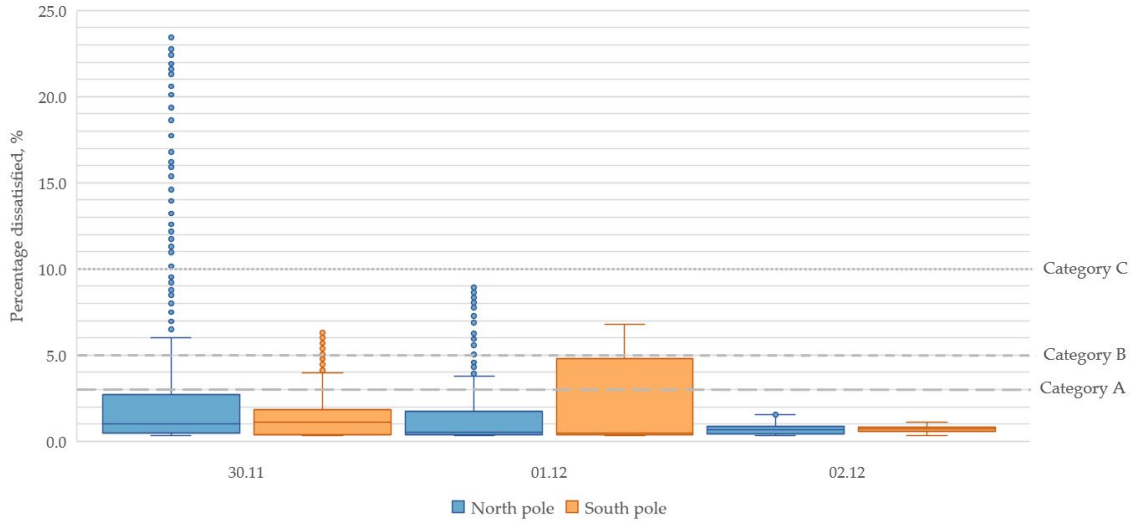

Figure 7.22: Percentage dissatisfied due to vertical air temperature difference between ankle (0.1m) and head of a sitting person (1.1m). (30.11.2023-02.12.2023; 8:00-15:00)

Floor surface temperature

The floor surface temperature is displayed in Figure 7.23, including all the measurement hours from 0-24. The tendency of increasing temperatures within the occupied hours and decreasing temperatures outside of the occupied hours can be observed.

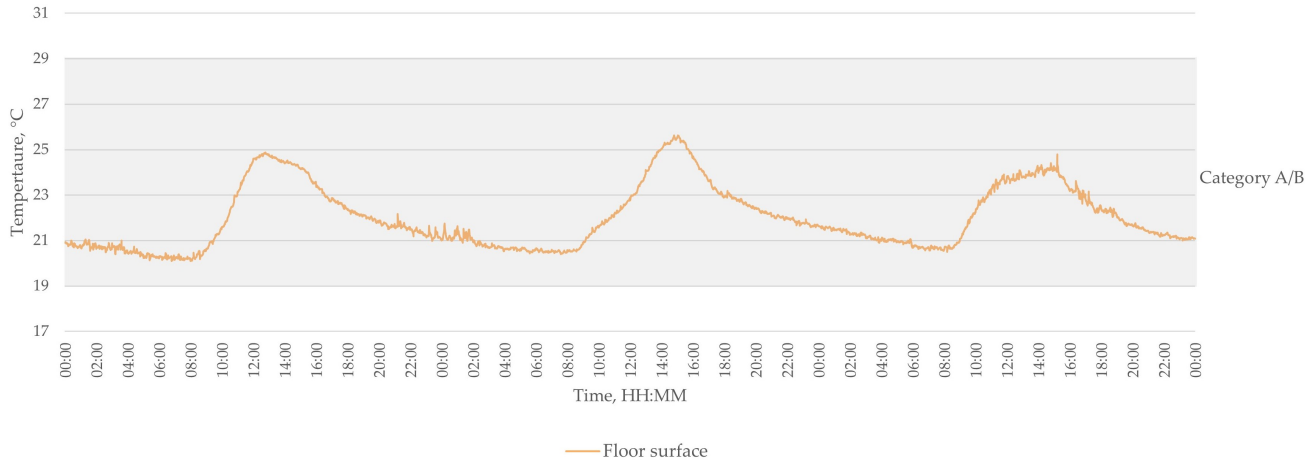

Figure 7.23: Floor surface temperature during all hours. (30.11.2023-02.12.2023; 00:00-23:59)

Within the occupied hours the lowest temperature is 20.1°C occurring on the first day, while the highest is 25.6°C on the second day. However, as the measurement results are within the range of 19-29°C defined by DS 7730, the best category is achieved for the whole measurement period.

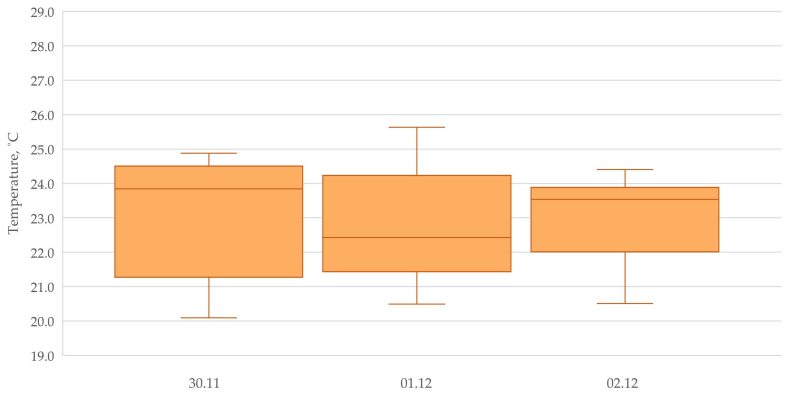

Figure 7.24: Floor surface temperature during occupied hours. (30.11.2023-02.12.2023; 8:00-15:00)

Furthermore, the calculated percentage of dissatisfied occupants due to the floor surface temperature ranges between 5.5% and 8.4%, therefore category A/B is fulfilled throughout the winter measurement period.

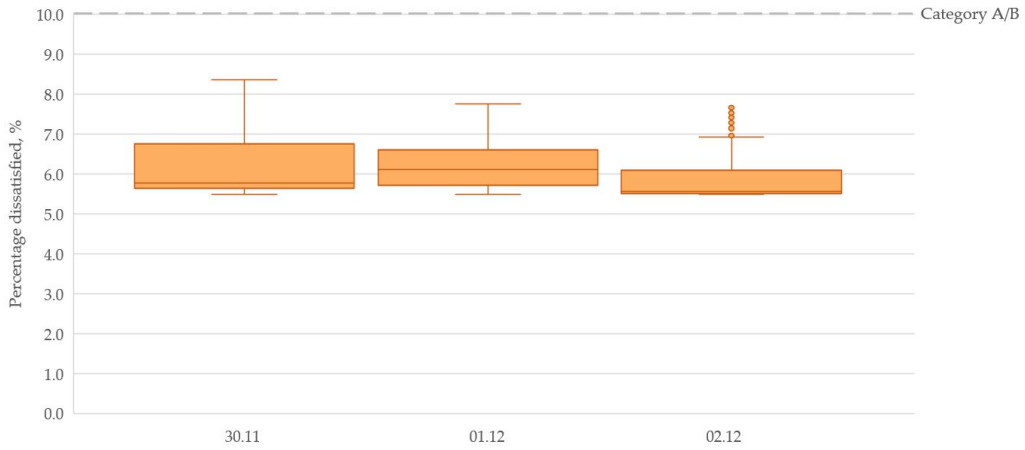

Figure 7.25: Percentage dissatisfied due to floor surface temperature during occupied hours. (30.11.2023-02.12.2023; 8:00-15:00)

Radiant temperature asymmetry

To assess the risk of thermal discomfort due to radiant asymmetry, the calculations are carried out for the cases of a sitting and a standing person placed in the middle of the room, 0.2m away from the North wall, and 0.2m away from the South wall during the occupied hours. The relevant angle factors are calculated according to DS 7726, and can be seen in 9.6 Appendix D. Additionally, as the case of a centrally placed sitting person occurred to be the only critical position, its results are displayed in this section. The RTA results for the sitting positions for the Northern and Southern locations, and all of the standing positions can be seen in Appendix 9.9

Sitting person in the middle of the room

In the case of a centrally located person in a sitting position, the radiant temperature asymmetry due to the North and South walls ranges from 0.9°C to 1.8°C, while for the West and East walls the values are between 0.0-0.9°C. Therefore, during the winter measurement period, all the values fall into category A/B as they are below 23°C.

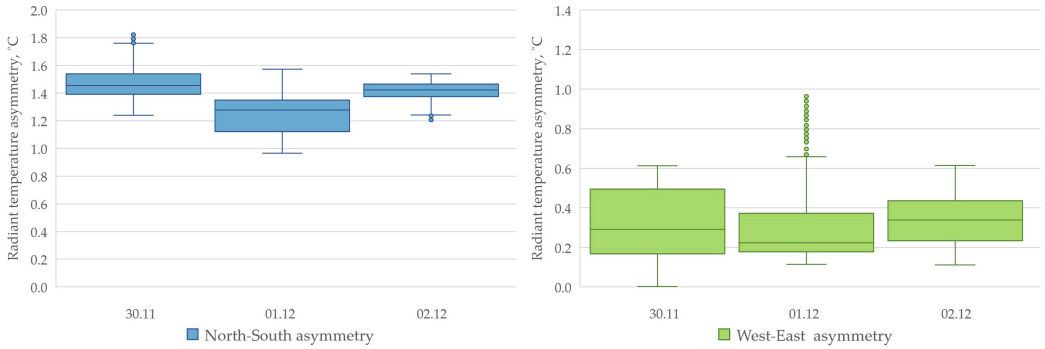

Figure 7.26: Radiant temperature asymmetry due to walls in the case of a sitting person located in the middle of the room during occupied hours. (30.11.2023-02.12.2023; 8:00-15:00)

Regarding the difference between the plane radiant temperatures of the floor and ceiling, the values during the three measurement days are between 4.3°C and 5.9°C. As the 5°C limit is exceeded, category A/B is only satisfied for 52.4%, while for 47.6% category C is achieved.

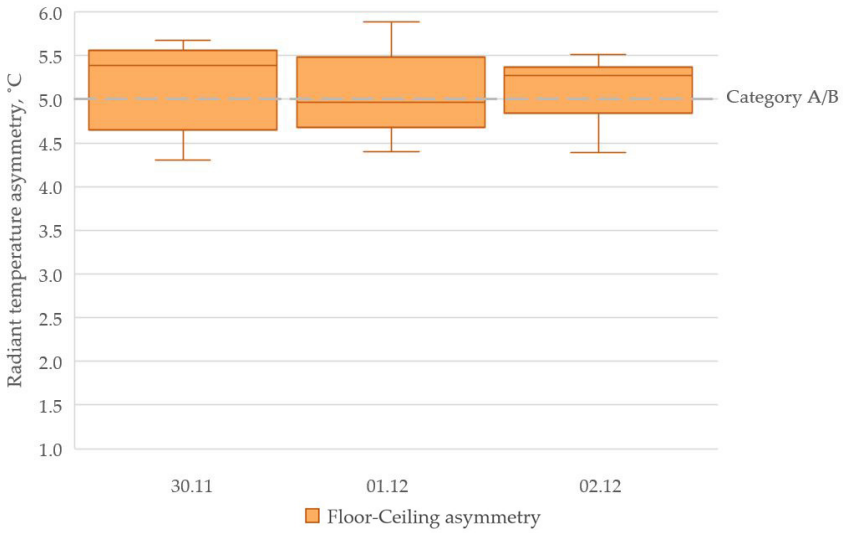

Figure 7.27: Radiant temperature asymmetry due to ceiling and floor in the case of a sitting person located in the middle of the room during occupied hours. (30.11.2023-02.12.2023; 8:00-15:00)

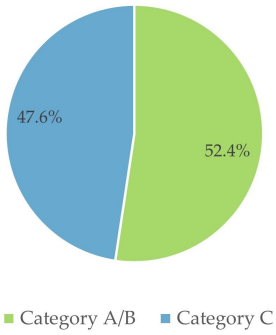

Figure 7.28: Comfort categories for radiant temperature asymmetry due to ceiling and floor in the case of a sitting person located in the middle of the room during occupied hours. (30.11.2023-02.12.2023; 8:00-15:00)

When considering the percentage of dissatisfied occupants due to the RTA, the walls do not pose any risk, while due to the warm ceiling 5.5-8.5% are expected to be dissatisfied and therefore only category C is reached during the winter measurement days.

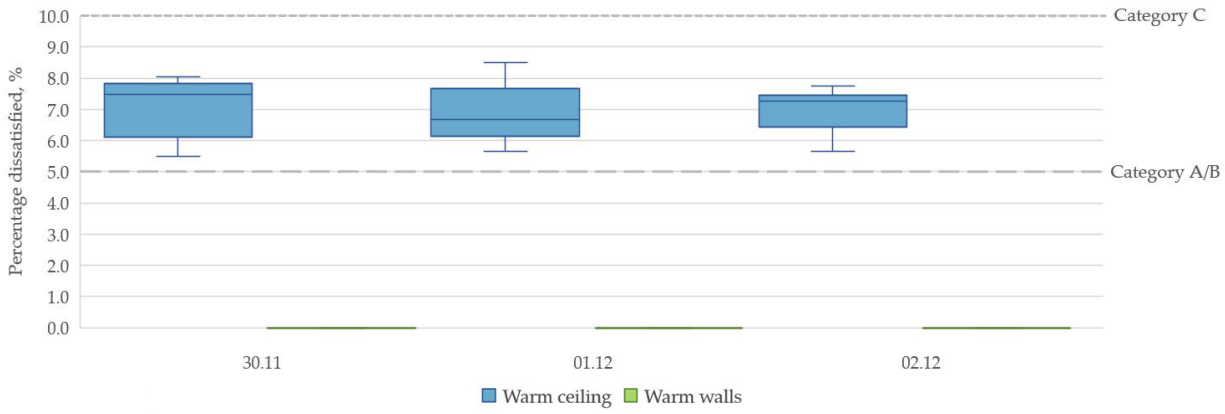

Figure 7.29: Percentage dissatisfied due to radiant temperature asymmetry in the case of a sitting person located in the middle of the room during occupied hours. (30.11.2023-02.12.2023; 8:00-15:00)

7.4 Summary

To sum up the evaluation of the local thermal comfort in the Test room, Figure 7.30 presents the measurement results considering the achieved thermal comfort categories according to DS7730 (2.8), while Figure 7.31 displays the calculated percentage of dissatisfied occupants.

The draught rate does not pose a risk of discomfort as the measurement results mainly fall into Category A for all the conducted measurement periods. The most favourable measurement week appears to be the summer case with 98.5% in category A, followed by the winter case with 97.6%, and lastly the intermediate case with 96.6% within the best category.

Considering the discomfort due to the vertical air temperature difference, the results primarily satisfied category A, with a tendency of the North pole position being the most critical. Regarding the calculated PD, the measurements from the intermediate week reached 100% in category A during the whole period for all three locations (North pole, Middle pole, South pole). The winter case presented the most critical results, as for the North pole 4.0% did not satisfy any of the comfort categories. Additionally, the evaluation of the Middle pole was not possible due to the thermocouple located at 0.1m providing inconclusive results. For the summer case, the PD results appear to be unproblematic, as category A was obtained for a minimum of 96.4% for all the positions.

The assessment of discomfort due to high or low surface temperatures of the floor was only conducted for the intermediate and winter cases, as the measurements from the summer week displayed unrealistic data. For both cases, the best category was achieved with a 100% satisfactory rate, indicating that there is no risk of discomfort.

Consequently to the lack of data regarding the floor surface temperature during the summer case, the radiant temperature asymmetry between the ceiling and the floor is also not possible to obtain. However, the results for the intermediate and winter cases indicate that only the sitting position in the middle of the room posed the risk of discomfort due to the warm ceiling, as the calculated PD 100% falls into category C. Regarding the RTA due to

the walls, no issue was detected as category A/B was achieved during all the measurement weeks for every position.

				SUMMER				INTERMEDIATE				WINTER			
				Category A	Category B	Category C	No category	Category A	Category B	Category C	No category	Category A	Category B	Category C	No category
Draught rate				98.5%	1.5%	0.0%	0.0%	96.6%	3.4%	0.0%	0.0%	97.6%	2.4%	0.0%	0.0%
Vertical air temperature difference			North	89.0%	8.3%	2.6%	0.1%	100.0%	0.0%	0.0%	0.0%	79.8%	10.4%	5.2%	4.5%
			Middle	100.0%	0.0%	0.0%	0.0%	100.0%	0.0%	0.0%	0.0%	N/A			
			South	92.6%	7.3%	0.1%	0.0%	100.0%	0.0%	0.0%	0.0%	79.7%	5.7%	14.6%	0.0%
Floor surface temperature				N/A				100.0%		0.0%	0.0%	100.0%		0.0%	0.0%
Radiant temperature asymmetry	Walls	Sitting position	North	100.0%		0.0%	0.0%	100.0%		0.0%	0.0%	100.0%		0.0%	0.0%
			Middle	100.0%		0.0%	0.0%	100.0%		0.0%	0.0%	100.0%		0.0%	0.0%
			South	100.0%		0.0%	0.0%	100.0%		0.0%	0.0%	100.0%		0.0%	0.0%
	Ceiling	Sitting position	North	N/A				100.0%		0.0%	0.0%	100.0%		0.0%	0.0%
			Middle	N/A				65.6%		34.4%	0.0%	52.4%		47.6%	0.0%
			South	N/A				100.0%		0.0%	0.0%	100.0%		0.0%	0.0%
	Walls	Standing position	North	100.0%		0.0%	0.0%	100.0%		0.0%	0.0%	100.0%		0.0%	0.0%
			Middle	100.0%		0.0%	0.0%	100.0%		0.0%	0.0%	100.0%		0.0%	0.0%
			South	100.0%		0.0%	0.0%	100.0%		0.0%	0.0%	100.0%		0.0%	0.0%
	Ceiling	Standing position	North	N/A				100.0%		0.0%	0.0%	100.0%		0.0%	0.0%
			Middle	N/A				100.0%		0.0%	0.0%	100.0%		0.0%	0.0%
			South	N/A				100.0%		0.0%	0.0%	100.0%		0.0%	0.0%

Figure 7.30: Summary of the evaluation of the local thermal comfort in the Test room.

				SUMMER				INTERMEDIATE				WINTER			
PERCENTAGE DISSATISFIED				Category A	Category B	Category C	No category	Category A	Category B	Category C	No category	Category A	Category B	Category C	No category
Vertical air temperature difference			North	96.4%	1.2%	2.4%	0.0%	100.0%	0.0%	0.0%	0.0%	86.8%	4.9%	4.3%	4.0%
			Middle	100.0%	0.0%	0.0%	0.0%	100.0%	0.0%	0.0%	0.0%	N/A			
			South	99.4%	0.6%	0.0%	0.0%	100.0%	0.0%	0.0%	0.0%	83.7%	6.6%	9.8%	0.0%
Floor surface temperature				N/A				100.0%		0.0%	0.0%	100.0%		0.0%	0.0%
Radiant temperature asymmetry	Walls	Sitting position	North	100.0%		0.0%	0.0%	100.0%		0.0%	0.0%	100.0%		0.0%	0.0%
			Middle	100.0%		0.0%	0.0%	100.0%		0.0%	0.0%	100.0%		0.0%	0.0%
			South	100.0%		0.0%	0.0%	100.0%		0.0%	0.0%	100.0%		0.0%	0.0%
	Ceiling	Sitting position	North	N/A				100.0%		0.0%	0.0%	98.3%		1.7%	0.0%
			Middle	N/A				0.0%		100.0%	0.0%	0.0%		100.0%	0.0%
			South	N/A				100.0%		0.0%	0.0%	98.3%		1.7%	0.0%
	Walls	Standing position	North	100.0%		0.0%	0.0%	100.0%		0.0%	0.0%	100.0%		0.0%	0.0%
			Middle	100.0%		0.0%	0.0%	100.0%		0.0%	0.0%	100.0%		0.0%	0.0%
			South	100.0%		0.0%	0.0%	100.0%		0.0%	0.0%	100.0%		0.0%	0.0%
	Ceiling	Standing position	North	N/A				100.0%		0.0%	0.0%	100.0%		0.0%	0.0%
			Middle	N/A				100.0%		0.0%	0.0%	100.0%		0.0%	0.0%
			South	N/A				100.0%		0.0%	0.0%	100.0%		0.0%	0.0%

Figure 7.31: Summary of the evaluation of the percentage dissatisfied due to local thermal comfort in the Test room.

Chapter 8

Discussion and conclusion

This research delves into the new renovation concept for schools, known as the Integrated Renovation Solution, Implementing a Double-Skin Facade with Diffuse Ceiling Ventilation (I-DIFFER). It focuses on an experimental investigation in a scaled-down classroom, explicitly examining the two primary control modes – heating and cooling – and their influence on thermal comfort for users during cooling, intermediate, and heating seasons.

The analysis presented in the paper supports previous findings, indicating that the system can maintain a draught-free environment (IEQ Category I) for 96.6% of the occupied time, even though outdoor air is supplied indirectly to the Test room, through the DSF and DCV cavities. The system poses no risk of radiant temperature asymmetry. However, some threats have been identified between floor and ceiling temperatures in the middle sitting area, which may be influenced by the location of the occupants and heat emitters. Previous studies have suggested that solar radiation significantly impacts the system. However, this research finds that the impact of solar radiation is moderate rather than high. The effect is more a result of the combination of various factors, including outdoor temperature, internal load, and thermal mass.

During the summer measurement period, the findings revealed that the dominating control mode was the cooling mode; however, the system switched to heating mode for a few hours at the beginning of the occupied period for 3 days. The cooling mode was operating with the temperature-controlled natural ventilation mode while implementing night cooling regularly throughout the evenings outside of occupancy. The heating mode was functioning with the gap ventilation, maintaining a consistent window opening percentage of 20%, while the pulsating ventilation mode opened the window to a larger percentage, concerning the outdoor conditions. The activation of the cooling mode occurred due to the Test room temperature reaching its setpoint, while the heating mode activated when this setpoint was not attained during the occupancy. Furthermore, interruptions in the heating mode occasionally occurred when the DSF cavity achieved its setpoint, causing the middle windows to open and cool down the cavity.

The operative temperature in the room in the summer week was effectively adjusted in accordance with the control modes. Nevertheless, the overheating experienced on the fifth day emphasizes the limitations of the system, due to its inability to manage the setpoints. This difficulty emerged as a result of the thermal mass of the constructions and the high

outdoor solar radiation combined with high outdoor temperatures. Consequently, night cooling appeared to be insufficient in achieving the necessary cooling effect that day. Furthermore, the switching from night cooling to heating mode on the second and third days suggests a need for optimization, by adjusting the night cooling schedule to end before the occupant period begins to possibly avoid the heating mode. Lastly, the rapid transition between cooling and heating modes demonstrates the system's fast reaction to the change in control, although the disadvantage of increased energy utilized by the control actions is posed.

The analysis conducted during the intermediate week has confirmed that only the heating mode was activated throughout the four days. As the temperature setpoints of either the cavities or the Test room were not achieved, the operation of WindowMaster was regulated by the CO_2 concentration of the room, during the occupancy period from 8:00 to 15:00. The maximum extent of window openings, initiated by the pulse ventilation mode, were limited by the outdoor conditions, primarily influenced by the wind speed. However, the gap ventilation mode ensured a steady airflow to maintain air quality with a consistent minimum window opening of 20%.

While the current heating control strategy led to the preheating of the supplied air via the cavities, and stable operative temperatures in the Test room; it also revealed the emerging issues regarding generally cool operative temperatures that are especially critical in the mornings, and the non-uniform supply air temperatures in the DCV cavity. Therefore, adjustments regarding the strategy are recommended with the aim of compensating for the low morning temperatures and satisfying the thermal comfort during the occupancy by integrating heaters into the room which are controlled unitedly with the WindowMaster.

The same control mode investigated during the winter measurements revealed the potential for enhancing the effect of the heating mode. However, the non-uniform temperature distribution experienced in the DCV cavity is also present during winter, similarly to the intermediate case. The measured temperatures in the test room exceeded the setpoint every day, which triggered the operation of the WindowMaster until the setpoint was no longer reached. This implies that the air temperatures dominated the control, and not the CO_2 concentration, resulting in an inconsistently regulated air supply. In addition, the combination of pulsating and gap ventilation defined the operation period, with limitations in window openings due to the outdoor conditions in both cases.

The tendency of low temperatures in the mornings during winter can be obtained, along with overheating occurring towards the end of occupancy, indicating the potential optimization of the control to avoid both too low and too high temperatures within the same day. Therefore, the heating control during winter is required to implement further actions to optimize the Test room temperature, possibly by increasing the window openings during the gap ventilation or by switching to cooling mode, resulting in reducing the overtemperatures.

Considering the above-mentioned findings regarding the currently applied control strategy, it can be concluded that the adjustment of the control is necessary across the diverse seasons. The incorporation of a space heating system and automatised solar shading into

the I-DIFFER renovation solution, integrated with the WindowMaster control is suggested with the purpose of preventing excessively low and high temperatures occurring the same day within the span of 7 hours. With this solution, the potential is enhanced to optimize occupant thermal comfort regarding operative temperatures, while achieving an equalized satisfaction rate of occupants situated in the different parts of the room due to the effect of shading reducing temperatures at South locations.

Moreover, it is necessary to reassess the current temperature setpoint of the Test room. The setpoint of 23°C during the occupied period implies an increased heat delivery to the room, while the DS 17772 defines the optimal thermal range during the heating season between 21-23°C for Category I. Consequently, this might lead to overheating, as observed in the winter scenario.

Lastly, it is essential to consider the age group of children occupying specific classrooms when establishing the control strategy for the I-DIFFER solution, as schools accommodate students from kindergarten until higher education. The thermal comfort of children differs from adults, due to the deviation in body surface area, subsequently achieving a higher metabolic rate of children at younger ages[16].

This renovation approach holds promise as an innovative solution for school refurbishments. However, it necessitates further investigation into its control strategy. The exploration could include assessing different window opening strategies and developing more advanced control systems that integrate window operations with ventilation, space heating and shading controls. Additionally, it is important to examine how this combined strategy affects other aspects of comfort, including acoustics, atmospheric, and visual elements. Equally crucial is the consideration of various parameters and guidelines when analyzing thermal comfort. These include metabolic rate, clothing insulation, body surface areas, and the PMV and PPD indices. Understanding how to adapt these factors for different age groups of schoolchildren in Denmark, could significantly enhance the I-DIFFER system's design and refine the control strategy to meet the occupants' needs more effectively.

Bibliography

[1] V. Angelakis D. Gundlegård A. Fredriksson A. An. Sezer. *Construction related urban disturbances: Identification and linking with an IoT-model*. 2022.

[2] Y. Hu A. K. Mikkelsen L. L. Pedersen V. Ø. Nyborg T. S. Larsen C. Zhang O. K. Larsen. *Experimental investigation of an integrated renovation solution combining diffuse ceiling ventilation and double skin façade*. 2023.

[3] EUROPEAN COMMISSION. *A Renovation Wave for Europe - greening our buildings, creating jobs, improving lives*. 2020. URL: https://eur-lex.europa.eu/legal-content/EN/TXT/?uri=CELEX:52020DC0662. (accessed: 02.01.2024).

[4] B. Occhiogrosso D. Minoli K. Sohraby. *IoT Considerations, Requirements, and Architectures for Smart Buildings — Energy Optimization and Next - Generation Building Management Systems*. 2017.

[5] P. A. B. James D. Teli M. F. Jentsch. *Naturally ventilated classrooms: An assessment of existing comfort models for predicting the thermal sensation and preference of primary school children*. 2012.

[6] G. Bekö E. P. Dam-Krogh A. B. Fangel K. Andersen G. Clausen J. Toftum. *Indeklima i skoler*. 2017.

[7] Carol S. Cash Glen I. Earthman. *Planning For A School Building Renovation*. 2016.

[8] S. Kempe C. Höfle-J. Görres K. E. Thomsen H. Erhorn-Kluttig H. Erhorn. *EU Project "School of the Future" — Refurbishment of School Buildings Toward Zero Emission with High - Performance Indoor Environment*. 2016.

[9] G. Havenith. *Metabolic rate and clothing insulation data of children and adolescents during various school activities*. 2007.

[10] P. Wargocki H. R. Menå E. M.N. Hansen G. Clausen J. Toftum B. U. Kjeldsen. *Association between classroom ventilation mode and learning outcome in Danish schools*. 2015.

[11] O. K. Larsen C. Zhang L. A. Bugenings M. Schaffer. *A novel solution for school renovations: Combining diffuse ceiling ventilation with double skin facade*. 2022.

[12] S. E. Maagaard K. B. Johannsen T. Østergaard M. K. Sørensen M. D. A. Andersen M. H. Vorre P. Noyé. *Branchevejledning for indeklima i skoler*. 2021.

[13] V. Hellstrand K. Thunshelle M. Mysena P. G. Schild. *Evaluation of simplified ventilation system with direct air supply through the facade in a school in a cold climate*. 2004.

[14] O. K. Larsen C. Zhang M. Schaffer L. A. Bugenings. *Exploring the potential of combining diffuse ceiling and double - skin facade for school renovations*. 2023.

[15] G. Marenzi N. Aste M. Manfren. *Building Automation and Control Systems and performance optimization: A framework for analysis*. 2017.

[16] V. P. de Freitas R. M.S.F. Almeida N. M.M. Ramos. *Thermal comfort models and pupils' perception in free-running school buildings of a mild climate country*. 2016.

[17] Dansk Standard. *DS 15251 Indoor environmental input parameters for design and assessment of energy performance of buildings addressing indoor air quality, thermal environment, lighting and acoustics*. 2007.

[18] Dansk Standard. *DS 17772-1 Energy performance of buildings - Indoor environmental quality - Part 1: Indoor environmental input parameters for the design and assessment of energy performance of buildings*. 2017.

[19] Dansk Standard. *DS 7726 Ergonomics of the thermal environment - Instruments for measuring physical quantities*. 2001.

[20] Dansk Standard. *DS 7730 Ergonomics of the thermal environment - Analytical determination and interpretation of thermal comfort using calculation of the PMV and PPD indices and local thermal comfort criteria*. 2006.

[21] Dansk Standard. *DS 8996 Ergonomics of the thermal environment - Determination of metabolic rate*. 2021.

[22] Building Ministry of Transport and Housing. *Executive order on building regulations (BR18)*. 2018.

[23] WindowMaster. *WLA 330 Wind/Rain sensor*. 2019.

[24] T. Hong Z. Wang. *Reinforcement learning for building controls: The opportunities and challenges*. 2020.

Chapter 9

Appendix

9.1 Desciprtion of IEQ categories

Category	Explanation
I	High level of expectation and is recommended for spaces occupied by very sensitive and fragile persons with special requirements like handicapped, sick, very young children and elderly persons
II	Normal level of expectation and should be used for new buildings and renovations
III	An acceptable, moderate level of expectation and may be used for existing buildings
IV	Values outside the criteria for the above categories. This category should only be accepted for a limited part of the year

NOTE In other standards like EN 13779 and EN ISO 7730 categories are also used; but may be named different (A, B, C or 1, 2, 3 etc.)

Figure 9.1: Desciprtion of IEQ categories. [17]

9.2 Setup of the control room

Written according to the guide *"Performing temperature measurements using Type K thermocouples and Fluke Helios Plus 2287A datalogger"* received from AAU.

Thermocouples
All the thermocouples setup in the test room are joined in a compensation box, which is placed in the control room located underneath the test room. The compensation box functions as an isolating environment for one end of a thermocouple with the aim of defining the temperature at the other end based on the measured voltage. Therefore, the temperature in the compensation box is measured by a resistance temperature detector (Pt100), in order to know the difference between the measurement point placed in the test room and in the compensation box. The Pt100 is connected to a National Instrument (NI 9216) module, that is further connected to a computer.

For each thermocouple, a copper wire is connected at the terminals of the Pt100. The copper wires make the connection between the compensation box and the Fluke Helios

Plus 2287A datalogger, as they join at the isothermal input connector at the back side of the datalogger. The Fluke Helios Plus 2287A datalogger is connected to power and is grounded in order to reduce the noise on the measured signal of the thermocouples. Furthermore, it is connected to a computer, where the measurements can be obtained via a LABVIEW script. In the script, calibration files are added to acquire accurate data, and the measurements are logged every 10 seconds in a text file format for all the thermocouples.

Anemometers
The anemometers from the test room are connected to two Dantec ComfortSense main frames, that are located in the control room. Each frame can accommodate 16 channels. Both Dantec devices are connected to a computer, where two LABVIEW scripts log the measurements. Within the scripts, calibration files are loaded with the aim of obtaining accurate data. As a result, the measurements are displayed in a text file, including the voltage, air velocity, draught rate, and turbulence logged at every 10 seconds. The draught rate and turbulence are calculated within the LABVIEW script according to the Danish Standards 7730.

9.3 Validation of equipment and measurement preparations

9.3.1 Calibration of thermocouples

Objective
The calibration of the thermocouples is performed with the aim of assessing the measurement preciseness. As the thermocouples have been previously calibrated, the calibration is executed only on a randomly selected bundle of thermocouples to determine whether the previous calibration is still valid. The calibration is performed according to the guide of *"Performing temperature measurements using Type K thermocouples and Fluke Helios Plus 2287A datalogger"* obtained from AAU.

Method
To prepare the thermocouples for calibration, the measuring points are covered with a thin tape with the aim of reducing noise. The selected thermocouples are: 35, 36, 41, 42, 43. A bundle of 5 thermocouples is formed for the measurement.

Then the thermocouples are placed into the calibration well of the ISOCAL Calibration bath and then covered with a paper towel. It is possible to manually set the desired temperature, or it can also be controlled by a LABVIEW script. The F200 Precision Thermometer is connected to the ISOCAL Calibration bath and is used to indicate the true temperature.

Figure 9.2: Setup of the ISOCAL Calibration bath (left) and F200 Precision Thermometer (right) for calibrating thermocouples.

With the LABVIEW script, first the correct port needs to be selected under the "VISA resource name". Then the events are defined according to the temperature setpoints (°C), elapsed time (seconds), and rate of change of temperature. The temperature setpoints for the calibration are 0°C, 10°C, 20°C, and 30°C. The elapsed time between each setpoint is set to 1 hour, as only positive temperature setpoints are defined. The setpoint rate is set to the maximum value, which is 999. The total runtime for the calibration is defined at "The End" event, which is 15000 seconds.

Then the LABVIEW script for the Fluke Helios Plus 2287A Datalogger can be run in order to log the measured temperatures by the investigated thermocouples (see Figure 9.3).

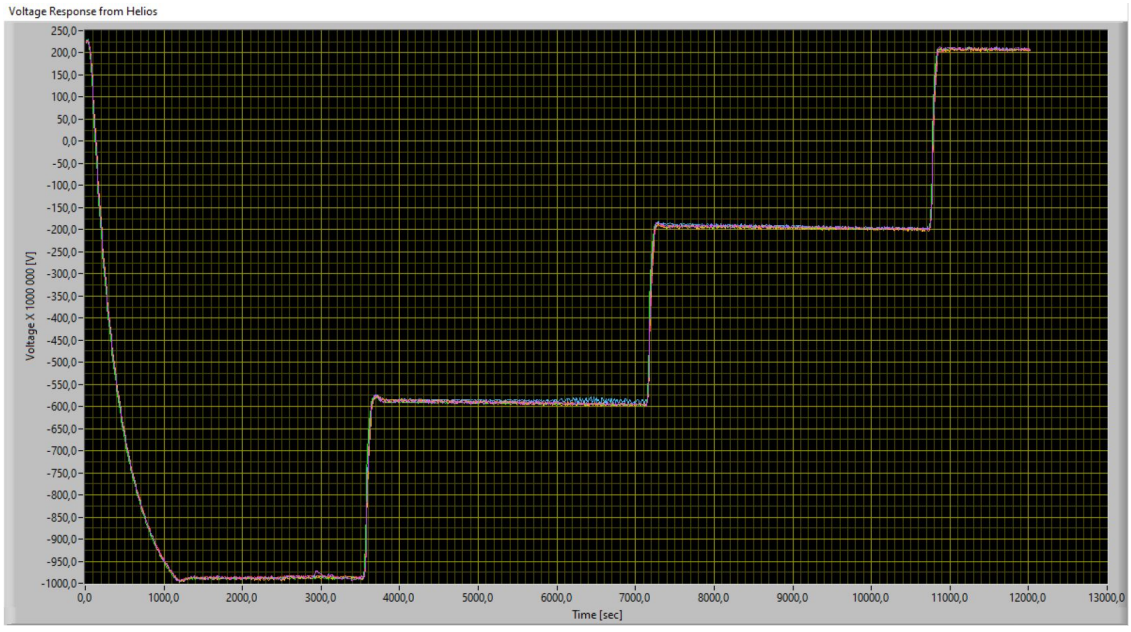

Figure 9.3: Voltage response to changing temperature setpoints from Fluke Helios Plus 2287A Datalogger as the function of time.

Results

The relation between real temperatures by the F200 Precision Thermometer and the measured voltage by the thermocouples can be illustrated on calibration curves in the form of a polynomial equation. The calibration measurements are displayed in Figure 9.4.

THERMOCOUPLE CALIBRATION						
SET POINT, °C	REAL VALUE, °C	MEASURED VALUE, V				
ISOCAL Calibration bath	F200 Precision Thermometer	Chanel 35	Chanel 36	Chanel 41	Chanel 42	Chanel 43
0	-0.135	-0.00097229	-0.00098535	-0.00098401	-0.00098743	-0.00098499
10	9.952	-0.00059155	-0.00059485	-0.00059302	-0.00059497	-0.00058618
20	20.160	-0.00019568	-0.00020056	-0.00019812	-0.00019959	-0.00019666
30	30.101	0.00020825	0.00020483	0.00020593	0.00020789	0.00020740

Figure 9.4: Calibration measurement results

The calibration curve for thermocouple 35 is the following:

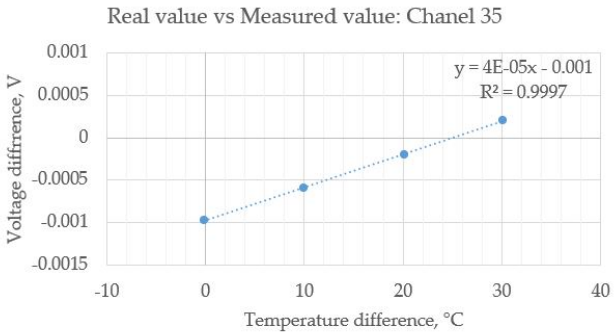

Figure 9.5: Calibration curve for thermocouple 35

The calibration curve for thermocouple 36 is the following:

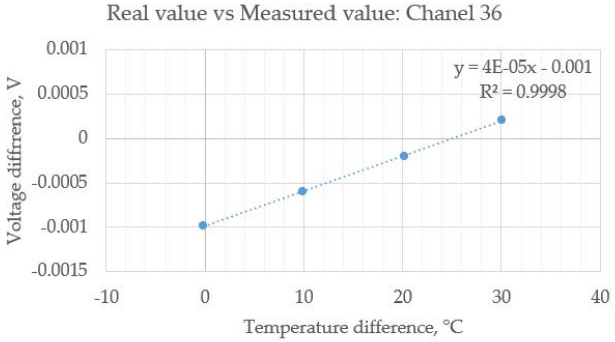

Figure 9.6: Calibration curve for thermocouple 36

The calibration curve for thermocouple 41 is the following:

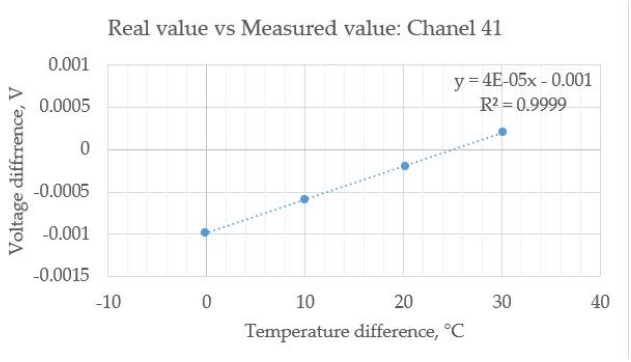

Figure 9.7: Calibration curve for thermocouple 41

The calibration curve for thermocouple 42 is the following:

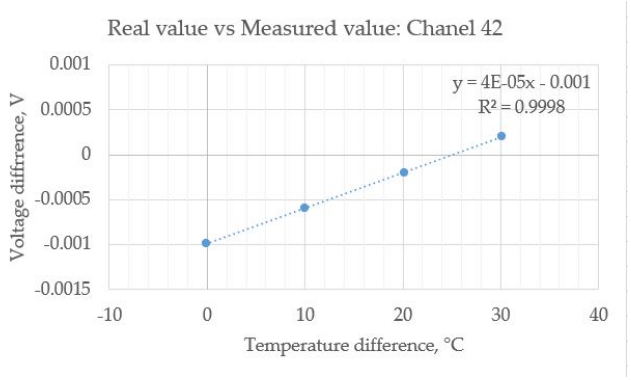

Figure 9.8: Calibration curve for thermocouple 42

The calibration curve for thermocouple 43 is the following:

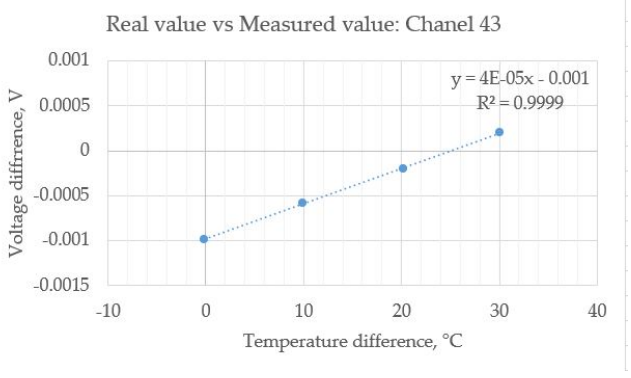

Figure 9.9: Calibration curve for thermocouple 43

The results show that the thermocouples measure accurately, therefore, no further calibration is performed.

9.3.2 Validation of WindowMaster monitor thermal sensors

WindowMaster automatically controls the openings in the outer layer of the DSF, in which the system's cooling or heating modes are set. The system is controlled according to a complex relationship within the logged air temperatures in all the WindowMaster monitors: in the Test Room, DSF and DCV cavities. Therefore, it is essential to validate the accuracy and reliability of the WindowMaster sensor before proceeding with measurements and data analysis.

To evaluate the performance of the thermal sensors of the WindowMaster system, the sensors at the DSF, DCV cavities and in the Test room are compared with K-type thermocouples and IC-meter placed at the exact location as the WindowMaster sensor. The two apparatus will also be used during the measurements. Having a clear understanding of how these tools behave is crucial for the validation process and overall experimentation.

The line graphs show time (HH:MM) for one day on the x-axis, the temperature logged with the apparatus in Celsius degrees on the left of the y-axis and solar radiation in W/m^2 on the right of the y-axis.

WindowMaster vs K-type thermocouples

Two K-type thermocouples are positioned in close proximity to the WindowMaster monitor, as depicted in Figure 9.10. This same approach is applied to the WindowMaster monitors in the DSF and DCV cavities. The reason for placing two thermocouples is to verify and give confidence in the accuracy of the received data for analysis. The tables contain 24-hour data logs from 03.09.2023. Given the sensitivity of K-type thermocouples, the graphs present running averages over 5-minute intervals.

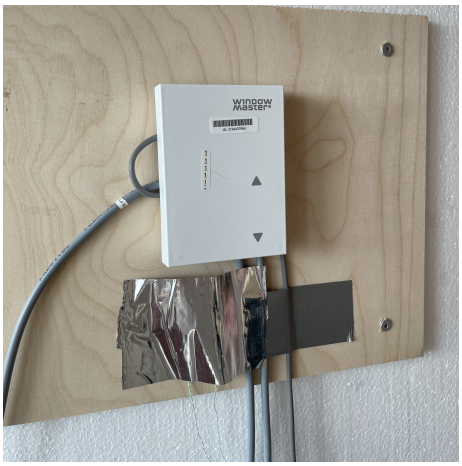

Figure 9.10: K-type thermocouple placement during the WindomMaster validation in the Test Room.

The graphs show that both sensors have the same trends as the rises and drops coincide. Across all three WindowMaster monitors, temperatures are consistently lower than those recorded by the K-type thermocouples, with an average difference of 1.16°C (channel 36) for the Test Room, 0.43°C (channel 99) for the DSF cavity, and 1.26°C (channel 51) for the DCV cavity compared to WindowMaster data.

While the thermocouples report similar temperatures in the Test Room, a noticeable variance emerges between the two thermocouples placed in the DSF cavity (channels 83 and 99), amounting to an average difference of 0.49°C. Furthermore, it is evident that greater temperature fluctuations occur when solar radiation is present.

The DCV cavity records the highest noise among the thermocouples.

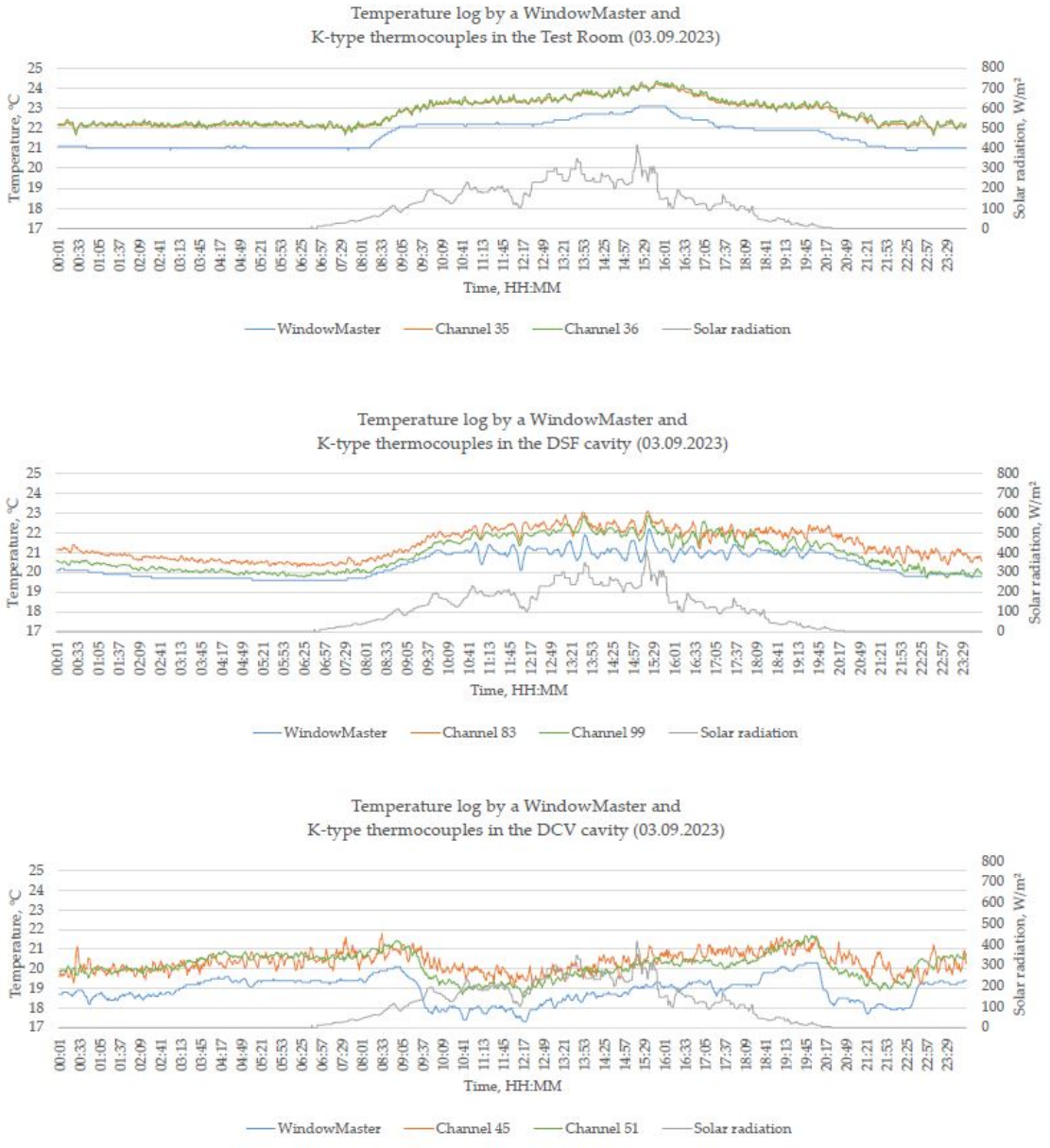

Figure 9.11: WindowMaster air temperature measures compared with K-type thermocouples measures.

WindowMaster vs IC-meters

The placement of the IC-meter device can be seen in Figure 9.12.

Figure 9.12: IC-meters placement during the WindomMaster validation. Test Room (Right), DSF cavity (Middle) and DCV cavity (Left).

The data for temperature logs are presented in Figure 9.13 for all day 29.09.2023 for the Test Room and DCV cavity and 19.09.2023 for the DSF cavity. The line graphs show that both apparatuses have the same pattern in data logs. However, the WindowMaster logs detect lower temperatures than the IC-meter. On average, the WindowMaster showed lower temperatures by 1.63°C for the Test Room, 2.09°C for the DSF cavity and 1.77°C for the DCV cavity compared with the IC-meter data. Notably, WindowMaster and IC-meter measurements tend to exhibit more pronounced fluctuations when solar radiation increases.

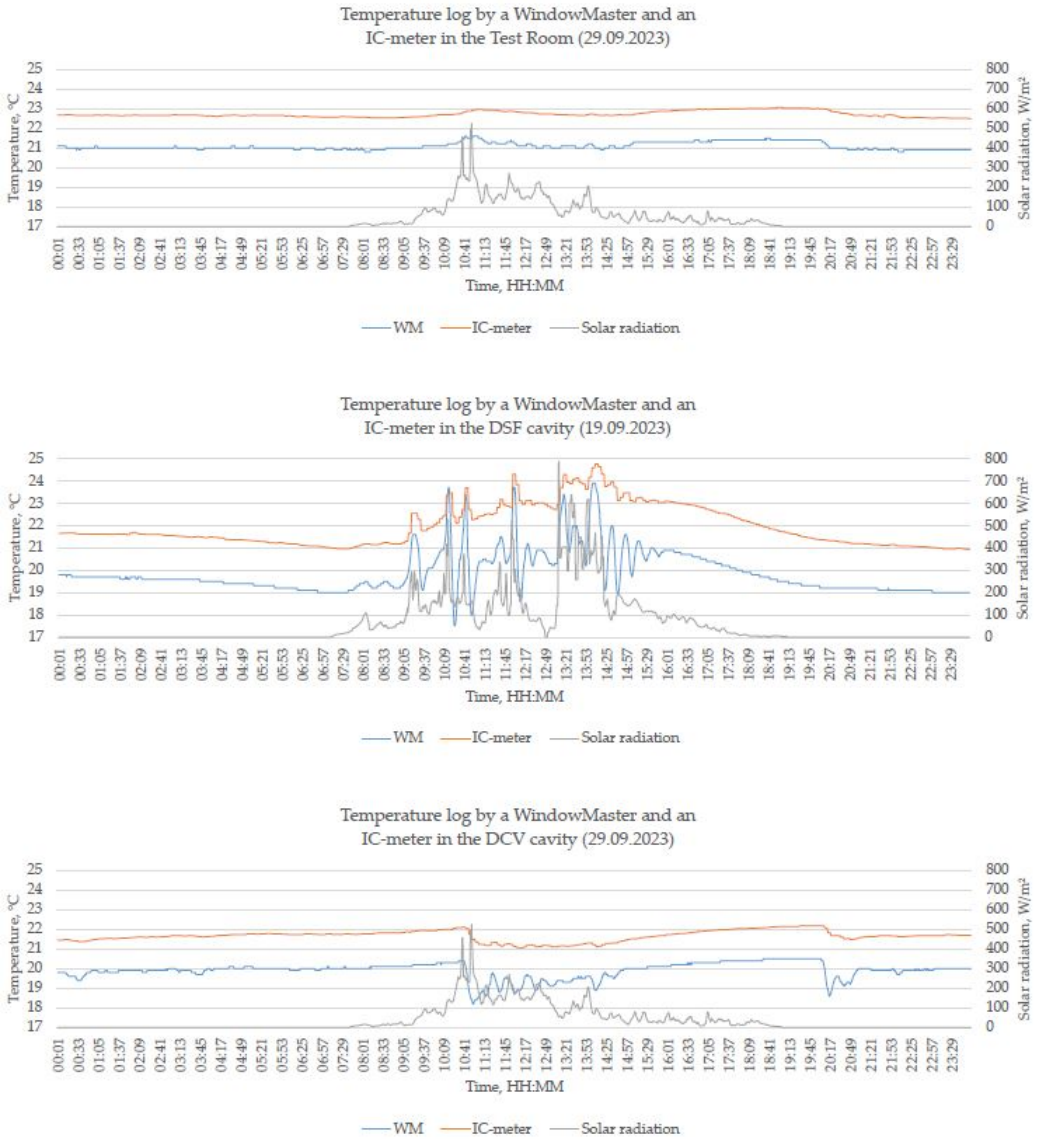

Figure 9.13: WindowMaster air temperature measures compared with IC-meter measures.

Summary

To summarise, the data indicates that WindowMaster tends to record slightly lower temperatures compared to the reference sensors, with variations in accuracy observed across different locations within the location of the WindowMaster monitor. This could mean it takes more time for the WindowMaster monitor to react and start the cooling/heating mode, which may indicate a risk of discomfort in the room regarding too low or too high indoor temperatures. This suggests there may be room for calibration improvements to ensure precise temperature management.

Furthermore, the noticeable variance between the reference thermocouples in the DSF cavity, particularly in the presence of solar radiation, highlights the importance of accounting for environmental factors when relying on automated systems like WindowMaster and checking the accuracy of the K-type thermocouples as they might require to be calibrated.

Therefore, the offsets for the WindowMaster values are as follows:

- DCV cavity: +1.8°C
- Test room: +1.6°C
- Test room: +2.0°C

Figure 9.3.2 shows how the change of the offset in the WindowMaster, the average difference between the WindowMAster and thermocouple measuring the air temperature near the WindowMaster in the Test room is 0.424°C and between Window Master and IC-meter is -0.003°C. The data in the figure is used from the intermediate measurement.

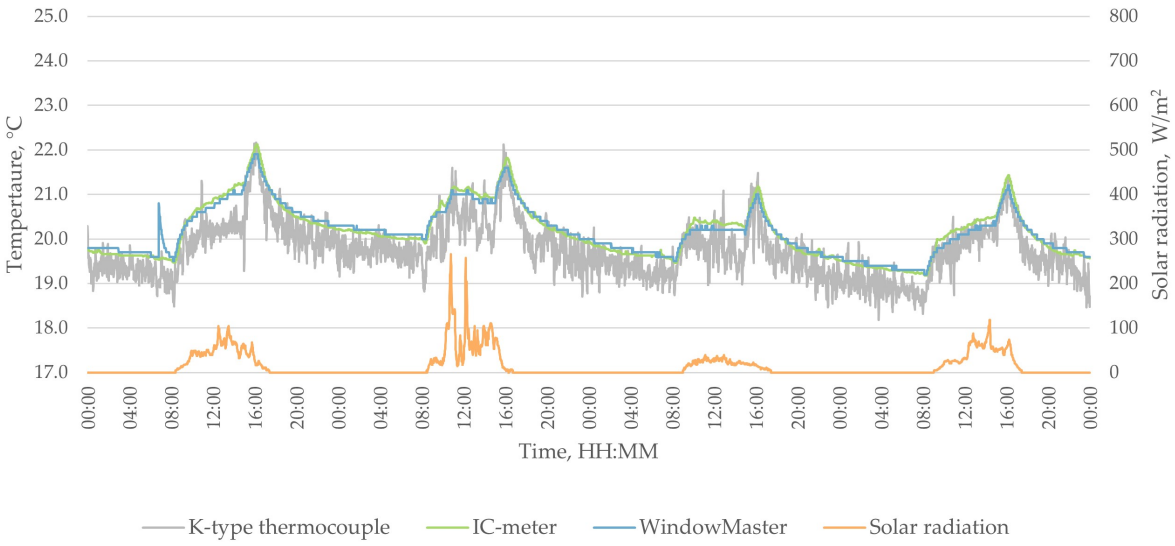

Figure 9.14: The effect on data between the WindowMaser, IC-meter and thermocouple after the change of offset of the WindowMaster. (23-26.10.2023)

9.3.3 Different types of protection for thermocouples against solar radiation

The performance of thermocouples with different types of protection against solar radiation is measured with the aim of defining the most adequate one. The measurement is conducted for three thermocouples placed on the middle line in the DSF cavity at the height of 1.34m. Thermocouple 71 is located inside a silver tube equipped with a mechanical mini fan with a produced air velocity of 1.5m/s. Thermocouple 11 is placed on the outside of the silver tube and is covered with silver foil that allows natural ventilation. Thermocouple 18 is also fixed on the side of the silver tube, however, without any protective measures against direct solar radiation. The setup of the thermocouples is displayed in Figure 9.15.

Figure 9.15: Eperimental setup of measuring the performance of thermocouples with different types of protection against solar radiation.

The measurement is conducted on a sunny day on 05.10.2023. The measured temperatures during this day are displayed in Figures 9.16-9.17. It can be observed that when the solar radiation was high (e.g. from 11:30-12:30 in Figure 9.17), the thermocouple placed inside the silver tube (71) showed the lowest average and maximum temperatures, while the thermocouple shielded with silver foil (18) showed the highest average and maximum temperatures. The thermocouple with no protection displayed intermediate temperatures. The high temperatures of the thermocouple with silver foil could be explained as the airflow around the measuring point is more limited than around the exposed thermocouple.

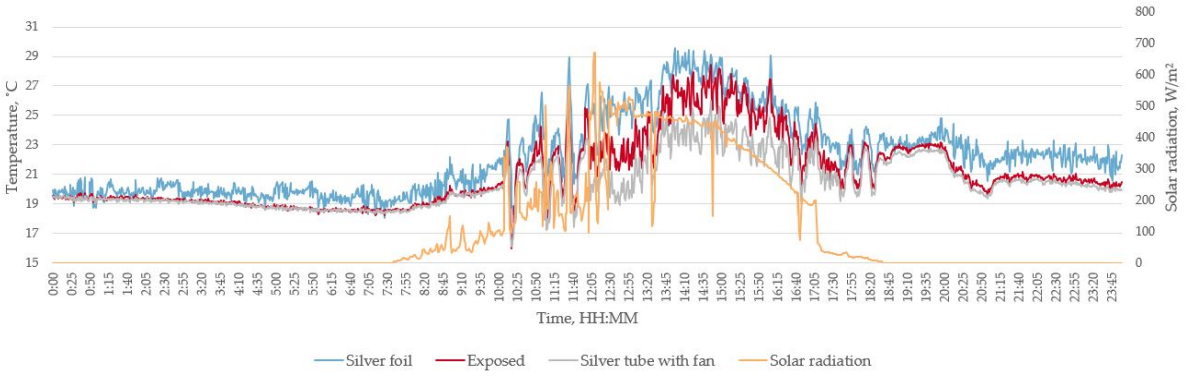

Figure 9.16: Performance of thermocouples with different types of protection against solar radiation for 24 hours on 05.10.2023.

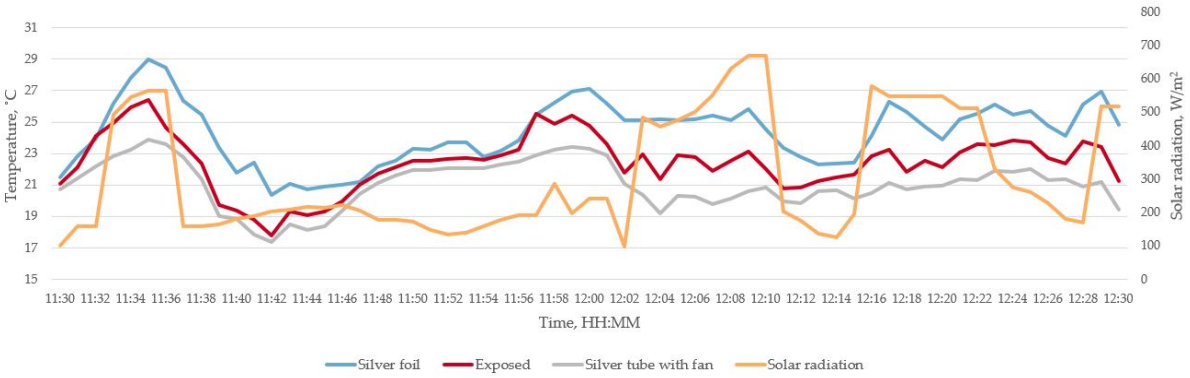

Figure 9.17: Performance of thermocouples with different types of protection against solar radiation at 11:30-12:30 on 05.10.2023.

In conclusion, the most adequate method for protecting the thermocouples against solar radiation, in order to obtain accurate temperature measurements, is to place them inside a silver tube, that is equipped with a mini fan to ensure airflow inside the silver tube which removes the radiative heat. Furthermore, as the mini fan is located at the bottom of the silver tube, a downward airflow is provided, thus the additional heat generated by the fans is not measured by the thermocouples.

9.3.4 Performance of thermocouples in polished vs. unpolished silver tubes

The thermocouples in the DSF cavity are placed inside a mechanically ventilated silver tube. As silver tarnishes over time when exposed to sulfur in the air, a test measurement is run with the aim of finding whether it has any effect on the performance of thermocouples.

Figure 9.18: Polished (left) and unpolished (right) silver tubes.

The silver tube of thermocouple 71 is polished, and the measurement results are compared with thermocouples 66 and 80, which are placed inside unpolished silver tubes. The selected thermocouples are located at the same height, at 1.5m. Thermocouple 66 is placed on the West line, thermocouple 71 is on the middle line, and thermocouple 80 is on the East line. The test measurement is conducted on 26.09.2023 between 12:30-15:30, and the results are displayed in Figure 9.19.

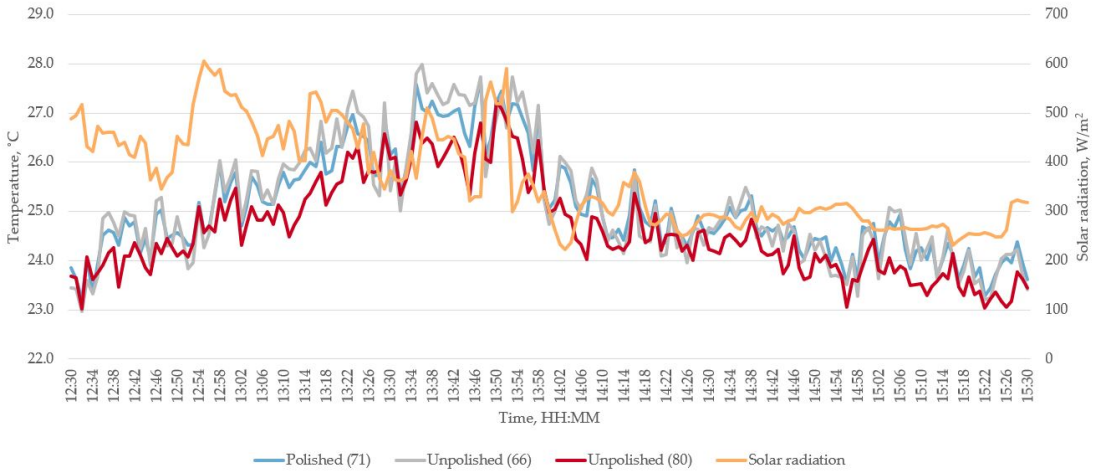

Figure 9.19: Performance of thermocouples in polished (71) and unpolished (66, 80) silver tubes, measured at 12:30-15:30 on 26.09.2023.

From the results, it can be observed that the polished and unpolished silver tubes perform similarly, as the peak temperatures occur at the same time and with small temperature differences.

Thermocouples, ˚C			
	71	66	80
Average	21.39	21.34	21.01
Min	17.36	18.18	18.61
Max	28.25	28.45	28.25

Figure 9.20: Average, minimum, and maximum temperatures measured at 12:30-15:30 on 26.09.2023.

Therefore, it can be concluded that the tarnishing of the silver tubes does not affect the performance of the thermocouples.

9.4 Wind speed scale according to the WindowMaster

Wind force in Beaufort	Speed in m/s	Speed in km/h	Wind intensity	Effects
0	0 – 0,2	< 1	calm	smoke rises straight
1	0,3 – 1,5	1 – 5	light air	only noticeable from the smoke
2	1,6 – 3,3	6 – 11	light breeze	noticeable on the face
3	3,4 – 5,4	12 – 19	gentle breeze	thin twigs are moved
4	5,5 – 7,9	20 – 28	moderate breeze	thin branches are moved
5	8 – 10,7	29 – 38	fresh breeze	small trees sway
6	10,8 – 13,8	39 – 49	strong breeze	thick branches are moved
7	13,9 – 17,1	50 – 61	moderate gale	entire trees are in motion
8	17,2 – 20,7	62 – 74	fresh gale	Branches break off trees
9	20,8 – 24,4	75 – 88	strong gale	minor damage to houses
10	24,5 – 28,4	89 – 102	whole gale	trees blown over
11	28,5 – 32,6	103 – 117	storm	severe storm damage
12	> 32,6	> 117	hurricane	

Figure 9.21: Wind speed scale according to the WindowMaster. [23]

9.5 Analysis of the temperature distribution in the DSF & DCV cavity

DSF cavity - Summer case

In this section, the figures display averages for three hours each day in the DSF cavity during the conducted measurement in the period of 24-30.07.2023.

Day 1				24/07/2023
Averages - 8:00-9:00			Average outdoor temperature:	16.47
	West line	Middle line	East line	Average solar radiation:	122
Bypass	18.53	17.85	17.82	
2.41m	21.09	20.57	20.48	
1.87m	21.10	20.68	20.46	
1.34m	21.11	20.78	20.79	
0.80m	21.15	20.88	20.61	
0.265m	21.18	21.14	20.59	
Averages - 11:00-12:00			Average outdoor temperature:	18.81
	West line	Middle line	East line	Average solar radiation:	280
Bypass	21.35	20.08	19.96	
2.41m	21.32	21.18	23.10	
1.87m	21.65	21.50	20.29	
1.34m	21.58	22.07	20.83	
0.80m	21.47	22.50	21.63	
0.265m	21.32	21.19	20.79	
Averages - 14:00-15:00			Average outdoor temperature:	17.57
	West line	Middle line	East line	Average solar radiation:	306
Bypass	20.26	19.16	19.14	
2.41m	20.91	20.94	21.74	
1.87m	21.24	21.15	20.34	
1.34m	21.20	21.65	20.72	
0.80m	21.16	21.81	21.20	
0.265m	21.06	20.58	20.36	

Figure 9.22: Hourly averages of the measured temperatures in the DSF cavity. (24.07.2023)

Day 2				25/07/2023
Averages - 8:00-9:00			Average outdoor temperature:	16.03
	West line	Middle line	East line	Average solar radiation:	307
Bypass	19.34	19.03	18.20	
2.41m	19.90	19.63	19.07	
1.87m	19.90	19.45	19.09	
1.34m	19.90	19.65	19.44	
0.80m	19.70	19.48	19.19	
0.265m	18.99	18.84	18.09	
Averages - 11:00-12:00			Average outdoor temperature:	17.59
	West line	Middle line	East line	Average solar radiation:	625
Bypass	23.83	23.58	22.66	
2.41m	24.02	23.35	22.16	
1.87m	24.26	23.73	23.02	
1.34m	24.05	24.06	25.95	
0.80m	23.78	23.50	23.09	
0.265m	23.76	23.84	23.10	
Averages - 14:00-15:00			Average outdoor temperature:	18.51
	West line	Middle line	East line	Average solar radiation:	767
Bypass	19.74	19.52	19.41	
2.41m	21.77	20.78	19.75	
1.87m	22.69	21.61	20.43	
1.34m	22.54	21.92	23.07	
0.80m	22.51	21.83	21.23	
0.265m	22.80	22.72	21.71	

Figure 9.23: Hourly averages of the measured temperatures in the DSF cavity. (25.07.2023)

Day 3					26/07/2023
	Averages - 8:00-9:00			Average outdoor temperature:	13.89
	West line	Middle line	East line	Average solar radiation:	249
Bypass	17.31	16.94	16.52		
2.41m	18.13	17.78	17.00		
1.87m	18.07	17.50	17.05		
1.34m	17.95	17.57	17.33		
0.80m	17.78	17.27	17.17		
0.265m	17.36	17.18	16.70		
	Averages - 11:00-12:00			Average outdoor temperature:	14.92
	West line	Middle line	East line	Average solar radiation:	604
Bypass	22.28	22.02	21.16		
2.41m	22.20	21.90	21.28		
1.87m	22.20	21.76	21.53		
1.34m	21.99	22.15	23.96		
0.80m	21.46	20.91	21.10		
0.265m	20.55	20.29	19.75		
	Averages - 14:00-15:00			Average outdoor temperature:	13.86
	West line	Middle line	East line	Average solar radiation:	330
Bypass	17.95	16.94	16.71		
2.41m	20.89	20.19	19.37		
1.87m	20.95	20.45	19.90		
1.34m	20.78	20.61	20.74		
0.80m	20.56	20.21	20.01		
0.265m	19.35	19.64	19.12		

Figure 9.24: Hourly averages of the measured temperatures in the DSF cavity. (26.07.2023)

Day 4					27/07/2023
	Averages - 8:00-9:00			Average outdoor temperature:	13.43
	West line	Middle line	East line	Average solar radiation:	125
Bypass	19.26	18.81	18.53		
2.41m	17.50	17.89	19.67		
1.87m	17.33	17.33	17.77		
1.34m	17.51	18.80	16.71		
0.80m	17.51	17.68	21.35		
0.265m	16.44	16.69	19.78		
	Averages - 11:00-12:00			Average outdoor temperature:	16.94
	West line	Middle line	East line	Average solar radiation:	418
Bypass	23.92	23.47	22.45		
2.41m	23.83	20.65	22.80		
1.87m	23.91	23.35	23.17		
1.34m	23.84	23.73	24.73		
0.80m	23.49	23.17	22.87		
0.265m	22.62	22.58	21.95		
	Averages - 14:00-15:00			Average outdoor temperature:	16.53
	West line	Middle line	East line	Average solar radiation:	666
Bypass	20.50	19.82	19.84		
2.41m	21.94	21.66	21.12		
1.87m	22.63	22.03	20.94		
1.34m	22.62	22.65	22.57		
0.80m	22.52	22.51	21.53		
0.265m	22.27	22.11	21.24		

Figure 9.25: Hourly averages of the measured temperatures in the DSF cavity. (27.07.2023)

Day 5				28/07/2023
Averages - 8:00-9:00			Average outdoor temperature:	14.43
	West line	Middle line	East line	Average solar radiation:	273
Bypass	16.62	16.25	16.26	
2.41m	19.15	19.04	18.88	
1.87m	19.25	19.01	18.82	
1.34m	19.28	19.10	19.11	
0.80m	19.37	19.04	18.99	
0.265m	19.43	19.40	19.03	
Averages - 11:00-12:00			Average outdoor temperature:	18.63
	West line	Middle line	East line	Average solar radiation:	733
Bypass	21.89	21.95	21.58	
2.41m	26.31	25.57	24.97	
1.87m	26.70	26.04	25.69	
1.34m	26.57	26.51	30.72	
0.80m	26.49	26.10	25.68	
0.265m	26.52	26.93	25.67	
Averages - 14:00-15:00			Average outdoor temperature:	20.73
	West line	Middle line	East line	Average solar radiation:	749
Bypass	25.60	25.69	25.51	
2.41m	31.20	30.49	30.42	
1.87m	31.85	31.21	31.20	
1.34m	32.01	31.91	34.26	
0.80m	31.70	31.18	31.08	
0.265m	31.16	31.71	30.34	

Figure 9.26: Hourly averages of the measured temperatures in the DSF cavity. (28.07.2023)

Day 6				29/07/2023
Averages - 8:00-9:00			Average outdoor temperature:	17.63
	West line	Middle line	East line	Average solar radiation:	255
Bypass	19.77	19.23	19.17	
2.41m	21.72	21.20	20.81	
1.87m	21.76	21.18	20.93	
1.34m	21.80	21.41	21.21	
0.80m	21.79	21.46	21.15	
0.265m	21.37	21.61	20.90	
Averages - 11:00-12:00			Average outdoor temperature:	21.26
	West line	Middle line	East line	Average solar radiation:	536
Bypass	21.99	21.63	21.66	
2.41m	24.15	23.41	22.75	
1.87m	24.27	23.54	23.15	
1.34m	24.25	23.89	26.51	
0.80m	24.45	24.04	23.67	
0.265m	24.26	24.50	23.59	
Averages - 14:00-15:00			Average outdoor temperature:	18.91
	West line	Middle line	East line	Average solar radiation:	269
Bypass	21.53	20.92	20.79	
2.41m	21.40	20.74	24.02	
1.87m	21.57	20.59	22.10	
1.34m	21.69	22.22	20.84	
0.80m	21.59	21.76	24.98	
0.265m	20.94	21.93	24.12	

Figure 9.27: Hourly averages of the measured temperatures in the DSF cavity. (29.07.2023)

Day 7					30/07/2023
	Averages - 8:00-9:00			Average outdoor temperature:	16.45
	West line	Middle line	East line	Average solar radiation:	275
Bypass	20.87	20.30	20.03		
2.41m	21.09	21.29	20.84		
1.87m	21.15	21.03	19.97		
1.34m	21.21	21.56	20.15		
0.80m	21.21	21.82	20.97		
0.265m	21.44	21.17	21.10		
	Averages - 11:00-12:00			Average outdoor temperature:	20.32
	West line	Middle line	East line	Average solar radiation:	540
Bypass	20.92	20.68	20.65		
2.41m	23.44	22.69	21.67		
1.87m	23.75	23.17	22.33		
1.34m	22.88	23.47	26.00		
0.80m	23.67	23.35	22.95		
0.265m	23.69	23.95	23.13		
	Averages - 14:00-15:00			Average outdoor temperature:	17.74
	West line	Middle line	East line	Average solar radiation:	66
Bypass	19.99	19.07	19.02		
2.41m	21.77	21.33	19.99		
1.87m	22.01	21.61	20.33		
1.34m	21.84	21.67	21.19		
0.80m	21.65	21.51	20.98		
0.265m	20.94	20.94	20.45		

Figure 9.28: Hourly averages of the measured temperatures in the DSF cavity. (30.07.2023)

DSF cavity - Intermediate case

In this section, the figures display averages for three hours each day in the DSF cavity during the conducted measurement in the period of 23-26.10.2023.

Day 1					23/10/2023
	Averages - 8:00-9:00			Average outdoor temperature:	10.20
	West line	Middle line	East line	Average solar radiation:	5
Bypass	19.22	17.58	19.91		
2.41m	17.11	15.77	16.48		
1.87m	16.87	15.99	14.34		
1.34m	16.76	16.68	13.93		
0.80m	16.16	16.53	16.49		
0.265m	14.98	15.63	15.06		
	Averages - 11:00-12:00			Average outdoor temperature:	10.04
	West line	Middle line	East line	Average solar radiation:	43
Bypass	20.19	18.86	20.54		
2.41m	18.17	16.32	17.69		
1.87m	17.89	16.70	15.03		
1.34m	17.89	17.71	14.41		
0.80m	17.16	17.45	17.68		
0.265m	16.27	16.69	16.47		
	Averages - 14:00-15:00			Average outdoor temperature:	10.65
	West line	Middle line	East line	Average solar radiation:	55
Bypass	22.05	20.49	22.25		
2.41m	19.70	17.51	18.95		
1.87m	19.37	17.97	15.79		
1.34m	19.31	19.29	15.01		
0.80m	18.38	18.97	19.22		
0.265m	17.80	18.29	18.27		

Figure 9.29: Hourly averages of the measured temperatures in the DSF cavity. (23.10.2023)

Day 2					24/10/2023
	Averages - 8:00-9:00			Average outdoor temperature:	9.94
	West line	Middle line	East line	Average solar radiation:	8
Bypass	18.56	17.58	19.41		
2.41m	16.87	15.91	15.82		
1.87m	15.62	15.98	14.67		
1.34m	15.55	16.37	14.29		
0.80m	15.26	15.85	16.21		
0.265m	14.82	15.30	14.71		
	Averages - 11:00-12:00			Average outdoor temperature:	10.52
	West line	Middle line	East line	Average solar radiation:	60
Bypass	19.06	17.97	19.26		
2.41m	17.47	16.20	16.61		
1.87m	17.28	16.40	14.98		
1.34m	17.00	16.94	14.48		
0.80m	15.94	16.37	16.75		
0.265m	15.21	16.18	15.35		
	Averages - 14:00-15:00			Average outdoor temperature:	9.82
	West line	Middle line	East line	Average solar radiation:	86
Bypass	17.38	16.52	17.70		
2.41m	16.09	15.12	15.61		
1.87m	15.94	15.22	14.09		
1.34m	15.66	15.58	13.75		
0.80m	14.75	14.90	15.50		
0.265m	13.53	14.79	14.16		

Figure 9.30: Hourly averages of the measured temperatures in the DSF cavity. (24.10.2023)

Day 3				25/10/2023
Averages - 8:00-9:00			Average outdoor temperature:	7.30
	West line	Middle line	East line	Average solar radiation:	0
Bypass	16.94	16.66	17.35	
2.41m	15.15	15.02	14.08	
1.87m	15.21	14.92	13.79	
1.34m	14.88	14.87	13.86	
0.80m	14.92	14.71	14.79	
0.265m	14.40	13.70	13.80	
Averages - 11:00-12:00			Average outdoor temperature:	7.41
	West line	Middle line	East line	Average solar radiation:	29
Bypass	16.26	15.64	16.89	
2.41m	14.52	13.84	13.79	
1.87m	14.33	13.86	12.89	
1.34m	14.22	14.13	12.67	
0.80m	13.60	13.80	14.12	
0.265m	11.62	13.07	14.84	
Averages - 14:00-15:00			Average outdoor temperature:	7.91
	West line	Middle line	East line	Average solar radiation:	21
Bypass	17.00	15.98	17.61	
2.41m	15.17	14.05	14.42	
1.87m	14.97	14.23	12.98	
1.34m	14.91	14.84	12.39	
0.80m	14.03	14.57	14.90	
0.265m	12.65	13.93	13.54	

Figure 9.31: Hourly averages of the measured temperatures in the DSF cavity. (25.10.2023)

Day 4				26/10/2023
Averages - 8:00-9:00			Average outdoor temperature:	5.67
	West line	Middle line	East line	Average solar radiation:	0
Bypass	16.60	16.24	17.01	
2.41m	14.80	14.78	13.77	
1.87m	14.60	14.67	13.62	
1.34m	14.54	14.60	13.69	
0.80m	14.35	14.47	14.50	
0.265m	13.35	13.76	13.87	
Averages - 11:00-12:00			Average outdoor temperature:	6.07
	West line	Middle line	East line	Average solar radiation:	26
Bypass	15.26	15.15	15.91	
2.41m	14.63	14.56	13.74	
1.87m	14.52	14.62	13.68	
1.34m	14.47	14.58	13.73	
0.80m	14.28	14.45	14.49	
0.265m	13.19	13.61	13.72	
Averages - 14:00-15:00			Average outdoor temperature:	6.43
	West line	Middle line	East line	Average solar radiation:	70
Bypass	15.24	15.24	15.81	
2.41m	14.96	15.03	14.12	
1.87m	14.91	15.03	14.10	
1.34m	14.85	14.99	14.14	
0.80m	14.71	14.79	14.83	
0.265m	13.74	13.90	14.08	

Figure 9.32: Hourly averages of the measured temperatures in the DSF cavity. (26.10.2023)

DSF cavity - Winter case

In this section, the figures display averages for three hours each day in the DSF cavity during the conducted measurement in the period of 30.11.2023-02.12.2023.

Day 1				30/11/2023
Averages - 8:00-9:00			Average outdoor temperature:	-2.13
	West line	Middle line	East line	Average solar radiation:	1
Bypass	16.16	15.72	16.45	
2.41m	12.12	12.09	11.20	
1.87m	11.92	11.92	11.19	
1.34m	11.82	11.85	11.23	
0.80m	11.73	11.79	11.79	
0.265m	11.57	11.77	11.73	
Averages - 11:00-12:00			Average outdoor temperature:	-1.65
	West line	Middle line	East line	Average solar radiation:	123
Bypass	22.84	27.12	21.75	
2.41m	25.84	25.67	24.99	
1.87m	26.04	25.55	25.00	
1.34m	25.27	25.62	25.07	
0.80m	24.66	24.40	25.08	
0.265m	22.65	23.05	23.44	
Averages - 14:00-15:00			Average outdoor temperature:	-0.95
	West line	Middle line	East line	Average solar radiation:	5
Bypass	20.37	21.14	20.25	
2.41m	20.55	20.51	19.74	
1.87m	20.18	20.28	19.57	
1.34m	20.02	20.17	19.50	
0.80m	19.81	19.75	19.98	
0.265m	18.79	18.80	19.22	

Figure 9.33: Hourly averages of the measured temperatures in the DSF cavity. (30.11.2023)

Day 2				01/12/2023
Averages - 8:00-9:00			Average outdoor temperature:	-1.31
	West line	Middle line	East line	Average solar radiation:	0
Bypass	16.44	16.04	16.76	
2.41m	12.85	12.83	11.98	
1.87m	12.71	12.71	11.98	
1.34m	12.62	12.64	12.02	
0.80m	12.52	12.60	12.59	
0.265m	12.37	12.61	12.55	
Averages - 11:00-12:00			Average outdoor temperature:	-1.44
	West line	Middle line	East line	Average solar radiation:	31
Bypass	17.73	17.82	18.04	
2.41m	14.66	14.70	13.82	
1.87m	14.62	14.66	13.85	
1.34m	14.44	14.60	13.86	
0.80m	14.36	14.52	14.46	
0.265m	14.28	14.49	14.42	
Averages - 14:00-15:00			Average outdoor temperature:	-1.07
	West line	Middle line	East line	Average solar radiation:	9
Bypass	24.47	28.11	24.80	
2.41m	28.92	28.90	28.41	
1.87m	28.77	28.61	28.10	
1.34m	28.35	28.70	27.89	
0.80m	27.43	27.66	27.97	
0.265m	25.91	26.31	26.66	

Figure 9.34: Hourly averages of the measured temperatures in the DSF cavity. (01.12.2023)

Day 3					02/12/2023
	Averages - 8:00-9:00			Average outdoor temperature:	-5.80
	West line	Middle line	East line	Average solar radiation:	4
Bypass	16.21	15.73	16.50		
2.41m	10.97	10.92	10.03		
1.87m	10.75	10.79	9.99		
1.34m	10.64	10.70	10.00		
0.80m	10.54	10.55	10.59		
0.265m	10.33	10.43	10.49		
	Averages - 11:00-12:00			Average outdoor temperature:	-3.29
	West line	Middle line	East line	Average solar radiation:	8
Bypass	18.50	20.17	18.45		
2.41m	18.50	18.52	17.87		
1.87m	18.60	18.48	17.70		
1.34m	18.39	18.50	17.77		
0.80m	18.26	18.26	18.32		
0.265m	17.81	18.01	18.20		
	Averages - 14:00-15:00			Average outdoor temperature:	-2.26
	West line	Middle line	East line	Average solar radiation:	41
Bypass	18.86	19.34	18.85		
2.41m	18.76	18.85	18.12		
1.87m	18.65	18.75	18.00		
1.34m	18.59	18.69	18.00		
0.80m	18.51	18.50	18.60		
0.265m	18.17	18.15	18.35		

Figure 9.35: Hourly averages of the measured temperatures in the DSF cavity. (02.12.2023)

DCV cavity - Summer case

In this section, the figures display averages for three hours each day in the DCV cavity during the conducted measurement in the period of 24-30.07.2023.

Day 1			24/07/2023
Averages - 8:00-9:00		Average outdoor temperature:	16.47
	East line	West line	Average solar radiation:	122
1m	N/A	18.91	
2m	N/A	N/A	
2.75m	19.16	18.70	
Averages - 11:00-12:00		Average outdoor temperature:	18.81
	East line	West line	Average solar radiation:	280
1m	N/A	19.30	
2m	N/A	N/A	
2.75m	19.11	19.10	
Averages - 14:00-15:00		Average outdoor temperature:	17.57
	East line	West line	Average solar radiation:	306
1m	N/A	18.64	
2m	N/A	N/A	
2.75m	18.33	18.40	

Figure 9.36: Hourly averages of the measured temperatures in the DCV cavity. (24.07.2023)

Day 2			25/07/2023
Averages - 8:00-9:00		Average outdoor temperature:	16.03
	East line	West line	Average solar radiation:	307
1m	N/A	18.18	
2m	N/A	N/A	
2.75m	17.83	17.84	
Averages - 11:00-12:00		Average outdoor temperature:	17.59
	East line	West line	Average solar radiation:	625
1m	N/A	22.74	
2m	N/A	N/A	
2.75m	22.19	22.14	
Averages - 14:00-15:00		Average outdoor temperature:	18.51
	East line	West line	Average solar radiation:	767
1m	N/A	19.88	
2m	N/A	N/A	
2.75m	19.56	19.64	

Figure 9.37: Hourly averages of the measured temperatures in the DCV cavity. (25.07.2023)

Day 3			26/07/2023
Averages - 8:00-9:00		Average outdoor temperature:	13.89
	East line	West line	Average solar radiation:	249
1m	N/A	16.73		
2m	N/A	N/A		
2.75m	16.73	16.37		
Averages - 11:00-12:00		Average outdoor temperature:	14.92
	East line	West line	Average solar radiation:	604
1m	N/A	21.14		
2m	N/A	N/A		
2.75m	20.96	20.64		
Averages - 14:00-15:00		Average outdoor temperature:	13.86
	East line	West line	Average solar radiation:	330
1m	N/A	19.31		
2m	N/A	N/A		
2.75m	18.31	18.06		

Figure 9.38: Hourly averages of the measured temperatures in the DCV cavity. (26.07.2023)

Day 4			27/07/2023
Averages - 8:00-9:00		Average outdoor temperature:	13.43
	East line	West line	Average solar radiation:	125
1m	N/A	18.39		
2m	N/A	N/A		
2.75m	19.04	18.58		
Averages - 11:00-12:00		Average outdoor temperature:	16.94
	East line	West line	Average solar radiation:	418
1m	N/A	22.04		
2m	N/A	N/A		
2.75m	21.68	21.57		
Averages - 14:00-15:00		Average outdoor temperature:	16.53
	East line	West line	Average solar radiation:	666
1m	N/A	19.52		
2m	N/A	N/A		
2.75m	19.23	19.35		

Figure 9.39: Hourly averages of the measured temperatures in the DCV cavity. (27.07.2023)

Day 5			28/07/2023
Averages - 8:00-9:00		Average outdoor temperature:	14.43
	East line	West line	Average solar radiation:	273
1m	N/A	17.42		
2m	N/A	N/A		
2.75m	17.58	17.69		
Averages - 11:00-12:00		Average outdoor temperature:	18.63
	East line	West line	Average solar radiation:	733
1m	N/A	21.32		
2m	N/A	N/A		
2.75m	21.27	21.07		
Averages - 14:00-15:00		Average outdoor temperature:	20.73
	East line	West line	Average solar radiation:	749
1m	N/A	24.82		
2m	N/A	N/A		
2.75m	24.69	24.50		

Figure 9.40: Hourly averages of the measured temperatures in the DCV cavity. (28.07.2023)

Day 6			29/07/2023
Averages - 8:00-9:00		Average outdoor temperature:	17.63
	East line	West line	Average solar radiation:	255
1m	N/A	19.64	
2m	N/A	N/A	
2.75m	19.32	19.38	
Averages - 11:00-12:00		Average outdoor temperature:	21.26
	East line	West line	Average solar radiation:	536
1m	N/A	21.40	
2m	N/A	N/A	
2.75m	21.36	21.33	
Averages - 14:00-15:00		Average outdoor temperature:	18.91
	East line	West line	Average solar radiation:	269
1m	N/A	20.55	
2m	N/A	N/A	
2.75m	20.68	20.48	

Figure 9.41: Hourly averages of the measured temperatures in the DCV cavity. (29.07.2023)

Day 7			30/07/2023
Averages - 8:00-9:00		Average outdoor temperature:	16.45
	East line	West line	Average solar radiation:	275
1m	N/A	19.79	
2m	N/A	N/A	
2.75m	20.20	19.72	
Averages - 11:00-12:00		Average outdoor temperature:	20.32
	East line	West line	Average solar radiation:	540
1m	N/A	20.56	
2m	N/A	N/A	
2.75m	20.51	20.50	
Averages - 14:00-15:00		Average outdoor temperature:	17.74
	East line	West line	Average solar radiation:	66
1m	N/A	19.86	
2m	N/A	N/A	
2.75m	19.34	19.53	

Figure 9.42: Hourly averages of the measured temperatures in the DCV cavity. (30.07.2023)

DCV cavity - Intermediate case

In this section, the figures display averages for three hours each day in the DCV cavity during the conducted measurement in the period of 23-26.10.2023.

Day 1			23/10/2023
Averages - 8:00-9:00		Average outdoor temperature:	10.20
	East line	West line	Average solar radiation:	5
1m	19.19	17.02	
2m	18.19	18.53	
2.75m	18.18	18.56	
Averages - 11:00-12:00		Average outdoor temperature:	10.04
	East line	West line	Average solar radiation:	43
1m	18.79	16.72	
2m	18.13	18.27	
2.75m	17.90	17.92	
Averages - 14:00-15:00		Average outdoor temperature:	10.65
	East line	West line	Average solar radiation:	55
1m	19.41	17.04	
2m	18.61	18.83	
2.75m	18.27	18.76	

Figure 9.43: Hourly averages of the measured temperatures in the DCV cavity. (23.10.2023)

Day 2			24/10/2023
Averages - 8:00-9:00		Average outdoor temperature:	9.94
	East line	West line	Average solar radiation:	8
1m	19.48	17.53	
2m	18.36	18.86	
2.75m	19.08	19.28	
Averages - 11:00-12:00		Average outdoor temperature:	10.52
	East line	West line	Average solar radiation:	60
1m	18.97	16.95	
2m	17.66	18.26	
2.75m	18.49	18.66	
Averages - 14:00-15:00		Average outdoor temperature:	9.82
	East line	West line	Average solar radiation:	86
1m	18.46	16.31	
2m	16.92	17.69	
2.75m	17.89	18.14	

Figure 9.44: Hourly averages of the measured temperatures in the DCV cavity. (24.10.2023)

Day 3			25/10/2023
Averages - 8:00-9:00		Average outdoor temperature:	7.30
	East line	West line	Average solar radiation:	0
1m	18.56	17.04	
2m	16.92	18.28	
2.75m	17.80	19.36	
Averages - 11:00-12:00		Average outdoor temperature:	7.41
	East line	West line	Average solar radiation:	29
1m	17.71	15.69	
2m	16.16	17.43	
2.75m	16.62	18.32	
Averages - 14:00-15:00		Average outdoor temperature:	7.91
	East line	West line	Average solar radiation:	21
1m	17.48	17.44	
2m	16.05	16.88	
2.75m	16.04	18.04	

Figure 9.45: Hourly averages of the measured temperatures in the DCV cavity. (25.10.2023)

Day 4			26/10/2023
Averages - 8:00-9:00		Average outdoor temperature:	5.67
	East line	West line	Average solar radiation:	0
1m	18.18	16.67	
2m	16.61	18.15	
2.75m	17.63	18.82	
Averages - 11:00-12:00		Average outdoor temperature:	6.07
	East line	West line	Average solar radiation:	26
1m	17.38	15.95	
2m	15.93	17.42	
2.75m	16.96	18.02	
Averages - 14:00-15:00		Average outdoor temperature:	6.43
	East line	West line	Average solar radiation:	70
1m	17.52	16.09	
2m	16.03	17.42	
2.75m	16.69	18.30	

Figure 9.46: Hourly averages of the measured temperatures in the DCV cavity. (26.10.2023)

DCV cavity - Winter case

In this section, the figures display averages for three hours each day in the DCV cavity during the conducted measurement in the period of 30.11.2023-02.12.2023.

Day 1			30/11/2023
Averages - 8:00-9:00		Average outdoor temperature:	-2.13
	East line	West line	Average solar radiation:	1
1m	N/A	17.98	
2m	N/A	N/A	
2.75m	22.14	21.82	
Averages - 11:00-12:00		Average outdoor temperature:	-1.65
	East line	West line	Average solar radiation:	123
1m	N/A	22.91	
2m	N/A	N/A	
2.75m	25.09	26.38	
Averages - 14:00-15:00		Average outdoor temperature:	-0.95
	East line	West line	Average solar radiation:	5
1m	N/A	22.60	
2m	N/A	N/A	
2.75m	25.37	28.90	

Figure 9.47: Hourly averages of the measured temperatures in the DCV cavity. (30.11.2023)

Day 2			01/12/2023
Averages - 8:00-9:00		Average outdoor temperature:	-1.31
	East line	West line	Average solar radiation:	0
1m	N/A	18.04	
2m	N/A	N/A	
2.75m	18.66	20.41	
Averages - 11:00-12:00		Average outdoor temperature:	-1.44
	East line	West line	Average solar radiation:	31
1m	N/A	19.87	
2m	N/A	N/A	
2.75m	21.13	22.95	
Averages - 14:00-15:00		Average outdoor temperature:	-1.07
	East line	West line	Average solar radiation:	9
1m	N/A	25.58	
2m	N/A	N/A	
2.75m	25.84	26.97	

Figure 9.48: Hourly averages of the measured temperatures in the DCV cavity. (01.12.2023)

Day 3			02/12/2023
Averages - 8:00-9:00		Average outdoor temperature:	-5.80
	East line	West line	Average solar radiation:	4
1m	N/A	18.11	
2m	N/A	N/A	
2.75m	17.94	20.57	
Averages - 11:00-12:00		Average outdoor temperature:	-3.29
	East line	West line	Average solar radiation:	8
1m	N/A	20.14	
2m	N/A	N/A	
2.75m	20.70	22.81	
Averages - 14:00-15:00		Average outdoor temperature:	-2.26
	East line	West line	Average solar radiation:	41
1m	N/A	19.02	
2m	N/A	N/A	
2.75m	21.47	25.68	

Figure 9.49: Hourly averages of the measured temperatures in the DCV cavity. (02.12.2023)

9.6 Calculation of angle factors

9.6.1 Sitting person

Located in the middle of the room

The subject is placed in the middle of the Test room in a sitting position. Accordingly, the floor, ceiling, West wall, North wall, and East wall are divided into 4 sections each for calculating the relevant angle factors. As on each surface, there is only one thermocouple placed for measuring, the temperatures of the surfaces are considered to be uniform in this project.

However, on the south wall, two additional thermocouples are placed on the two windows. Therefore, the wall is divided into 2 sections for the windows, and 8 sections for the walls due to the shape.

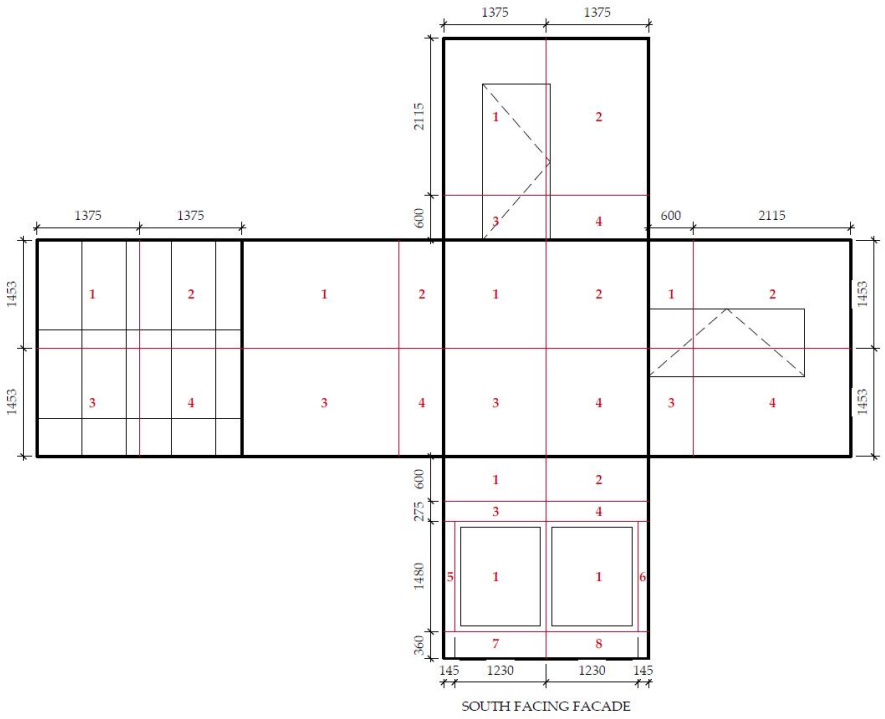

Figure 9.50: Illustration of the Test room for calculating the angle factors in the case of a person sitting in the middle of the room.

In Figure 9.51, the calculated angle factors according to DS7726 are displayed for each surface.

Angle factor input												
	a	b	c	A	B	C	D	E	Fmax	τ	γ	Angle factor
North wall 1	1.375	2.115	1.453	1.216	0.169	0.717	0.087	0.052	0.118	1.376	0.893	0.047
North wall 2	1.375	2.115	1.453	1.216	0.169	0.717	0.087	0.052	0.118	1.376	0.893	0.047
North wall 3	1.375	0.600	1.453	1.216	0.169	0.717	0.087	0.052	0.118	1.376	0.802	0.024
North wall 4	1.375	0.600	1.453	1.216	0.169	0.717	0.087	0.052	0.118	1.376	0.802	0.024
West wall 1	1.453	2.115	1.375	1.216	0.169	0.717	0.087	0.052	0.118	1.395	0.906	0.051
West wall 2	1.453	0.600	1.375	1.216	0.169	0.717	0.087	0.052	0.118	1.395	0.810	0.026
West wall 3	1.453	2.115	1.375	1.216	0.169	0.717	0.087	0.052	0.118	1.395	0.906	0.051
West wall 4	1.453	0.600	1.375	1.216	0.169	0.717	0.087	0.052	0.118	1.395	0.810	0.026
East wall 1	1.453	0.600	1.375	1.216	0.169	0.717	0.087	0.052	0.118	1.395	0.810	0.026
East wall 2	1.453	2.115	1.375	1.216	0.169	0.717	0.087	0.052	0.118	1.395	0.906	0.051
East wall 3	1.453	0.600	1.375	1.216	0.169	0.717	0.087	0.052	0.118	1.395	0.810	0.026
East wall 4	1.453	2.115	1.375	1.216	0.169	0.717	0.087	0.052	0.118	1.395	0.906	0.051
South wall 1	1.375	0.600	1.453	1.216	0.169	0.717	0.087	0.052	0.118	1.376	0.802	0.024
South wall 2	1.375	0.600	1.453	1.216	0.169	0.717	0.087	0.052	0.118	1.376	0.802	0.024
South wall 3	1.375	0.275	1.453	1.216	0.169	0.717	0.087	0.052	0.118	1.376	0.783	0.013
South wall 4	1.375	0.275	1.453	1.216	0.169	0.717	0.087	0.052	0.118	1.376	0.783	0.013
South wall 5	0.145	1.480	1.453	1.216	0.169	0.717	0.087	0.052	0.118	1.233	0.811	0.007
South wall 6	0.145	1.480	1.453	1.216	0.169	0.717	0.087	0.052	0.118	1.233	0.811	0.007
South wall 7	1.375	0.360	1.453	1.216	0.169	0.717	0.087	0.052	0.118	1.376	0.788	0.016
South wall 8	1.375	0.360	1.453	1.216	0.169	0.717	0.087	0.052	0.118	1.376	0.788	0.016
West window 1	1.230	1.480	1.453	1.216	0.169	0.717	0.087	0.052	0.118	1.359	0.850	0.038
East window 1	1.230	1.480	1.453	1.216	0.169	0.717	0.087	0.052	0.118	1.359	0.850	0.038
Floor 1	1.375	1.453	0.600	1.396	0.130	0.951	0.080	0.055	0.116	1.694	1.271	0.073
Floor 2	1.375	1.453	0.600	1.396	0.130	0.951	0.080	0.055	0.116	1.694	1.271	0.073
Floor 3	1.375	1.453	0.600	1.396	0.130	0.951	0.080	0.055	0.116	1.694	1.271	0.073
Floor 4	1.375	1.453	0.600	1.396	0.130	0.951	0.080	0.055	0.116	1.694	1.271	0.073
Ceiling 1	1.375	1.453	2.115	1.396	0.130	0.951	0.080	0.055	0.116	1.481	1.042	0.020
Ceiling 2	1.375	1.453	2.115	1.396	0.130	0.951	0.080	0.055	0.116	1.481	1.042	0.020
Ceiling 3	1.375	1.453	2.115	1.396	0.130	0.951	0.080	0.055	0.116	1.481	1.042	0.020
Ceiling 4	1.375	1.453	2.115	1.396	0.130	0.951	0.080	0.055	0.116	1.481	1.042	0.020
												1.017

Figure 9.51: Angle factors: Sitting person - middle of the room.

Located on the South of the room

The subject is placed 0.2m from the South wall of the Test room in a sitting position. Accordingly, the floor, ceiling, West wall, North wall, and East wall are divided into 4 sections each for calculating the relevant angle factors. As on each surface, there is only one thermocouple placed for measuring, the temperatures of the surfaces are considered to be uniform in this project.

However, the south wall is divided into 6 sections as two additional thermocouples are placed on the windows, and with the aim to achieve the sum of angle factors in the room to be close to 1.

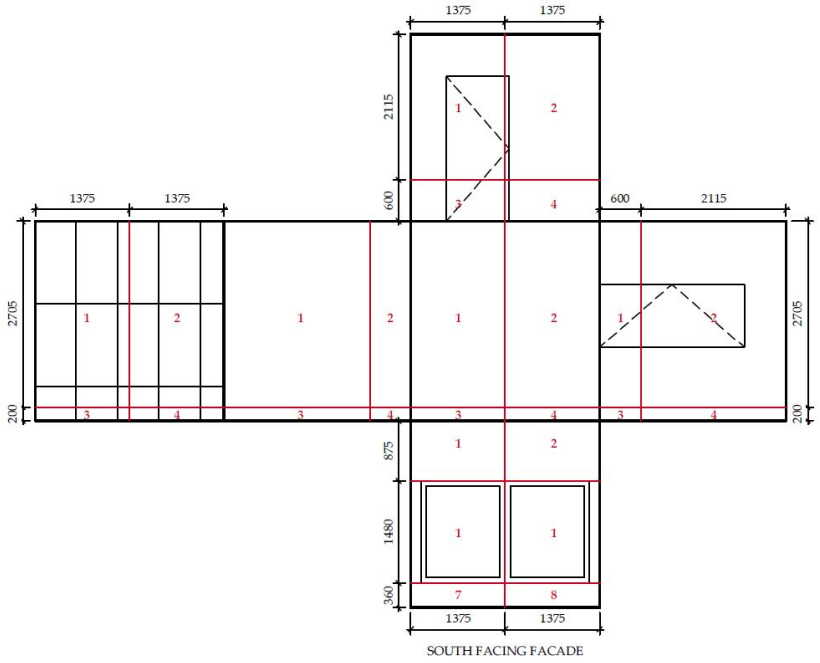

Figure 9.52: Illustration of the Test room for calculating the angle factors in the case of a person sitting in the South of the room.

Angle factor input												
	a	b	c	A	B	C	D	E	Fmax	τ	γ	Angle factor
North wall 1	1.375	2.115	2.705	1.216	0.169	0.717	0.087	0.052	0.118	1.302	0.811	0.024
North wall 2	1.375	2.115	2.705	1.216	0.169	0.717	0.087	0.052	0.118	1.302	0.811	0.024
North wall 3	1.375	0.600	2.705	1.216	0.169	0.717	0.087	0.052	0.118	1.302	0.763	0.010
North wall 4	1.375	0.600	2.705	1.216	0.169	0.717	0.087	0.052	0.118	1.302	0.763	0.010
West wall 1	2.705	2.115	1.375	1.216	0.169	0.717	0.087	0.052	0.118	1.548	0.953	0.068
West wall 2	2.705	0.600	1.375	1.216	0.169	0.717	0.087	0.052	0.118	1.548	0.857	0.034
West wall 3	0.200	2.115	1.375	1.216	0.169	0.717	0.087	0.052	0.118	1.241	0.858	0.011
West wall 4	0.200	0.600	1.375	1.216	0.169	0.717	0.087	0.052	0.118	1.241	0.763	0.006
East wall 1	2.705	0.600	1.375	1.216	0.169	0.717	0.087	0.052	0.118	1.548	0.857	0.034
East wall 2	2.705	2.115	1.375	1.216	0.169	0.717	0.087	0.052	0.118	1.548	0.953	0.068
East wall 3	0.200	0.600	1.375	1.216	0.169	0.717	0.087	0.052	0.118	1.241	0.763	0.006
East wall 4	0.200	2.115	1.375	1.216	0.169	0.717	0.087	0.052	0.118	1.241	0.858	0.011
South wall 1	1.375	0.875	0.200	1.216	0.169	0.717	0.087	0.052	0.118	2.378	1.455	0.106
South wall 2	1.375	0.875	0.200	1.216	0.169	0.717	0.087	0.052	0.118	2.378	1.455	0.106
South wall 7	1.375	0.360	0.200	1.216	0.169	0.717	0.087	0.052	0.118	2.378	1.231	0.086
South wall 8	1.375	0.360	0.200	1.216	0.169	0.717	0.087	0.052	0.118	2.378	1.231	0.086
West window 1	1.375	1.480	0.200	1.216	0.169	0.717	0.087	0.052	0.118	2.378	1.718	0.110
East window 1	1.375	1.480	0.200	1.216	0.169	0.717	0.087	0.052	0.118	2.378	1.718	0.110
Floor 1	1.375	2.705	0.600	1.396	0.130	0.951	0.080	0.055	0.116	1.694	1.438	0.082
Floor 2	1.375	2.705	0.600	1.396	0.130	0.951	0.080	0.055	0.116	1.694	1.438	0.082
Floor 3	1.375	0.200	0.600	1.396	0.130	0.951	0.080	0.055	0.116	1.694	1.104	0.022
Floor 4	1.375	0.200	0.600	1.396	0.130	0.951	0.080	0.055	0.116	1.694	1.104	0.022
Ceiling 1	1.375	2.705	2.115	1.396	0.130	0.951	0.080	0.055	0.116	1.481	1.089	0.028
Ceiling 2	1.375	2.705	2.115	1.396	0.130	0.951	0.080	0.055	0.116	1.481	1.089	0.028
Ceiling 3	1.375	0.200	2.115	1.396	0.130	0.951	0.080	0.055	0.116	1.481	0.994	0.004
Ceiling 4	1.375	0.200	2.115	1.396	0.130	0.951	0.080	0.055	0.116	1.481	0.994	0.004
												1.180

Figure 9.53: Angle factors: Sitting person - south of the room.

Located on the North of the room

The subject is placed 0.2m from the North wall of the Test room in a sitting position. Accordingly, the floor, ceiling, West wall, North wall, and East wall are divided into 4 sections each for calculating the relevant angle factors. As on each surface, there is only one thermocouple placed for measuring, the temperatures of the surfaces are considered to be uniform in this project.

However, on the south wall, two additional thermocouples are placed on the two windows. Therefore, the wall is divided into 2 sections for the windows, and 8 sections for the walls due to the shape.

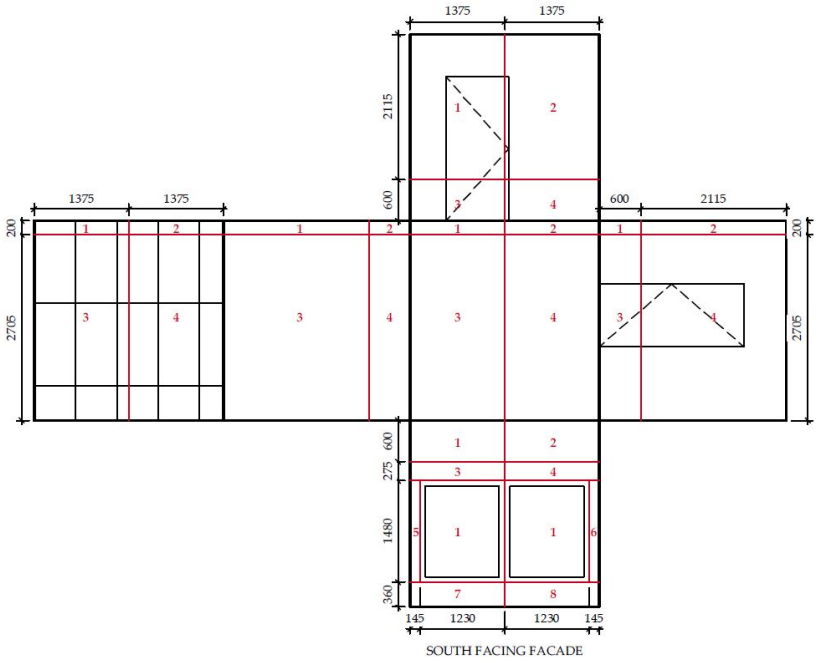

Figure 9.54: Illustration of the Test room for calculating the angle factors in the case of a person sitting in the North of the room.

Angle factor input												
	a	b	c	A	B	C	D	E	Fmax	τ	γ	Angle factor
North wall 1	1.375	2.115	0.200	1.216	0.169	0.717	0.087	0.052	0.118	2.378	1.995	0.111
North wall 2	1.375	2.115	0.200	1.216	0.169	0.717	0.087	0.052	0.118	2.378	1.995	0.111
North wall 3	1.375	0.600	0.200	1.216	0.169	0.717	0.087	0.052	0.118	2.378	1.336	0.100
North wall 4	1.375	0.600	0.200	1.216	0.169	0.717	0.087	0.052	0.118	2.378	1.336	0.100
West wall 1	0.200	2.115	1.375	1.216	0.169	0.717	0.087	0.052	0.118	1.241	0.858	0.011
West wall 2	0.200	0.600	1.375	1.216	0.169	0.717	0.087	0.052	0.118	1.241	0.763	0.006
West wall 3	2.705	2.115	1.375	1.216	0.169	0.717	0.087	0.052	0.118	1.548	0.953	0.068
West wall 4	2.705	0.600	1.375	1.216	0.169	0.717	0.087	0.052	0.118	1.548	0.857	0.034
East wall 1	0.200	0.600	1.375	1.216	0.169	0.717	0.087	0.052	0.118	1.241	0.763	0.006
East wall 2	0.200	2.115	1.375	1.216	0.169	0.717	0.087	0.052	0.118	1.241	0.858	0.011
East wall 3	2.705	0.600	1.375	1.216	0.169	0.717	0.087	0.052	0.118	1.548	0.857	0.034
East wall 4	2.705	2.115	1.375	1.216	0.169	0.717	0.087	0.052	0.118	1.548	0.953	0.068
South wall 1	1.375	0.600	2.705	1.216	0.169	0.717	0.087	0.052	0.118	1.302	0.763	0.010
South wall 2	1.375	0.600	2.705	1.216	0.169	0.717	0.087	0.052	0.118	1.302	0.763	0.010
South wall 3	1.375	0.275	2.705	1.216	0.169	0.717	0.087	0.052	0.118	1.302	0.752	0.005
South wall 4	1.375	0.275	2.705	1.216	0.169	0.717	0.087	0.052	0.118	1.302	0.752	0.005
South wall 5	0.145	1.480	2.705	1.216	0.169	0.717	0.087	0.052	0.118	1.225	0.767	0.003
South wall 6	0.145	1.480	2.705	1.216	0.169	0.717	0.087	0.052	0.118	1.225	0.767	0.003
South wall 7	1.375	0.360	2.705	1.216	0.169	0.717	0.087	0.052	0.118	1.302	0.755	0.006
South wall 8	1.375	0.360	2.705	1.216	0.169	0.717	0.087	0.052	0.118	1.302	0.755	0.006
West window 1	1.230	1.480	2.705	1.216	0.169	0.717	0.087	0.052	0.118	1.293	0.788	0.018
East window 1	1.230	1.480	2.705	1.216	0.169	0.717	0.087	0.052	0.118	1.293	0.788	0.018
Floor 1	1.375	0.200	0.600	1.396	0.130	0.951	0.080	0.055	0.116	1.694	1.104	0.022
Floor 2	1.375	0.200	0.600	1.396	0.130	0.951	0.080	0.055	0.116	1.694	1.104	0.022
Floor 3	1.375	2.705	0.600	1.396	0.130	0.951	0.080	0.055	0.116	1.694	1.438	0.082
Floor 4	1.375	2.705	0.600	1.396	0.130	0.951	0.080	0.055	0.116	1.694	1.438	0.082
Ceiling 1	1.375	0.200	2.115	1.396	0.130	0.951	0.080	0.055	0.116	1.481	0.994	0.004
Ceiling 2	1.375	0.200	2.115	1.396	0.130	0.951	0.080	0.055	0.116	1.481	0.994	0.004
Ceiling 3	1.375	2.705	2.115	1.396	0.130	0.951	0.080	0.055	0.116	1.481	1.089	0.028
Ceiling 4	1.375	2.705	2.115	1.396	0.130	0.951	0.080	0.055	0.116	1.481	1.089	0.028
												1.013

Figure 9.55: Angle factors: Sitting person - north of the room.

9.6.2 Standing person

Located in the middle of the room

The subject is placed in the middle of the Test room in a standing position. Accordingly, the floor, ceiling, West wall, North wall, and East wall are divided into 4 sections each for calculating the relevant angle factors. As on each surface, there is only one thermocouple placed for measuring, the temperatures of the surfaces are considered to be uniform in this project.

However, on the south wall, two additional thermocouples are placed on the two windows. Therefore, the wall is divided into 4 sections for the windows, and 8 sections for the walls due to the shape.

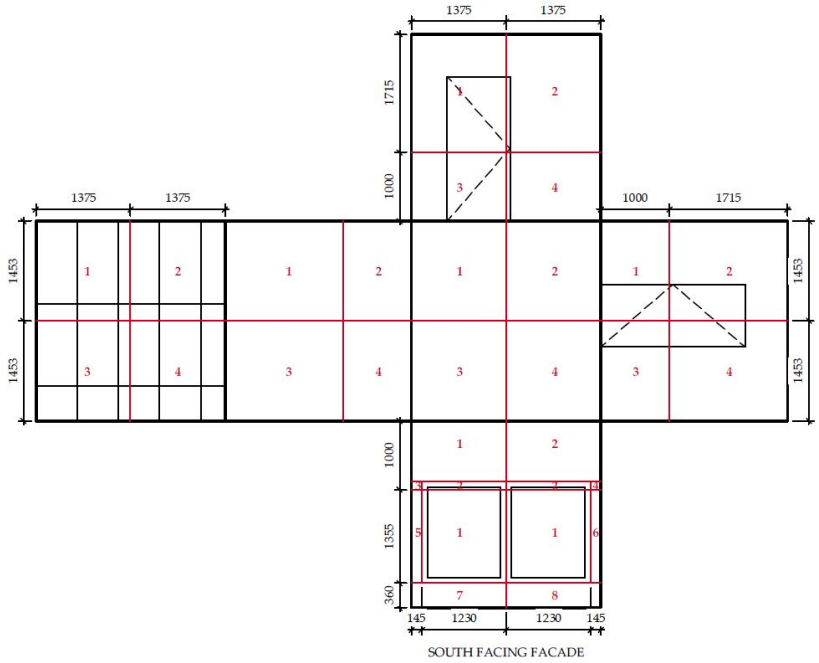

Figure 9.56: Illustration of the Test room for calculating the angle factors in the case of a person standing in the middle of the room.

Angle factor input												
	a	b	c	A	B	C	D	E	Fmax	τ	γ	Angle factor
North wall 1	1.375	1.715	1.453	1.242	0.167	0.616	0.082	0.051	0.12	1.400	0.761	0.046
North wall 2	1.375	1.715	1.453	1.242	0.167	0.616	0.082	0.051	0.12	1.400	0.761	0.046
North wall 3	1.375	1.000	1.453	1.242	0.167	0.616	0.082	0.051	0.12	1.400	0.721	0.036
North wall 4	1.375	1.000	1.453	1.242	0.167	0.616	0.082	0.051	0.12	1.400	0.721	0.036
West wall 1	1.453	1.715	1.375	1.242	0.167	0.616	0.082	0.051	0.12	1.418	0.772	0.050
West wall 2	1.453	1.000	1.375	1.242	0.167	0.616	0.082	0.051	0.12	1.418	0.730	0.040
West wall 3	1.453	1.715	1.375	1.242	0.167	0.616	0.082	0.051	0.12	1.418	0.772	0.050
West wall 4	1.453	1.000	1.375	1.242	0.167	0.616	0.082	0.051	0.12	1.418	0.730	0.040
East wall 1	1.453	1.000	1.375	1.242	0.167	0.616	0.082	0.051	0.12	1.418	0.730	0.040
East wall 2	1.453	1.715	1.375	1.242	0.167	0.616	0.082	0.051	0.12	1.418	0.772	0.050
East wall 3	1.453	1.000	1.375	1.242	0.167	0.616	0.082	0.051	0.12	1.418	0.730	0.040
East wall 4	1.453	1.715	1.375	1.242	0.167	0.616	0.082	0.051	0.12	1.418	0.772	0.050
South wall 1	1.375	0.875	1.453	1.242	0.167	0.616	0.082	0.051	0.12	1.400	0.714	0.034
South wall 2	1.375	0.875	1.453	1.242	0.167	0.616	0.082	0.051	0.12	1.400	0.714	0.034
South wall 3	0.145	0.125	1.453	1.242	0.167	0.616	0.082	0.051	0.12	1.259	0.628	0.001
South wall 4	0.145	0.125	1.453	1.242	0.167	0.616	0.082	0.051	0.12	1.259	0.628	0.001
South wall 5	0.145	1.355	1.453	1.242	0.167	0.616	0.082	0.051	0.12	1.259	0.698	0.007
South wall 6	0.145	1.355	1.453	1.242	0.167	0.616	0.082	0.051	0.12	1.259	0.698	0.007
South wall 7	1.375	0.360	1.453	1.242	0.167	0.616	0.082	0.051	0.12	1.400	0.685	0.018
South wall 8	1.375	0.360	1.453	1.242	0.167	0.616	0.082	0.051	0.12	1.400	0.685	0.018
West window 1	1.230	1.355	1.453	1.242	0.167	0.616	0.082	0.051	0.12	1.383	0.736	0.039
West window 2	1.230	0.125	1.453	1.242	0.167	0.616	0.082	0.051	0.12	1.383	0.666	0.007
East window 1	1.230	1.355	1.453	1.242	0.167	0.616	0.082	0.051	0.12	1.383	0.736	0.039
East window 2	1.230	0.125	1.453	1.242	0.167	0.616	0.082	0.051	0.12	1.383	0.666	0.007
Floor 1	1.375	1.453	1.000	1.595	0.128	1.226	0.046	0.044	0.116	1.771	1.353	0.041
Floor 2	1.375	1.453	1.000	1.595	0.128	1.226	0.046	0.044	0.116	1.771	1.353	0.041
Floor 3	1.375	1.453	1.000	1.595	0.128	1.226	0.046	0.044	0.116	1.771	1.353	0.041
Floor 4	1.375	1.453	1.000	1.595	0.128	1.226	0.046	0.044	0.116	1.771	1.353	0.041
Ceiling 1	1.375	1.453	1.715	1.595	0.128	1.226	0.046	0.044	0.116	1.698	1.300	0.021
Ceiling 2	1.375	1.453	1.715	1.595	0.128	1.226	0.046	0.044	0.116	1.698	1.300	0.021
Ceiling 3	1.375	1.453	1.715	1.595	0.128	1.226	0.046	0.044	0.116	1.698	1.300	0.021
Ceiling 4	1.375	1.453	1.715	1.595	0.128	1.226	0.046	0.044	0.116	1.698	1.300	0.021
												0.986

Figure 9.57: Angle factors: Standing person - middle of the room.

Located on the South of the room

The subject is placed 0.2m from the South wall of the Test room in a standing position. Accordingly, the floor, ceiling, West wall, North wall, and East wall are divided into 4 sections each for calculating the relevant angle factors. As on each surface, there is only one thermocouple placed for measuring, the temperatures of the surfaces are considered to be uniform in this project.

However, the south wall is divided into 6 sections as two additional thermocouples are placed on the windows, and with the aim to achieve the sum of angle factors in the room to be close to 1.

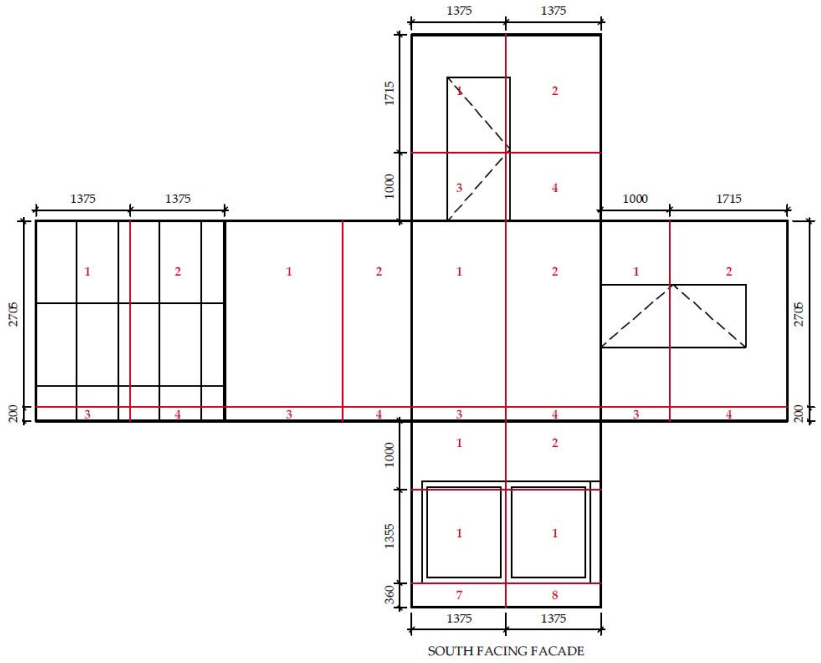

Figure 9.58: Illustration of the Test room for calculating the angle factors in the case of a person standing in the South of the room.

Angle factor input												
	a	b	c	A	B	C	D	E	Fmax	τ	γ	Angle factor
North wall 1	1.375	1.715	2.705	1.242	0.167	0.616	0.082	0.051	0.12	1.327	0.694	0.023
North wall 2	1.375	1.715	2.705	1.242	0.167	0.616	0.082	0.051	0.12	1.327	0.694	0.023
North wall 3	1.375	1.000	2.705	1.242	0.167	0.616	0.082	0.051	0.12	1.327	0.672	0.016
North wall 4	1.375	1.000	2.705	1.242	0.167	0.616	0.082	0.051	0.12	1.327	0.672	0.016
West wall 1	2.705	1.715	1.375	1.242	0.167	0.616	0.082	0.051	0.12	1.571	0.819	0.067
West wall 2	2.705	1.000	1.375	1.242	0.167	0.616	0.082	0.051	0.12	1.571	0.776	0.052
West wall 3	0.200	1.715	1.375	1.242	0.167	0.616	0.082	0.051	0.12	1.266	0.726	0.011
West wall 4	0.200	1.000	1.375	1.242	0.167	0.616	0.082	0.051	0.12	1.266	0.683	0.009
East wall 1	2.705	1.000	1.375	1.242	0.167	0.616	0.082	0.051	0.12	1.571	0.776	0.052
East wall 2	2.705	1.715	1.375	1.242	0.167	0.616	0.082	0.051	0.12	1.571	0.819	0.067
East wall 3	0.200	1.000	1.375	1.242	0.167	0.616	0.082	0.051	0.12	1.266	0.683	0.009
East wall 4	0.200	1.715	1.375	1.242	0.167	0.616	0.082	0.051	0.12	1.266	0.726	0.011
South wall 1	1.375	1.000	0.200	1.242	0.167	0.616	0.082	0.051	0.12	2.390	1.377	0.110
South wall 2	1.375	1.000	0.200	1.242	0.167	0.616	0.082	0.051	0.12	2.390	1.377	0.110
South wall 7	1.375	0.360	0.200	1.242	0.167	0.616	0.082	0.051	0.12	2.390	1.114	0.091
South wall 8	1.375	0.360	0.200	1.242	0.167	0.616	0.082	0.051	0.12	2.390	1.114	0.091
West window 1	1.375	1.355	0.200	1.242	0.167	0.616	0.082	0.051	0.12	2.390	1.522	0.112
East window 1	1.375	1.355	0.200	1.242	0.167	0.616	0.082	0.051	0.12	2.390	1.522	0.112
Floor 1	1.375	2.705	1.000	1.595	0.128	1.226	0.046	0.044	0.116	1.771	1.411	0.053
Floor 2	1.375	2.705	1.000	1.595	0.128	1.226	0.046	0.044	0.116	1.771	1.411	0.053
Floor 3	1.375	0.200	1.000	1.595	0.128	1.226	0.046	0.044	0.116	1.771	1.296	0.009
Floor 4	1.375	0.200	1.000	1.595	0.128	1.226	0.046	0.044	0.116	1.771	1.296	0.009
Ceiling 1	1.375	2.705	1.715	1.595	0.128	1.226	0.046	0.044	0.116	1.698	1.334	0.030
Ceiling 2	1.375	2.705	1.715	1.595	0.128	1.226	0.046	0.044	0.116	1.698	1.334	0.030
Ceiling 3	1.375	0.200	1.715	1.595	0.128	1.226	0.046	0.044	0.116	1.698	1.267	0.004
Ceiling 4	1.375	0.200	1.715	1.595	0.128	1.226	0.046	0.044	0.116	1.698	1.267	0.004
												1.174

Figure 9.59: Angle factors: Standing person - south of the room.

Located on the North of the room

The subject is placed 0.2m from the North wall of the Test room in a standing position. Accordingly, the floor, ceiling, West wall, North wall, and East wall are divided into 4 sections each for calculating the relevant angle factors. As on each surface, there is only one thermocouple placed for measuring, the temperatures of the surfaces are considered to be uniform in this project.

However, on the south wall, two additional thermocouples are placed on the two windows. Therefore, the wall is divided into 4 sections for the windows, and 8 sections for the walls due to the shape.

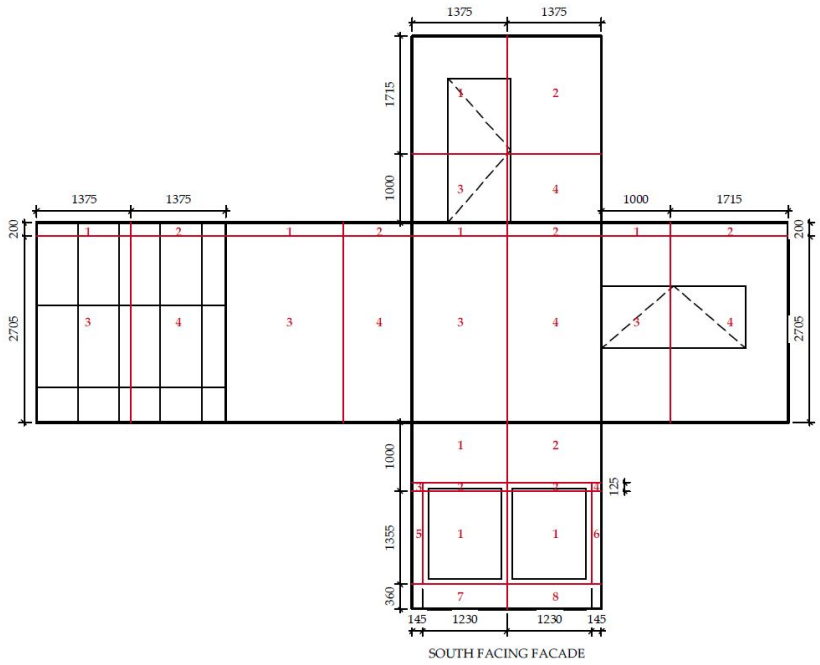

Figure 9.60: Illustration of the Test room for calculating the angle factors in the case of a person standing in the North of the room.

Angle factor input												
	a	b	c	A	B	C	D	E	Fmax	τ	γ	Angle factor
North wall 1	1.375	1.715	0.200	1.242	0.167	0.616	0.082	0.051	0.12	2.390	1.670	0.113
North wall 2	1.375	1.715	0.200	1.242	0.167	0.616	0.082	0.051	0.12	2.390	1.670	0.113
North wall 3	1.375	1.000	0.200	1.242	0.167	0.616	0.082	0.051	0.12	2.390	1.377	0.110
North wall 4	1.375	1.000	0.200	1.242	0.167	0.616	0.082	0.051	0.12	2.390	1.377	0.110
West wall 1	0.200	1.715	1.375	1.242	0.167	0.616	0.082	0.051	0.12	1.266	0.726	0.011
West wall 2	0.200	1.000	1.375	1.242	0.167	0.616	0.082	0.051	0.12	1.266	0.683	0.009
West wall 3	2.705	1.715	1.375	1.242	0.167	0.616	0.082	0.051	0.12	1.571	0.819	0.067
West wall 4	2.705	1.000	1.375	1.242	0.167	0.616	0.082	0.051	0.12	1.571	0.776	0.052
East wall 1	0.200	1.000	1.375	1.242	0.167	0.616	0.082	0.051	0.12	1.266	0.683	0.009
East wall 2	0.200	1.715	1.375	1.242	0.167	0.616	0.082	0.051	0.12	1.266	0.726	0.011
East wall 3	2.705	1.000	1.375	1.242	0.167	0.616	0.082	0.051	0.12	1.571	0.776	0.052
East wall 4	2.705	1.715	1.375	1.242	0.167	0.616	0.082	0.051	0.12	1.571	0.819	0.067
South wall 1	1.375	0.875	2.705	1.242	0.167	0.616	0.082	0.051	0.12	1.327	0.668	0.015
South wall 2	1.375	0.875	2.705	1.242	0.167	0.616	0.082	0.051	0.12	1.327	0.668	0.015
South wall 3	0.145	0.125	2.705	1.242	0.167	0.616	0.082	0.051	0.12	1.251	0.623	0.000
South wall 4	0.145	0.125	2.705	1.242	0.167	0.616	0.082	0.051	0.12	1.251	0.623	0.000
South wall 5	0.145	1.355	2.705	1.242	0.167	0.616	0.082	0.051	0.12	1.251	0.660	0.003
South wall 6	0.145	1.355	2.705	1.242	0.167	0.616	0.082	0.051	0.12	1.251	0.660	0.003
South wall 7	1.375	0.360	2.705	1.242	0.167	0.616	0.082	0.051	0.12	1.327	0.653	0.007
South wall 8	1.375	0.360	2.705	1.242	0.167	0.616	0.082	0.051	0.12	1.327	0.653	0.007
West window 1	1.230	1.355	2.705	1.242	0.167	0.616	0.082	0.051	0.12	1.318	0.680	0.018
West window 2	1.230	0.125	2.705	1.242	0.167	0.616	0.082	0.051	0.12	1.318	0.643	0.002
East window 1	1.230	1.355	2.705	1.242	0.167	0.616	0.082	0.051	0.12	1.318	0.680	0.018
East window 2	1.230	0.125	2.705	1.242	0.167	0.616	0.082	0.051	0.12	1.318	0.643	0.002
Floor 1	1.375	0.200	1.000	1.595	0.128	1.226	0.046	0.044	0.116	1.771	1.296	0.009
Floor 2	1.375	0.200	1.000	1.595	0.128	1.226	0.046	0.044	0.116	1.771	1.296	0.009
Floor 3	1.375	2.705	1.000	1.595	0.128	1.226	0.046	0.044	0.116	1.771	1.411	0.053
Floor 4	1.375	2.705	1.000	1.595	0.128	1.226	0.046	0.044	0.116	1.771	1.411	0.053
Ceiling 1	1.375	0.200	1.715	1.595	0.128	1.226	0.046	0.044	0.116	1.698	1.267	0.004
Ceiling 2	1.375	0.200	1.715	1.595	0.128	1.226	0.046	0.044	0.116	1.698	1.267	0.004
Ceiling 3	1.375	2.705	1.715	1.595	0.128	1.226	0.046	0.044	0.116	1.698	1.334	0.030
Ceiling 4	1.375	2.705	1.715	1.595	0.128	1.226	0.046	0.044	0.116	1.698	1.334	0.030
												1.006

Figure 9.61: Angle factors: Standing person - north of the room.

9.7 Air velocity and air temperature distribution in the Test room

9.7.1 Summer case

Day 1				Day 2				Day 3				Day 4			
Averages - 8:00-9:00				Averages - 8:00-9:00				Averages - 8:00-9:00				Averages - 8:00-9:00			
	North pole	Middle pole	South pole		North pole	Middle pole	South pole		North pole	Middle pole	South pole		North pole	Middle pole	South pole
1.8m	N/A	N/A	N/A	1.8m	N/A	N/A	N/A	1.8m	N/A	N/A	N/A	1.8m	N/A	N/A	N/A
1.1m	N/A	0.08	0.06	1.1m	N/A	0.08	0.06	1.1m	N/A	0.08	0.07	1.1m	N/A	0.06	0.10
0.6m	0.09	0.09	0.01	0.6m	0.09	0.09	0.02	0.6m	0.09	0.09	0.03	0.6m	0.08	0.05	0.02
0.1m	0.09	0.06	0.03	0.1m	0.09	0.06	0.04	0.1m	0.09	0.07	0.06	0.1m	0.09	0.09	0.04
Averages - 11:00-12:00				Averages - 11:00-12:00				Averages - 11:00-12:00				Averages - 11:00-12:00			
	North pole	Middle pole	South pole		North pole	Middle pole	South pole		North pole	Middle pole	South pole		North pole	Middle pole	South pole
1.8m	N/A	N/A	N/A	1.8m	N/A	N/A	N/A	1.8m	N/A	N/A	N/A	1.8m	N/A	N/A	N/A
1.1m	N/A	0.08	0.04	1.1m	N/A	0.08	0.08	1.1m	N/A	0.08	0.09	1.1m	N/A	0.08	0.05
0.6m	0.11	0.09	0.06	0.6m	0.09	0.10	0.07	0.6m	0.10	0.10	0.09	0.6m	0.10	0.09	0.08
0.1m	0.11	0.07	0.03	0.1m	0.09	0.10	0.04	0.1m	0.11	0.08	0.04	0.1m	0.11	0.08	0.05
Averages - 14:00-15:00				Averages - 14:00-15:00				Averages - 14:00-15:00				Averages - 14:00-15:00			
	North pole	Middle pole	South pole		North pole	Middle pole	South pole		North pole	Middle pole	South pole		North pole	Middle pole	South pole
1.8m	N/A	N/A	N/A	1.8m	N/A	N/A	N/A	1.8m	N/A	N/A	N/A	1.8m	N/A	N/A	N/A
1.1m	N/A	0.08	0.05	1.1m	N/A	0.08	0.08	1.1m	N/A	0.07	0.04	1.1m	N/A	0.09	0.06
0.6m	0.10	0.09	0.04	0.6m	0.10	0.13	0.05	0.6m	0.11	0.07	0.05	0.6m	0.10	0.12	0.05
0.1m	0.11	0.06	0.04	0.1m	0.09	0.14	0.05	0.1m	0.12	0.03	0.04	0.1m	0.10	0.11	0.04

Day 1				Day 2				Day 3				Day 4			
Averages - 8:00-9:00				Averages - 8:00-9:00				Averages - 8:00-9:00				Averages - 8:00-9:00			
	North pole	Middle pole	South pole		North pole	Middle pole	South pole		North pole	Middle pole	South pole		North pole	Middle pole	South pole
1.8m	27.43	23.38	24.51	1.8m	27.12	22.13	22.59	1.8m	27.90	21.51	22.40	1.8m	27.80	21.96	22.55
1.1m	23.41	23.01	23.07	1.1m	22.09	21.78	22.07	1.1m	21.53	21.15	21.27	1.1m	22.00	21.60	21.73
0.6m	N/A	23.55	23.04	0.6m	N/A	22.32	22.12	0.6m	N/A	21.63	21.31	0.6m	N/A	22.15	21.68
0.1m	23.89	23.03	24.42	0.1m	23.53	21.79	22.66	0.1m	23.31	21.13	22.28	0.1m	22.91	21.61	22.88
Averages - 11:00-12:00				Averages - 11:00-12:00				Averages - 11:00-12:00				Averages - 11:00-12:00			
	North pole	Middle pole	South pole		North pole	Middle pole	South pole		North pole	Middle pole	South pole		North pole	Middle pole	South pole
1.8m	28.67	24.71	26.56	1.8m	29.26	25.30	25.71	1.8m	28.12	24.23	25.18	1.8m	27.97	24.90	23.45
1.1m	24.76	24.39	24.52	1.1m	25.22	24.99	25.18	1.1m	24.21	23.94	24.15	1.1m	24.85	24.61	24.82
0.6m	N/A	25.09	24.47	0.6m	N/A	25.69	25.16	0.6m	N/A	24.64	24.16	0.6m	N/A	25.35	24.79
0.1m	24.16	24.53	26.41	0.1m	23.89	24.98	25.24	0.1m	23.58	23.98	24.92	0.1m	23.32	24.64	23.14
Averages - 14:00-15:00				Averages - 14:00-15:00				Averages - 14:00-15:00				Averages - 14:00-15:00			
	North pole	Middle pole	South pole		North pole	Middle pole	South pole		North pole	Middle pole	South pole		North pole	Middle pole	South pole
1.8m	27.45	24.19	24.07	1.8m	32.52	26.57	25.96	1.8m	31.26	25.38	26.68	1.8m	28.20	25.75	25.08
1.1m	24.26	23.84	24.11	1.1m	26.32	26.22	26.50	1.1m	25.48	25.01	25.26	1.1m	25.76	25.46	25.58
0.6m	N/A	24.51	24.11	0.6m	N/A	26.87	26.49	0.6m	N/A	25.76	25.23	0.6m	N/A	26.13	25.57
0.1m	24.18	23.91	24.15	0.1m	24.38	26.01	25.62	0.1m	23.94	25.08	26.47	0.1m	23.75	25.41	24.76
Outdoor temp.:		16-19	°C	Outdoor temp.:		16-19	°C	Outdoor temp.:		16-19	°C	Outdoor temp.:		13-18	°C
Solar radiation:		88-1088	W/m2	Solar radiation:		100-1055	W/m2	Solar radiation:		90-1055	W/m2	Solar radiation:		100-1055	W/m2

Figure 9.62: Air velocity and air temperature distribution in the occupied zone in the Test room. (24-30.07.2023)

Figure 9.63: North, Middle and South pole air temperatures at 0.1m, 0.6m, 1.1m and 1.7m from the ground (Occupied zone) in the Test room during the occupied hours. (24-30.07.2023; 8:00-15:00)

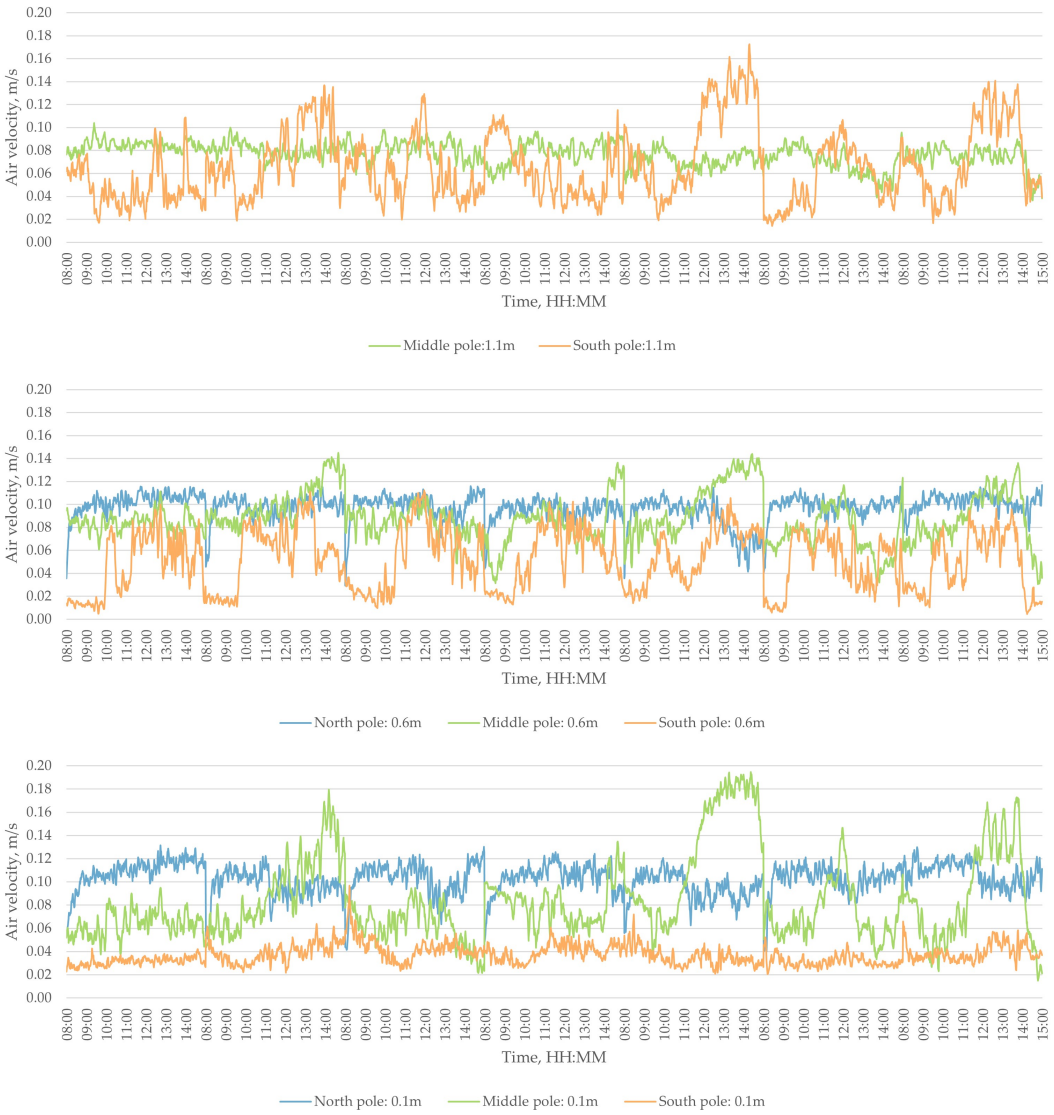

Figure 9.64: North, Middle and South pole air velocities at 0.1m, 0.6m, 1.1m and 1.7m from the ground (Occupied zone) in the Test room during the occupied hours. (24-30.10.2023; 8:00-15:00)

9.7.2 Intermediate case

Day 1				Day 2				Day 3				Day 4			
Averages - 8:00-9:00				**Averages - 8:00-9:00**				**Averages - 8:00-9:00**				**Averages - 8:00-9:00**			
	North pole	Middle pole	South pole		North pole	Middle pole	South pole		North pole	Middle pole	South pole		North pole	Middle pole	South pole
1.7m	0.07	0.07	0.02	1.7m	0.06	0.07	0.02	1.7m	0.05	0.07	0.01	1.7m	0.06	0.07	0.02
1.1m	0.07	0.07	0.04	1.1m	0.07	0.08	0.04	1.1m	0.05	0.08	0.03	1.1m	0.06	0.08	0.04
0.6m	0.05	0.06	0.10	0.6m	0.04	0.06	0.09	0.6m	0.03	0.08	0.09	0.6m	0.03	0.08	0.10
0.1m	0.05	0.10	0.04	0.1m	0.03	0.10	0.03	0.1m	0.05	0.10	0.03	0.1m	0.05	0.09	0.04
Averages - 11:00-12:00				**Averages - 11:00-12:00**				**Averages - 11:00-12:00**				**Averages - 11:00-12:00**			
	North pole	Middle pole	South pole		North pole	Middle pole	South pole		North pole	Middle pole	South pole		North pole	Middle pole	South pole
1.7m	0.08	0.10	0.04	1.7m	0.08	0.10	0.03	1.7m	0.07	0.10	0.03	1.7m	0.07	0.10	0.03
1.1m	0.09	0.11	0.06	1.1m	0.09	0.10	0.07	1.1m	0.08	0.11	0.06	1.1m	0.07	0.11	0.06
0.6m	0.06	0.09	0.10	0.6m	0.06	0.09	0.09	0.6m	0.06	0.09	0.10	0.6m	0.05	0.10	0.10
0.1m	0.06	0.12	0.04	0.1m	0.05	0.12	0.04	0.1m	0.06	0.11	0.04	0.1m	0.07	0.11	0.04
Averages - 14:00-15:00				**Averages - 14:00-15:00**				**Averages - 14:00-15:00**				**Averages - 14:00-15:00**			
	North pole	Middle pole	South pole		North pole	Middle pole	South pole		North pole	Middle pole	South pole		North pole	Middle pole	South pole
1.7m	0.07	0.09	0.03	1.7m	0.08	0.10	0.03	1.7m	0.08	0.10	0.03	1.7m	0.07	0.10	0.03
1.1m	0.08	0.09	0.06	1.1m	0.10	0.11	0.08	1.1m	0.09	0.11	0.07	1.1m	0.08	0.11	0.06
0.6m	0.05	0.08	0.10	0.6m	0.07	0.09	0.11	0.6m	0.06	0.09	0.11	0.6m	0.05	0.09	0.10
0.1m	0.06	0.11	0.04	0.1m	0.06	0.12	0.05	0.1m	0.07	0.13	0.05	0.1m	0.07	0.10	0.04

0.13
0.12
0.11
0.10
0.09
0.08
0.07
0.06
0.05
0.04
0.03
0.02
0.01

Day 1				Day 2				Day 3				Day 4			
Averages - 8:00-9:00				**Averages - 8:00-9:00**				**Averages - 8:00-9:00**				**Averages - 8:00-9:00**			
	North pole	Middle pole	South pole		North pole	Middle pole	South pole		North pole	Middle pole	South pole		North pole	Middle pole	South pole
1.7m	20.24	20.49	21.30	1.7m	20.74	21.00	21.01	1.7m	20.35	20.54	20.50	1.7m	20.07	20.19	20.21
1.1m	20.54	20.90	20.48	1.1m	21.03	21.39	20.95	1.1m	20.58	20.94	20.48	1.1m	20.25	20.59	20.17
0.6m	19.78	20.82	20.45	0.6m	20.19	21.30	20.92	0.6m	19.75	20.80	20.44	0.6m	19.45	20.48	20.12
0.1m	21.24	20.78	21.20	0.1m	21.58	21.23	20.94	0.1m	20.90	20.62	20.50	0.1m	21.00	20.42	20.17
Averages - 11:00-12:00				**Averages - 11:00-12:00**				**Averages - 11:00-12:00**				**Averages - 11:00-12:00**			
	North pole	Middle pole	South pole		North pole	Middle pole	South pole		North pole	Middle pole	South pole		North pole	Middle pole	South pole
1.7m	21.19	21.58	22.45	1.7m	21.58	21.86	21.92	1.7m	20.86	21.13	21.15	1.7m	20.74	20.96	20.97
1.1m	21.58	22.07	21.52	1.1m	21.89	22.38	21.88	1.1m	21.13	21.65	21.11	1.1m	20.94	21.47	20.94
0.6m	20.76	22.05	21.44	0.6m	21.06	22.34	21.79	0.6m	20.37	21.62	21.07	0.6m	20.20	21.41	20.88
0.1m	21.95	21.96	22.29	0.1m	22.41	22.26	21.70	0.1m	21.72	21.56	21.06	0.1m	21.51	21.29	20.91
Averages - 14:00-15:00				**Averages - 14:00-15:00**				**Averages - 14:00-15:00**				**Averages - 14:00-15:00**			
	North pole	Middle pole	South pole		North pole	Middle pole	South pole		North pole	Middle pole	South pole		North pole	Middle pole	South pole
1.7m	21.39	21.73	22.44	1.7m	21.46	21.66	21.73	1.7m	20.82	21.04	21.06	1.7m	20.99	21.20	21.26
1.1m	21.76	22.21	21.67	1.1m	21.74	22.20	21.68	1.1m	21.09	21.58	21.02	1.1m	21.21	21.73	21.23
0.6m	20.88	22.14	21.59	0.6m	20.91	22.18	21.62	0.6m	20.28	21.55	20.96	0.6m	20.43	21.68	21.14
0.1m	22.17	22.07	22.27	0.1m	22.40	22.08	21.51	0.1m	21.94	21.50	20.97	0.1m	21.68	21.60	21.15
Outdoor temp.:		10-11	°C	Outdoor temp.:		10-11	°C	Outdoor temp.:		7-8	°C	Outdoor temp.:		6-7	°C
Solar radiation:		0-104	W/m2	Solar radiation:		0-266	W/m2	Solar radiation:		0-39	W/m2	Solar radiation:		0-118	W/m2

22.50
22.00
21.50
21.00
20.50
20.00
19.50
19.00

Figure 9.65: Air velocity and air temperature distribution in the occupied zone in the Test room. (23-26.10.2023)

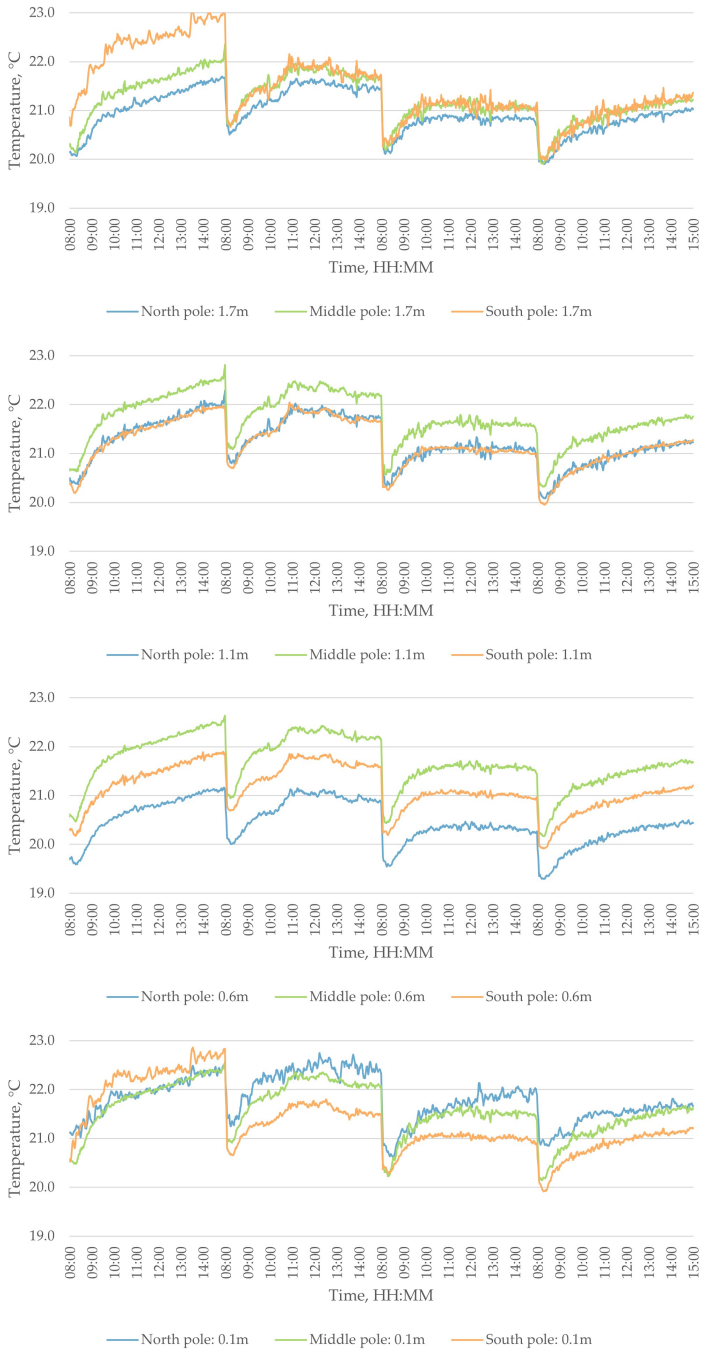

Figure 9.66: North, Middle and South pole air temperatures at 0.1m, 0.6m, 1.1m and 1.7m from the ground (Occupied zone) in the Test room during the occupied hours. (23-26.10.2023; 8:00-15:00)

Figure 9.67: North, Middle and South pole air velocities at 0.1m, 0.6m, 1.1m and 1.7m from the ground (Occupied zone) in the Test room during the occupied hours. (23-26.10.2023; 8:00-15:00)

9.7.3 Winter case

Figure 9.68: North, Middle and South pole air temperatures at 0.1m, 0.6m, 1.1m and 1.7m from the ground (Occupied zone) in the Test room during the occupied hours. (30.11.2023-06.12.2023; 8:00-15:00)

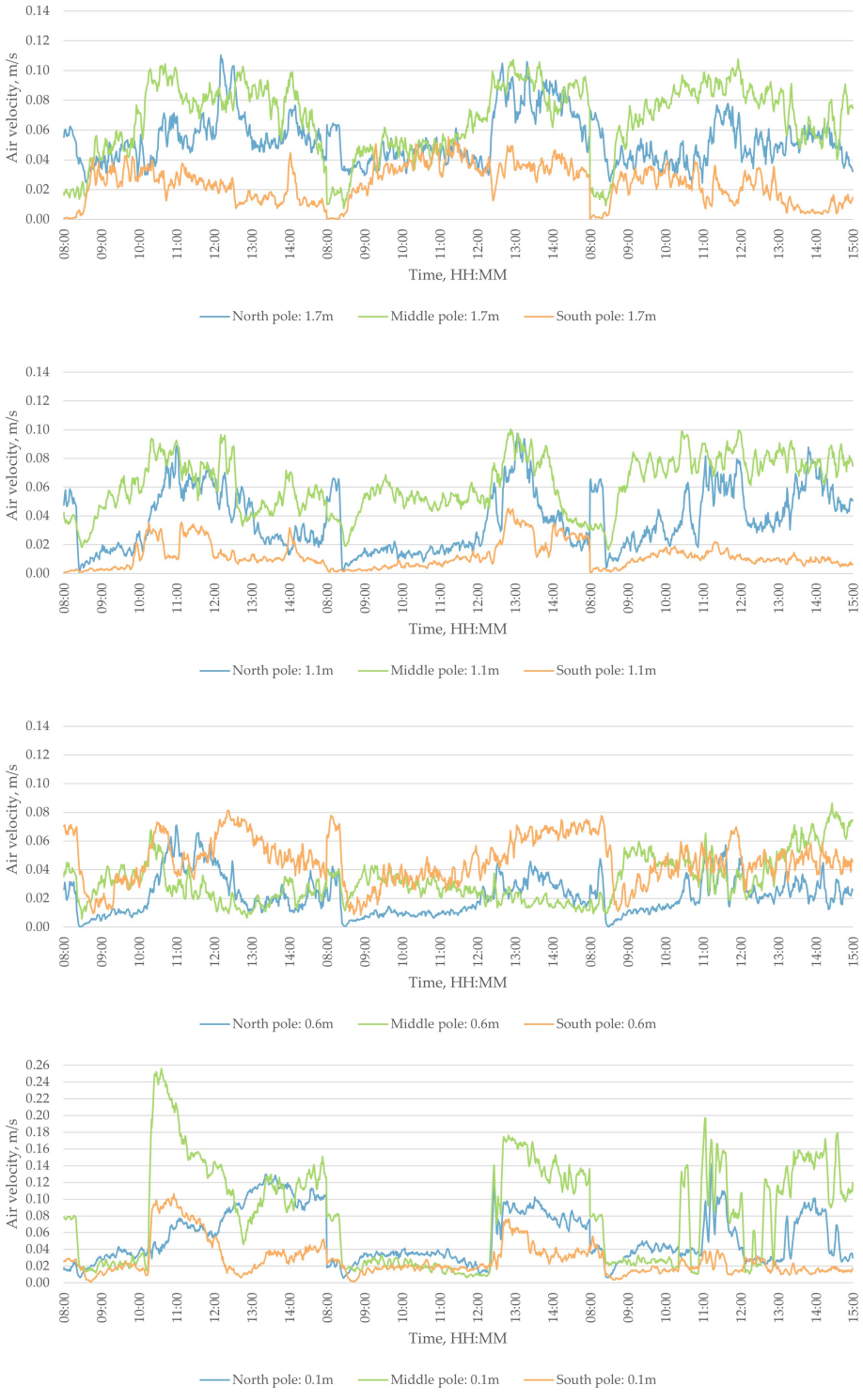

Figure 9.69: North, Middle and South pole air velocities at 0.1m, 0.6m, 1.1m and 1.7m from the ground (Occupied zone) in the Test room during the occupied hours. (30.11.2023-06.12.2023; 8:00-15:00)

9.8 Classroom vs. Kindergarten

PMV and PPD: 1.2 met vs 1.4 met

Figures 9.70 and 9.71 present the estimated PMV and PPD for both classroom and kindergarten scenarios in the cooling and heating season, focusing on air temperature averages from 0.1 meters up to 1.1 meters. This range is selected to account for the difference in height between kindergarten children and the standard adult heights referenced in DS 7726. The missing data is attributed to measurement errors logged for the North pole in summer and the Middle pole in winter. Consequently, these measurements are not presented.

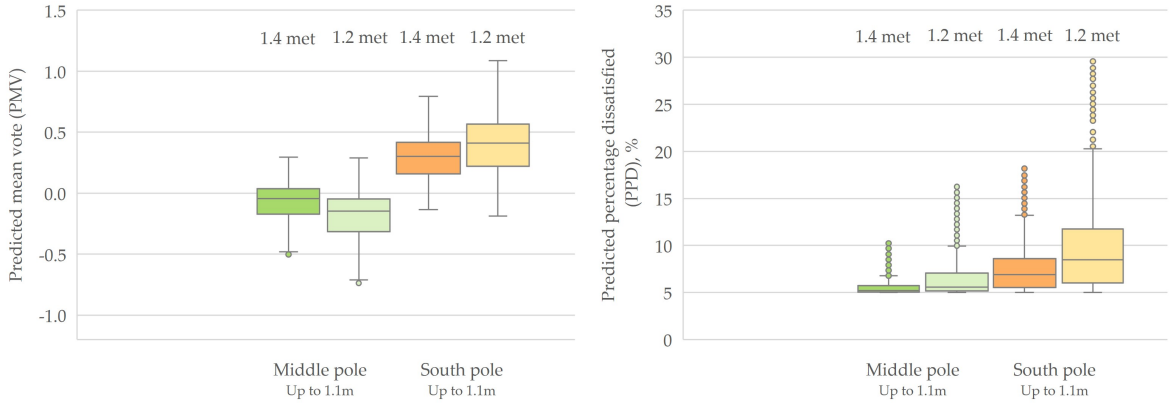

Figure 9.70: Predicted mean vote (PMV) and Predicted percentage dissatisfied (PPD) for an up to 1.1 height from the floor person with metabolic rate of 1.4 and 1.2 in two positions (Middle and South) in the Test room during the occupied hours. (24-30.07.2023 SUMMER; 8:00-15:00)

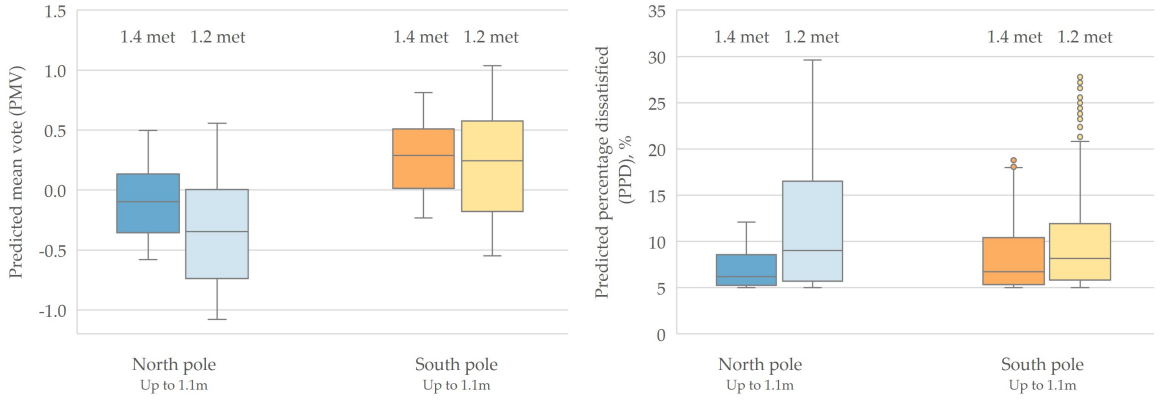

Figure 9.71: Predicted mean vote (PMV) and Predicted percentage dissatisfied (PPD) for an up to 1.1 height from the floor person with metabolic rate of 1.4 and 1.2 in two positions (North and South) in the Test room during the occupied hours. (30.11.2023-06.12.2023 WINTER; 8:00-15:00)

In summer, centrally located, those with a 1.4 met rate experience a more comfortable thermal environment, while a 1.2 met rate indicates a preference for a slightly cooler sensation. At the South pole, higher PMVs for both metabolic rates suggest increased warmth, with the 1.4 met rate feeling closer to neutral than the 1.2 met. Overall, there is a lower PPD, indicating greater satisfaction with the thermal environment for the 1.4 met rate than for the 1.2 met at both locations.

In winter at the North Pole, individuals with a metabolic rate of 1.4 met experience a range of PMV closest to zero, indicating neutral thermal comfort. For those with a metabolic rate of 1.2 met at the North Pole, the PMV values are generally lower, indicating cooler conditions. At the South Pole, 1.4 met and 1.2 met metabolic rates show PMV medians closer to zero. However, the range for 1.4 met is narrower and closer to neutral comfort, whereas 1.2 met has a broader spread, indicating more significant variability in comfort perception. Similar to the summer case, a lower Predicted Percentage of Dissatisfied (PPD) is observed, indicating greater satisfaction with the thermal environment for the 1.4 met rate compared to the 1.2 met at both locations.

PMV and PPD: different clothing insulation

In Figure 9.72, the impact of varying clothing insulation levels on thermal comfort during the cooling season at the Middle and South Poles, focusing on insulation levels slightly lower and slightly higher than the DS recommendations for heights up to 1.1 meters. A similar analysis is conducted for the heating season for the available poles, as depicted in Figure 9.73).

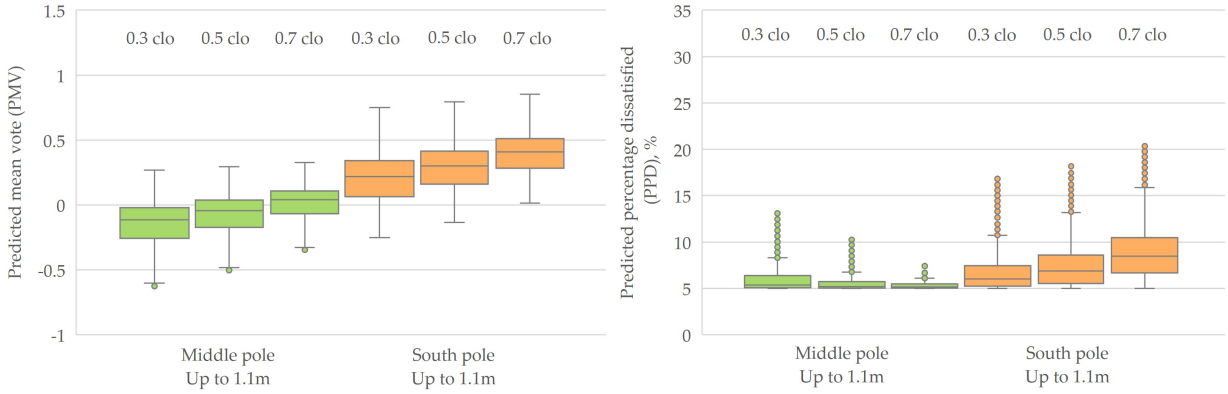

Figure 9.72: Predicted mean vote (PMV) and Predicted percentage dissatisfied (PPD) for an up to 1.1 height from the floor person with a metabolic rate of 1.4 and clothing insulation of 0.3 clo, 0.5 clo and 0.7 clo in two positions (North and South) in the Test room during the occupied hours. (24-30.07.2023 SUMMER; 8:00-15:00)

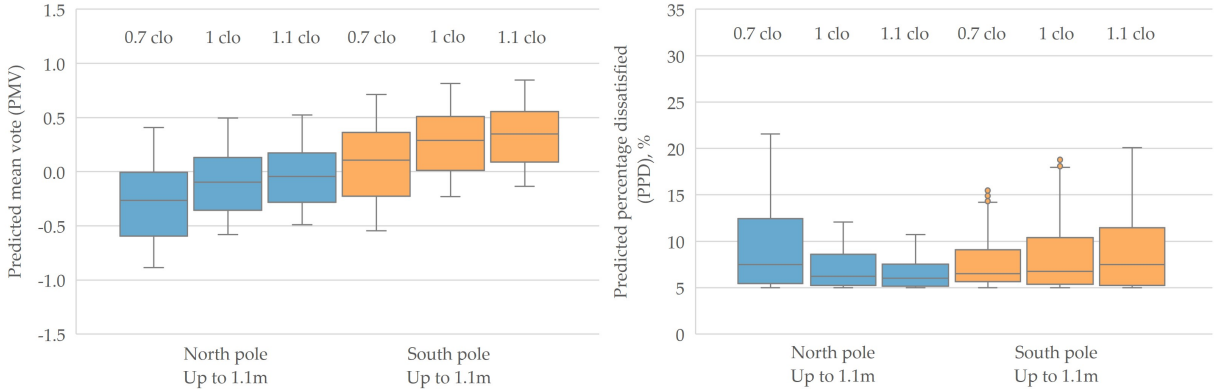

Figure 9.73: Predicted mean vote (PMV) and Predicted percentage dissatisfied (PPD) for an up to 1.1 height from the floor person with a metabolic rate of 1.4 and clothing insulation of 0.7 clo, 1 clo and 1.1 clo in two positions (North and South) in the Test room during the occupied hours. (30.11.2023-06.12.2023 WINTER; 8:00-15:00)

It is unsurprising that higher clothing insulation levels increase the PMV value, as clothing provides thermal insulation for the human body. Consequently, we observe that in both seasons, the PMV gradually increases with higher levels of thermal insulation. During the cooling season at the Middle Pole, occupants with 0.7 clo experience less PPD, suggesting greater comfort, whereas at the South Pole, the lower insulation level of 0.3 clo is more conducive to comfort.

In the heating season, occupants at the North Pole find the warmest analysed clothing insulation of 1.1 clo to be more acceptable, while at the South Pole, the lowest analysed insulation of 0.7 clo is preferred for optimal thermal comfort.

9.9 Local discomfort due to radiant temperature asymmetry

The evaluation of results concerning the RTA in the Test room is displayed in detail in this section.

9.9.1 Summer case

Sitting person located in the North of the room

When the sitting subject is moved to the Northern part of the Test room, the plane radiant temperature between the North and South walls is enhanced, resulting in values between 8.1°C and 11.5°C. As the subject is not moved in West-East directions, the RTA results between the West and East walls are similar to the central position, as they range between 0.2-1.5°C. Eventually, category A/B is achieved throughout the summer measurement period.

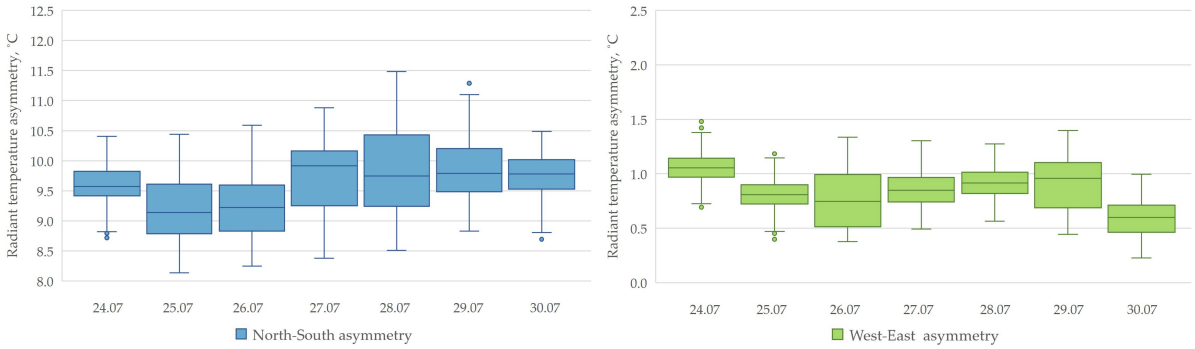

Figure 9.74: Radiant temperature asymmetry due to walls in the case of a sitting person located in the middle of the room during occupied hours. (24-30.07.2023; 8:00-15:00)

The calculated PD is illustrated in Figure 9.75. It can be concluded that there is no dissatisfaction due to the asymmetry from the West-East walls. However, the North-South temperature asymmetry causes 0.1-0.7% to be thermally dissatisfied.

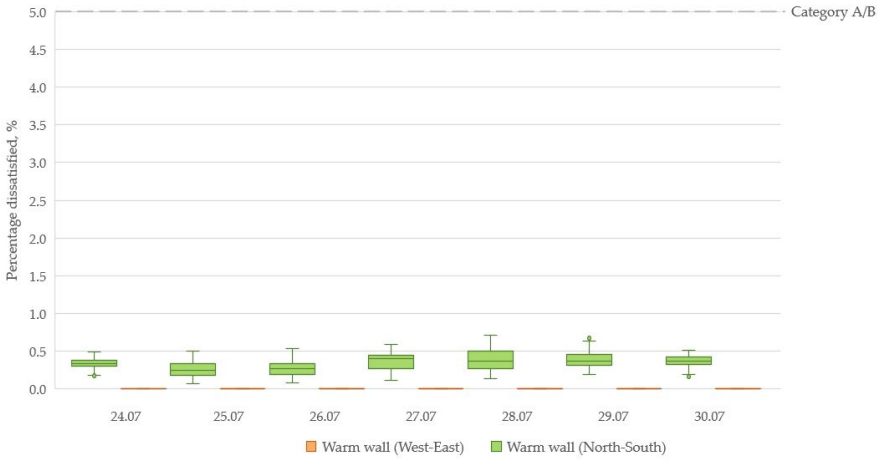

Figure 9.75: Percentage dissatisfied due to radiant temperature asymmetry in the case of a sitting person located in the middle of the room during occupied hours. (24-30.07.2023; 8:00-15:00)

Sitting person located in the South of the room

In the case of the subject located close to the Southern wall, the North-South radiant temperature asymmetry further increases. However, it still fulfils category A/B as the maximum RTA is 17.5°C, which is lower than the category limit of 23°C defined in DS7730. The temperature range is also wider, as the minimum value is 13.0°C. On the other hand, the West-East asymmetry remains unchanged, as the values vary between 0.2-1.5°C.

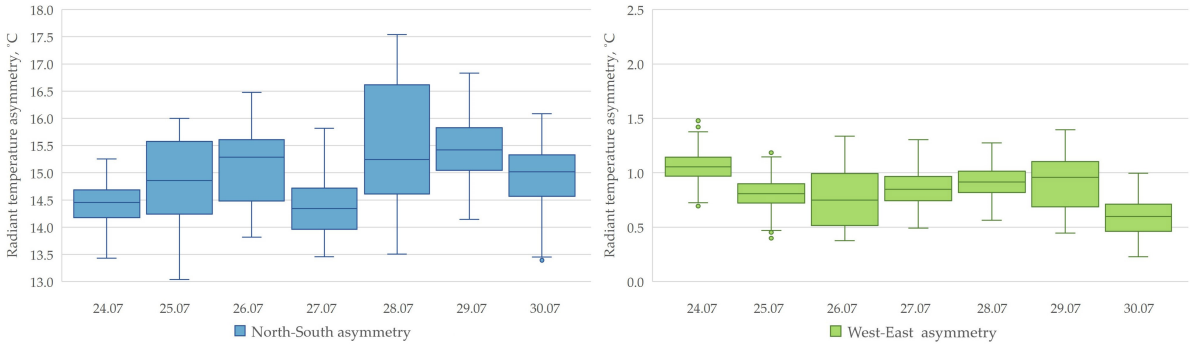

Figure 9.76: Radiant temperature asymmetry due to walls in the case of a sitting person located in the middle of the room during occupied hours. (24-30.07.2023; 8:00-15:00)

The percentage of dissatisfied occupants was between 1.0-2.2% due to warm walls (North-South asymmetry). Additionally, there is no discomfort due to the RTA from the West- East walls.

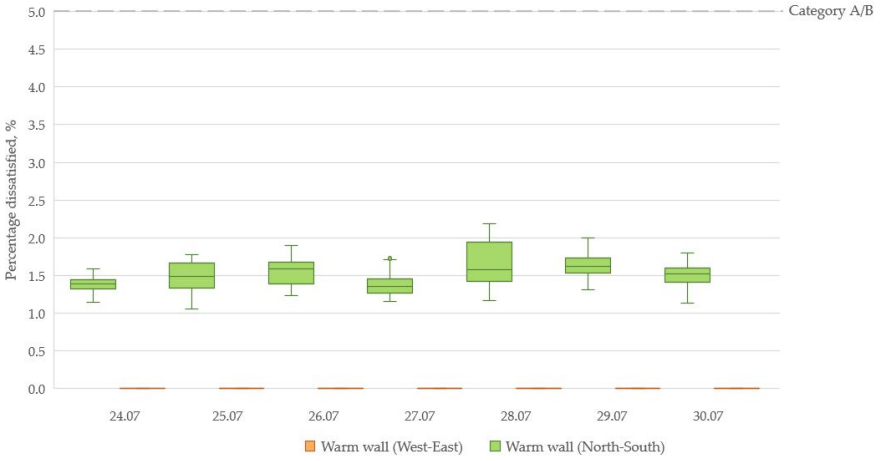

Figure 9.77: Percentage dissatisfied due to radiant temperature asymmetry in the case of a sitting person located in the middle of the room during occupied hours. (24-30.07.2023; 8:00-15:00)

Standing person in the middle of the room

When the subject's position is changed from sitting to standing while being centrally located in the Test room, the results are illustrated in Figure 9.78. It can be observed, that the radiant temperature asymmetry between the North and South walls ranges from 0.4°C to 1.9°C, while for the West-East walls it ranges from 0.3°C to 2.3°C. Consequently, category A/B is fulfilled during all measurement days.

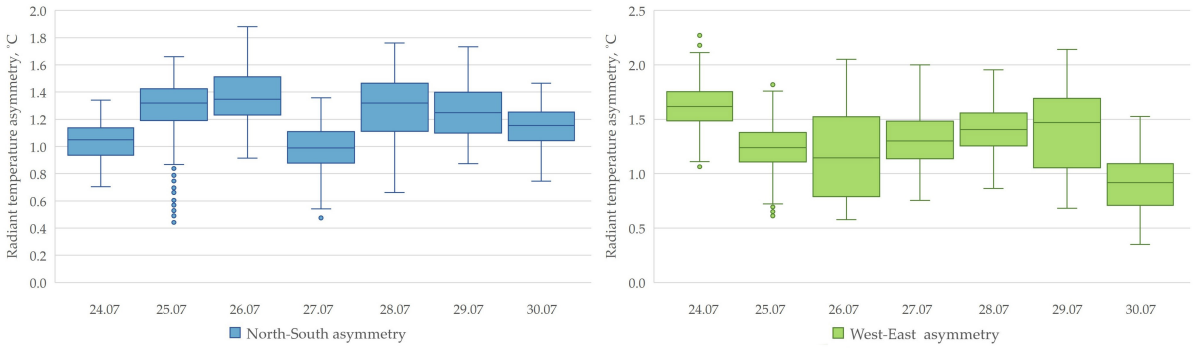

Figure 9.78: Radiant temperature asymmetry due to walls in the case of a sitting person located in the middle of the room during occupied hours. (24-30.07.2023; 8:00-15:00)

The calculated percentage of dissatisfied occupants displays that there is no risk of thermal discomfort due to the warm walls.

Standing person located in the North of the room

In the case when the standing person is located close to the Northern wall, the RTA due to the North and South walls increases to 8.5-12.0°C, while the West-East asymmetry ranges between 0.2-1.7°C. Accordingly, category A/B is fulfilled.

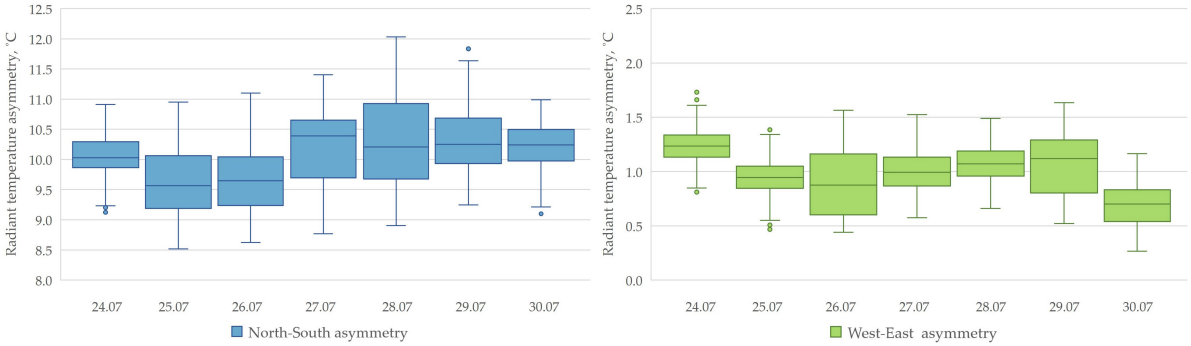

Figure 9.79: Radiant temperature asymmetry due to walls in the case of a sitting person located in the middle of the room during occupied hours. (24-30.07.2023; 8:00-15:00)

As the percentage of dissatisfied occupants can be obtained from Figure 9.80, it can be concluded that category A/B is fulfilled, since the maximum calculated PD due to warm walls is 0.8% from the North-South asymmetry.

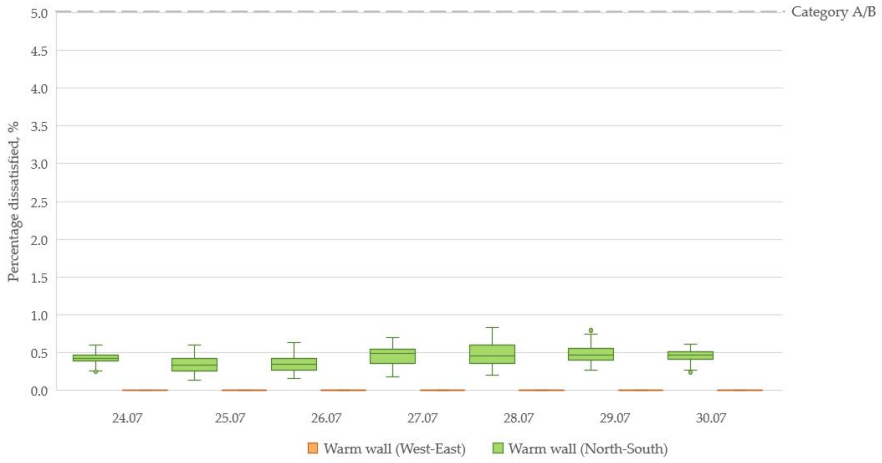

Figure 9.80: Percentage dissatisfied due to radiant temperature asymmetry in the case of a sitting person located in the middle of the room during occupied hours. (24-30.07.2023; 8:00-15:00)

Standing person located in the South of the room

Similarly to the Northern case, when the subject is standing in the Southern part of the room, the North-South asymmetry increases up to 17.9°C, with a minimum of 13.3°C. The difference between the plane radiant temperatures of the West and East walls remains unchanged and within the range of 0.2-1.7°C.

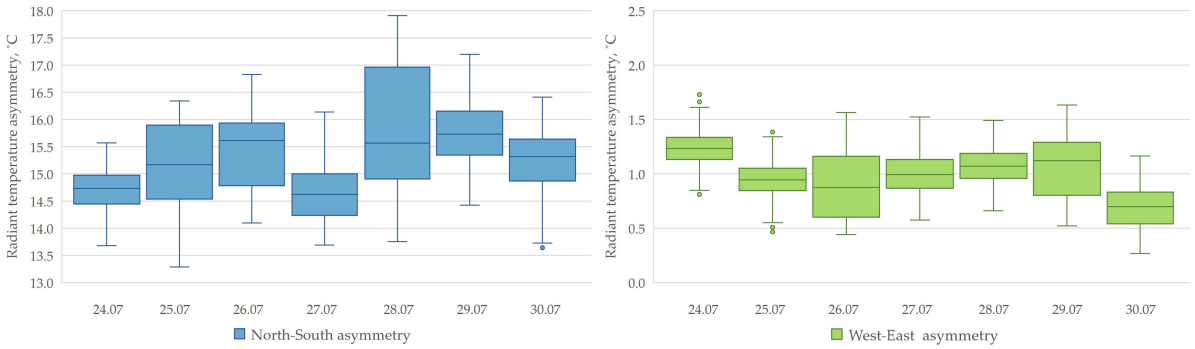

Figure 9.81: Radiant temperature asymmetry due to walls in the case of a sitting person located in the middle of the room during occupied hours. (24-30.07.2023; 8:00-15:00)

The PD due to warm walls is displayed in Figure 9.82.The highest PD is caused by the warm walls due to the asymmetry from the North-South walls, which ranges from 1.1% up to 2.3%.

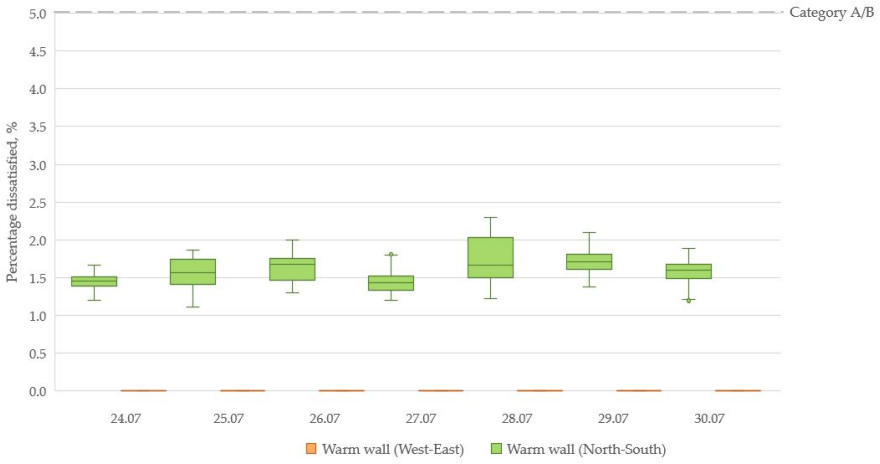

Figure 9.82: Percentage dissatisfied due to radiant temperature asymmetry in the case of a sitting person located in the middle of the room during occupied hours. (24-30.07.2023; 8:00-15:00)

9.9.2 Intermediate case

Sitting person located in the North of the room

When the sitting subject is placed 0.2m away from the North wall, the radiant temperature asymmetry between the North and South walls increases to a range of 6.7-7.3°C. However, the values for the West and East walls remain unchanged as it is between 0.0-0.3°C. As the RTA for all the walls is below 23°C, category A/B is fulfilled.

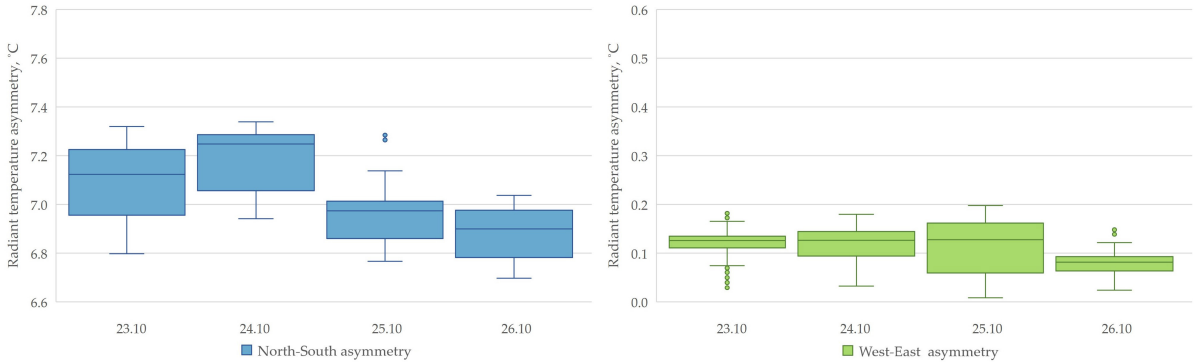

Figure 9.83: Radiant temperature asymmetry due to walls in the case of a sitting person located on the North of the room during occupied hours. (23-26.10.2023; 8:00-15:00)

As the sitting subject is moved to the Northern part of the room, the RTA due to the ceiling is reduced to 3.2-3.6°C, which fulfills category A/B as it is below 5°C.

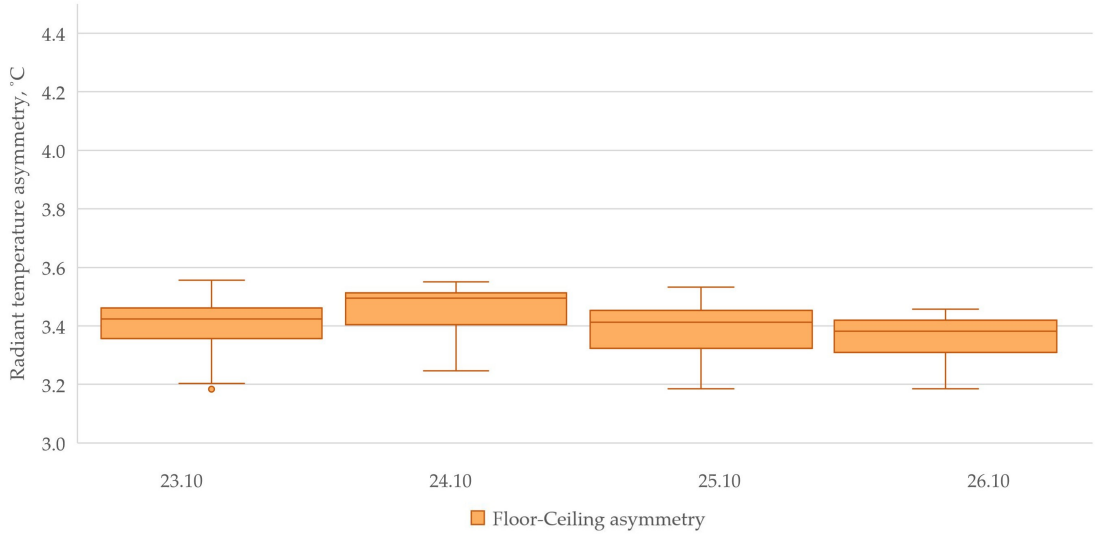

Figure 9.84: Radiant temperature asymmetry due to ceiling and floor in the case of a sitting person located on the North of the room during occupied hours. (23-26.10.2023; 8:00-15:00)

When calculating the percentage of dissatisfied, it can be concluded that the RTA from warm walls does not cause any issues. Although, 3.7-4.2% of the occupants are experiencing discomfort due to RTA from the ceiling, category A/B is still achieved during the whole measurements period.

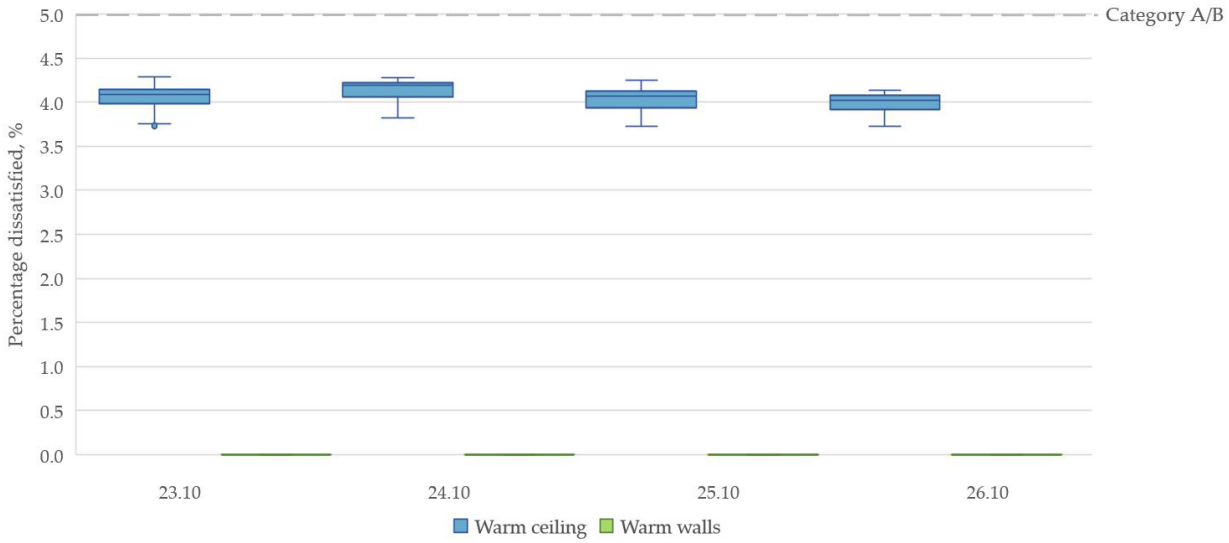

Figure 9.85: Percentage dissatisfied due to radiant temperature asymmetry in the case of a sitting person located on the North of the room during occupied hours. (23-26.10.2023; 8:00-15:00)

Sitting person located in the South of the room

As the subject is placed 0.2m away from the South wall in a sitting position, the RTA for the North-South walls further increases. Even though the values range between 10.4-11.3°C, category A/B is fulfilled. For the West and East walls, the difference in the plane radiant temperatures remains unchanged, with variations between 0.0-0.3°C.

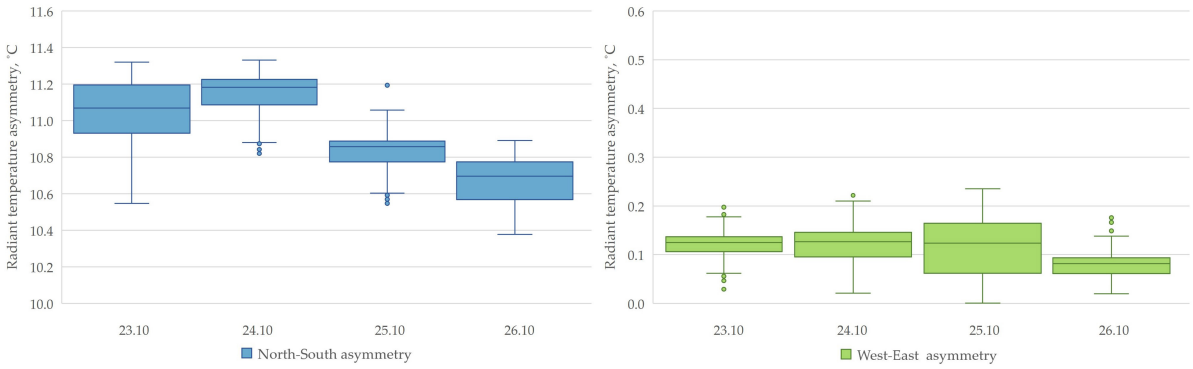

Figure 9.86: Radiant temperature asymmetry due to walls in the case of a sitting person located on the South of the room during occupied hours. (23-26.10.2023; 8:00-15:00)

Similarly to the case of the subject sitting in the Northern part of the room, the RTA from the ceiling ranges between 3.2-3.6°C. Therefore, no discomfort is experienced and category A/B is achieved.

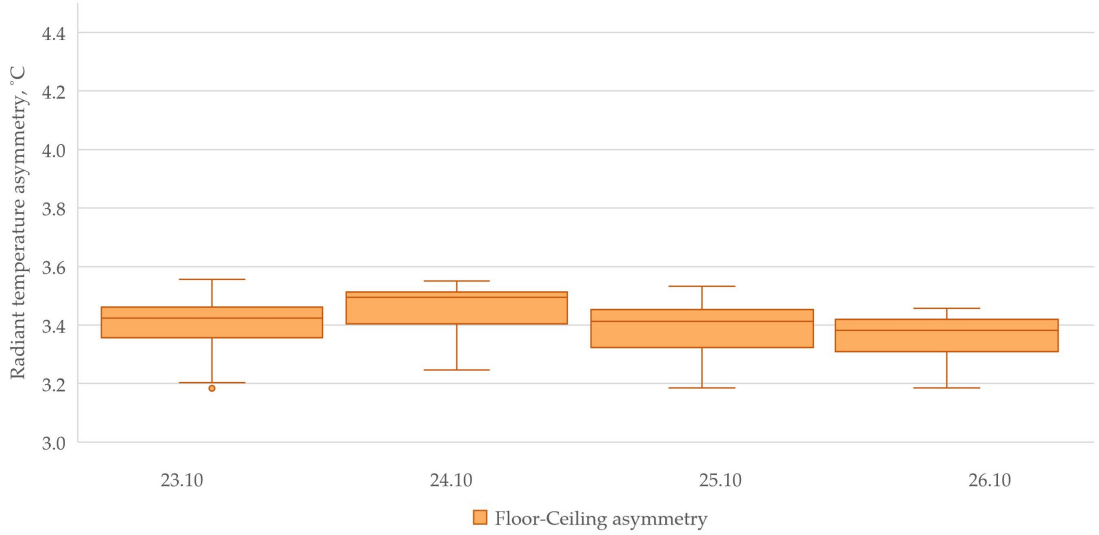

Figure 9.87: Radiant temperature asymmetry due to ceiling and floor in the case of a sitting person located on the South of the room during occupied hours. (23-26.10.2023; 8:00-15:00)

The results of calculating the PD are displayed in Figure 9.88, and it can be obtained that PD due to the RTA from the North-South walls is between 0.5-0.7%. Due to the West-East walls, there is no discomfort expected. For the ceiling, the PD remains the same as for the Northern placement, as it ranges between 3.7-4.2%.

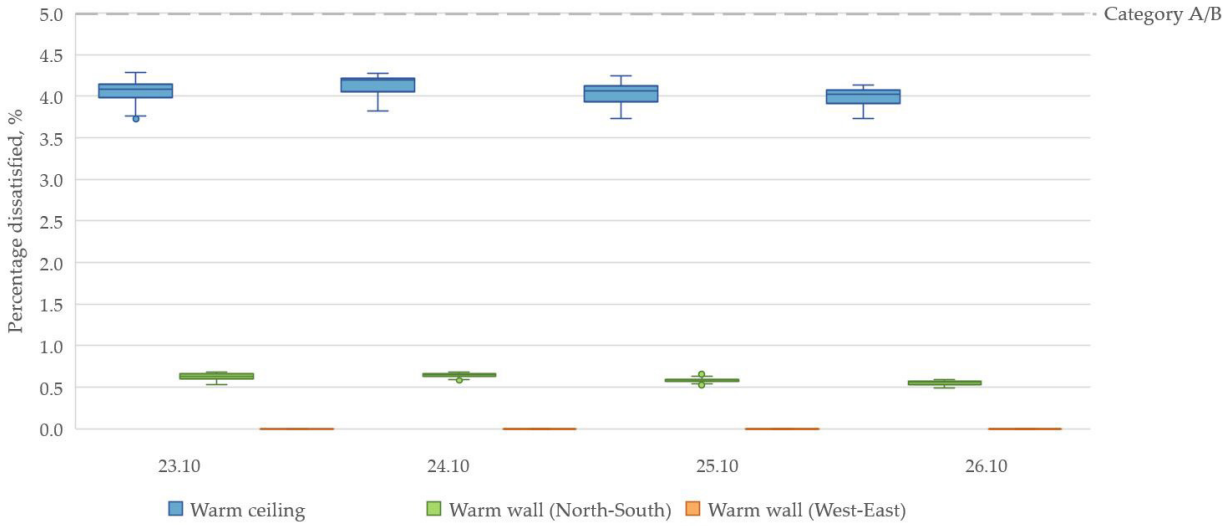

Figure 9.88: Percentage dissatisfied due to radiant temperature asymmetry in the case of a sitting person located on the South of the room during occupied hours. (23-26.10.2023; 8:00-15:00)

Standing person in the middle of the room

In the case of a person standing in the middle of the room, the difference between the plane radiant temperatures of the North and South walls varies between 0.8-0.9°C during the measurement period. For the West and East walls, this range is between 0.0-0.3°C, as it

is illustrated in Figure 9.89. Therefore, it can be established that there is no discomfort due to RTA from the walls.

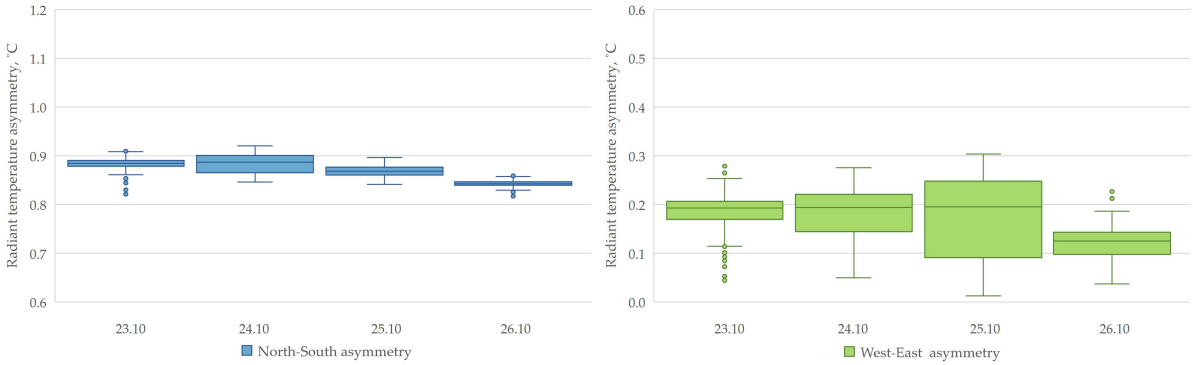

Figure 9.89: Radiant temperature asymmetry due to walls in the case of a standing person located in the middle of the room during occupied hours. (23-26.10.2023; 8:00-15:00)

In figure 9.90 the analysis of RTA due to ceiling is displayed. As the values vary between 1.9-2.2°C, category A/B is achieved.

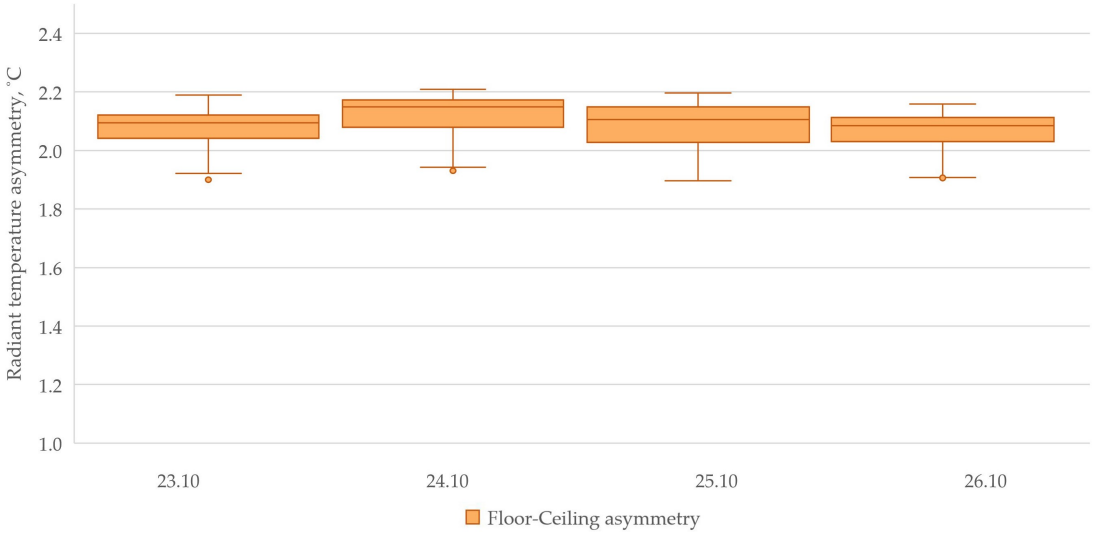

Figure 9.90: Radiant temperature asymmetry due to ceiling and floor in the case of a standing person located in the middle of the room during occupied hours. (23-26.10.2023; 8:00-15:00)

As the RTA is below 1°C for all the walls, no discomfort is expected. However, due to the difference in plane radiant temperatures between the ceiling and floor, 2.0-2.4 percent of the occupants are calculated to be dissatisfied.

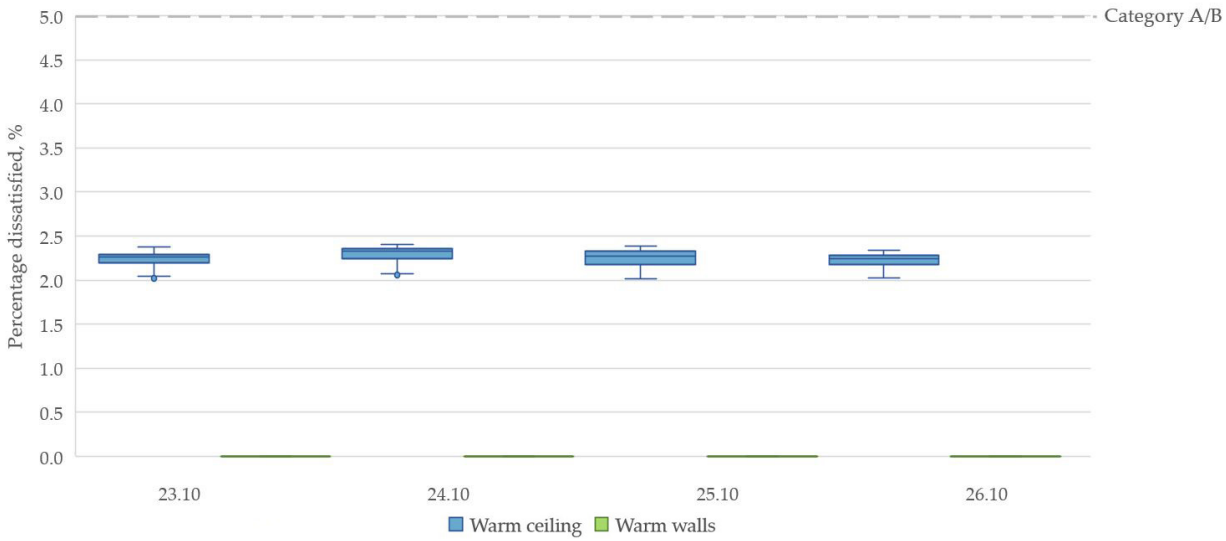

Figure 9.91: Percentage dissatisfied due to radiant temperature asymmetry in the case of a standing person located in the middle of the room during occupied hours. (23-26.10.2023; 8:00-15:00)

Standing person located in the North of the room

When the standing person is positioned 0.2m from the Northern wall, the RTA due to the North-South walls varies between 7.0-7.7°C, and for the West-East walls it is between 0.0-0.3°C. Therefore, both of them fulfill category A/B as the values are below 23°C.

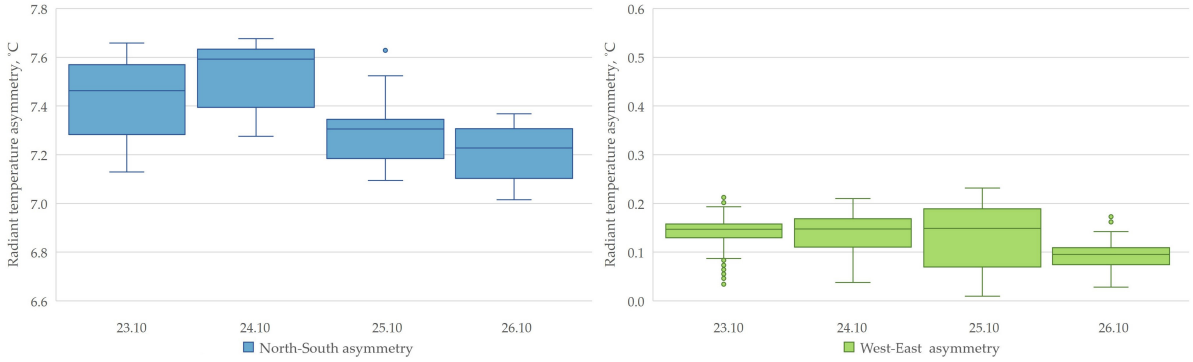

Figure 9.92: Radiant temperature asymmetry due to walls in the case of a standing person located on the North of the room during occupied hours. (23-26.10.2023; 8:00-15:00)

When analysing the RTA between the ceiling and the floor, category A/B is achieved as the value-range is from 1.4°C to 1.6°C.

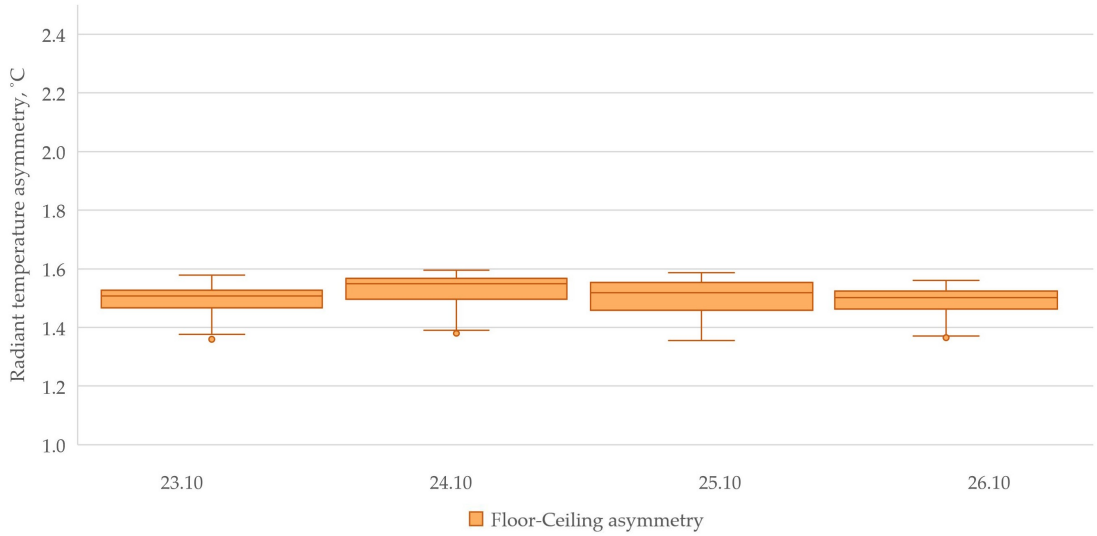

Figure 9.93: Radiant temperature asymmetry due to ceiling and floor in the case of a standing person located on the North of the room during occupied hours. (23-26.10.2023; 8:00-15:00)

From Figure 9.94 it can be concluded that there is no discomfort occurring due to the radiant temperature asymmetry from the walls. Although 1.4-1.7% of the occupants are calculated to be dissatisfied due to the difference in plane radiant temperatures between the ceiling and floor, category A/B is achieved.

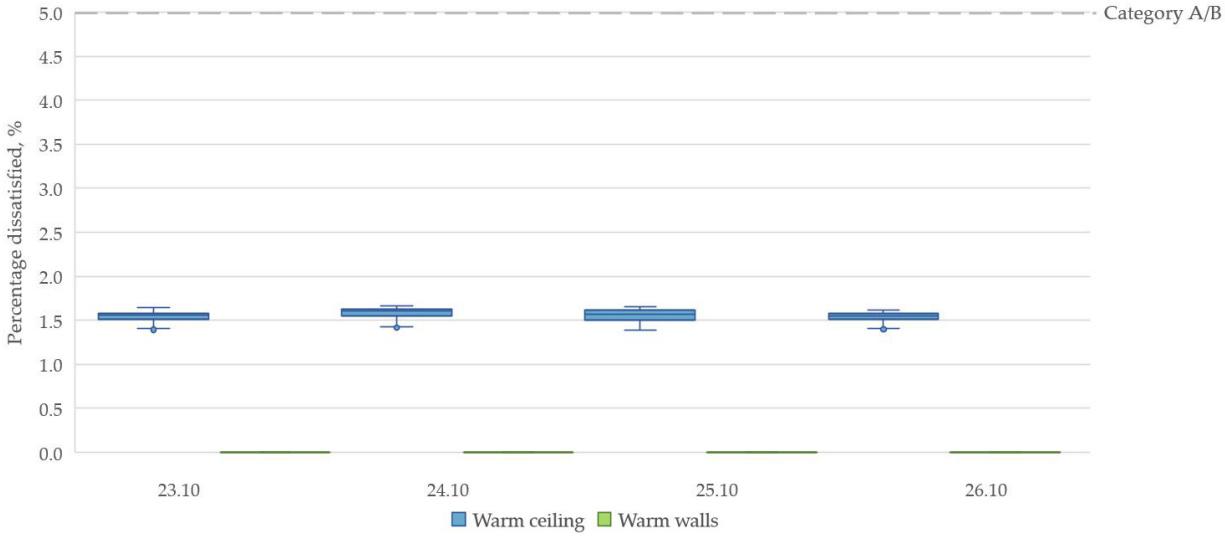

Figure 9.94: Percentage dissatisfied due to radiant temperature asymmetry in the case of a standing person located on the North of the room during occupied hours. (23-26.10.2023; 8:00-15:00)

Standing person located in the South of the room

When the standing person is located in the South part of the room, 0.2m away from the South wall, the RTA for the North-South walls is between 10.6-11.6°C. For the West and East walls, the values remain unchanged as the range is between 0.0-0.3°C. In conclusion, the RTA due to the walls is fulfilling the requirements for category A/B.

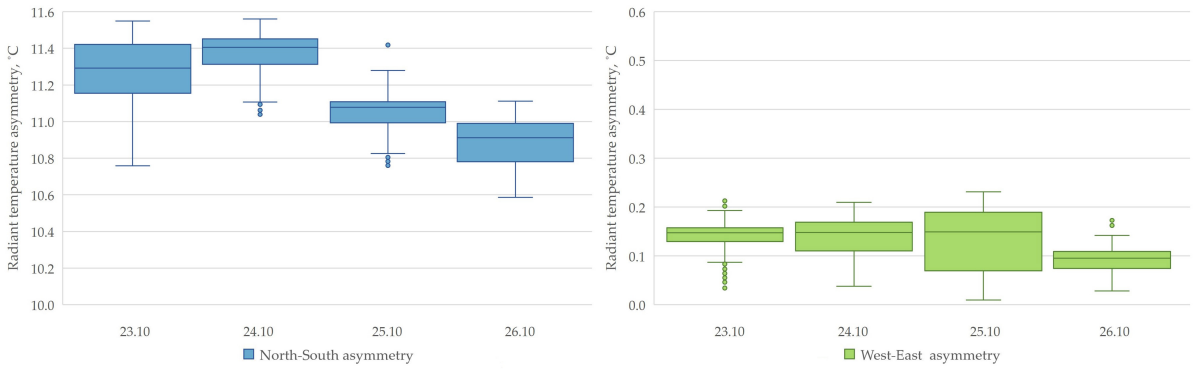

Figure 9.95: Radiant temperature asymmetry due to walls in the case of a standing person located on the South of the room during occupied hours. (23-26.10.2023; 8:00-15:00)

The RTA from the ceiling also appears to be in category A/B, as it ranges between 1.4-1.6°C, similarly to the Northern position.

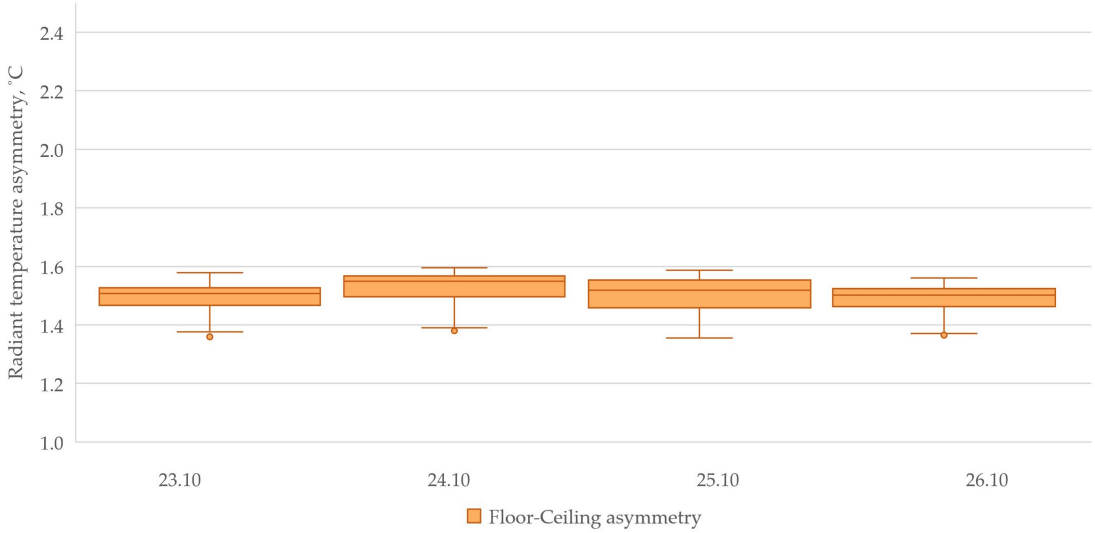

Figure 9.96: Radiant temperature asymmetry due to ceiling and floor in the case of a standing person located on the South of the room during occupied hours. (23-26.10.2023; 8:00-15:00)

In Figure 9.97 the values are displayed for calculating the percentage of occupants dissatisfied due to the RTA in the room. It can be obtained that 0.0% is dissatisfied due to the RTA from the West-East walls, 0.5-0.7% is dissatisfied due to the North-South walls, and 1.4-1.7% is dissatisfied due to the warm ceiling. As all the PD values are below 5%, category A/B is fulfilled during the measurement period.

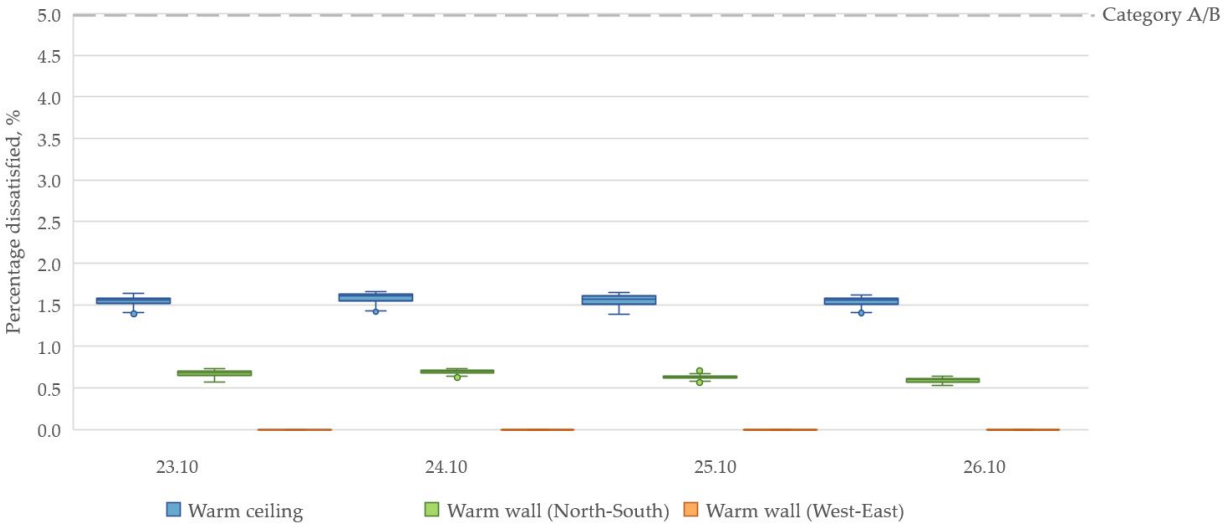

Figure 9.97: Percentage dissatisfied due to radiant temperature asymmetry in the case of a standing person located on the South of the room during occupied hours. (23-26.10.2023; 8:00-15:00)

9.9.3 Winter case

Sitting person in the North of the room

When the subject is located 0.2m away from the North wall in a sitting position, the RTA increases between the North and South walls up to 11.1°C; though, category A/B is still fulfilled. For the West-East walls, the RTA slightly decreases, as the values vary between 0.0-0.7°C.

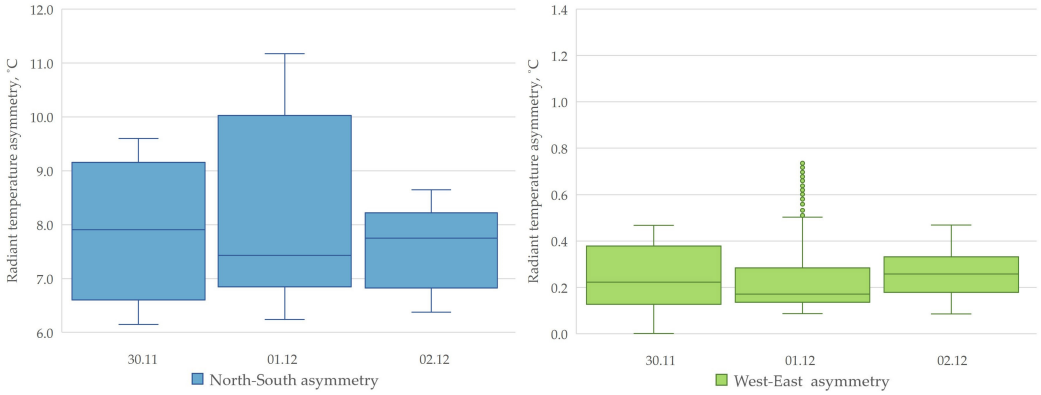

Figure 9.98: Radiant temperature asymmetry due to walls in the case of a sitting person located in the North of the room during occupied hours. (30.11.2023-02.12.2023; 8:00-15:00)

With the location change, the floor-ceiling RTA improved, and category A/B was satisfied during all three measurement days, as the values range between 2.9-4.0°C.

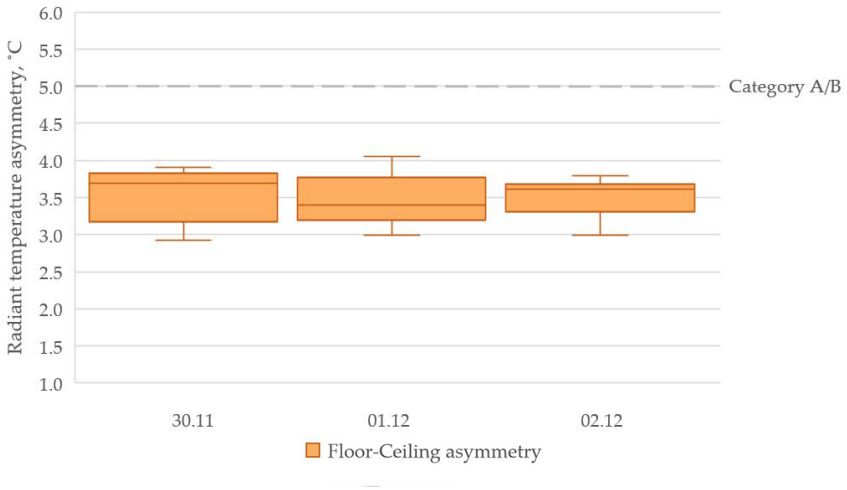

Figure 9.99: Radiant temperature asymmetry due to ceiling and floor in the case of a sitting person located in the North of the room during occupied hours. (30.11.2023-02.12.2023; 8:00-15:00)

Furthermore, the calculated PD for the North-South walls is between 0.0-0.6%, while there is no risk of discomfort due to the West-East walls. The floor-ceiling RTA is calculated to cause 3.3-5.1% to be thermally dissatisfied. As the limit of 5% is exceeded, 1.7% falls into category C.

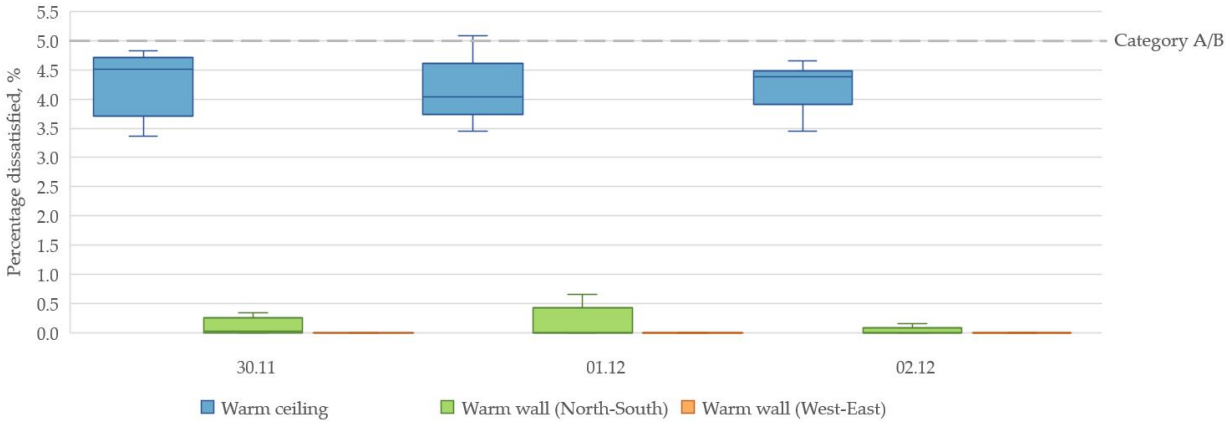

Figure 9.100: Percentage dissatisfied due to radiant temperature asymmetry in the case of a sitting person located in the North of the room during occupied hours. (30.11.2023-02.12.2023; 8:00-15:00)

Sitting person in the South of the room

In the case of a sitting person 0.2m away from the South wall, the West-East asymmetry remains unchanged compared to the Northern location, while the North-South RTA further increases and varies between 11.0°C and 15.4°C. However, category A/B is reached during the whole occupancy as the temperature asymmetry between the walls is less than 23°C.

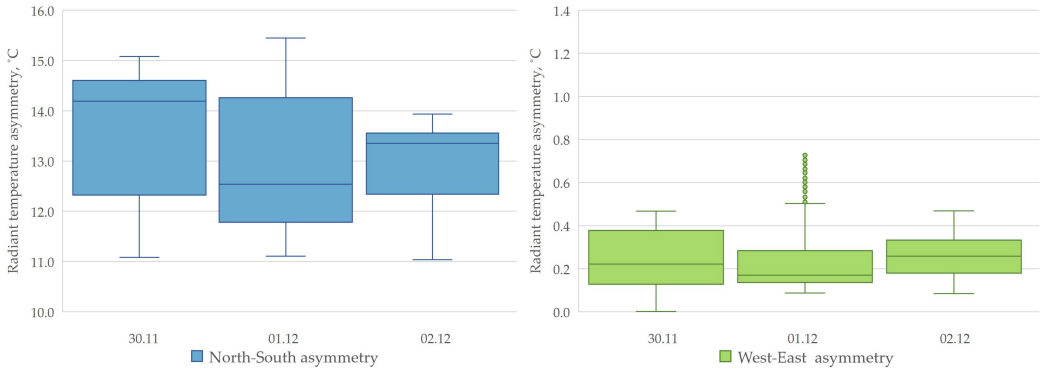

Figure 9.101: Radiant temperature asymmetry due to walls in the case of a sitting person located in the South of the room during occupied hours. (30.11.2023-02.12.2023; 8:00-15:00)

Equally to the Northern position, the RTA due to the floor-ceiling fulfils category A/B, as the values range from 2.9°C up to 4.0°C.

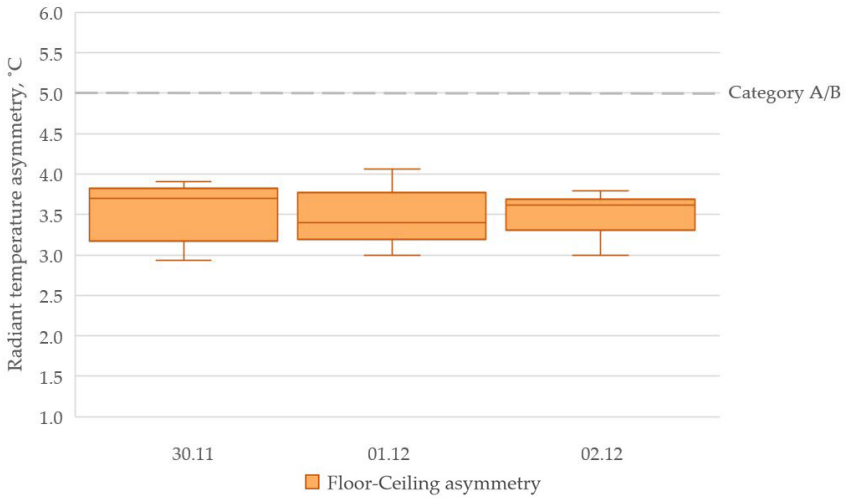

Figure 9.102: Radiant temperature asymmetry due to ceiling and floor in the case of a sitting person located in the South of the room during occupied hours. (30.11.2023-02.12.2023; 8:00-15:00)

Due to the North-South RTA, 0.6-1.6% is expected to be thermally dissatisfied, while the West-East walls do not cause any discomfort. The PD calculated due to the warm ceiling displays that 98.3% is in category A/B, similarly to the Northern position.

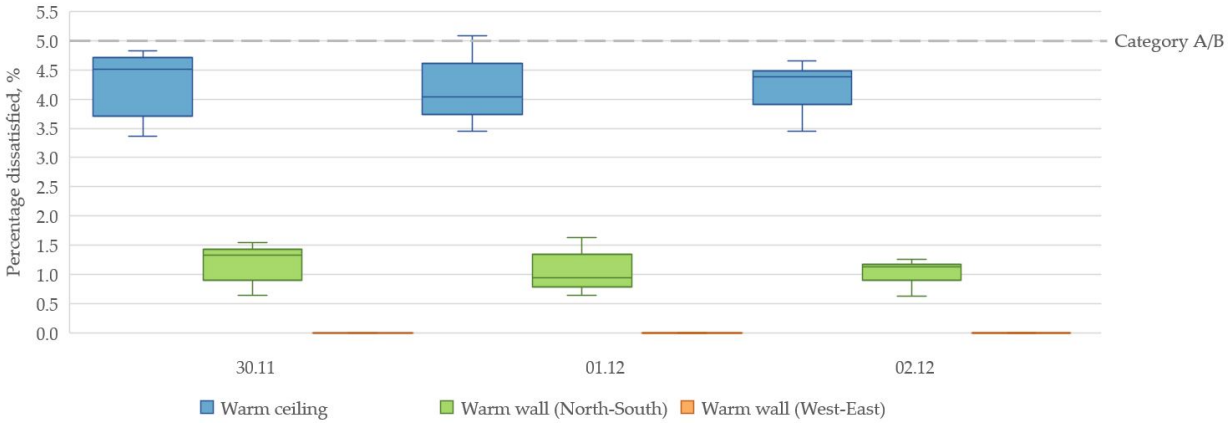

Figure 9.103: Percentage dissatisfied due to radiant temperature asymmetry in the case of a sitting person located in the South of the room during occupied hours. (30.11.2023-02.12.2023; 8:00-15:00)

Standing person in the middle of the room

In the case of a centrally located person in a standing position, the RTA due to the North and South walls varies between 0.7-1.7°C, while the values for the West and East walls are between 0.0-1.1°C. Therefore category A/B is fulfilled.

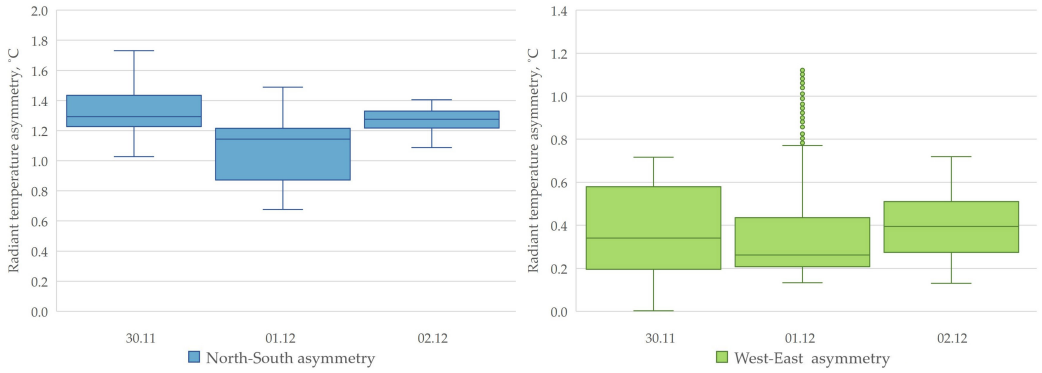

Figure 9.104: Radiant temperature asymmetry due to walls in the case of a standing person located in the middle of the room during occupied hours. (30.11.2023-02.12.2023; 8:00-15:00)

Considering the difference between the plane radiant temperatures of the floor and ceiling, the results are between 1.6°C and 2.5°C. As category A/B is satisfied during the three measurement days, an improvement is evident when the position is changed from sitting to standing, with a central placement in the room.

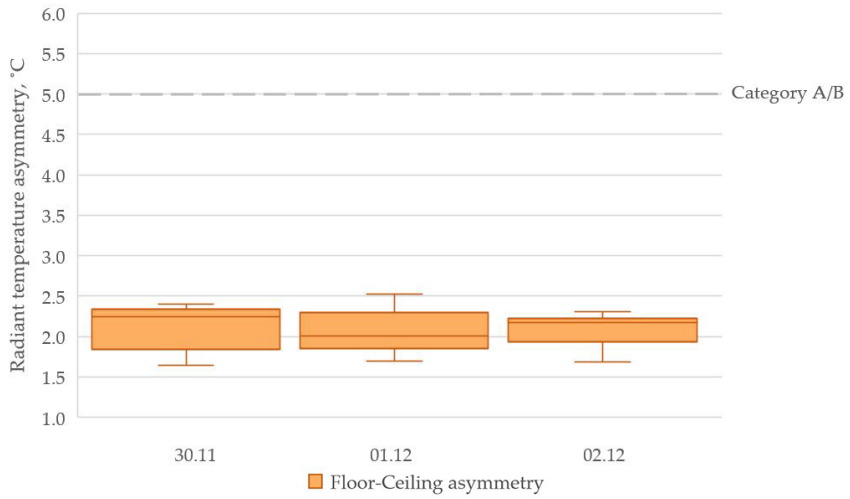

Figure 9.105: Radiant temperature asymmetry due to ceiling and floor in the case of a standing person located in the middle of the room during occupied hours. (30.11.2023-02.12.2023; 8:00-15:00)

Correspondingly, the calculated PD displays no discomfort due to warm walls, and a maximum of 2.8% dissatisfaction rate due to the warm ceiling.

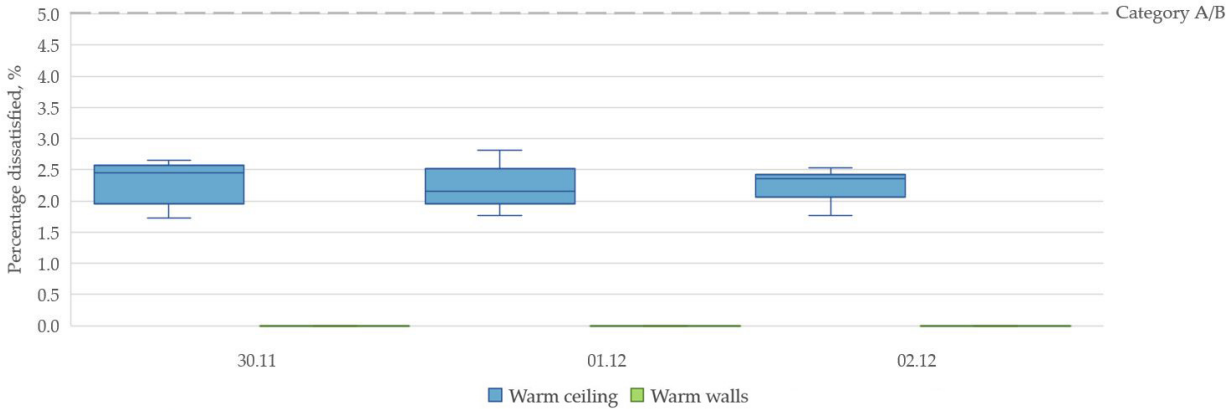

Figure 9.106: Percentage dissatisfied due to radiant temperature asymmetry in the case of a standing person located in the middle of the room during occupied hours. (30.11.2023-02.12.2023; 8:00-15:00)

Standing person in the North of the room

When the standing subject is located 0.2m away from the North wall, the RTA due to the North-South walls increases as the results vary between 6.4°C and 11.7°C, although Category A/B is achieved. In contrast, the RTA due to the West-East asymmetry decreases, as the maximum asymmetry is 0.8°C. Furthermore, with the standing position, slightly larger RTA results are calculated, than with a sitting position.

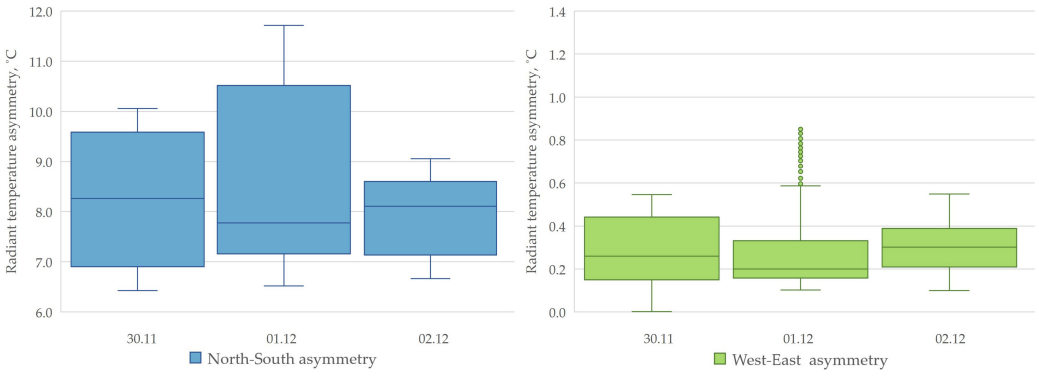

Figure 9.107: Radiant temperature asymmetry due to walls in the case of a standing person located in the North of the room during occupied hours. (30.11.2023-02.12.2023; 8:00-15:00)

The RTA due to the ceiling and floor ranges between 1.1°C and 1.8°C, indicating a minor improvement compared to the centrally placed standing position. Therefore, category A/B is satisfied.

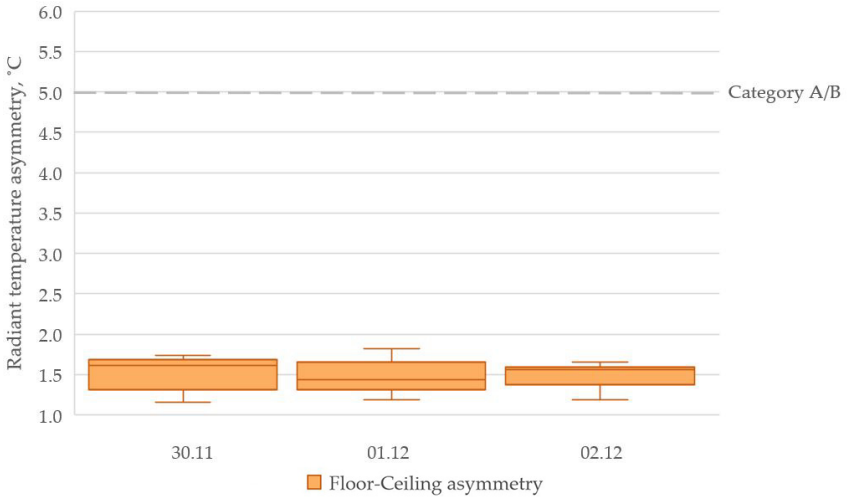

Figure 9.108: Radiant temperature asymmetry due to ceiling and floor in the case of a standing person located in the North of the room during occupied hours. (30.11.2023-02.12.2023; 8:00-15:00)

The calculated PD displays no discomfort due to the RTA of the West-East walls. For the North and South walls up to 0.8% is expected to be thermally dissatisfied, while the results due to the warm ceiling vary between 1.2-1.9%.

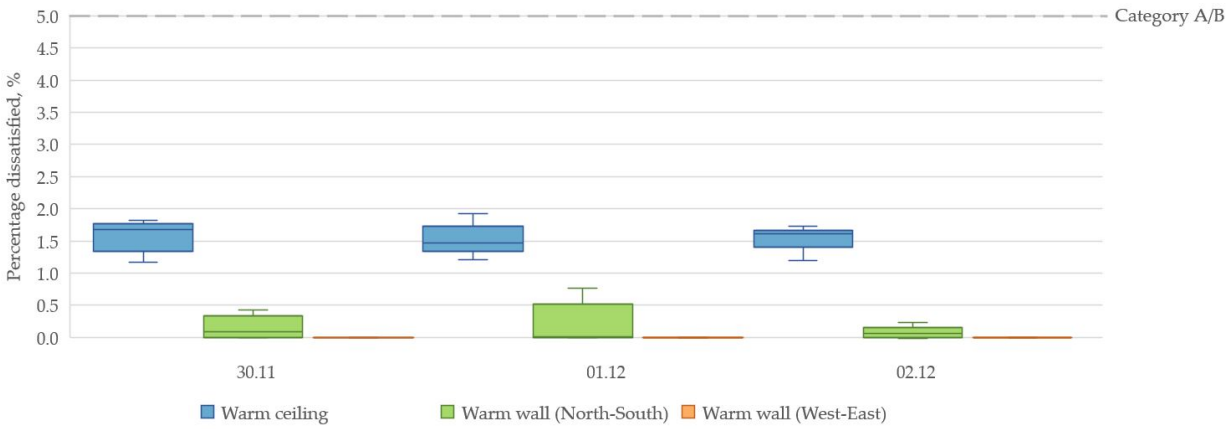

Figure 9.109: Percentage dissatisfied due to radiant temperature asymmetry in the case of a standing person located in the North of the room during occupied hours. (30.11.2023-02.12.2023; 8:00-15:00)

Standing person in the South of the room

Considering a standing subject 0.2m away from the South wall, the RTA of the West-East walls remains unchanged compared to the Northern position. However, the plane radiant temperature difference between the North and South walls increases up to 15.7°C. As both RTA results are below 23°C, category A/B is achieved.

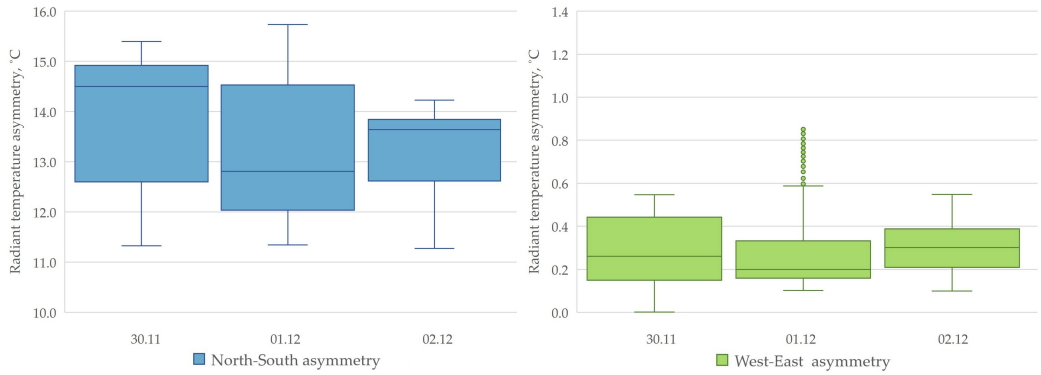

Figure 9.110: Radiant temperature asymmetry due to walls in the case of a standing person located in the South of the room during occupied hours. (30.11.2023-02.12.2023; 8:00-15:00)

Similarly to the Northern position, the result of RTA due to the floor and ceiling is classified as category A/B, as it ranges from 1.1°C up to 1.8°C.

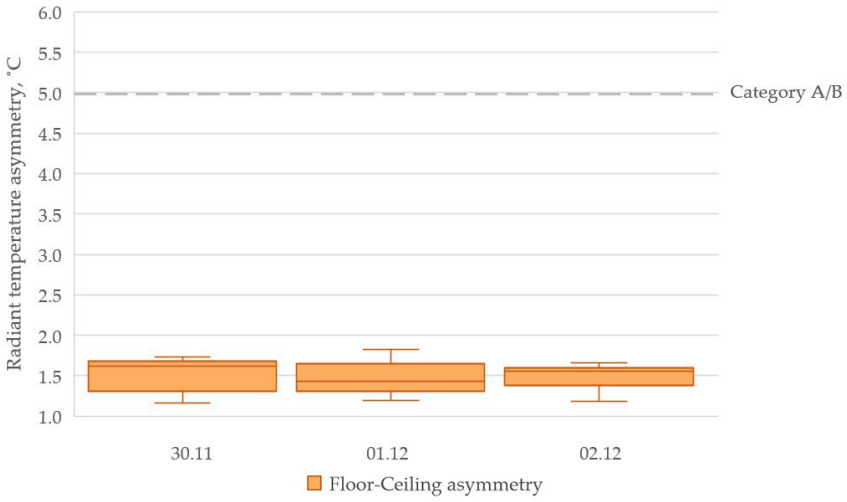

Figure 9.111: Radiant temperature asymmetry due to ceiling and floor in the case of a standing person located in the South of the room during occupied hours. (30.11.2023-02.12.2023; 8:00-15:00)

Lastly, it can be concluded that the occupants are not thermally dissatisfied due to the RTA between the West-East walls, and the expected percentage of dissatisfaction is under 2.0% for the North-South walls and floor-ceiling.

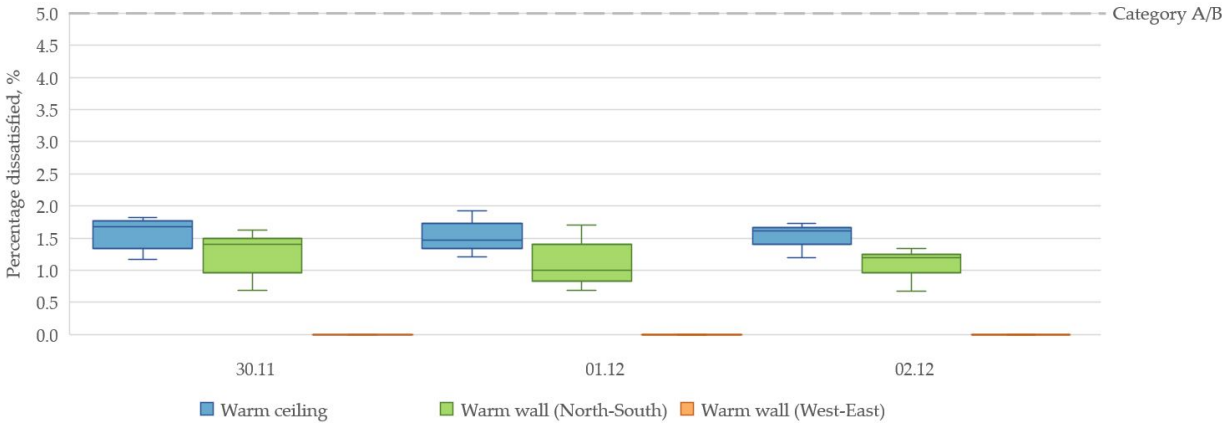

Figure 9.112: Percentage dissatisfied due to radiant temperature asymmetry in the case of a standing person located in the South of the room during occupied hours. (30.11.2023-02.12.2023; 8:00-15:00)

9.10 Thermal imaging with FLIR thermal camera

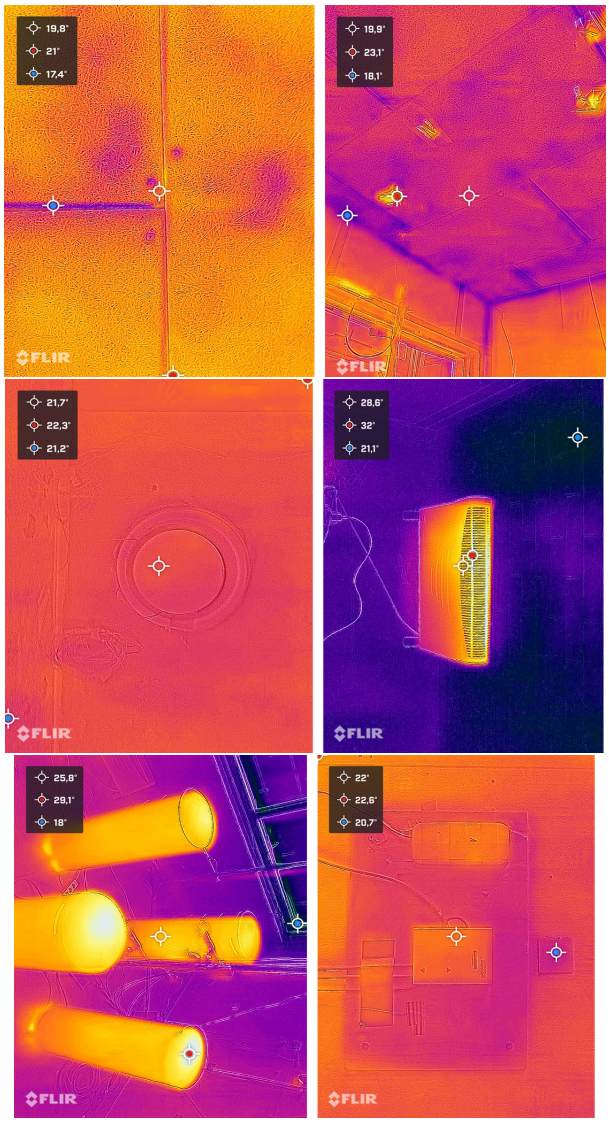

Figure 9.113: Various pictures taken in the Test room with a thermal imaging camera FLIR.